Physiological responses to genomic instability

Hannah S. E. Tivey

Department of Pathology

School of Medicine

Cardiff University

UK

A thesis submitted to the School of Medicine, Cardiff University for the degree of Doctor of Philosophy.

September 2010

UMI Number: U584495

UMI

Dissertation Publishing

ProQuest

DECLARATION

This work has not previously been accepted in substance for any degree and is not concurrently submitted in candidature for any degree.

Signed .... (candidate)   Date ...2/.11/.10..........
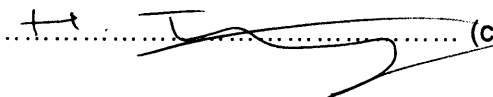
STATEMENT 1

This thesis is being submitted in partial fulfillment of the requirements for the degree of PhD

Signed .... (candidate)   Date ...2/.11/.10..........
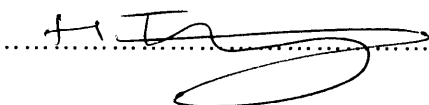
STATEMENT 2

This thesis is the result of my own independent work/investigation, except where otherwise stated.

Other sources are acknowledged by explicit references.

Signed .... (candidate)   Date ...2/.11/.10..........

STATEMENT 3

I hereby give consent for my thesis, if accepted, to be available for photocopying and for inter-library loan, and for the title and summary to be made available to outside organisations.

Signed .... (candidate)   Date ...2/.11/.10..........

Acknowledgments

Contributions to study

The studies described were all carried out by HT unless stated otherwise including cell culture studies, passaging, inhibitor studies, analysis of cell morphology, immunoblots studies, cell cycle studies, genotoxic drug response studies and single cell analyses. The hTert immortalisation was performed in collaboration with Dr. Terence Davis and used a pBABE-puro-hTert vector from laboratory stocks. Samples analysed on the FACS Vantage were acquired in collaboration with Marie Wiltshire; image analysis acquisition and time-lapse microscopy were supported by Dr. Rachel Errington and TRAP assays were performed in collaboration with Rebecca Capper.

Table of Contents

List of Figures

List of Tables

Summary

Abnormalities in the cellular senescence programme may contribute to premature ageing and cancer predisposition. Primary human cells have a limited proliferative capacity, entering a state of irreversible growth arrest/senescence arising from telomere attrition (replicative senescence). Stress-induced premature senescence (SIPS) can additionally limit cellular lifespan and there are several human genomic instability (GI) disorders - cancer-prone/premature ageing syndromes - in which SIPS may prematurely limit cellular lifespan. The hypothesis is that increased GI is a critical factor in limiting the lifespan of somatic cells by activating common pathways leading to SIPS. This study examines the extent to which GI cells present restraints on cellular proliferation with a focus on the degree to which they share similar properties – not least a common dependence on the p38 mitogen-activated protein kinase (MAPK) mediated stress response pathway. The study utilised a panel of normal (N) and a GI panel of fibroblasts comprising: Rothmund Thomson syndrome (RTS), Bloom syndrome (BS), Cockayne syndrome A (CSA), Hutchinson-Gilford Progeria syndrome (HGPS), Nijmegen Breakage syndrome (NBS), Werner syndrome (WS), Seckel syndrome (SS), Dyskeratosis Congenita (DKC) and Ligase 4 syndrome (LIG4). The study revealed a commonality of response to p38 inhibitors – increased clonogenicity and lifespan - for normal and GI syndrome cells, suggesting that all cells undergo some degree of p38-mediated proliferation restraint/SIPS. A degree of inter-strain heterogeneity for reduced replicative potential and/or altered morphology was apparent for both normal and GI syndrome primary fibroblasts. This study revealed truncated lifespans for LIG4, SS, HGPS, BS, RTS, DKC and NBS cells. GM18366(SS) and GM07166(NBS) cell strains show an altered morphology and increased p38 inhibitor responses suggesting elevated SIPS operation. Growth and DNA damage studies using a newly created bank of hTert-immortalised cell strains [AG16409(N), AG18371(RTS), GM02548(BS), GM07166(NBS), GM01856(CSA), AG11498(HGPS) and GM17523(LIG4)] showed that GI syndrome cells, alleviated from the stress of telomere attrition, remain susceptible to SIPS. Of these RTS cells were hTert-immortalised for the first time, showing that senescence in these strains is telomere-dependent. Cell cycle analysis revealed a common p38-associated mechanism that limits retention in cycle. The specific p38 inhibitor BIRB796 was found to increase clonogenic potential of both normal and GI syndrome cells. The findings suggest that both RTS and WS cells show a higher proportion of cells that are non-dividing. Furthermore, the study suggests that WS cells have an altered cell cycle transit time that is reduced by BIRB796 treatment. Overall, the study highlights successful single cell analysis approaches for testing the impact of p38 inhibitors by teasing out the nature of cellular heterogeneity arising from different sources for specific cell strains. These findings support and expand previous evidence that WS cells undergo higher levels of SIPS compared to normal cells and provide new evidence that RTS cells may also show an increased propensity for SIPS.

Abbreviations List

4NQO	4-Nitroquinoline 1-oxide
AD	Autosomal Dominant
ALT	Alternative telomere lengthening
APS	Ammonium persulphate
AT	Ataxia telangiectasia
ATM	Ataxia telangiectasia mutated
ATP	Adenine triphosphate
ATR	ATM-related
BER	Base excision repair
BR	BIRB796-responsive
BS	Bloom syndrome
BSA	Bovine Serum Albumin
Cdk	Cyclin dependent kinase
CdkI	Cyclin dependent kinase inhibitor
CIN	Chromosomal instability
CisPt	Cisplatin
CPT	Camptothecin
CSA	Cockayne syndrome A
DKC	Dyskeratosis congenita
DMSO	Dimethyl sulphoxide
DOX	Doxorubicin
DSB	Double strand break
Eb	Ethidium bromide
ECL	Enhanced chemiluminescence
ECM	Extracellular matrix
EDTA	Ethylenediaminetetraacetate
EGTA	Ethylene glycerolbis (2-aminoethyl)- N, N, N'-tetraacetic acid
EMEM	Eagle's minimum essential medium
ERK	Extracellular signal regulated kinase
ES	Embryonic stem
FCP	Full clonogenic potential
FCS	Foetal calf serum
FCS	Forward scatter
FHA	Forkhead-associated domain
FITC	Fluorescein isothiocyanate
G_1	Gap phase 1
G_2	Gap phase 2
GI	Genomic instability
H_2O_2	Hydrogen peroxide
HGPS	Hutchinson-Gilford progeria syndrome
HR	Homologous recombination
HRP	Horseradish peroxidase
HSP27	Heat shock protein 27
IL-1	Interleukin-1
IMT	Intermitotic time
IR	Ionising radiation
JNK/SAPK	c-jun N-terminal/Stress-activated protein kinase

LIG4	Ligase 4
M	Mitosis
MAP3K	Mitogen activated protein kinase kinase kinase
MAPK	Mitogen activated protein kinase
MCP	Minimal clonogenic potential
MIN	Minisatellite instability
MKK	Mitogen activated protein kinase kinase
MMC	Mitomycin C
MMP	Matrix metalloproteinase
MMR	Mismatch repair
NBS	Nijmegen breakage syndrome
NC	Non-clonogenic
NER	Nucleotide excision repair
NHEJ	Non-homologous end joining
OD	Optical density
P	Passage
PCR	Polymerase chain reaction
PD	Population doubling
PE	Plating efficiency
PMSF	phenylmethylsulfonyl fluoride
RDS	Radioresistant DNA synthesis
RNP	Replication protein A
ROS	Reactive oxygen species
RPA	Replication protein A
RTS	Rothmund Thomson syndrome
S-phase	Synthesis phase
SA β-gal	Senescence-associated β-galactosidase
SCE	Sister-chromatid exchange
SD	Standard deviation
SDS	Sodium dodecyl sulphate
SIPS	Stress-induced premature senescence
SS	Seckel syndrome
SSC	Side scatter
TC-NER	Transcription-coupled repair
TEMED	N, N, N', N'-tetramethylethylenediamine
TNF	Tumour necrosis factor
TOF	Time of flight
Topo	Topoisomerase
TRF1/2	Telomere repeat factor 1/2
UV	Ultraviolet
VEGF	Vascular endothelial growth factor
WCE	Whole cell extract
WS	Werner syndrome
XP	Xeroderma pigmentosum

Chapter 1   General Introduction

It is widely accepted that cell proliferation involves numerous processes that need to be tightly coordinated to ensure the preservation of genome integrity and to promote faithful genome propagation. Numerous studies have established that efficient and error-free DNA replication is key for faithful duplication of chromosomes before their segregation (Smith and Jones 2000). Central to this is the need to coordinate DNA replication, DNA-damage sensing and repair and cell cycle progression to ensure genome integrity is maintained during cell division and genomic instability (GI) is avoided. When coordination fails or fidelity is compromised, cells may accumulate genomic defects that initiate cancer and its progression (Anderson 2001; Kerzendorfer and O'Driscoll 2009; Negrini et al. 2010). Indeed, multisystem syndromes, for example Bloom syndrome (German et al. 2007) often show signs of abnormalities in replication control at the cellular level resulting in disruption of normal physiology and function or the acquisition of cancer predisposition (Coppede and Migliore 2010; Duker 2002). Some disorders also show *in vitro* indicators of significant limitation on replicative potential (Capell et al. 2009), for example Werner syndrome. The enforcement of a normal limitation on replicative potential of cells can be viewed as a process of 'cellular senescence' with implications for dynamic tissue management and the suppression of neoplasia (Campisi 2005). This has lead to a search for molecular mechanisms involved in the limitation of replicative potential. There has been a recent focus on the signalling pathways potentially operating in senescence with evidence that p38 pathway modulation may be critical in the commitment of cells to the senescence process (Davis et al. 2005; Deng et al. 2004; Haq et al. 2002; Iwasa et al. 2003; Wang et al. 2002). The p38 MAP kinases are a family of serine/threonine protein kinases. p38 MAP kinase (MAPK), also called RK or CSBP, is the mammalian orthologue of the yeast HOG kinase which participates in a signalling cascade controlling cellular responses to cytokines and stress. Such studies could reveal target proteins that may be available for manipulation in attempts to interfere with the senescence process. Recently, the availability of potent p38 inhibitors with

different modes of action (Goldstein et al. 2010) has opened the possibility of exploring senescence pathway interference in different genetic backgrounds.

The conceptual framework for this thesis is that there are significant overlaps between the processes driving senescence (Figure 1.1), the control of the cell cycle under stress and the acquisition of genomic instability. This thesis addresses aspects of these interdependencies. GI syndromes present an attractive group of relevant disorders with known, and in some cases well-characterised, molecular defects for such studies. The principal approach was to investigate the cell cycle and progression to senescence of dermal fibroblasts derived from normal and GI syndrome individuals under p38 inhibitor exposure. The studies have employed techniques for single cell evaluation, immortalisation, stress induction, and cell cycle monitoring of p38 inhibitor responses.
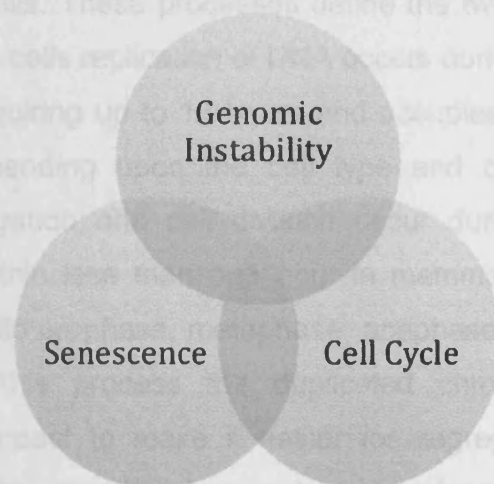
Figure 1.1. Thesis framework:
The interdependency of genomic instability, senescence and the cell cycle.

1.1 The cell cycle

In multicellular eukaryotic organisms, two fundamental types of cell division occur depending on the cell type and developmental stage involved. Mitosis is the process of cell division resulting in two identical nuclei and is performed by somatic cells during tissue development. During gametogenesis meiosis is a reductional division process, performed by diploid or haploid precursor cells undergoing cell

2

division and differentiation to form mature haploid gametes. The sequence of stages that a given cell undergoes while progressing to division is known as the cell cycle, the functional structure of which was described in 1953 (Howard and Pelc 1953), has been extensively reviewed [for example: (Schafer 1998; Sclafani and Holzen 2007; Vermeulen et al. 2003)].

The somatic cell cycle can be defined as the temporal sequence of structural and functional transitions that a cell undergoes during processes of cell growth, replication of genetic material, nuclear division, and cytoplasmic separation (Smith et al. 2006). Its most basic function is to duplicate accurately the vast amount of DNA in the chromosomes and then segregate the copies into two genetically identical daughter cells. These processes define the two major phases of the cell cycle. In mammalian cells replication of DNA occurs during the synthesis phase (S-phase), normally requiring up to 12 hours and occupies approximately half of the cell cycle time depending upon the cell type and origin. Following S-phase, chromosome segregation and cell division occur during mitosis (M), which is usually complete within less than one hour in mammalian cells. Mitosis can be further subdivided into prophase, metaphase, anaphase and telophase (Alberts et al. 2002). During this process the duplicated chromosomes become more condensed and compact to make it easier for segregation into the respective daughter cells. Subsequently, the nuclear envelope breaks down, and the chromosomes attach to the microtubules of the mitotic spindle. As mitosis proceeds, the cell pauses briefly in metaphase, when the chromosomes are aligned at the equator of the mitotic spindle, awaiting segregation. The sudden separation of sister chromatids marks the beginning of anaphase, during which the chromosomes move to opposite poles of the spindle, where they decondense and reform intact nuclei. The cell is then pinched in two by cytoplasmic division (cytokinesis) and cell division/daughter separation is complete. There are also two "gap" phases (G_1 prior to S-phase, and G_2 between S-phase and mitosis), which allow time for the cell to grow and double their mass of proteins and organelles required to replicate their DNA and divide. The balance between the cell cycle stages and the timing of S-phase is modified during early embryogenesis and as

homeostatic mechanisms control tissue formation. Thus, the eukaryotic somatic cell cycle is traditionally divided into four phases: G_1, S-phase, G_2 and M. G_1, S-phase and G_2 together are often referred to as interphase since they make up the interlude between mitoses (Figure 1.2). Although the duration of the cell cycle varies from organism to organism and within tissue lineages, it typically takes at least 24 hours for mammalian cell to complete a full cell cycle, for example as found for explanted human dermal fibroblasts *in vitro*.

The two gap phases serve as more than simple time delays to cell growth, they also provide time for the cell to monitor the internal and external environment to ensure that conditions are suitable and allow time for repair of DNA damage and replication errors, before the cell commits to DNA replication or cell division. G_1 is of particular importance in this respect (Massague 2004). Its length can vary greatly depending on external conditions and extracellular signals from other cells. If extracellular conditions are unfavourable, cells can delay progress through G_1 and may enter a resting state called G_0 prior to commitment to DNA replication. Cells can remain for extended periods of time in this state before resuming proliferation. Indeed, cells in G_0 account for the majority of non-growing, non-proliferating cells in the human body (Vermeulen et al. 2003). Conversely, if extracellular conditions are favourable and signals to grow and divide are present, cells in early G_1 or G_0 progress through a commitment point near the end of G_1 known as the restriction point. The restriction point is thought to be regulated largely by pRb (Zetterberg et al. 1995). After passing this point, cells are committed to DNA replication, even if the extracellular signals that stimulate cell growth and division are removed.

G₂/M checkpoint
- DNA damage
- cell size
- DNA replication

Spindle assembly checkpoint

Cell cycle arrest

Prophase · Metaphase · Anaphase · Telophase

M

G₂

G₁

S

G₀

Cell cycle exit and arrest

G₁/S checkpoint
- DNA damage
- cell size
- nutrients
- growth factors

Intra S checkpoint
- Replication fork stalling
- Intra-S-phase damage
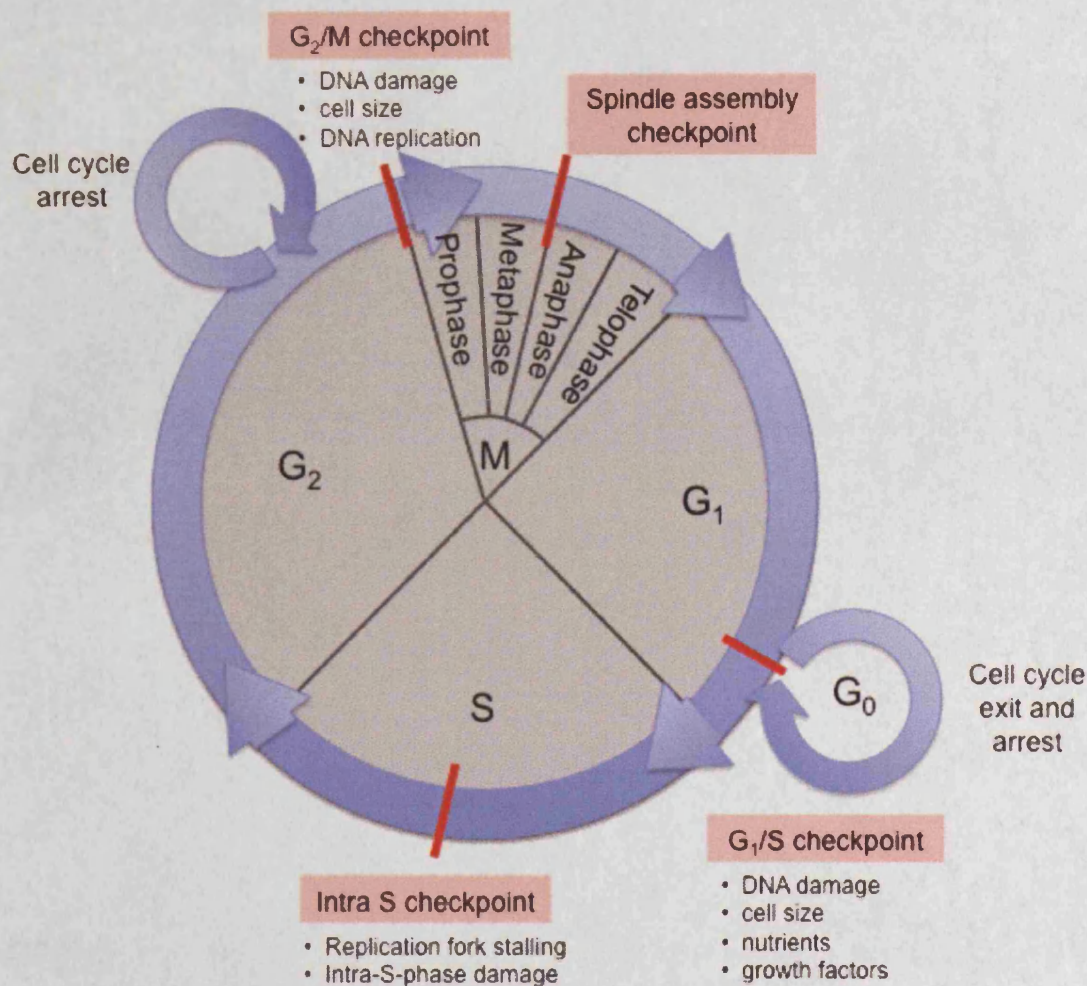
Figure 1.2. Schematic representation of the human cell cycle.

Actively dividing cells pass through a series of stages known collectively as the cell cycle: two gap phases (G_1 and G_2); a synthesis (S) phase, in which the genetic material is duplicated; and mitosis (M), in which the chromosomes are segregated and the cell divides. A series of DNA checkpoints act at different stages of the cell cycle to ensure the fidelity of cell division. DNA damage checkpoints are positioned before S-phase (G_1/S checkpoint), after DNA replication (G_2/M checkpoint) and during S-phase (Intra-S checkpoint). Defects in mitotic spindle assembly activate the spindle checkpoint and arrest cells in anaphase.

1.1.1 Cell cycle regulation

Regulation of the cell cycle involves processes crucial to the survival of a cell, including the detection and repair of genetic damage as well as the prevention of uncontrolled cell division. The transition from one cell cycle phase to another is a highly ordered process that is regulated by a number of different cellular proteins. Two key classes of regulatory molecules, cyclins and cyclin-dependent kinases

5

(Cdks), determine a cell's progress through the cell cycle (Morgan 2007). In 2001, Hartwell, Hunt and Nurse were awarded a Nobel Prize in Physiology and Medicine for their discovery of these central molecules (Hartwell et al. 2001). Many of the genes encoding cyclins and Cdks are conserved among all eukaryotes, but in general complex organisms have more elaborate cell cycle control systems that incorporate more individual components. In yeast, there is one major Cdk (designated Cdk1, equivalent to $p34^{Cdc28}$ in *Saccharomyces cerevisae* and $p34^{Cdc2}$ in *Schizosaccharomyces pombe*), the activity of which oscillates during cell cycle progression and is capable of regulating diverse cell cycle transitions by associating with different cell cycle stage-specific cyclins (Satyanarayana and Kaldis 2009). In contrast, approximately 20 Cdk-related proteins have been identified higher eukaryotes. In higher eukaryotic cells the problems of coordinating the growth and proliferation of multicellular states results in additional complexity in cell cycle events although the cell cycle 'engine' is still driven by Cdks and cyclins.

Cdks are a family of serine/threonine protein kinases that require binding to a cyclin subunit to become catalytically competent (Morgan 1995, 1997; Murray 2004). The role of Cdks in cell cycle regulation and in particular their role in cancer has been extensively studied [reviewed by (Malumbres and Barbacid 2005; Sanchez and Dynlacht 2005; Satyanarayana and Kaldis 2009)]. Different members of the Cdk family, in association with different cyclins, regulate progression through the cell cycle (Figure 1.3). The principal Cdks in most mammalian cells are Cdk1, Cdk2, Cdk4 and Cdk6, whereas other Cdks regulate transcription, differentiation, nutrient uptake and other functions (Massague 2004). Cyclin-Cdk complexes are regulated by post-translational modifications (phosphorylation/dephosphorylation) and protein interaction events that tightly control the timing and extent of Cdk activation. When activated, Cdks induce downstream processes by phosphorylating selected proteins (Morgan 1995; Pines 1995). Whereas Cdk protein levels remain stable during the cell cycle, the levels of cyclin proteins rise and fall and in this way periodically activate the necessary Cdks required for cell cycle progression (Evans et al. 1983; Pines 1991). Different cyclins are required at

different phases of the cell cycle; for instance, cyclins A and B function in the S-phase, G_2, and early mitosis, whereas D-type cyclins (Cyclin D1, D2 and D3) and cyclin E are expressed in G_1 (Figure 1.3).

The prototypic Cdk, Cdk1, associates with cyclins A and B, and acts at the G_2/M interface. Synthesis of cyclin A begins as cells approach the G_1 to S-phase transition, and the protein is immediately transported into the nucleus. Cyclin A binds to Cdk2 and is required for the cell to progress through S-phase (Pagano et al. 1992). In late G_2 and early M-phase, cyclin A complexes with Cdk1 to promote entry in to mitosis (Pagano et al. 1992). Mitosis is further regulated by cyclin B in complex with Cdk1 (Arellano and Moreno 1997; King et al. 1994). In cycling mammalian cells, cyclin B is first synthesised during S-phase and increases in concentration as cells proceed through G_2, peaking in early mitosis and dropping after anaphase. Thus, the progressive accumulation of cyclins A and B during the cell cycle and their abrupt degradation at the onset of anaphase, mediates entry and exit from mitosis, respectively. The G_1 cyclin, Cyclin D, forms an active complex with Cdk4 and Cdk6 and is required for cells to pass through the restriction point and enter G_1 (Sherr 1994; Sherr et al. 1994). Unlike the other cyclins, cyclin D is not expressed periodically, but is synthesised as long as growth factor stimulation persists (Assoian and Zhu 1997). Another G_1 cyclin is cyclin E which associates with Cdk2 to regulate progression from G_1 to S-phase (Ohtsubo et al. 1995). Cyclin A binds with Cdk2 and this complex is required during S-phase (Girard et al. 1991; Walker and Maller 1991). Thus, a cycling cell exits the cell cycle phases in association with the synthesis and degradation of specific cyclins. In general, before a cell can enter the next cell cycle phase, the appropriate cyclin of the previous phase is degraded, and the cyclin of the next phase is synthesised: Cyclins A and B contain a destruction box and cyclins D and E contain a PEST sequence [protein motifs rich in proline (P), glutamine (E), serine (S), and threonine (T) residues], which target them for ubiquitin-mediated degradation at specific times (Glotzer et al. 1991; Rechsteiner and Rogers 1996).
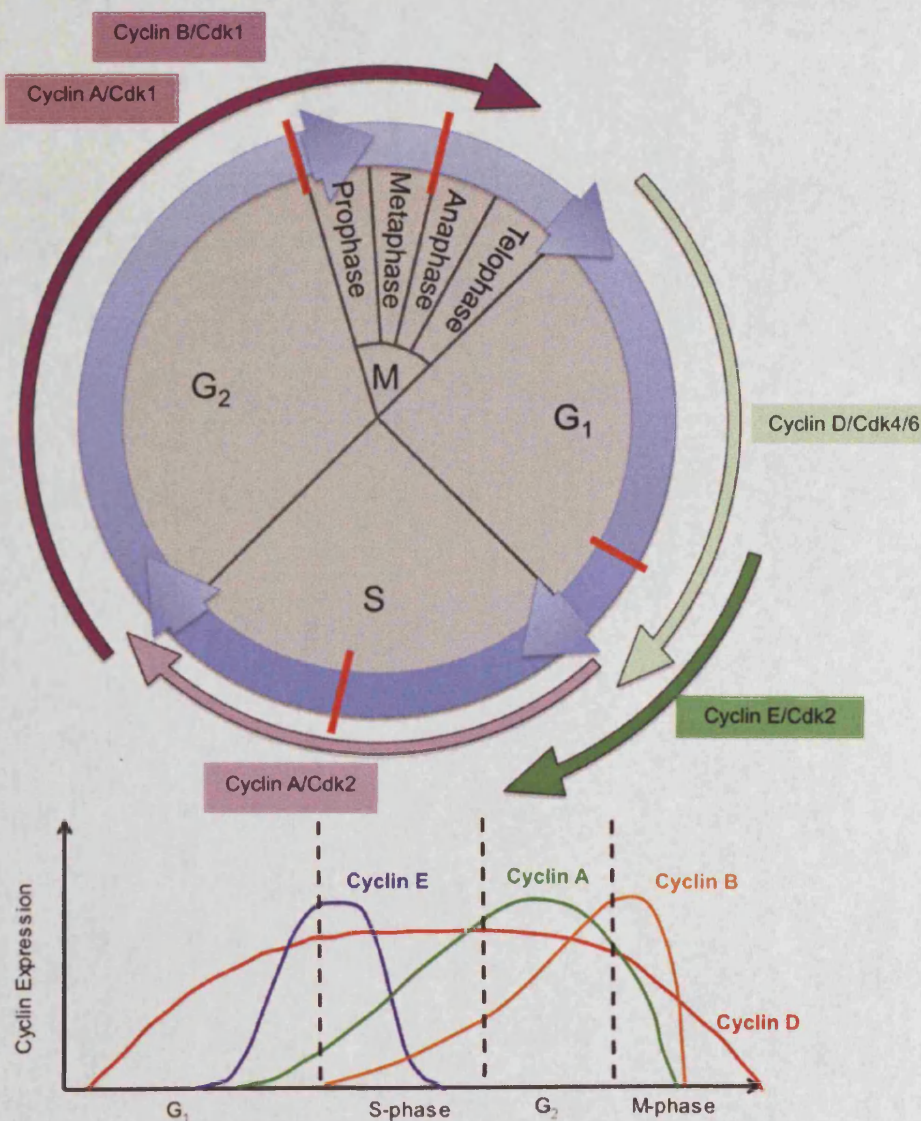
Figure 1.3. Schematic representation of the activity of mammalian Cdk-cyclin complexes and the oscillating expression levels of cyclins throughout the cell cycle.

Cyclin D refers to all three D-type cyclins.

The activities and functions of Cdk/cyclin complexes under normal, as well as extreme conditions, such as stress, DNA damage, telomere dysfunction and others, are regulated by Cdk inhibitors (CdkIs). Two distinct families of CdkIs have been discovered: the INK4 family (p15[INK4b], p16[INK4a], p18[INK4c], p19[INK4d]) specifically bind to Cdk4 and Cdk6 (Guan et al. 1994; Hirai et al. 1995) and prevent D-type cyclin activity, thus preventing the phosphorylation and activation of pRb (Carnero

and Hannon 1998); and the Cip/Kip family (p21$^{Waf1/Cip1}$, p27^{Kip1}, p57^{Kip2}) (Toyoshima and Hunter 1994; Xiong 1996) inhibit Cdk2/cyclinE, Cdk2/cyclin A, Cdk1/cylin A, as well as Cdk1/cyclin B activity (Harper et al. 1995; Resnitzky et al. 1995) thereby preventing the Cdk from phosphorylating pRb and inducing its dissociation from E2F (Chen et al. 1996; Hall et al. 1995).

Cdk activity is further regulated by post-translational modification (phosphorylation). Phosphorylation on conserved threonine and tyrosine residues is required for full activation of Cdks, for example, Cdk1 requires phosphorylation of Thr-161 (Thr-172 in Cdk4 and Thr-160 in Cdk2), by the Cdk7-cyclin H complex (CAK) (Drapkin et al. 1996; Jeffrey et al. 1995). Conversely, phosphorylation of Cdk1 at Tyr-15 and/or Thr-14, which are located within the active site of the kinase, prevents kinase activity (Borgne and Meijer 1996). This phosphorylation is performed by the wee1 and Myt1 kinases (Heald et al. 1993; McGowan and Russell 1993, 1995; Mueller et al. 1995). The wee1 kinase phosphorylates Cdk1 upon entry of the Cdk-cyclin complex into the nucleus, thereby protecting the nucleus from premature exposure to an active mitotic kinase (Heald et al. 1993). When the cell is ready to divide, Cdc25 dephosphorylates Cdk1 at Tyr-15 and Thr-14, thereby activating Cdk1 and allowing further progression through the cell cycle (Devault et al. 1991; Honda et al. 1993; Lew and Kornbluth 1996). Intracellular localisation of different Cdks and cyclins may also contribute to cell cycle regulation (Vermeulen et al. 2003). For example, in human cells, cyclin B first accumulates in the cytoplasm then enters the nucleus just before the nuclear envelope breaks down early in mitosis.

1.1.2 The Restriction Point and Checkpoints

Cell cycle checkpoints are control mechanisms that ensure the fidelity of cell division that have been extensively studied [reviewed by (Hartwell and Weinert 1989; Satyanarayana and Kaldis 2009; Warmerdam and Kanaar 2010)] (Figure 1.2). Growth factors primarily act on cells in G_0 and G_1. The point in G_1 after which cells no longer respond to withdrawal of growth factors has been termed the restriction point. Studies show that cells starved of serum before the restriction

9

point enter a G_0-like state, while cells starved after are unaffected and continue through mitosis (Pardee 1974). Additional 'checkpoints' exist further in the cell cycle that monitor the integrity of DNA and serve to coordinate DNA replication with repair, chromosome segregation and cell cycle progression, ensuring an orderly sequence of events in the cell cycle (Hartwell and Weinert 1989). As an example, the completion of cellular DNA replication is a checkpoint that must be passed before the biochemically unrelated event of chromosome separation in mitosis can begin (Hartwell and Weinert 1989). Cell cycle arrest is produced by a variety of factors that may be intrinsic or extrinsic and may affect several different checkpoints according to the pathway affected. Understanding the downstream consequences of unresolved events, supra-threshold levels of genomic damage or abnormal checkpoint maintenance appears to be critical in determining the dynamic responses of cellular systems undergoing commitment to senescence.

In response to DNA damage, checkpoints arrest the cell in order to provide time for DNA repair. DNA damage checkpoints are positioned before the cell enters S-phase (G_1/S checkpoint) or after DNA replication (G_2/M checkpoint). In addition, there appear to be DNA damage checkpoints during S-phase and mitosis, for example the spindle assembly checkpoint arrests cells in anaphase if the mitotic spindle is assembled improperly (Rudner and Murray 1996). Under normal conditions, DNA is most vulnerable to DNA breaks during S-phase. This is mainly due to the fact that during replication the replisome must overcome obstacles (such as DNA adducts, secondary structures or tightly bound proteins) that can cause replication fork stalling and can compromise genomic integrity if not properly processed. The S-phase checkpoint responds to replication fork stalling and intra-S-phase damage by preventing replication fork collapse and breakdown, and is therefore crucial for maintaining genome integrity (Segurado and Tercero 2009).

At the G_1/S checkpoint, cell cycle arrest induced by DNA damage is p53-dependent. This is supported by the observation that cells derived from p53-null transgenic mice do not arrest in G_1 in response to DNA damage such as ionising radiation (Little et al. 1995). Under normal conditions, the cellular level of p53 is low

but DNA damage can lead to rapid induction of p53 activity (el-Deiry et al. 1993; Perry et al. 1993). This stabilisation and activation of p53 is achieved by ATM-mediated phosphorylation (Sancar et al. 2004; Shiloh 2003). ATM (ataxia telangiectasia mutated) and ATR (ATM-related) protein kinases sense and respond to DNA damage by activating the transducer checkpoint kinases Chk2 and Chk1, respectively. ATM/ATR and Chk1/Chk2 phosphorylate p53 at serine 15 and serine 20, respectively (Jowsey et al. 2004). These events increase the stability and transcriptional activity of p53 causing upregulation of p53 target genes. These include p21, various pro-apoptotic factors (Puma, Bax, Noxa) (Clarke et al. 1994), DNA-repair and oxidative stress response genes, and the negative feedback regulator Hdm2 (Agarwal et al. 1998). The induction of p21 results in Cdk inhibition and cell cycle arrest, preventing the replication of damaged DNA (Ko and Prives 1996). The p53 protein also has an autoregulatory feedback loop in which p53 stimulates the transcription of Hdm2, which in turn contributes to the proteolytic degradation of p53 by facilitating its ubiquitination (Oren 1999). When DNA damage occurs during G_2, cells are able to initiate cell cycle arrest in the presence or absence of p53. The entry into mitosis is prevented by maintaining Cdk1 in its inhibited form through inhibitory phosphorylation (Devault et al. 1991; Honda et al. 1993; Lew and Kornbluth 1996), as discussed previously, or by sequestration of components of the Cdk1-cyclin B complex out of the nucleus (Vermeulen et al. 2003).

Regulation of the cell cycle is therefore a complex process involving the coordination of a number of pathways and is crucial to the survival of a cell. Failure of cell cycle checkpoints and repair processes can lead to uncontrolled proliferation and the accrual of genomic defects leading to GI and chromosomal instability (CIN) that can contribute to carcinogenesis (Negrini et al. 2010). Therefore, in order to preserve genomic integrity and prevent carcinogenesis, damaged cells rely on two different mechanisms to halt their progression: they can either enter into a permanent cell cycle arrest (cellular senescence) or trigger programmed cell death (apoptosis). Although it is not clear what determines whether a cell undergoes

senescence or apoptosis it is thought to depend largely on the nature and duration of the stress, as well as the cell type (Rebbaa et al. 2003; Seluanov et al. 2001).

1.2 Genomic Instability (GI)

Genomic instability refers to a range of genetic alterations from point mutations to chromosomal rearrangements and can be divided into classes according to the type of event stimulated (Aguilera and Gomez-Gonzalez 2008). Chromosomal instability (CIN) is defined as a persistently high rate of loss and gain of whole chromosomes (Draviam et al. 2004) and is caused by mis-segregation of chromosomes during mitosis (Thompson et al. 2010).The consequence of CIN is aneuploidy, which is widely known to be a hallmark of tumour cells (Lengauer et al. 1997). Micro- and minisatellite instability (MIN) leads to repetitive DNA expansions and contractions and can occur by replication slippage, by mismatch repair (MMR) impairment or by homologous recombination (HR) (Aguilera and Gomez-Gonzalez 2008). Instability leading to mutations, including base substitutions, micro-insertions, and micro-deletions, is mainly associated with replication errors, impairment of base excision repair (BER) and MMR, or error-prone translesion synthesis (Friedberg et al. 2006). Instability, leading to rearrangements refers to events that involve changes in the genetic linkage of two DNA fragments. Increases in HR-mediated events, such as unequal sister-chromatid exchange (SCE) and ectopic HR between non-allelic repeated DNA, or in end-joining between non-homologous DNA fragments can result in gross chromosomal rearrangements such as translocation, duplications, inversions or deletions. The downstream consequences of GI have been described previously (Aguilera and Gomez-Gonzalez 2008; Anderson 2001; Negrini et al. 2010) but can include a drive towards aneuploidy, a mutator phenotype, loss of integrity of proliferation control pathways (e.g. checkpoints), insufficiencies of biological responses or biochemical problems due to segregation of material and abnormalities in progression to senescence or programmed cell death. These differ depending on the cell type and the extent to which cell types normally have lifespan control.

1.2.1 DNA Damage and Repair

Genomic instability can arise either from increased rates of damage that overwhelm the ability of normal repair systems to restore genomic integrity, or defective repair systems being unable to cope with normal rates of damage being generated through normal cellular and environmental mechanisms, or a combination of the two. Increased rates of damage may arise from either exogenous or endogenous sources. DNA is subject to continuous modification from exogenous factors such as radiation damage, industrial genotoxins, food agents and chemical agents (such as chemotherapy drugs) (Lindahl 1993). While these are highly relevant to therapy-induced secondary cancers, exogenous damage cannot directly underlie the ongoing heritable GI seen within cultured tumour cells. Endogenous factors that actively increase genomic damage can include by-products of metabolism, including reactive oxygen species (ROS) (such as superoxide anions, hydrogen peroxide and hydroxyl radicals) (De Bont and van Larebeke 2004) and telomere deficiencies that can generate breakage-fusion-bridge events (Davoli et al. 2010; McEachern et al. 2000; Russo et al. 1995).

DNA repair is essential to preserve the fidelity of genomic information, removing damage generated by naturally occurring environmental insults as well as inevitable replication errors that may occur. Inefficient or defective repair that is unable to cope with normally occurring damage is well documented as a means of generating GI (Kerzendorfer and O'Driscoll 2009; Lindahl and Wood 1999; Zha et al. 2007). This can arise from deficiencies in the repair proteins themselves, or from checkpoint defects that fail to halt the cell cycle until repair can be completed. In recent years, the characterisation of many proteins involved in sensing and responding to DNA damage has enhanced our understanding of DNA damage responses extensively (Wood et al. 2001). Mutations in the genes that encode DNA damage response proteins are associated with a number of GI syndromes (Coppede and Migliore 2010; Hoeijmakers 2009; Musich and Zou 2009). Interestingly, these disorders often result in a predisposition to cancer and/or premature ageing (Duker 2002) and highlight the clinical significance of pathways

that sense, relay, or transduce signals associated with DNA damage (Capell et al. 2009). Ataxia telangiectasia (AT), for example, provides an example of how defects in DNA damage sensing can contribute to genomic instability and malignancy (Peltomaki 2001). Briefly, AT is caused by mutations in ATM, a protein kinase involved in cell cycle checkpoint and genotoxic stress responses (Abraham 2001; Shiloh 2003) particularly those responses elicited by exposure to ionising radiation (IR) or 'radiomimetic' agents (e.g. neocarzinostatin and bleomycin). At a clinical level, AT presents a complex multisystem disorder characterised by immunodeficiency, neurodegeneration, premature ageing, striking sensitivity to ionizing radiation delivered at therapeutic doses, and susceptibility to cancer, in particular lymphoma and leukaemia (Boder and Sedgwick 1958). Xeroderma pigmentosum (XP) is another human disorder that is associated with defects in DNA repair genes associated with nucleotide excision repair (NER) genes. The impact of the defect(s) is a deficiency in the repair of cyclobutane pyrimidine dimers and 6-4 photo products, major DNA photoproducts resulting from ultraviolet (UV) light exposure (Friedberg et al. 2006). Individuals with XP are extremely sensitive to UV and display an increased incidence of skin cancer, such as basal cell carcinoma (Friedberg 2001; Peltomaki 2001). In an attempt to reveal the environmental relevance of inducers of carcinogenesis and to reveal the molecular pathways involved in responding to these types of damage syndromes, such as AT and XP have become paradigms for studying the cellular responses to IR and UV, respectively. The question therefore remains as to whether the wider role of GI at the cellular level can be studied in other syndromes that show hallmarks at a chromosomal and genome level of putative abnormalities in stress response pathways. In the following section a prospective panel of GI syndromes is described and their relevance to the aims of this thesis.

1.3 Genomic Instability Syndromes

1.3.1 Werner Syndrome (WS)

Werner syndrome (WS) was first characterised by Dr Otto Werner (Werner 1904) and is a rare autosomal recessive disorder affecting approximately ten per

million individuals (Thannhauser 1945). The first sign of this disorder is often the lack of the pubertal growth spurt and WS individuals are typically short in height (Kipling et al. 2004; Martin et al. 1999). WS is characterised by juvenile bilateral cataracts, skin atrophy and sclerosis, premature hair-greying and thymic atrophy. The premature ageing phenotypes associated with WS usually manifest themselves in the twenties or thirties with the median age of diagnosis being the early thirties. WS individuals show increased predisposition to age-related diseases such as type II diabetes mellitus, osteoporosis and atherosclerosis. An elevated incidence of cancer is observed in WS, although this is generally limited to rare non-epithelial cancers, especially mesenchymal cancers such as sarcomas (Epstein et al. 1966; Goto et al. 1996). Several of the clinical features are much more severe that seen in normal ageing, including calcification of the cardiac valves and atrophy of the testicles and skin appendages. WS individuals do not seem to have any obvious immune system dysfunction despite the thymic atrophy, and they lack notable pathology of the central nervous system (Postiglione et al. 1996), although there are some reports of premature senile dementia (Hofer et al. 2005). Death generally occurs in the fourth or fifth decade of life, primarily from cancer or cardiovascular disease.

1.3.1.1 Properties of the WRN protein

WS is caused by mutations in the *WRN* gene that encodes a 1432 amino acid protein with several functional domains, including a helicase domain with significant homology to the RecQ helicases, and a 3' to 5' exonuclease activity (Hickson 2003; Moser et al. 1997; Yu et al. 1996). The vast majority of known mutations in the *WRN* gene result in the creation of premature stop codons that would produce truncated proteins and lead to complete absence of WRN (Moser et al. 1999).

The WRN protein has numerous interacting partners, including replication protein A (RPA), p53, proliferating cell nuclear antigen, topoisomerase I, DNA polymerases β and δ, the Ku complex, the MRN complex, the telomeric proteins TRF1 and TRF2, and telomeric DNA in human cells (Blander et al. 1999;

Constantinou et al. 2000; Johnson et al. 2001; Kamath-Loeb et al. 2000; Li and Comai 2000; Opresko et al. 2004; Opresko et al. 2002; Shen and Loeb 2001). A number of studies have indicated that WRN can unwind and/or hydrolyse a number of distinctive DNA structures, such as duplex DNA, branched DNA structures, displacement loops (D-loops), and four-way DNA junctions (Brosh et al. 2002; Fry and Loeb 1999; Kamath-Loeb et al. 2001; Mohaghegh et al. 2001; Opresko et al. 2002; Orren et al. 2002), although recent data suggest that WRN is not necessary for D-loop processing, at least *in vitro* (Verdun and Karlseder 2006). Of particular interest is the ability of WRN to efficiently resolve G-quadruplexes that are thermodynamically stable intramolecular structures containing four hydrogen-bonded guanine residues on G-rich telomeric sequences (Chang et al. 2004; Mohaghegh et al. 2001). Many of these structures may form during processes of DNA metabolism, suggesting that WRN plays a role in DNA replication, recombination and repair processes. In normal human cells WRN is localised to the nucleolus (Marciniak et al. 1998); however, in cells with DNA damage or undergoing ALT (alternative telomere lengthening), a significant fraction of WRN re-localises to the sites of damage or to telomeres (Johnson et al. 2001; Opresko et al. 2004; Opresko et al. 2002). More recent data suggests that the localisation of WRN changes throughout the cell cycle, for example WRN was shown to localise to sites of DNA replication (Rodriguez-Lopez et al. 2003). The observed interactions between WRN and telomere binding proteins (Opresko et al. 2002), and its ability to metabolise many telomeric substrates, suggests that WRN plays a central role in telomere biology. Mounting evidence suggests that WRN may also play a critical role in the rescue of replication fork stalls (Franchitto et al. 2008; Pichierri and Franchitto 2004; Sidorova et al. 2008).

1.3.1.2 Cellular phenotype

Primary WS cells display genomic instability, manifested by an elevated rate of chromosomal translocation and genomic deletions (Fukuchi et al. 1989), and are hypersensitive to a subset of DNA damaging agents, including 4NQO, camptothecin and cisplatin (Comai and Li 2004; Pichierri et al. 2000; Poot et al. 2002; Poot et al. 2001), suggesting that the WRN protein plays a key role in the

cellular response to specific types of DNA damage. WS is also associated with an increased level of pro-oxidant stress (Pagano et al. 2005), which has been connected to increased genomic instability and premature cellular senescence (Passos et al. 2010). Furthermore it has been linked to ageing, diabetes, cancer, atherosclerosis and osteoporosis, all of which are features of WS (Pagano et al. 2005). In addition, cultured fibroblasts from WS individuals have an aged appearance (Davis et al. 2005; Davis et al. 2006) and undergo premature replicative senescence, with 90% of WS cultures tested having a lifespan of less than 20 population doublings (PDs) (Salk et al. 1981; Tollefsbol and Cohen 1984). This compares to a lifespan for normal adult dermal fibroblasts that ranges from 20 to 85 PDs (Cristofalo et al. 1998a). Similarly, WS fibroblasts manifest a poor rate of growth compared to normal cells (Davis et al. 2005; Salk et al. 1981), partially due to a delayed passage through the S-phase of the cell cycle (Fujiwara et al. 1977; Rodriguez-Lopez et al. 2002). Moreover, WS fibroblasts, even at low population doublings, have an enlarged cellular morphology with extensive F-actin stress fibres and resemble senescent normal fibroblasts (Davis et al. 2005; Davis et al. 2006). Overall, WS fibroblasts resemble normal cells that have undergone stress-induced premature senescence (SIPS) (Brack et al. 2000). Evidence in the literature suggests that activation of the p38 signalling pathway is involved in commitment to SIPS (Huot et al. 1997; Wang et al. 2002). In addition, WS cells have been shown to have high levels of activated p38 (Davis et al. 2005) (See Appendix A). This together with the genome instability, increased pro-oxidant state, and the frequent replication fork stalling seen in WS cells, provides a plausible trigger for intracellular stress in WS cells.

1.3.2 Bloom Syndrome (BS)

A second syndrome associated with mutations in a member of the RecQ family, in this case the BLM protein, is Bloom syndrome (BS). BS is an extremely rare autosomal recessive disorder that is characterised by proportional dwarfism with a disproportionately small head, sun-sensitive facial skin erythema, learning disabilities, and occasional mental deficiency. Major clinical features are immune

deficiency and cancer (German 1969; German and Ellis 1998). BS is unique among cancer predisposition syndromes in that the frequencies of most types of cancer are elevated, including leukaemias, lymphomas and the common solid epithelial cancers, although lung and prostate cancers are rare (Hickson et al. 2001). However, although classified as a progeroid syndrome, there is little evidence of a premature ageing defect apart from a high incidence of type II diabetes in young individuals, and the elevated cancer incidence.

1.3.2.1 Properties of the BLM protein

The gene mutated in BS encodes a 1417 amino acid DNA helicase member of the RecQ family (BLM). Most mutations lead to truncation of BLM, and BS individuals usually lack detectable BLM protein, although some mis-sense mutations have been found (German et al. 2007). The BLM protein has numerous interacting partners including, BRCA1, PML, p53, RAD51, TopIIIα, MLH1, RPA, WRN, TRF2, and telomeric DNA in human cells (Bachrati and Hickson 2003). A number of studies have indicated that BLM is a structure-specific helicase that can unwind a large array of substrates, such as synthetic Holliday junctions, D-loops, and G-quadruplexes (Mohaghegh et al. 2001), although recent data suggest that BLM is not necessary for D-loop processing, at least *in vitro* (Verdun and Karlseder 2006). Many of these structures may form during processes of DNA metabolism, suggesting that that BLM plays a role in DNA replication, recombination and repair processes. The BLM protein localises with TRF2 and telomeric foci in telomerase negative cells undergoing ALT and promotes telomeric DNA synthesis, but not in telomerase positive cells or primary cell strains (Stavropoulos et al. 2002). As no telomeric association of BLM is seen in normal cells, it is perhaps not surprising that no telomere defects have yet been reported in BS.

1.3.2.2 Cellular phenotype

Cells from BS have a markedly increased level of genomic instability that is characterised by the formation of spontaneous genetic exchanges, which are apparently error prone, with gaps, breaks, and structurally rearranged chromosomes occurring at an elevated frequency (German 1969; Poppe et al.

2001; Wang et al. 2000a). However, the hallmark of BS cells, which is used in human diagnosis, is the ten-fold increase in SCEs, with isolated ES cells, lymphoblasts, and fibroblasts all showing this phenotype (Chaganti et al. 1974; German et al. 1977). The SCEs are thought to represent HR events occurring between sister chromosomes during S-phase or G_2 phase of the cell cycle, as HR is elevated in BS cells (Sonoda et al. 1999; Wu et al. 2001). Surprisingly, BS cells are only moderately deficient in the known DNA repair pathways, although non-homologous end-joining (NHEJ) processes are abnormal with an increased frequency of inaccurate rejoining of DSBs found in BS cells (Bachrati and Hickson 2003; Friedberg et al. 1979).

1.3.3 Rothmund-Thomson Syndrome (RTS)

RTS is a rare autosomal recessive genetic disorder, first described in 1866 (Rothmund 1868; Thomson 1936). The most characteristic feature of RTS is cutaneous poikiloderma (dry and colour-flecked flesh), which usually appears in infancy, with red oedematous plaques and blistering occurring on the cheeks, forehead and ears, and is most severe in sun-exposed areas. Other features include short stature, hair greying, alopecia, sparse eyebrows and eyelashes, and juvenile cataracts, all of which are associated with normal ageing; thus, RTS is classified as a premature ageing syndrome. Two clinical subforms of RTS have been defined: RTS type I characterised by poikiloderma, ectodermal dysplasia and juvenile cataracts, and RTS type II characterised by poikiloderma, congenital bone defects and an increased risk of osteosarcoma in childhood and skin cancer in later life. Despite its long history only 300 individuals with RTS have been described in the literature, and relatively little is known about it. Moreover, whether RTS I and II represent distinct syndromes with overlapping clinical signs or intersecting nosological entities involving genes acting on the same pathway, remains to be assessed.

1.3.3.1 Properties of the RECQL4 protein

Approximately two-thirds of individuals with RTS have mutations in the RECQL4 gene that are predicted to result in a truncated protein due to premature

19

termination of protein synthesis (Lindor et al. 2000; Wang et al. 2003). The *RECQL4* gene is located on chromosome 8q24.3 and encodes a 1208 amino acid protein with a central helicase domain that is characteristic of RecQ helicases (Kitao et al. 1998). However, RECQL4 does not share homology to two other conserved RecQ motifs; RQC and helicase and RNaseD C-terminal (HRDC) (Burks et al. 2007; Singh et al. 2010), which are present in human BLM and WRN helicases. Recently, RECQL4 was shown to possess two N-terminal nuclear localisation signal sequences (Burks et al. 2007). In addition, RECQL4 has an intrinsic ATPase activity and single-stranded DNA annealing activity and has been shown to interact with the ubiquitin ligases UBR1/2 (Macris et al. 2006; Yin et al. 2004). Since RECQL4 expression is cell cycle regulated, the association with UB1 and 2 in the cytoplasm may be linked to the process of RECQL4 degradation at specific times during the cell cycle. More recently, RECQL4 has also been shown to have helicase activity *in vitro* (Capp et al. 2009; Suzuki et al. 2009; Xu and Liu 2009).

Although the precise role of RECQL4 is largely unknown, recent evidence suggests its involvement in multiple DNA metabolic pathways. The RECQL4 protein is significantly expressed in the S-phase of the cell cycle, suggesting a role in DNA replication (Sengupta et al. 2005). Indeed, RECQL4 N-terminal region plays a role in recruiting DNA polymerase α to nascent DNA replication forks in Xenopus egg extract (Matsuno et al. 2006; Sangrithi et al. 2005). The possible involvement of RECQL4 in the repair of DNA DSBs has been demonstrated by the localisation of RECQL4 nuclear foci with the foci formed by RAD51, a crucial protein which functions in homologous recombination of DNA DSBs (Petkovic et al. 2005), as well as by the sensitivity of RTS fibroblasts from RTS patients to ionising radiation (Vennos et al. 1992), and by the participation of RECQL4 in DSB repair in Xenopus egg extracts (Kumata et al. 2007). In addition, RECQL4 interacts with poly (ADP-ribose) polymerase-1 (PARP-1), which is implicated in DNA recombination, DNA repair (Wang et al. 2006), transcriptional regulation and BER (Malanga and Althaus 2005). Similarly, RECQL4 colocalises with XPA in human cells treated with UV, suggesting that RECQL4 might facilitate NER-mediated

repair of UV-induced damage (Fan and Luo 2008). It has also been reported that RECQL4 plays a role in oxidative stress and its amount increases in the nucleolus after treatment of cells with agents that induce ROS (Woo et al. 2006).

1.3.3.2 Cellular phenotype

At a cellular level, defects in RECQL4 manifest themselves as CIN that is mainly represented by mosaic aneuploidies and isochromosomes (Larizza et al. 2006). For example, multiple evidence for *in vivo* mosaicism of trisomy 8 and/or 7 and /or 2 has been found (Der Kaloustian et al. 1990; Lindor et al. 1996; Miozzo et al. 1998; Ying et al. 1990). As compared to chromosomal instability features of other RecQ helicase defects, RTS has apparently no overlap with BS. No increase in SCE, which is characteristic of BS, has been recorded in RTS cells (Mann et al. 2005). Although RTS resembles WS with regards to a few clinical features, the spectrum of chromosomal rearrangements appears to be more restricted in RTS than in WS (Ouyang et al. 2008). It is conceivable that accumulation of CIN can drive neoplastic transformation in RTS cells and may explain the predisposition of RTS individuals to developing osteosarcoma. Inconsistencies have been found in the *in vitro* response of RTS cells to different genotoxic agents and this aspect will be reviewed in a later chapter.

1.3.4 Cockayne Syndrome A (CSA)

CS is a rare autosomal genetic disorder characterised by failure to grow, abnormal sun sensitivity and premature ageing. Hearing loss, cataracts, and severe tooth decay are other common features (Nance and Berry 1992). Individuals with CS are often normal at birth but experience failure of brain growth which progresses during the first year of life (Kraemer et al. 2007). They have a characteristic facial appearance, with large ears and nose, sunken eyes and thinning hair, and are thin due to progressive loss of subcutaneous fat (Nance and Berry 1992). However, they do not have the pigmentary changes and increased frequency of skin cancers seen in XP (Rapin et al. 2000). The vast majority of CS individuals have defects in either the *CKN1 (CSA)* or *CSB* gene (Licht et al. 2003). Here only the CSA subtype is discussed.

1.3.4.1 Cellular phenotype

At a cellular level, cultured CSA fibroblasts cells show increased sensitivity to UV irradiation, and display dramatic delay in the recovery of RNA synthesis after DNA damage, and impaired repair of actively transcribed genes or transcription-coupled nucleotide excision repair (TC-NER), (Anindya et al. 2010; Mayne and Lehmann 1982; van Hoffen et al. 1993; Venema et al. 1990).

1.3.4.2 Properties of the CSA protein

The 44 kDa CSA protein is encoded by the *CKN1* gene located on chromosome 5 and contains multiple WD-repeats (tryptophan-aspartate repeats) (Henning et al. 1995). Approximately 70% of the mutations reported in CSA are mis-sense, nonsense, or splice site mutations in the *CKN1* gene, whereas the other 30% are large, partial deletions of *CKN1* (Cao et al. 2004; Ren et al. 2003; Ridley et al. 2005). The CSA protein is a component of a ubiquitin ligase complex (Anindya et al. 2010; Groisman et al. 2003), that plays a role in TC-NER (de Waard et al. 2004), a DNA repair process that preferentially removes UV-induced pyrimidine dimers and other transcription-blocking lesions from actively transcribed genes; however, the exact role of CSA in TC-NER remains unclear. The deficiency of TC-NER is sufficient to explain the cutaneous photosensitivity observed in CSA individuals; however, it does not explain the growth failure and neurodegeneration that typify CSA, therefore it is likely that CSA has other functions that are yet to be elucidated.

1.3.5 Nijmegen-Breakage Syndrome (NBS)

Nijmegen breakage syndrome (NBS) was first described in two Dutch brothers with microcephaly, mental retardation, and immunodeficiency, and is a rare autosomal recessive condition (Hustinx et al. 1979; Ochs et al. 1997). The hallmarks of NBS are growth retardation, microcephaly, mental retardation, and immunodeficiency, accompanied by recurrent infections and a predisposition to lymphoid malignancy, in particular B and T cell lymphomas (van der Burgt et al. 1996). Interestingly, despite severe immunodeficiency, life expectancy is reduced most commonly due to malignancy, and the frequently occurring infections rarely

lead to complications and are only occasionally fatal. NBS individuals also have progeroid-like features, such as sparse hair and distinctive 'bird-like' facial appearance, characterised by a receding forehead, a prominent mid-face with a long nose and a receding mandible, all of which become more pronounced with age (Seemanova et al. 1985). Other common symptoms include skin abnormalities, particularly café-au-lait spots, sun-sensitivity of the eyelids, and congenital malformations, particularly clinodactyly and syndactyly (Hiel et al. 2000).

1.3.5.1 Properties of the NBS1 protein

NBS is caused by mutations in the NBS1 gene located on chromosome 8 that encodes the protein nibrin (Carney et al. 1998; Matsuura et al. 2004; Varon et al. 1998). The N-terminal part of nibrin has two domains; an FHA (forkhead-associated domain) and an adjacent BRCT (BRCA1 carboxy-terminal) domain, that are shared by many proteins involved in DNA replication, cell-cycle regulation or responses to DNA damage (Featherstone and Jackson 1998; Varon et al. 1998). It is generally accepted that nibrin plays a role in DSB repair (Zhang et al. 2006), although its exact roles in this process, and the effect of lack of nibrin in the aetiology of NBS, are not fully understood. Briefly, nibrin, together with RAD50 and Mre11, make up the MRN complex that co-localises with γH2AX at sites of DSBs, or at sites of V(D)J rearrangement processes (Kobayashi et al. 2002; Nelms et al. 1998). Nibrin is required for both nuclear localisation of Mre11/RAD50, and foci formation at sites of DNA damage, particularly DSBs (Carney et al. 1998; Desai-Mehta et al. 2001). In addition, nibrin physically interacts with ATM, which recruits it to sites of DNA damage and facilitates its activation (Digweed et al. 1999; Maser et al. 1997; Matsuura et al. 2004; Petrini 1999). Although the interaction between ATM and MRN is complex, studies clearly show that both ATM and nibrin are required for proper cell cycle regulation and DNA repair in response to DSBs (Petrini 2000). Therefore NBS illustrates how defects in proteins involved in DSB-repair can contribute to genomic instability and the development of cancer (Antoccia et al. 2006; Varon et al. 1998). A more recent report also provides evidence for a role of NBS1 in DNA maintenance by the BER pathway, with NBS

cells showing impaired processing of damaged bases by BER following genotoxic treatment with H_2O_2 (Sagan et al. 2009).

To date, seven mutations in *NBS1* have been found in NBS individuals (Maraschio et al. 2001; Resnick et al. 2002; Varon et al. 1998). The founder mutation, also known as the Slavic mutation, is a 5 bp deletion (657del5) in exon 6 of the *NBS1* gene resulting in a premature stop codon. The other *NBS* mutations also lead to premature protein truncation downstream of the FHA/BRCT domains. In *Nbs1*[657del5/657del5] cells no wild-type nibrin is seen, however, abbreviated polypeptides of both N-terminal (~ 26 kDa) and C-terminal (~ 70 kDa) nibrin are expressed at low levels, and appear to be sufficient to allow cell survival (Maser et al. 2001). The C-terminal protein (nibrin[p70]) is produced by internal translation and has the ability to interact with Mre11, which could be crucial for embryogenesis and cell growth. This may explain why embryonic-viable *NBS1* mutations are all in the limited region from exon 6 to exon 10, and suggests that a null mutation would be embryonic lethal. Thus NBS individuals are effectively hypomorphic for nibrin expression.

1.3.5.2 Cellular phenotype

At a cellular level, cultured lymphocytes and fibroblasts from NBS individuals show a marked hypersensitivity to the cytotoxicity and clastogenic effects of IR and radiomimetic drugs compared with normal cells (Tauchi et al. 2002; Yamazaki et al. 1998). Following γ-irradiation, NBS cells exhibit abnormal cell-cycle regulation, including radioresistant DNA synthesis (RDS) in which cells have an inability to halt or slow S-phase progression (D'Amours and Jackson 2002; Hiel et al. 2000; Shiloh 1997), and delayed induction of p53 at the G_1/S phase checkpoint; however, NBS cells apparently only exhibit mild defects in the DNA-damage dependent G_2 checkpoint following IR (Buscemi et al. 2001; Shiloh 1997). Primary NBS lymphocytes and fibroblasts typically show slow growth in culture and undergo premature replicative senescence (Ranganathan et al. 2001). This may reflect the *in vivo* situation, where lymphocytes are defective in T cell dependent antibody responses and show reduced responses to mitogenic signals, such as

phytohaemagglutinin, leading to failure of clonal T cell expansion resulting from infection (Digweed et al. 1999; Hiel et al. 2000). In addition, NBS Lymphocytes are predisposed to chromosomal translocations that interrupt the immunoglobulin heavy (IgH) chain loci and the T cell receptor loci $TCR\beta$ and $TCR\gamma$ (Shiloh 1997; van der Burgt et al. 1996), a phenotype not seen in NBS fibroblasts. Many of these aberrations occur at sites that undergo V(D)J recombination, however V(D)J recombination is apparently not deficient in NBS individuals (Harfst et al. 2000). The failure of T cell clonal expansion, and the premature senescence of fibroblasts, may well underlie some of the phenotypic characteristics of NBS, such as immunodeficiency and skin abnormalities.

1.3.6 Hutchinson-Gilford Progeria Syndrome (HGPS)

Hutchinson-Gilford progeria syndrome (HGPS) is a rare disorder associated with a characteristic aged appearance very early in life, and was originally described more than 100 years ago (Gilford 1904; Hutchinson 1886). The reported incidence is one in eight million and since 1886 just over 100 cases have been reported (Pollex and Hegele 2004). Children born with HGPS typically appear normal at birth but within a year they begin to display the effects of ageing, and as such HGPS is termed a childhood progeria that is distinct from the adult progeroid syndromes such as WS. The initial symptoms of HGPS include severe growth retardation and individuals are short in stature and below average weight. In addition, HGPS individuals have micrognathia, craniofacial disproportion, alopecia, arteriosclerosis, prominent eyes and scalp veins, and dystrophic nails. A lack of subcutaneous fat makes the skin appear wrinkled and aged. Moreover, HGPS individuals show skeletal abnormalities that may reflect deficient osteogenesis, principally in the extremities, and severe osteolysis (Fernandez-Palazzi et al. 1992). In short, children with HGPS appear several decades older than they actually are, showing signs of respiratory, cardiovascular and arthritic conditions similar to those seen in senior citizens. The average age of death is 13, with at least 90% of HGPS individuals dying from atherosclerosis (Baker et al. 1981; Brown 1992).

1.3.6.1 Cellular phenotype of HGPS

At the cellular level, HGPS is associated with significant changes in the interphase nucleus, including blebbing of the nuclear envelope, thickening of the nuclear lamina, loss of peripheral heterochromatin, and clustering of nuclear pores (Goldman et al. 2004). Additional analyses describe HGPS lymphocytes as having *'strikingly altered nuclear sizes and shapes with envelope interruptions accompanied by chromatin extrusion'* and expressing only 25% of the lamin A levels seen in normal controls (De Sandre-Giovannoli et al. 2003). Cells from HGPS individuals show an accumulation of prelamin A, either as a full-length protein or as various truncated forms, and the nuclei have a reduced deformability (Dahl et al. 2006) similar to that observed in ageing normal cells (Lans and Hoeijmakers 2006).

Premature replicative senescence is popularly considered a canonical feature of HGPS cells, although early studies gave mixed results, showing impaired proliferation compared to normal age-matched controls but not to the same extent as seen in other progeroid syndromes, such as WS. More recent studies suggest that HGPS fibroblasts undergo approximately 20-30 PDs compared to approximately 60 PDs in the controls (Bridger and Kill 2004), although lifespans up to 53 PDs have been recorded. These studies also suggest that HGPS fibroblasts undergo a period of hyperproliferation, followed by rapid apoptotic death (Bridger and Kill 2004).

The telomeres of skin fibroblasts derived from HGPS individuals are seen to be shorter that those of age-matched controls (Allsopp et al. 1992), and telomere shortening is accelerated in HGPS cells, or in normal cells ectopically over-expressing normal lamin A (Huang et al. 2008). In addition, ectopic expression of TERT results in the immortalisation of HGPS cells, although there are some cell clones that fail to immortalise (Ouellette et al. 2000; Wallis et al. 2004). These data suggest that that the premature senescence may be due to accelerated telomere shortening. However, these studies did not take into account the much-elevated rate of apoptosis seen in HGPS cells that would result in altered dynamics of

cellular growth, similar to that proposed for WS cells (Section 1.7, Figure 1.6). Thus, it is possible that the shortened telomeres in recently explanted HGPS cells and the accelerated telomere erosion rates seen *in vitro*, are due simply to elevated cell turnover resulting from cell loss, and there are, as yet, no data definitively linking the shortened cellular lifespan to defects in telomere biology.

1.3.6.2 Properties of the Lamin A protein

HGPS is caused by mutations in the *LMNA* gene that encodes the nuclear lamina component lamin A/C. Nuclear lamins are intermediate filament proteins that constitute major components of the nuclear lamina, a dynamic filamentous meshwork comprising A- and B-type lamins that forms an interface between the nuclear membrane and chromatin (Aebi et al. 1986). The nuclear lamina has long been thought to protect the genome from mechanical stress. More recently, it has been shown that lamin A interacts with chromatin in the nucleoplasm, suggesting a regulatory role in chromatin organisation, assembly and disassembly of the nucleus during cell division, and gene expression, (Goldman et al. 2002; Gruenbaum et al. 2005): indeed transcriptional misregulation has been reported in HGPS fibroblasts (Ly et al. 2000).

The most common mutation in HGPS, G608G (GGC>GGT), is a silent *de novo* single nucleotide substitution in exon 11 (~90% HGPS cases). A second mutation in the same codon, G608S (GGC>AGC), that results in a conservative substitution of serine for glycine is also observed in HGPS, although this mutation is less common (~10% HGPS cases). Both of these mutations activate a cryptic splice site and result in deletion of the 3' terminal 150 nucleotides of exon 11 mRNA, causing a 50 amino acid internal truncation near the C-terminus of prelamin A, denoted LAΔ50/progerin (De Sandre-Giovannoli et al. 2003; Eriksson et al. 2003). The mutant progerin protein becomes inserted into the nuclear membrane rather than the lamina (Navarro et al. 2006) and acts in a dominant negative fashion, causing the aberrant nuclear morphology and shortened lifespan seen in HGPS cells, even in the presence of wild-type lamin A (Goldman et al. 2004). Support for this theory comes from studies showing that the these

phenotypes can be corrected using RNA interference against the truncated mRNA (Huang et al. 2005), and by the use of specifically targeted oligonucleotides to block the HGPS splice site (Scaffidi and Misteli 2005).

1.3.7 Dyskeratosis Congenita

Dyskeratosis congenita (DKC) is a rare inherited disorder characterised by multisystem failure of highly proliferating tissues (Drachtman and Alter 1992; Morgan 1997). Individuals with DKC typically present with progressive bone marrow failure and a classic triad of mucocutaneous features, including abnormal skin pigmentation, nail dystrophy and oral leukoplakia (Dokal 1996, 2000; Knight et al. 1998). Other features include signs of premature ageing, such as hair loss, early hair greying, aplastic anaemia, osteoporosis, and pulmonary and hepatic fibrosis (Dokal 2000). DKC individuals have a predisposition to malignancy, although bone marrow failure is the main cause of early mortality. The prevalence is approximately one in a million individuals with death occurring at the median age of 16 with a maximum of 50 years (Drachtman and Alter 1995; Marciniak et al. 2000). DKC is clinically heterogeneous displaying a range of cutaneous, dental, gastrointestinal, neurological, ophthalmic and pulmonary abnormalities (Marrone and Dokal 2004). This reflects the genetic heterogeneity of DKC in which X-linked recessive, autosomal dominant (AD) and autosomal recessive (AR) forms have been identified.

The X-linked recessive is the most severe subtype of DKC, with over 85% of affected males having a peripheral cytopenia of at least one lineage and 76% develop pancytopenia at a median age of 10 years (Garcia et al. 2007). A severe variant of X-linked DKC, known as Hoyeraal-Hreidarrson syndrome, is characterised by intrauterine growth retardation, microcephaly, cerebellar hypoplasia, mental retardation, progressive combined immune deficiency, and aplastic anaemia (Bessler et al. 2007). Conversely, AD-DKC is often much milder, with a later onset of disease manifestations and a longer life expectancy. Individuals with AD-DKC display bone marrow failure, pulmonary fibrosis and liver cirrhosis, but the mucocutaneous manifestations characteristic of the X-linked

28

disease are often absent or very mild (Armanios et al. 2007). Interestingly, myelodysplatic syndrome and acute myeloid leukaemia, which are rare in X-linked DKC, are more frequent in AD-DKC, perhaps reflecting the time required for malignant transformation (Garcia et al. 2007).

1.3.7.1 Aetiology of DKC

The aetiology of DKC is complex as it caused by mutations in at least five separate genes. In those cases of DKC where the aetiology is known, the vast majority of causative mutations are in components of the telomerase multimeric ribonucleoprotein (RNP) complex. This complex consists of two core components: the telomerase reverse transcriptase (TERT) that catalyses the addition of telomeric repeats to the end of chromosomes (Feng et al. 1995), and an RNA component (TERC) that contains the template region complementary to the telomeric sequence (Greider and Blackburn 1985). Several other proteins associate with the core RNP of telomerase, including dyskerin, NOP10, GAR1 and NHP2, and are thought to aid the function and localisation of the telomerase core (Tollervey and Kiss 1997). Although mutations in a number of these proteins have been associated with DKC approximately 60% of clinically diagnosed DKC individuals have uncharacterised mutations.

The X-linked form makes up 35% of diagnosed cases of DC and is caused by mis-sense mutations in DKC1, the gene encoding the highly conserved nucleolar protein dyskerin (Heiss et al. 1998). Dyskerin is thought to have a structural role in the telomerase complex as it physically interacts with TERC (Heiss et al. 1999; Mitchell et al. 1999b), and DKC1 mutations result in lower TERC levels. AD-DKC is a rare subtype (approx 5% of cases) that has been linked to mutations in TERC (Vulliamy et al. 2001a; Vulliamy et al. 2004), although in some cases TERT mutations have been recorded (Armanios et al. 2005; Vulliamy et al. 2005). The majority of mutations in AD-DKC are predicted to reduce telomerase activity when present in vivo (Chen and Greider 2004). Another common mutation in AD-DC is a 3' truncation of the last 74 bases of TERC (Westin et al. 2007). Interestingly, this region is important for binding to dyskerin, thus potentially linking the X-linked and

AD forms of DC (Mitchell et al. 1999a). Until recently the genetic basis of AR-DKC was completely unknown. However, a recent study identified mutations in the RNP component, *NOP10* (Walne et al. 2007). Individuals with homozygous mutations in *NOP10* have short telomeres and reduced levels of TERC (Walne et al. 2007). Heterozygous individuals also have reduced TERC levels, but to a lesser extent than the affected homozygotes. Recently, individuals with DKC that lack mutations in *DKC1, NOP10, TERC* or *TERT*, were found to have mutations in the *TINF2* gene that encodes TIN2, a component of the shelterin complex that protects the ends of chromosomes (Savage et al. 2008). As these individuals are heterozygotes, this is a form of AD-DC. The *TINF2* mutations disrupt the TIN2-TRF1-TRF2 complex resulting in telomere instability, and these individuals have very short telomeres. This represents the first time that mutations in the shelterin complex have been linked to human disease.

The tissues that are most affected in DKC are those that require constant renewal, including skin, oral mucosa, and bone marrow (Garcia et al. 2007; Luzzatto and Karadimitris 1998). This is reflected by the *in vitro* behaviour of cells from DKC individuals, and it has been reported that skin fibroblasts grow poorly *in vitro* (Dokal et al. 1992; Marsh et al. 1992). In separate reports, fibroblasts derived from individuals with AD-DKC were shown to proliferate at rates similar to normal cells at early passage but undergo premature replicative senescence, with a proliferative lifespan of approximately half that of their normal counterparts (Westin et al. 2007). Similarly, fibroblasts from individuals with X-linked DKC have a reduced replicative lifespan but also show reduced growth rates at early passage (Wong and Collins 2006). Thus, it appears that all DKC fibroblasts have a replicative defect, whereas the growth rate defects are variable and depend on the genetic origin of the cells. Cultured primary DKC fibroblasts have also been reported to have an abnormal morphology, (including polygonal cell shape, ballooning, and dendritic-like projections), a longer doubling time and abnormal chromosomal rearrangements (Dokal et al. 1992). Finally, female carriers of the X-linked mutant allele show a skewed pattern of X-chromosome inactivation that is also consistent with a proliferative defect (Devriendt et al. 1997; Vulliamy et al.

1997). These data all support the hypothesis that the clinical manifestations of DKC can be explained by a defect in cellular proliferative capacity.

An additional cellular phenotype is genomic instability, with fibroblasts and lymphocytes from DKC individuals showing an age-dependent increase in chromosomal rearrangements that are consistent with telomere shortening (Davidson and Connor 1988). As the disease progresses, unbalanced chromosomal rearrangements including dicentrics, Robertsonian translocations, and ring-chromosomes become detectable in the skin, bone marrow and peripheral blood cells; however, there is no elevated sensitivity of DKC cells to most DNA damaging agents (Dokal 1996; Dokal et al. 1992). This suggests that the molecular defects predispose DKC cells to developing chromosomal rearrangements (Dokal et al. 1992) but do not affect DNA repair processes.

1.3.8 Ligase 4 syndrome

1.3.8.1 Clinical and cellular phenotype of LIG4 syndrome

Ligase 4 (LIG4) syndrome is a rare autosomal recessive disorder that exhibits microcephaly, unusual facial features, growth retardation, developmental delay, skin abnormalities and pancytopenia (O'Driscoll et al. 2001) and shares similar clinical phenotypes with NBS (Ben-Omran et al. 2005; O'Driscoll et al. 2004). LIG4 is characterised by, genomic instability, malignancy, immunodeficiency and bone marrow abnormalities. LIG4 syndrome cells also show pronounced radiosensitivity, however, unlike NBS cells, they show normal cell cycle checkpoint responses but impaired DNA DSB rejoining (O'Driscoll et al. 2001).

1.3.8.2 Aetiology of LIG4 syndrome

LIG4 syndrome is caused by mutations in the LIG4 gene that encodes DNA ligase IV, a component of the DNA NHEJ machinery (O'Driscoll et al. 2001), which represents the major process in mammalian cells for the repair of DNA DSBs (Jeggo 1998). In the current model of NHEJ [reviewed by (Hartlerode and Scully 2009; Poplawski et al. 2009)], the first step involves binding of the heterodimeric Ku protein (comprising two subunits, Ku70 and Ku80) to double stranded DNA

ends. DNA-bound Ku recruits the DNA-dependent protein kinase catalytic subunit (DNA-PKcs) and activates its kinase activity. DNA-bound Ku also serves to recruit DNA ligase IV and Xrcc4, which is tightly associated with it. The DNA ligase IV/Xrcc4 complex then carries out the final ligation step (Grawunder et al. 1997; Wilson et al. 1997). DNA ligase IV has been shown to be essential for development and knock out mice die at an early embryonic stage (Barnes et al. 1998; Frank et al. 2000). Thus, biallelic null mutations have not been described in LIG4 syndrome to date, and instead LIG4 syndrome individuals have hypomorphic mutations that retain some residual DNA ligase IV function and allow viability (O'Driscoll et al. 2001).

1.3.9 Seckel syndrome

Seckel syndrome (SS) is a rare autosomal recessive disorder that is characterised by marked microcephaly and developmental delay (Seckel 1960). Other clinical features of SS include severe proportionate dwarfism evident even *in utero*, a characteristic facial appearance (small chin, protruding nose, receding forehead), mental retardation and isolated skeletal abnormalities (Faivre and Cormier-Daire 2001; O'Driscoll et al. 2004). Since it was first described in 1960, >70 cases have been reported, but there is considerable heterogeneity in their clinical characteristics (Faivre et al. 2002). This disorder shares many clinical features with NBS (Section 1.3.5) and LIG4 syndrome (Section 1.3.8), both of which are syndromes involving DNA damage response genes.

1.3.9.1 Aetiology of SS

Given the varied clinical presentation of SS it is not surprising that several loci have been linked to SS. Several homozygosity mapping studies using different SS families have shown that it was likely that at least three different genes (designated as SCKL1, SCKL2 and SCKL3 loci) are responsible for this disorder. Recently, mutations in *ATR* were identified as the gene mutated at the SCKL1 locus (O'Driscoll et al. 2003). Sequencing of *ATR* cDNA revealed a silent A2101G transition in exon 9 that results in low levels of ATR activity allowing viability, although with severe clinical features. Whilst not all SS individuals are mutated in

ATR, all classical SS individuals are defective in ATR-pathway function (Alderton et al. 2004). More recently a second genetic defect in ATR-pathway defective SS was identified, namely mutations in the *pericentrin(PCNT2)/kendrin* gene, which encodes a structural centrosomal protein, (Griffith et al. 2008).

1.3.9.2 Cellular phenotype of SS

SS fibroblasts are reported to have slow cycling time (Alderton et al. 2004) and are associated with increased chromosome breakage following replication stress, particularly at fragile sites (Casper et al. 2004; Casper et al. 2002). In addition, SS cells have been reported to show impaired phosphorylation of a range of ATR-dependent substrates (H2AX, p53 Nbs1 and Rad17) following exposure to UV irradiation but a normal ATM-dependent response to IR (O'Driscoll et al. 2003). A similar response was observed in SS following exposure to hydroxyurea (O'Driscoll et al. 2004). However, reports of CIN in SS cells are inconsistent. For example, spontaneous CIN has been reported in some SS individuals (Woods et al. 1995), whereas others show increased CIN following exposure to mitomycin C (MMC) (Bobabilla-Morales et al. 2003; Syrrou et al. 1995). However, other SS individuals have been reported to be resistant to MMC (Abou-Zahr et al. 1999). In addition, increased SCE has been observed in some SS individuals (Cervenka et al. 1979; Syrrou et al. 1995). Despite the heterogeneous cellular phenotype of SS cells, it is generally accepted that SS cells are unusually sensitive to agents that cause replication stalling (Casper et al. 2004), suggesting that the low levels of ATR present in SS individuals are insufficient to respond appropriately to replication stress.

1.4 Cellular senescence

Normal human fibroblasts undergo only a limited number of divisions in culture and eventually enter a state of irreversible cell cycle arrest designated senescence or mortality stage 1 (M1) (Hayflick 1965; Hayflick and Moorhead 1961). Even at low passage numbers cell cultures are made up of a mixture of highly replicating cells and senescent cells, although replicating cells make up the greater proportion. Over time the percentage of senescent cells progressively

increases as clones reach the end of their lifespan and arrest, until the whole culture stops dividing (Ostler et al. 2000). This is thought to be due to the selective repression of growth-promoting genes and the overexpression of repressive factors. In fibroblasts, this includes repression of the c-fos proto-oncogene (Seshadri and Campisi 1990) and components of the E2F transcription factor (Dimri et al. 1995), amongst others, and overexpression of the cell cycle inhibitors, p21^{WAF1} and p16^{INK4A} (Noda et al. 1994). This is likely to lead to hypophosphorylation of the retinoblastoma gene product, pRb, in senescent cells and ultimately trigger growth arrest.

Cellular senescence was first described in human fibroblasts, which were shown to senesce after approximately 60-80 PD. Since then a number of other cell types, including keratinocytes (Noda et al. 1994; Rheinwald and Green 1975), endothelial cells (Mueller et al. 1980), and lymphocytes (Tice et al. 1979) have been shown to undergo replicative senescence. The replicative lifespan of normal cells can be measured in cumulative PDs and depends on the age and genetic background of the donor, and also the species and cell type (Hayflick 1965). In contrast to quiescent cells which exhibit transient and reversible growth arrest, senescent cells are arrested in the G_1/G_0 phase of the cell cycle and do not re-enter the S-phase, even when they are treated with strong mitogenic stimuli (Campisi and d'Adda di Fagagna 2007; Cristofalo et al. 1989).

There are two types of cellular senescence: replicative senescence and stress-induced premature senescence (SIPS). Replicative senescence is thought to be induced by progressive telomere shortening and is often referred to as a telomere-dependent process (see section 1.4.2). SIPS, on the other hand, is induced when cells are exposed to stressful stimuli (including DNA damage, overexpression of oncogenes and oxidative stress) and is thought to be a telomere-independent process (see section 1.4.3). Although this distinction is useful, it probably does not refer to two independent cellular mechanisms but, rather, to the fact that disparate signals can elicit a common cellular response. Most studies indicate that senescence is activated once a cell has suffered a

critical level of damage. It is therefore possible that senescence can result from the cumulative effect of multiple stresses acting on a population of cells. Moreover, extrinsic stresses, such as oxidative stress, may affect intrinsic factors, such as DNA damage accumulation and telomere shortening rates (Passos et al. 2010). Thus, a combination of various stressors may exert a complex cumulative effect on a heterogeneous population of cells, ultimately triggering the senescence of the population as a whole. Here, the terms replicative senescence and SIPS are used to make a distinction between the different inducers of senescence with particular attention given to the signalling pathways involved in senescence and specifically of the role of p38 MAPK in senescence.

1.4.1 Characteristics of senescent cells

At senescence, the most obvious change is irreversible growth arrest. Whilst the hallmark of senescent cells is the cessation of responsiveness to mitogens (Seshadri and Campisi 1990), the senescent phenotype is typically characterised by marked alterations in growth kinetics, morphological appearance and dysregulation of biological processes. Senescent cells maintained under routine culture conditions are morphologically characterised by an increase in cell size, with a marked flattened and vacuolated appearance coupled with an associated increase in nucleus and nucleoli size (Cristofalo and Kritchevsky 1969; Greenberg et al. 1977; Mitsui and Schneider 1976). A marked increase in the number of lysosomes and golgi (Cristofalo and Kabakjian 1975; Maciera-Coelho et al. 1971) and a pronounced increase in the number of cytoplasmic microfilaments are also features indicative of senescence (Brandes et al. 1972; Lipetz and Cristofalo 1972). In addition to the morphological alterations, senescent cell populations exhibit a pronounced increase in the number of multinucleated cells (Matsumura 1980; Yanishevsky and Carrano 1975) and heterochromatic foci are observed (Narita et al. 2003). Although senescent cells remain metabolically active, the progressive accumulation of senescent cells causes attenuation in tissue function (Dimri et al. 1995; Minamino et al. 2002).

The complete cessation of proliferation in senescent fibroblasts is associated with alterations in gene expression patterns and posttranslational modifications in a cell-type specific manner, resulting in an altered phenotype compared to their young isogenic counterparts (Cristofalo et al. 1998b; Park et al. 2001; Shelton et al. 1999). For example, altered patterns of gene expression are seen in the transduction and secretory pathways. Impairment in cell mobility, secretion of matrix degrading proteins, secretion of growth factors and pro-inflammatory cytokines are considered as significant changes associated with cellular senescence. These changes are thought to have a detrimental impact on neighbouring cells, the surrounding extracellular matrix and other structural components, leading to aged tissues (Burton et al. 2005; Burton et al. 2007; Campisi 1997a).

Microarray analysis of senescent dermal fibroblasts, retinal pigment epithelial cells and vascular endothelial cells demonstrate overlap in gene expression changes but overall display cell-type specific changes (Shelton et al. 1999). In particular, the differential regulation of proteases and constituents of the extracellular matrix, such as: extracellular matrix (ECM)-degrading secreted proteases, collagenase (West et al. 1989), and tissue plasminogen activator (West et al. 1996); ECM-modifying proteins, matrix metalloproteinases (MMPs) and tissue inhibitor of metalloproteinase family (Millis et al. 1992a; Millis et al. 1992b); growth factors and inflammatory cytokines, have been reported (Campisi 1998; Faragher and Kipling 1998; Shay and Wright 2005). Additionally, senescent fibroblasts express reduced levels of MMP inhibitors, tissue inhibitor of metalloprotease (TIMP1) (Millis et al. 1992b) and Ras-related C3 botulinium toxin substrate 1 (MIG5) (Wick et al. 1994), a reduction in ECM components, including elastin, laminin (Linskens et al. 1995) and constituents of collagen (Furth 1991). Secreted levels of growth factors, such as vascular endothelial growth factor (VEGF), are also reported to be elevated in senescent cell cultures (Coppe et al. 2006). These findings lead to the idea that while cellular senescence may be a mechanism to suppress tumourigenesis early in life, it may promote cancer in aged organisms

(Campisi 1997a). Indeed, co-cultivation of senescent fibroblasts with epithelial cells can promote the growth of pre-neoplastic cells (Krtolica and Campisi 2002).

One of the most commonly used markers of senescence is the upregulation of senescence associated β-galactosidase (SA β-gal) activity. It was proposed that SA β-gal, which is active at pH 6.0, was distinct from the lysosomal β-gal with an optimum pH of 4.5 (Dimri et al. 1995). Results showed an age-dependent increase in SA β-gal staining in dermal fibroblasts and epidermal keratinocytes at senescence (Dimri et al. 1995). Despite the extensive application of the SA β-gal assay as an indicator of senescence, the validity and reliability of the assay has been challenged. An increase in SA β-gal has been reported in immortalised cells following serum starvation (Yegorov et al. 1998) and oxidative stress induced by H_2O_2, and can even be reversed under some conditions (Cristofalo 2005).

More recently, studies have used novel biomarkers to detect cellular senescence in mitotic tissues in order to re-evaluate the significance of cellular senescence in organismal ageing (Herbig et al. 2006; Jeyapalan et al. 2007). These studies investigated markers of cellular senescence such as telomere damage, active checkpoint kinase ATM, high levels of heterochromatin proteins and elevated levels of p16 in skin biopsies from baboons with advancing age. The number of dermal fibroblasts containing damaged telomeres reached a value of over 15% of total fibroblasts in very old animals (26-30 years) compared to young (5-6 years) where DNA damage was rarely detected.

1.4.2 Replicative senescence

Telomere attrition is thought to be the predominant mechanism by which a cell ultimately becomes "replicatively" senescent (Harley et al. 1990; Olovnikov 1973). Telomeres are the DNA-protein structures that cap the ends of eukaryotic linear chromosomes. They function to protect chromosomal ends from normal cellular activity and genome instability promoting events. Human telomeres consist of TTAGGG repeat sequences, the lengths of which vary greatly among mammalian species and interestingly in the same individual depending on cell type (Allshire et al. 1989; Campisi 2001; de Lange et al. 1990; Moyzis et al. 1988).

Telomeres form a higher-order chromatin structure that physically hides the 3'-overhang at the chromosome end. Studies suggest that the double-stranded telomere folds back on itself to form large terminal loops known as a T-loop (de Lange 2005; Greider 1999). The 3' G-rich single-stranded overhang at the end of the T-loop then invades the double-stranded telomere and produces a D-loop. This structure performs a number of essential roles in chromosome preservation. For example, capping allows the cell to differentiate chromosome ends from DSBs in the genome. This is essential since uncapped chromosome ends are susceptible to degradation (leading to loss of genetic information), recombination (leading to chromosomal rearrangements) or fusion (resulting in the formation of dicentric chromosomes and breakage-fusion-bridge cycles) (Stansel et al. 2001; van Steensel et al. 1998).

During the replicative lifespan of normal diploid somatic cells, telomere attrition is thought to occur at approximately 50-200 base pairs (bp) per cell division (Harley et al. 1990). The progressive attrition of telomeric sequences has been attributed to the inability of DNA polymerase to completely replicate chromosome ends during lagging strand synthesis (Harley et al. 1990; Olovnikov 1973). This phenomenon is known as the end replication problem and occurs when somatic diploid fibroblasts undergo each cell division. Telomeres can be extended by addition of TTAGGG repeats onto pre-existing telomeres. Telomerase, a cellular reverse transcriptase, provides the main regulator of telomere length and facilitates the replication of telomeric DNA. Telomerase is composed of two essential constituents: the reverse transcriptase subunit, hTert, and the RNA component, hTERC, the latter of which contains the template for the synthesis of new tandem repeats (Blasco 2003). Most normal human somatic cells either completely lack telomerase activity or possess residual levels that are insufficient for telomere maintenance (Harley et al. 1990; Kim et al. 1994). This, coupled with the end replication problem, leads to progressive telomere shortening with each round of replication.

Support for this theory comes from the observations that the mean telomere length in cells that do not express telomerase, such as primary human fibroblasts, decreases with subcultivation (Harley et al. 1990). In contrast, telomerase activity is reactivated in approximately 90% of human cancers, which may contribute to the continued growth of cancer cells (Artandi 2006). Similarly, the introduction of telomerase into normal somatic cells, such as retinal pigment epithelial cells and foreskin fibroblasts, has been shown to extend replicative lifespan (Bodnar et al. 1998).

1.4.2.1 Immortalisation by ectopic expression of hTert

The observation that normal human somatic cells have a finite life span and enter senescence after a limited number of divisions (Hayflick 1965; Hayflick and Moorhead 1961) is the main drawback of working with primary cultures. It represents an obstacle to the study of normal human cells, especially since large quantities of cells are often required for analysis. This limitation is of particular concern for the study of rare hereditary human diseases, such as those studied here, since the volume of the biological samples collected from biopsies is often small and contain limited numbers of cells. The establishment of permanent cell lines is one way to avoid this lack of material. Conventional methods of immortalisation involve the utilisation of oncogenic viral proteins to establish permanent fibroblast cell lines. However, such transformed cells typically exhibit significant alterations in physiological and biological properties from their normal counterparts (Ouellette et al. 2000). Most notably, these cells are associated with aneuploidy, spontaneous hypermutability, loss of contact inhibition and alterations in biochemical functions related to cell cycle checkpoints (Ouellette et al. 2000). These differences pose significant limitations to the analysis of many cellular functions, in particular those related to genomic integrity and the study of genomic instability syndromes. To overcome the technical barrier of senescence whilst avoiding problems associated with transformation, immortalisation of cells by ectopic expression of hTert can be achieved. The utilisation of hTert permits an extension of proliferative lifespan whilst maintaining normal cell cycle controls, functional p53 and pRb checkpoints and retention of contact inhibition and

anchorage dependence (Jiang et al. 1999; Morales et al. 1999). Specifically, the ectopic expression of hTert cDNA in normal fibroblasts and retinal pigment cells has been shown to bypass the senescence barrier leading to immortalisation (Bodnar et al. 1998; Vaziri and Benchimol 1998) without inducing alterations that resemble a malignant phenotype (Jiang et al. 1999; Morales et al. 1999; Vaziri and Benchimol 1998).

1.4.3 Stress-induced premature senescence (SIPS)

While it is widely recognised that telomere shortening is a universal mechanism that limits proliferative potential of normal cells lacking telomerase, evidence of telomere-independent senescence processes have been reported. Studies have shown that mouse embryonic fibroblasts (MEFs) have functional telomerase and long telomeres but they exhibit replicative senescence-like cell cycle arrest after several rounds of cell division (Wright and Shay 2000). In addition, exposure to stressful stimuli can elicit a permanent state of growth arrest that is indistinguishable from replicative senescence. Furthermore, expression of hTert does not prevent SIPS in normal human fibroblasts in response to UV, γ-irradiation or H_2O_2 (Gorbunova et al. 2002), suggesting that SIPS is not triggered by telomere shortening but rather that nonspecific DNA damage serves as a signal for the induction of SIPS.

An early observation linking DNA damage to premature senescence was the permanent and irreversible proliferation arrest observed in irradiated human fibroblasts (Di Leonardo et al. 1994). Since then, a number of other DNA damaging agents have been shown to induce senescence. The most frequently reported causes of SIPS include: oxidative DNA damage (Chen and Ames 1994; Parrinello et al. 2003) or nucleotide damage (Rai 2010), DNA damage induced by genotoxic agents (Schmitt et al. 2002; te Poele et al. 2002), oncogenic dysregulation (Serrano et al. 1997), and suboptimal culture conditions (Ramirez et al. 2001).

Oxidative stress and the accumulation of intracellular ROS play an important role in the induction of senescence (Chen and Ames 1994). Human fibroblasts are

shown to undergo premature senescence when grown at high oxygen conditions (40-50% oxygen) (Ben-Porath and Weinberg 2005). Conversely, a reduced partial pressure of oxygen (equivalent 2-3% oxygen) allows an increase in growth rate and an increased frequency in colony formation (Balin et al. 1977; Honda and Matsuo 1983; Packer and Fuehr 1977). Similarly, an increase in intracellular ROS levels through H_2O_2 treatment or through the inhibition of ROS scavenging enzymes, such as superoxide dismutase (Sod1), causes premature senescence (Blander et al. 2003). Although there is some evidence that minimal doses of H_2O_2 (10 nM) stimulate growth of transformed and normal fibroblasts (Bladier et al. 1997; Burdon et al. 1989), exposure to higher doses (50-100 μM) is shown to induce growth arrest with cells displaying a characteristic senescent-like morphology (Bladier et al. 1997).

The direct damaging of DNA, either achieved by irradiating cells or treatment with DNA-damaging agents, can induce cells to undergo senescence (Wahl and Carr 2001). However, often the cellular response to such damage is cell death or reversible cell-cycle arrest, depending on the type of agent, the dose, and the cell type (Wahl and Carr 2001). Many chemotherapeutic drugs that cause severe DNA damage have been shown to induce senescence in normal cells. For example, exposure of human dermal fibroblasts to anti-neoplastic molecules such as MMC and bleomycin has been shown to result in a marked decrease in proliferation capacity, appearance of SA β-gal activity and a senescent-like morphology (Niggli et al. 1989; Rodemann et al. 1989). However, the distinction between arrested cells and those undergoing senescence as indicated by SA β-gal may not be clear. It has also been reported that topoisomerase inhibitors, such as doxorubicin (DOX), can induce irreversible growth arrest in tumour cells along with morphological and biochemical changes that are associated with senescence (te Poele et al. 2002). In conclusion, several lines of evidence suggest that the exposure of normal human cells to sub-cytotoxic stress triggers the appearance of a senescent-like phenotype.

The introduction of activated oncogenes into primary cells triggers defence responses that prevent cell growth. Some oncogenes, such as c-Myc, trigger apoptosis, whereas others, such as activated Ras, trigger a permanent and irreversible arrest that is reminiscent of senescence (Serrano et al. 1997). Oncogene-induced senescence is conserved not only in fibroblasts (Serrano et al. 1997), but also in epithelial cells of human and murine origin (Jones et al. 2000; Lin and Lowe 2001). This response has been suggested to represent a tumour-suppressive mechanism by which cells prevent uncontrolled proliferation in response to the aberrant activation of proliferation-driving oncogenes.

1.4.4 Regulators of senescence

There are two major signalling pathways that have been implicated in the activation and regulation of senescence including the $p53/p21^{WAF1/CIP1}$ and $pRb/16^{INK4A}$ tumour suppressor pathways (Alcorta et al. 1996; Beausejour et al. 2003; Lin et al. 1998; Serrano et al. 1997). These pathways interact but can independently halt cell cycle progression. To some extent, they also respond to different stimuli. In addition, there are both cell-type specific and species-specific differences in the propensity with which cells engage one or the other pathway, and in the ability of each pathway to induce senescence (Campisi and d'Adda di Fagagna 2007). Finally, although most cells senesce due to engagement of the p53 pathway, p16 pathway, or both, there are some examples of senescence that appear to be independent of these pathways (Olsen et al. 2002). In these cases there is evidence that the p38 pathway plays a role in cell cycle arrest. For example, the cell cycle checkpoint function of p38 was shown to be essential for cell cycle arrest in cells with defective p53 (Reinhardt et al. 2007).

Stimuli that generate a DNA-damage response, for example ionizing radiation and telomere dysfunction, induce senescence primarily through the $p53/p21^{WAF1/CIP1}$ pathway (Campisi and d'Adda di Fagagna 2007). p53 is an important downstream target of the DNA damage response pathway, which is activated via ATM through several mechanisms (Kastan and Bartek 2004). ATM activates downstream kinases Chk1 and Chk2, which mediate the phosphorylation

of p53 at Ser20. Subsequently, the interaction of p53 with Mdm2 is disrupted leading to the stabilisation of p53. In this way, p53 regulates cellular proliferation and senescence, which is thought to provide a protective mechanism that suppresses tumourigenesis (Campisi 2005). p21$^{WAF1/CIP1}$ is a crucial transcriptional target of p53 that mediates p53-dependent senescence (Brown et al. 1997). However, p21$^{WAF1/CIP1}$ also mediates a transient DNA-damage-induced growth arrest. It is currently unknown what determines whether cells senesce or arrest transiently. It is possible that rapid DNA repair quickly terminates p53/p21$^{WAF1/CIP1}$ signalling, whereas, slow, incomplete or faulty repair results in sustained signalling and induces senescence (Campisi and d'Adda di Fagagna 2007; Passos et al. 2010). The role of p21$^{WAF1/CIP1}$ in senescence is highlighted by the finding that the level of p21$^{WAF1/CIP1}$ gradually increases as cells progress into a state of senescence (Alcorta et al. 1996). Furthermore, targeted deletion of p21$^{WAF1/CIP1}$ in fibroblasts results in the bypass of cellular senescence (Brown et al. 1997).

Stimuli that produce a DNA-damage response can also engage the pRb/16^{INK4A} pathway. Although this is usually secondary to activation of the p53/p21$^{WAF1/CIP1}$ pathway, there are some senescence-inducing stimuli, such as oncogenic Ras, that act primarily through the pRb/16^{INK4A} pathway (Jacobs and de Lange 2004; Lowe and Sherr 2003; Stein et al. 1999). p16 is an inhibitor of cyclin D/Cdk4,6 complexes (Lowe and Sherr 2003) that is induced in various situations of stress and is highly expressed in senescent cells (Alcorta et al. 1996; Palmero et al. 1997). Active p16 prevents the phosphorylation of pRb, thus keeping it in the active hypophosphorylated form, thereby preventing E2F from transcribing genes that are required for proliferation (Sherr and McCormick 2002). The final outcome is irreversible senescence.

1.4.5 Significance of senescence *in vivo*

Hayflick's original observations of cellular senescence were made using cultured cells, and much of the current understanding of the causes and consequences of senescence still derives from cell cultures. It has only been in

recent years that cellular senescence has been shown to occur and to be important *in vivo*.

Senescence-associated markers (see section 1.4.1) have been used to identify senescent cells *in vivo*, with the caveat that none of these markers are exclusive to the senescent state. In rodents, primates and humans, senescent cells are found in many renewable tissues, including the vasculature, haematopoietic system, many epithelial organs and the stroma (Campisi 2005; Dimri et al. 1995; Jeyapalan et al. 2007; Krishnamurthy et al. 2004). Notably, cells that express one or more senescence markers are relatively rare in young organisms, but their number increases with age (Herbig et al. 2006). Among the senescence markers that accumulate with age are senescence-associated DNA-damage foci (SDFs) that co-localise with telomeres, suggesting that, at least in some tissues, telomere dysfunction causes senescence *in vivo* (Campisi and d'Adda di Fagagna 2007). Cells that express senescence markers are also found at sites of age-related pathology, such as osteo-arthritis and atherosclerosis (Chang and Harley 1995; Price et al. 2002; Vasile et al. 2001). As discussed previously, prior to senescence, dermal fibroblasts express high levels of matrix-producing genes and low levels of matrix degrading enzymes, such as collagenase and stromelysin. However, upon senescence these expression levels reverse, reflecting a clear switch to a matrix-degrading phenotype (Campisi 1997a). This can have profound effects on tissue function and is postulated to contribute to the progression of disease and the overall functional decline that is associated with ageing *in vivo*. In particular, secretion of matrix metalloproteases by senescent cells has been suggested to play a role in the pathogenesis of coronary heart disease (Nanni et al. 2007), and osteoporosis (Logar et al. 2007). In addition, some studies suggest that this process may be responsible for the thinning and wrinkling of the skin during ageing (Furth 1991). Another change that occurs when a cell becomes senescent is the increased secretion of pro-inflammatory cytokines. These not only affect local tissue but also have much wider impacts throughout the organism. Enhanced inflammation during ageing is thought to contribute to many of the diseases of ageing. For example, vascular smooth muscle cells that have become senescent

due to the activation of Ras have been shown to drastically increase the expression of pro-inflammatory cytokines, such as Interleukin 1α (IL1 α), IL 1β, IL-6 and IL-8, which are thought to contribute to the progression of atherosclerosis (Minamino et al. 2003). Thus, senescent cells are associated with ageing and age-related diseases *in vivo*.

The demonstration of a senescent-like arrest mediated by p53 and p16^{INK4A} after ectopic expression of oncogenic Ras in primary normal human and rodent cells introduced the concept of oncogene-induced senescence as a mechanism to restrain the growth of potentially cancerous cells (Serrano et al. 1997). This idea is further supported by the fact that essentially all human cancer cells have acquired mechanisms to maintain telomeres, generally through the expression of high levels of telomerase (Stewart and Weinberg 2006). Recently, replicative senescence has been shown to act as a tumour suppressor mechanism in telomerase-deficient mice expressing the oncogene Myc in B cells (Feldser and Greider 2007). Short telomeres reduced the incidence of cancer in these animals even when apoptosis was blocked by overexpression of the anti-apoptotic protein Bcl2. Examination of the lymph nodes of these apoptosis-resistant mice revealed clear signs of senescence induction, demonstrating that telomere-dependent senescence is an efficient mechanism to suppress cancer *in vivo* (Feldser and Greider 2007). Moreover, senescent cells are associated with benign dysplastic or pre-neoplastic lesions (Braig et al. 2005; Collado et al. 2005) and benign prostatic hyperplasia (Castro et al. 2003), but not with malignant tumours. They are also found in normal and tumour tissues following DNA-damaging chemotherapy (Roninson 2003; Schmitt et al. 2002; te Poele et al. 2002). These findings support the idea that cellular senescence has evolved as a tumour-suppression mechanism and that ageing may simply be an unwanted by-product of this.

1.5 Stress signalling, MAPKs and senescence

Cells respond to stress in a variety of ways ranging from activation of pathways that promote survival to those eliciting senescence or programmed cell death (apoptosis). One of the major pathways that is activated in response to

stress is the mitogen-activated protein kinase (MAPK) pathway. Here the focus is on the p38 MAPK pathway and its role in senescence.

All eukaryotic cells possess multiple MAPK pathways, which are activated in response to a variety of extracellular stimuli and mediate signal transduction from the cell surface to the nucleus. They regulate diverse physiological and pathological cellular activities, including inflammation, apoptotic cell death, oncogenic transformation, tumour cell invasion, and metastasis thereby exerting a profound effect on cell physiology (Kyriakis and Avruch 2001; Pearson et al. 2001; Roux and Blenis 2004). MAPKs, in combination with several other signalling pathways, can differentially alter the phosphorylation status of transcription factors in a pattern unique to a given external signal. Although MAPKs are expressed in all eukaryotic cell types, they regulate very specific biological responses that differ between cell types.

To date, four distinct groups of MAPKs have been reported in mammalian cells that respond synergistically to different upstream signals: extracellular signal-regulated kinases (ERKs), c-jun N-terminal or stress-activated protein kinase (JNK/SAPK), ERK5/big MAPK1 (BMK1), and the p38 group (Chen et al. 2001; Kyriakis and Avruch 2001). Each of these MAPKs form part of a three-tiered phospho-relay cascade along with a MAP kinase kinase (MKK), and a MAP kinase kinase kinase (MAP3K) (Kyriakis and Avruch 2001; Widmann et al. 1999). Signals are transmitted through the module by sequential phosphorylation and activation of these components. The MAP3Ks are often activated through phosphorylation and/or interaction with small GTPase proteins of the Ras/Rho family in response to extracellular stimuli (Kolch 2000; Marinissen et al. 2001; Zhang et al. 1995). Upon activation, the MAP3Ks phosphorylate a MKK on conserved serine and threonine residues, which in turn stimulates MAPK activity through dual phosphorylation on threonine and tyrosine residues located in the activation loop of kinase subdomain VIII (Crews et al. 1992; Kosako et al. 1992; Wu et al. 1993). Once activated, the MAPK proteins elicit a cellular response by transferring the γ-phosphate of ATP to

46

a serine or threonine residue in specific S(T)P sequences in target proteins within the cell (Roux and Blenis 2004).

The ERK cascade is activated mainly by growth factors and induces cell proliferation, survival and differentiation (Pearson et al. 2001; Roux and Blenis 2004). Conversely, JNKs and p38 were originally identified as kinases activated in response to a diverse array of cellular stresses such as proinflammatory cytokines, UV irradiation, ROS, heat, osmotic shock, and DNA damage, and are therefore known as stress-activated MAPKs (Derijard et al. 1994; Han et al. 1994; Raingeaud et al. 1995). The JNK and p38 pathways have been shown to be critically involved in the control of cellular stress responses such as cell death and survival (Kyriakis and Avruch 2001; Widmann et al. 1999). It has gradually become clear that the involvement of these stress-activated MAPK cascades in cellular senescence is dependent on the cellular context and cell type (Maruyama et al. 2009). In the following sections, the focus is on the roles of stress-activated MAPKs, in particular the p38 pathway, in cellular senescence.

1.5.1 The p38 pathway

p38α was first isolated as a 38-kDa protein that is rapidly tyrosine phosphorylated in response to lipopolysaccharide (LPS) stimulation and osmotic shock (Freshney et al. 1994; Han et al. 1994; Rouse et al. 1994). Later, p38 was identified as the molecular target of pyridinyl-imidazole cytokine inhibitors, which are known to inhibit biosynthesis of inflammatory cytokines such as interleukin-1 (IL-1) and tumour necrosis factor (TNF) in LPS stimulated monocytes (Lee et al. 1994). Since then, three other isoforms have been isolated: p38β (Jiang et al. 1996; Stein et al. 1997), p38γ (Li et al. 1996) and p38δ (Jiang et al. 1997). The p38α and p38β are ubiquitously expressed while the p38γ and p38δ are differentially expressed depending on tissue type. The p38γ isoform is predominantly expressed in skeletal muscle (Li et al. 1996), whereas p38δ is enriched in lung, kidney, pancreas, testis and small intestine and is thought to be developmentally regulated (Hale et al. 1999; Kumar et al. 1997). The four isoforms of p38 share high sequence homology and a signature Thr-Xaa-Tyr (TXY)

phosphorylation motif in the activation loop (Wilson et al. 1996). The p38 MAPK isoforms appear to mediate distinct functions *in vivo* due, in part, to differences in substrate phosphorylation by individual p38 MAPKs and also to selective activation by MKKs.
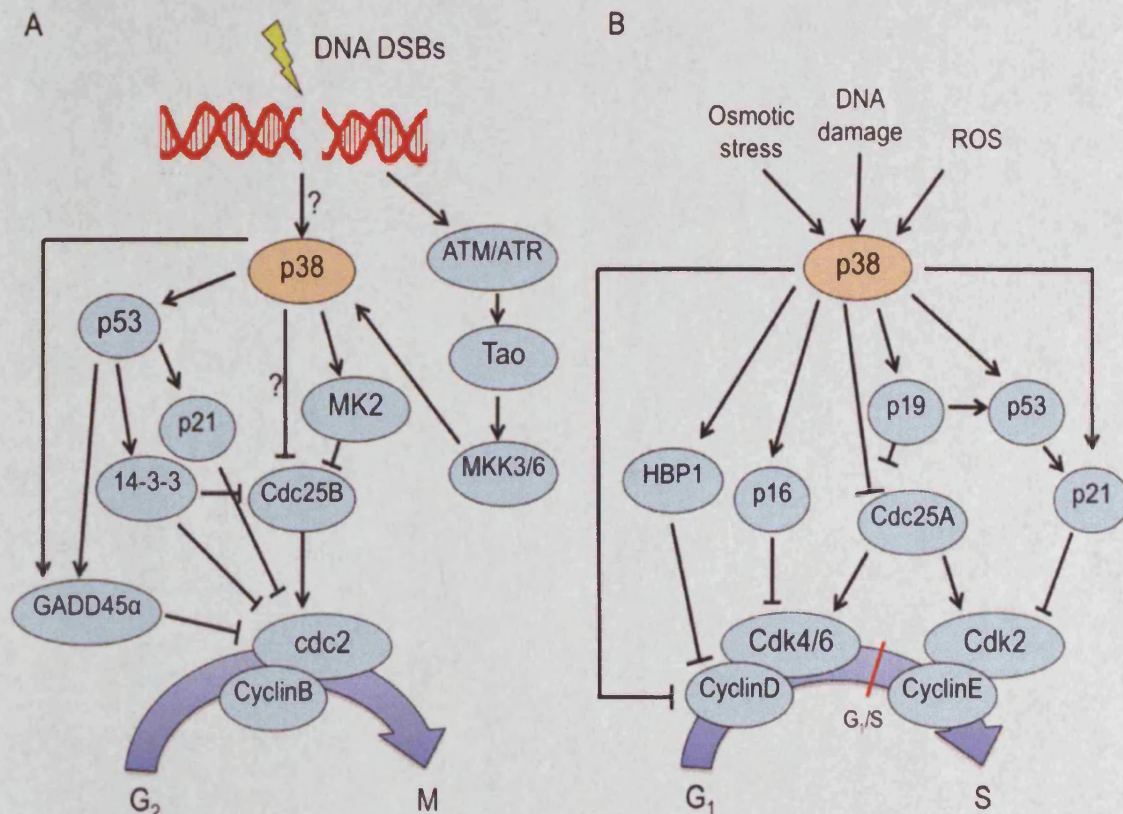
Figure 1.4. The role of p38 in the G_2/M (A) and G_1/S (B) checkpoints.

Stress signals are delivered to this cascade by members of the Rho family small GTPases (Rac, Rho, Cdc42). A large group of proteins, acting as MAP3Ks, activate the MKK/p38 pathway, which explains why this cascade can be activated by such a variety of stimuli. Downstream of the MAP3Ks in the p38 signal transduction cascade are the dual kinases known as MKKs. There are two main MKKs that are known to activate p38, MKK3 and MKK6, which show a high degree of specificity for p38 and do not activate ERK1/2 or JNK. In addition, MKK4, an upstream kinase of JNK, can also contribute to the activation of p38α and p38δ in specific cell types, suggesting that MKK4 represents a site of integration for the p38 and JNK pathways (Brancho et al. 2003; Meier et al. 1996). Despite conserved

dual phosphorylation sites among p38 isoforms, selective activation by distinct MKKs has been observed. For example, while MKK6 activates all p38 isoforms, MKK3 is somewhat selective, as it preferentially phosphorylates the p38α and p38γ and p38δ isoforms, but not p38β (Enslen et al. 1998). Furthermore, p38α is activated by low levels of MKK6 activity, whereas other p38 isoforms are only activated by high levels of MKK6 activity (Alonso et al. 2000). This suggests a mechanism for the specific activation of p38 MAPKs depending on the level of MKK6 activity triggered by a given stimulus. In addition, whereas MKK6 is activated by all known p38 activators, MKK3 appears to be more restricted with regard to activation by upstream stimuli (Kyriakis and Avruch 2001).

The p38 MAPK pathway regulates diverse biological functions by phosphorylation of specific target molecules found within the cell membrane, cytoplasm and nucleus. In particular p38 MAPK substrates include protein kinases and transcription factors, such as ATF-2 (Tan et al. 1996). The first p38α substrate to be identified was the MAPK-activated protein kinase 2 (MAPKAPK2 or MK2) (Stokoe et al. 1992a) and its closely related family member MK3. MK2 and MK3 are serine/threonine kinases with proline rich N-termini, highly conserved catalytic domains, and C-terminal autoinhibitory regions, both of which are shown to activate various substrates including small heat shock protein 27 (HSP27) (Stokoe et al. 1992b). HSP27 is an F-actin binding protein involved in cytoskeletal structure. Unphosphorylated HSP27 normally exists in high molecular multimers that serve as molecular chaperones; however, upon phosphorylation on conserved serine residues (Ser 15, 78, 82 and 90) HSP27 disassociates into monomers and dimers. This leads to redistribution of HSP27 to the actin cytoskeleton and the formation of actin stress fibres (Guay et al. 1997; Huot et al. 1997). Transcription factors activated by p38 include CREB homologous protein (CHOP), which is transcriptionally induced in response to genotoxic and inflammatory stresses (Wang and Ron 1996). Activation of CHOP mediates in part cell cycle arrest at G_1/S, an important consequence of DNA damage in that it allows for DNA repair before DNA replication (Kyriakis and Avruch 2001). This provides evidence for a role of p38 in the preservation of genomic integrity.

1.5.1.1 The p38 pathway and senescence

The role of p38α in inflammatory and stress responses is well established (Coulthard et al. 2009; Schieven 2005, 2009). However, recently, several lines of evidence suggest that p38 also negatively regulates cell cycle progression and plays a crucial role in replicative senescence (Davis et al. 2010; Han and Sun 2007; Maruyama et al. 2009) and in SIPS induced by overexpression of oncogenes, oxidative stress and inappropriate culture conditions (Chen and Ames 1994; Han and Sun 2007; Ishikawa 2006). It was suggested that p38 is activated not directly by the initial stimuli, but in response to unidentified cellular conditions caused by these stimuli. Importantly, this p38-activating condition appears to be defined quantitatively as a sum of continuous and low-level stresses and remains even after the initial stimuli are withdrawn (Passos et al. 2010). As previously discussed, overexpression of oncogenic Ras has been reported to promote cell proliferation in transformed cell lines but to induce premature senescence in normal primary cells (Lin et al. 1998). Inhibition of p38 by the inhibitor SB203580 (see section 1.6.1.1) or by expression of a dominant-negative mutant of MKK3 or MKK6 abrogated Ras-induced premature senescence, suggesting that Ras-induced premature senescence requires activation of the p38 pathway (Iwasa et al. 2003; Wang et al. 2002). Moreover, constitutive activation of p38 by expression of an active mutant of MKK3 or MKK6 is shown to induce premature senescence in primary human fibroblasts (Iwasa et al. 2003; Wang et al. 2002). Similarly, the depletion or inactivation of Wip1 phosphatase, a p53-regulated gene product that suppresses p38 activity (Takekawa et al. 2000), is shown to activate the p38 pathway causing cells to enter premature senescence (Bulavin et al. 2004; Iwasa et al. 2003; Wang et al. 2002). In addition, inhibition of p38 activity by SB203580 is shown to increase the lifespan and rescue the senescent-like phenotype of fibroblasts from individuals with WS (Davis et al. 2005; Davis et al. 2006) (see Appendix A). These findings demonstrate that the p38 pathway plays a crucial role in inducing SIPS. In addition, treatment of WI38 cells with SB203580 has been shown to increase the growth rate and lifespan of cells that were almost senescent, but has no effect on young cells (Iwasa et al. 2003), suggesting that shortened

telomeres in cells approaching replicative senescence may provide a stress signal in addition to the telomere-driven p53 activating signal. Support for this theory comes from the finding that PD-matched cells that have been immortalised by hTert expression, show a reduction in activated p38 levels (Iwasa et al. 2003).

1.6 Methodologies and choices

The techniques chosen were considered to be the best options given the problems of temporal heterogeneity, asynchronous events, differences in stages of the cell cycle that can lead to subset responses, differences in senescence commitment and variations in pharmacokinetic and pharmacodynamic responses of inhibitors:

1 *Cell Growth Analysis* by taking cell counts at each subculture giving the population doubling (PD) allows analysis of the variations in growth rate throughout the lifespan of a culture (Frisa and Jacobberger 2010).

2 *Flow Cytometric Analysis* with the advantages of rapid assessment of cell cycle dynamics in large population samples (~10,000 cells analysed).

3 *Live cell Imaging and Time-Lapse* with the advantage of allowing morphological and time dependent single cell analysis of adherent cell populations. Time-lapse has the advantage that each acquisition setting can be applied as a function of time, thus providing moving videos of visual events (such as mitoses) within the monitored cell population.

1.6.1 Studying p38 pathway: Use of selective inhibitors

Small cell-permeable inhibitors of protein kinases have become invaluable reagents with which to investigate the physiological roles of protein kinases, because they can be used simply and rapidly to block endogenous kinase activity in normal cells and tissues, as well as transformed cell lines. Since the initial discovery in 1994 of p38 as the molecular target for a novel class of cytokine suppressive inhibitors (Lee et al. 1994), hundreds of p38 inhibitors have been developed. These compounds are thought to be promising therapeutic tools in the

treatment of inflammatory diseases and as such several compounds have progressed to clinical trials and have dropped but for various reasons. More recently, there have been some positive phase II trials in inflammatory diseases such as rheumatoid arthritis and psoriasis (Lee and Dominguez 2005; Regan et al. 2003).

The majority of small-molecule inhibitors of p38 target the ATP binding site (Lee and Dominguez 2005) (Figure 1.5). p38α has a classical bi-lobar structure wherein the ATP binding site consists of a flexible P-loop, a hinge region (connecting the lobes) and a substrate-binding groove designed to accommodate protein substrates for phosphorylation. X-ray crystallographic structures of p38 and other kinases co-complexed with ATP suggest that bound ATP forms hydrogen bonds to His-107 and Met-109 at the hinge region. In addition, highly conserved residues such as Lys-53, Glu-71, and Asp-168, in concert with metal ions, are most likely involved in the coordination of the triphosphate group (Figure 1.5A). All of the potent p38α inhibitors to date fill an additional non-polar pocket known as the gatekeeper pocket, which mediates ligand binding. In p38α, the important residue is a relatively small amphiphilic threonine (Thr-106). Conversely, both p38γ and p38δ possess a larger methionine residue at the same position in the ATP binding pocket that prevents inhibitor binding (Cuenda and Rousseau 2007; Lee and Dominguez 2005). It is reported that the molecular basis for the specificity of the p38 inhibitors is attributed largely to Thr-106 in p38α, and that Met-109 contributes to increased binding affinity for imidazole-based inhibitors (Lisnock et al. 1998).

While there have been several reviews of p38 inhibitors (Lee et al. 1999; Lee and Dominguez 2005; Lisnock et al. 1998), this section will focus on three inhibitors, SB203580, BIRB796 and VX-745, and their relevant binding interactions with p38.

1.6.1.1 SB203580

The first p38 inhibitor to be released was SB203580, published by SmithKline & French in 1994, and is classified as a pyrimidinyl imidazole inhibitor (Lee et al. 1994). Since its discovery, SB203580 has been used widely to elucidate

the role of p38 in various physiological processes (Lee et al. 1999; Lee et al. 1994). The basis of inhibition was revealed by the crystal structure of p38α bound to SB203580. These studies showed that SB203580 contains an aryl ring that functions to fill the gatekeeper pocket and a heterocyclic aromatic ring that serves to form the critical hydrogen bond with the Met-109 linker residue. While bound to p38, SB203580 adopts a three-dimensional shape that is analogous to that of a teardrop, in which the aromatic ring filling the gatekeeper pocket forms the teardrop apex and the remainder of the inhibitor sits in the adenosine pocket and forms the large convex base of the teardrop (Figure 1.5B) (Lee and Dominguez 2005). In addition, the gatekeeper residue (Thr-106) in the hinge of the p38α ATP-binding pocket interacts with a fluorine atom in the SB203580 structure. This orients the drug to interact with His-107 and Leu-108 of the pocket, preventing ATP binding and thereby, specifically inhibiting p38 enzymatic activity (Eyers et al. 1998; Gum et al. 1998). Interestingly, studies show that treatment with SB203580 has no effect on Thr-180 and Tyr-182 phosphorylation, and hence activation of p38 *in vivo*. SB203580, however, potently inhibits the activity of p38 as demonstrated by the inhibition of activation of MK2 and HSP27, specific physiological substrates of p38. These data clearly indicate that SB203580 specifically inhibits the activity of p38 but not its activation by upstream MKKs (Kumar et al. 1999).

SB203580 has been reported to inhibit JNKs, as well as p38, and some additional targets in the epidermal growth factor receptor pathway were identified (Mayer and Callahan 2006). SB203580 has been shown to inhibit GAK (cyclin G-associated kinase) and CK1 (casein kinase) with similar potency to p38 and RIP2 (receptor-interacting protein 2) with even greater potency (Godl et al. 2003). In addition, SB203580 inhibits c-Raf (Hall-Jackson et al. 1999) and GSK3 *in vitro*, albeit less strongly, and inhibits the formation of ZMP (aminoimidazole-4-carboxamide-1-β-D-ribofuranoside monophosphate), an activator of AMPK, from its inactive precursor AICAR (aminoimidazole-4-carboxamide-1-β-D-ribofuranoside), probably by inhibiting adenosine transporters (Fryer et al. 2002). Thus there is a danger that the observed effects of SB203580 on cells result from the inhibition of a target(s) distinct from p38α/p38β MAPKs. Mechanistic studies with SB203580,

therefore, must be interpreted carefully and even repeated with more selective compounds.

1.6.1.2 BIRB796

A second p38 inhibitor, BIRB796, was developed by Boehringer Ingelheim and is a more potent inhibitor of human p38α and p38β than SB203580 (Pargellis et al. 2002). It is a member of the pyrazole-naphthyl urea class of p38 inhibitors. These compounds interact with p38α in a manner distinct from that exhibited by SB203580, in which binding induces a slow conformational change that locks the kinase into an inactive conformation (Bain et al. 2007; Pargellis et al. 2002). This is achieved by binding of another allosteric binding pocket on the kinase that is spatially distinct from the ATP pocket that allows a large conformational change in the conserved DFG (Asp168-Phe169-Gly170 in p38α) motif of the kinase activation loop (extended binding mode) (Pargellis et al. 2002). In all of the known protein Ser/Thr kinase structures, the DFG motif assumes a conformation with the Phe residue buried in a hydrophobic pocket in the groove between the two lobes of the kinase (DFG-in conformation). When bound to BIRB796, however, the Phe side chain moves to a new position (DFG-out conformation) revealing a large hydrophobic pocket in the kinase (Pargellis et al. 2002). Subsequently, the vacated Phe pocket is filled with the *t*-butyl group of the inhibitor (Regan et al. 2003). Figure 1.5C graphically depicts key interactions made between BIRB796 and p38.

The selectivity of BIRB796 for p38α is high. In contrast to SB203580, BIRB796 does not inhibit CK1δ, GSK3β, RIP2 or GAK *in vitro* (Bain et al. 2007). However, unlike SB203580, BIRB796 also inhibits p38γ, p38δ and JNK2α2. Although BIRB796 is a potent inhibitor of JNK2 in vitro, it does not affect the phosphorylation of JNK substrates (c-Jun and ATF2) in cells at the low (0.1 µM) concentration that abolishes p38α activity in cells (Bain et al. 2007). This is probably due to the fact the JNK1 is the dominant isoform that phosphorylates c-Jun and activates the AP1 transcription factor in cells that have been studied (Jaeschke et al. 2006). In conclusion, some reports recommend using SB203580

and BIRB796 in parallel to assess the physiological roles of p38 in cell-based assays (Bain et al. 2007).

1.6.1.3 VX745

In 1999, Vertex Pharmaceuticals disclosed a new class of p38α, ATP competitive inhibitors, including the clinical candidate VX745 (Natarajan and Doherty 2005). This compound displayed potent activity at 5.0 nM concentration and 1000-fold selectivity for p38 over closely related kinases, including ERK1, JNK1-3 and MK2, adopting a linear rather than a teardrop or extended binding mode (Figure 1.5D) (Lee and Dominguez 2005). Since VX745 does not inhibit JNKs this compound can be used in parallel with SB203580 and BIRB796 to assess the role of p38 whilst reducing the issue of off-target effects.
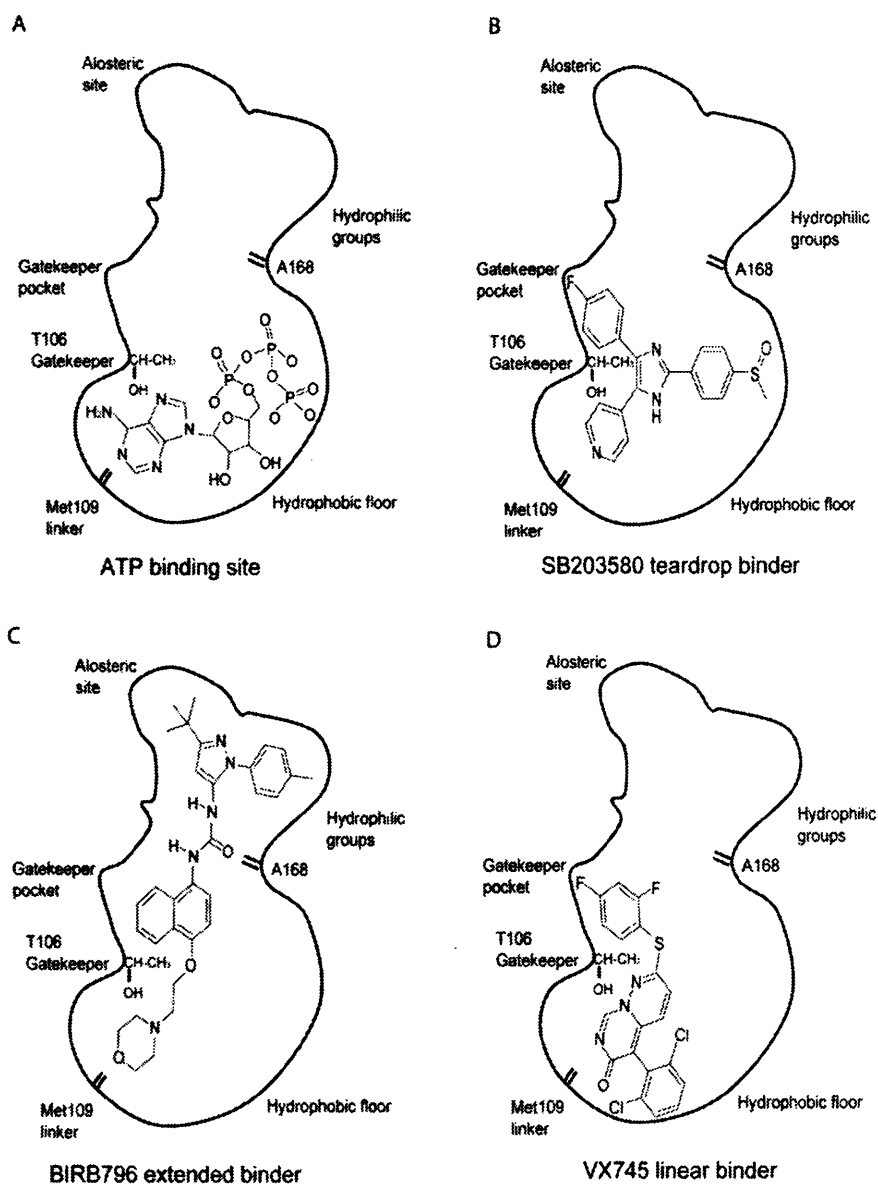
Figure 1.5. Schematic representation of ATP-binding site of p38 protein and binding mode of p38 inhibitors.

(A) shows the binding of ATP (B) SB203580, (C) BIRB796 and (D) VX745 and their different binding modes.

1.7 Rationale and Aims

- The thesis is based on a background of evidence that WS cells show evidence of SIPS, including reduced proliferative potential, senescent-like morphology and activation of p38. The hypothesis here is that other cells with underlying GI may trigger a common pathway leading to SIPS – namely the p38 pathway. **The primary aim of this thesis is therefore to assess the potential impact of SIPS in a panel of cells derived from individuals with defined genetically determined conditions associated with genomic instability.** In terms of a contribution to knowledge, addressing such complexity should improve our understanding of the nature of senescence barrier operation in premature ageing and possibly the breaching of senescence barriers at early stages of neoplasia.

- The approach adopted is to employ both primary and hTert-immortalised GI syndrome cells to determine whether these show evidence of differences in the level of commitment to cell cycle exit compared to normal fibroblasts. The focus of the project was to reveal the impact of exposure to p38 inhibitors in the modulation of replicative potential. Thus the study draws upon a panel of GI syndrome cells, in which normal DNA replication may be disrupted and genome integrity compromised. Accordingly GI panel cells provide an opportunity to study the effects of p38 inhibition on replicative potential.

- The Introduction outlines the known *in vitro* and/or *in vivo* characteristics for human conditions that present evidence of premature aging and aspects of GI. Whilst much attention has been given to the mutational consequences of the molecular defects in GI syndrome cells, there is little information in the literature about the cellular responses to ongoing GI in these cells. Furthermore, the evidence of a restriction of replicative potential in GI syndrome cells is limited. Taking the paradigm of Werner Syndrome, it was hypothesized that human disorders presenting evidence of progeroid characteristics and/or evidence of

underlying GI, may also present common features for the limitation of replicative potential. Therefore there is a need to determine whether GI cells express significant limitations on their replicative potential *in vitro*.

- The concept brought to this thesis is that there is a hierarchy of influences that result in the limitation of lifespan. The driving principle is that of ongoing telomere attrition. However, given current evidence there appears to be a role for SIPS in GI cells. It appears that ongoing disturbances in replication related pathways are modified in GI cells and therefore provide additional routes to increase the likelihood of cell cycle exit. The contribution of these pathways may be additive or perhaps synergistic to the telomere-driven limitations on *in vitro* lifespan. The population dynamics model for the impact of SIPS is outlined in Figure 1.6. This model assumes that SIPS is realised through a finite probability of cell cycle exit exercised pre- or post-mitosis, although it is unknown whether daughter cells show similar characteristics for future cell cycle exit. The timing and probability of cell cycle exit clearly generates complexity and heterogeneity in populations progressing to senescence and a challenge for attempts to determine the impact of ongoing GI at any given stage in that process.

- The working hypothesis, based on previous studies highlighted in the Introduction, is that underlying stress signalling – arising from ongoing replicative stress - could drive p38-dependent signalling in the active restriction of replicative potential at the population level. The model for the potential p38-mediated restraint on cell cycle progression and replicative potential in cells responding to genomic stress is outlined in Figure 1.7. This model proposes that replicative stress can arise from extrinsic factors (such as DNA damage induced by genotoxic agents), telomere uncapping at senescence, or an increase in replication errors associated with DNA repair defects (as seen in GI syndromes) and is realised by the activation of stress response pathways. Furthermore, the activation of stress response pathways is likely to restrain cell cycle progression and increase the probability of cell cycle exit. Thus, it was

proposed that there could be common roles for p38 in GI syndrome cells in restraining replicative potential and that their relative contribution within a given GI cell strain could be revealed by the degree of responsiveness to p38 inhibition.
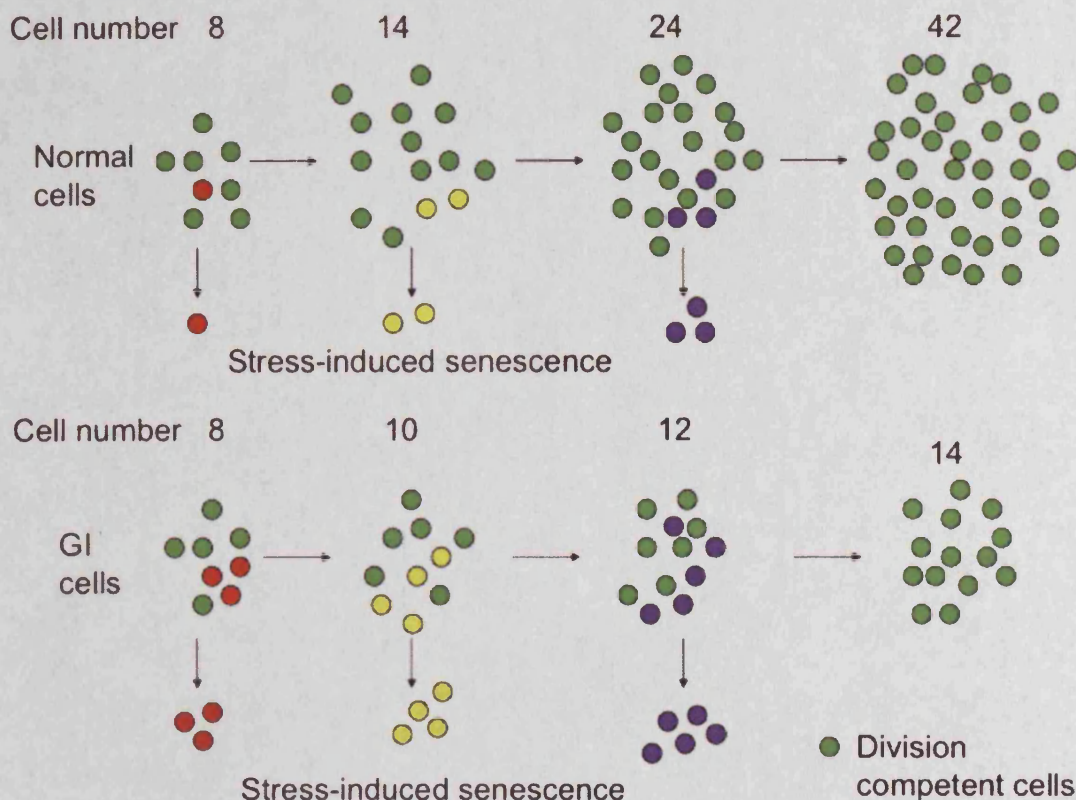
Figure 1.6. Population dynamics model for the impact of SIPS.

This model assumes that a cell in a given population has a small probability of undergoing SIPS at each cell division. In the model the green circles represent division competent cells that at the end of their replicative lifespan senesce and adopt an altered morphology. The other colours represent cells that undergo premature senescence at each division. For normal cells in culture, the majority of cells are division competent and the degree of premature senescence is low, thus after three divisions a colony of 48 cells, containing 42 division competent cells and 6 cells that have undergone SIPS, is produced. For GI syndrome cells however, this model predicts that the level of SIPS is much greater, thus after three divisions a colony of only 26 cells, containing 14 division competent and 12 cells that have undergone SIPS, is produced. Thus simply by increasing the rate of SIPS the model produces a much-reduced replicative capacity and a reduced growth rate.

Inducers of genomic stress
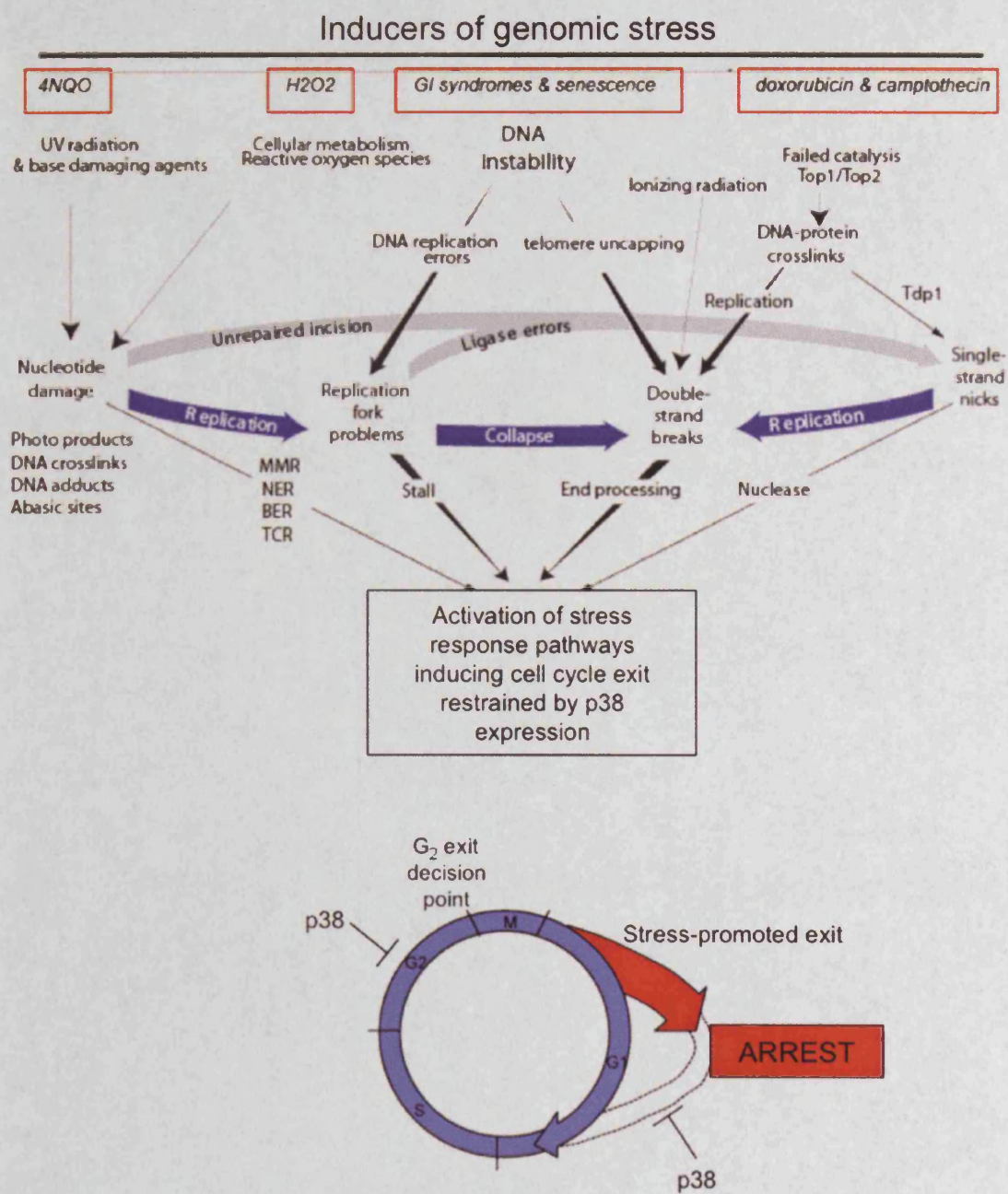
Figure 1.7. Model for the potential p38-mediated restraint on cell cycle progression and replicative potential in cells responding to genomic stress.

60

To examine the hypotheses the following studies were undertaken:

- As a fundamental basis for the thesis, the growth patterns and replicative potential of primary fibroblasts from normal and GI syndrome individuals were measured to determine the prevailing limitations on proliferation in cells with different genetic backgrounds (Chapter 3). Given the extended period over which studies needed to be undertaken the pragmatic decision was made to simultaneously determine the impact of different p38 inhibitors on the growth potential of primary cells. **Here the aim was to investigate whether there is a commonality of involvement of p38-driven pathways in limiting replicative potential.**

- It was recognised that there is an ongoing need to identify morphological biomarkers for SIPS, with recent findings suggesting that changes in morphology and stress fibre presentation as shown by cells undergoing lifespan limitation. The potential of such biomarkers for use in correlative studies on the impact of inhibitors was assessed (Chapter 4). **The aim was to assess morphological changes and stress fibre presentation in primary cells as candidate biomarkers for the extent of commitment to SIPS was made – a unique study given the range of disorders investigated.**

- A significant activity was to undertake the establishment of a new resource (Chapter 5). **The aim was to generate a panel of hTert-immortalised cells in which lifespan was not limited that could be used in more extensive studies.** Pragmatically, this effort addressed the problems associated with working with primary fibroblasts that have a limited replicative lifespan, by removing the restriction on generating sufficient cell numbers for various analyses. Conceptually, the removal of the stress signals arising from telomere attrition also allows for an analysis of the role of SIPS and the functionality of p38 in these cells without the background of stress signals leading to replicative senescence.

- Having established the hTert panel, **the aim was to determine the limitations on replicative lifespan in these cells**. The approach was to identify common features of lifespan limitation by screening the entire hTert panel and to use individual strains of interest to identify specific differences in lifespan limitation. Here flow cytometry and colony forming assays were undertaken to:

  o Test whether hTert-immortalised cells remain susceptible to SIPS. Here GI cell strains are exposed to a range of genotoxic agents, that are known to induce SIPS, and evidence of cell cycle arrest and reduced colony forming ability is assessed (Chapter 6).

  o Reveal any differences in cell cycle dynamics between members of the GI panel, with a particular focus on identifying evidence of cell cycle arrest, and the impact of p38 inhibition on these dynamics (Chapter 7).

  o Assess the impact of potential differences in the level of SIPS on the colony-forming ability, as a monitor of lineage viability and proliferation, of the GI panel members and whether these parameters can be modulated by p38 inhibition (Chapter 7).

The topics in the following chapters are given a brief introduction and materials and methods specific to the techniques used are provided within those chapters. Tables and figures are provided at the end of each chapter for ease of reference. The final chapter (Chapter 9) addresses hypotheses generated during the course of the study.

Chapter 2   Materials and Methods

All general chemicals were purchased from Fisher (Leicestershire, UK) and all molecular biology grade chemicals and reagents obtained from Sigma® (chemical Co., Dorset, UK) or Invitrogen™ (Paisley, UK) unless otherwise stated. Water was prepared by reverse osmosis (Millipore).

2.1 Cell Strains and Routine Culture Conditions

All cells were grown as monolayer cultures in either T25cm^2 flasks to which 3 ml medium was added, or T75cm^2 flasks to which 10 ml medium was added (Becton Dickinson) and maintained in a humidified incubator at 37°C, 20% O_2 and 5% CO_2. All cells were cultured in Eagle's minimum essential medium with Earle's salts (EMEM; Gibco) supplemented with 10% foetal calf serum (FCS; Autogen Bioclear), 1X MEM non-essential amino acids (NEAA) without L-glutamine (Sigma®), 2mM MEM L-glutamine (Invitrogen™), 0.002% $NaHCO_3$ (Invitrogen™), 1M NaOH, 1X vitamins (Invitrogen™), 1 mM sodium pyruvate (Sigma®) and 10,000U/ml penicillin (Sigma®) and 10mg/ml streptomycin (Sigma®). Medium was prepared to the correct concentration with autoclaved milliQ H_2O. For drug treatments, cells were fed daily with medium containing 2.5µM SB203580 (Tocris Chemical Co. Bristol, U.K), 2.5µM BIRB796 or 0.5µM VX745 (both produced 'in-house' as part of a BBSRC funded project: Bagley et al 2006; Bagley et al 2007), dissolved in dimethyl sulphoxide (DMSO). Control cells were supplemented with an equivalent volume of DMSO, added to the medium. p38 inhibitor concentrations were chose based on previous studies (see Appendix B).

Fibroblasts were sub-cultured close to confluence (~80-90%). Briefly, the medium was removed, cells washed with a mixture of 0.05% Trypsin; 0.2% EDTA (Invitrogen™) to remove any residual medium, this was then discarded and 1ml of fresh trypsin/EDTA was added. The cells were incubated at 37°C for approximately 5 minutes, or until the cells had visibly detached. 9 ml of fresh medium was added and cells were transferred to a 15 ml Falcon tube (Becton Dickinson). To determine total cell numbers, 10 µl of the cell suspension was added to a haemocytometer,

cell counts were taken, and the number of cells per ml was calculated. Cumulative PDs were calculated according to the formula: $PD=\log(N_t/N_0)/\log 2$, where N_t is the number of cells counted and N_0 is the number of cells seeded. The number of population doublings (PDs) for each passage (P) was calculated from the cell count by comparing the total cell count following trypsinisation with the initial number of cells seeded. For routine passaging of cells, fibroblasts were reseeded into a fresh T25cm^2 flask at a density of 6×10^4/flask.

At each passage, excess cells were cryo-stored in liquid nitrogen for future use. Briefly, cells were centrifuged at 90 x g for 5 minutes at room temperature in a Centaur 2 centrifuge (Sanyo). The supernatant was discarded and the cell pellet was re-suspended in 0.5 ml culture medium before mixing with 0.5 ml of freezing mix (1:4 FCS:DMSO), thus permitting the cryopreservation of cell cultures. The cell suspension was transferred to a freezing CryoTube™ (Nunc™, Denmark) and stored at -80°C in a storage box containing isopropanol for a minimum of 2 hours to reduce the temperature by 1°C/min over 120 minutes to a final temperature of -80°C, before transferring the ampoule to liquid nitrogen. When recovering viable cell cultures from liquid nitrogen, the ampoule was rapidly thawed in a 37°C sterile water bath. Once thawed, the cell suspension was transferred to a 15 ml Falcon tube and 9 ml of warm (~37°C) medium was added in a drop-wise manner. The cell suspension was centrifuged at 90 x g for 5 minutes at room temperature and the pellet resuspended in fresh culture medium.

Table 2.1. Cell Strains

Syndrome	Strain	Donor Age	P*	PD	Mutation	Reference
Normal	AG16409	12	2	4	Donor is clinically normal	
Normal	AG06234	17	7	15	Donor is clinically normal	Mendonsa et al 2008; Cristofalo et al 1998
Normal	AG013152	80	5	6	Donor is clinically normal	Kipling 2008; Cristofalo et al 1998
RTS	AG18371	12			Donor is homozygous for a truncating mutation in the RECQL4 gene: an 11 bp deletion at nucleotide g.2746 (g.2746del11) in intron 8 which results in an intron that is too short to be efficiently spliced.	Petkovic et al 2005
RTS	AG18375	22			Donor is a compound heterozygote; in allele one at nucleotide g.2626 there is a G>A substitution (g.2626G>A) in exon 8 of the RECQL4 gene which leads to disrupted splicing; in allele two there is a 1 bp deletion at g.2886 (g.2886delT) in exon 9 of the RECQL4 gene which leads to a truncation.	Wang et al 2003; Lindor et al 2000
RTS	AG17524	4			Donor is a compound heterozygote; both alleles carry truncating mutations in the RECQL4 gene: allele one carries a G>A substitution at g.2626 (g.2626G>A) in exon 8 resulting in alternative splicing; allele two carries a 2 bp deletion at g.4644delAT in exon 15 resulting in a frameshift; in addition, there are three mutations which result in amino acid changes: a homozygous substitution at g.1551G>T in exon 5 resulting in an amino acid change GLU267ASP (E267D), a heterozygous substitution at g.4470G>A in exon 14 resulting in an amino acid change GLU>ASP (E>D), and a homozygous substitution at g.5321G>A in exon 17 resulting in an amino acid change ARG1005GLN (R1005Q); there was one silent homozygous mutation at nucleotide g.1488C>T in exon 5 resulting in no change S246S.	
BS	GM02520	10	11		Donor is a compound heterozygote: one allele has a deletion at nucleotide 2923 of the RECQL3 gene [2923delC] resulting in a frameshift [fs:974+23-X] and a second allele has a deletion of exon 15 resulting in a frameshift [fs:941+26-X].	Trikka et al 2002; Lu et al 1993
BS	GM02548	6	8		Donor is a compound heterozygote: one allele has a 1-bp insertion at nucleotide 1544 of the RECQL3 gene [1544insA] resulting in a frameshift and premature termination [fs:514+1-X] and a second allele has a C>T transition at nucleotide 2328 of the RECQL3 g	Lu et al 1993; Warren et al 1981
BS	GM02932	28	6		Donor is homozygous for a 6-bp deletion/7-bp insertion [6-bp del/7-bp ins] at nucleotide 2,281 of the open reading frame of the RECQL3 gene, which results in a frameshift and a stop codon	Schawalder et al 2003; Collister et al 1998
HGPS	AG10677	4	11	6	Donor has a Glu-to-Lys substitution at codon 145 [Glu145Lys (E145K)] in exon 2 of the Lamin A gene (LMNA).	Bridger and Kill 2004; Eriksson et al 2003
HGPS	AG11498	14	6	10	Donor has a de novo single base substitution, a C>T change at nucleotide 2036 (2036C>T), which results in a silent change at codon 608 [Gly608Gly (G608G)] in exon 11 of the Lamin A gene (LMNA).	Moulson et al 2007; Scaffidi and Misteli 2005
HGPS	AG01972	14	11		Donor has a de novo single base substitution, a C>T change at nucleotide 2036 (2036C>T), which results in a silent change at codon 608 [Gly608Gly (G608G)] in exon 11 of the Lamin A gene (LMNA).	Moulson et al 2007; Scaffidi and Misteli 2006; Huang et al 2005

65

Table 2.1 continued. Cell Strains

Syndrome	Strain	Donor Age (yr)	P*	PD	Mutation	Reference
NBS	RO202					Der Kaloustian 1996
NBS	RO242					Der Kaloustian 1996
NBS	GM07166	20	10	6	Donor is homozygous for a deletion of 5 nucleotides in exon 6 of the NBS1 gene, resulting in a frameshift and a premature termination at codon 218 [657-661delACAAA (657del5)].	Alt et al 2005; Nove et al 1986
LIG4	GM17523	10	10		Donor is a compound heterozygote: one allele carries a G-to-A transition at nucleotide 1406 (1406C>A) of the LIG4 gene resulting in a gly469-toglu substitution (GLY469GLU; the other allele has a C-to-T transition at nucleotide 2440 (2440C>T, resulting in a nonsense codon at amino acid 814 [ARG814TER (R814X)].	Muylaert et al 2007; O'Driscoll et al 2001
LIG4	GM16088	15			Donor carries an Arg278 to His mutation in the LIG4 gene [ARG278HIS (R278H)], resulting from a G-to-A transition at nucleotide 833 (833G>A).	Al Rashid et al 2005
CSA	GM01856	13	7		Donor is CS3BE; complementation group A.	Ridley et al 2004; Andrews et al 1978
DKC	GM01774	7	7	7	Donor is hemizygous for an in frame 3 bp deletion of nucleotides 201_203 of the DKC1 gene (201_203delCTT) resulting in the deletion of leucine at position 37 [Leu37del].	Agarwal et al 2010; Wong et al 2006
SS	GM09812	15	5		Donor is clinically affected but the mutation has not been confirmed.	
SS	GM18366	6	15		Donor carries a mutation at nucleotide 2101A>G, which causes increased levels of skipping exon 9 and activation of two cryptic splicing events from sites in exon 9 leading to termination in exon 10. Splicing of exon 9 is inefficient in mutant cells, but a small amount of correctly spliced mRNA is observed. Cells showed a low level of expression of the ATR protein.	Stokes et ah 2007
WS	AG03141	30	8	6	The donor had features of premature aging, pigmented and atrophic skin, cataracts and hyperlipidemia type V. The biopsy was taken ante-mortem on 9/20/78. The culture was initiated using explants of minced skin tissue. The cell morphology is fibroblast-like. The karyotype is 46,XX with 80% of cells examined showing random chromosomal abnormalities. Homozygous for a C to T transition at nucleotide 2476 in the WRN gene (2476C>T), resulting in a stop codon at 748 {Gln748TER (Q748X)}.	Li et al 2008, Kipling et al 2008, Faragher et al 1993

All cell strains were obtained from Coriell Cell Repositories (Camden, New Jersey), unless otherwise stated (Note AG = NIA; GM = NIGMS).

*P refers to passage information provided by the repository

2.1.1 p38 Inhibitors

2.1.1.1 SB203580
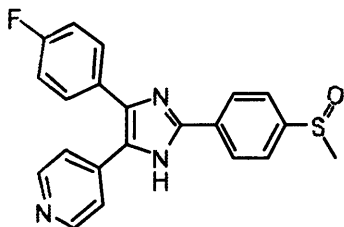
Figure 2.1. Chemical structure of SB203580.

(4-(4-Fluorophenyl)-2-(4-methylsulfonylphenyl)-5-(4-pyridyl)-1H-imidazole) was obtained from Tocris Chemical Co. Bristol, U.K (Lee et al. 1994).

2.1.1.2 BIRB796
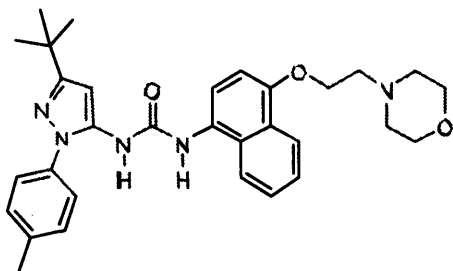
Figure 2.2. Chemical structure of BIRB796.

(1-[3-tert-Butyl-1-p-tolyl-1H-pyrazol-5-yl]-3-[4-(2-morpholin-4-yl-ethoxy)naphthalen-1-yl]urea) was produced 'in-house' as part of a BBSRC funded project (Bagley et al. 2006).

2.1.1.3 VX745
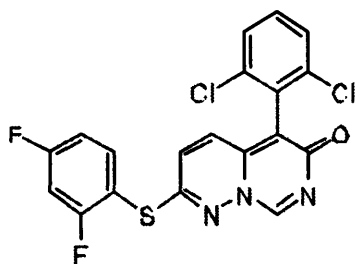
Figure 2.3. Chemical structure of VX745.

(5-(2,6-Dichlorophenyl)-2-(2,4-difluorophenylthio)-6H-pyrimido[1,6-b]pyridazin-6-one) was produced 'in-house' as part of a BBSRC funded project (Bagley et al. 2007)

2.2 Phalloidin-FITC Staining of Stress Fibres

Actin staining for fluorescence microscopy was performed essentially as previously described (Huot et al. 1997) and specific details are given in chapter 3 material and methods. Imaging was performed as described in section 2.9.1.

2.3 Western Blotting

2.3.1 Reagents

1X ELISA lysis buffer:	20 mM Tris (pH7.5), 150 mM NaCl, 1 mM EDTA, 1 mM EGTA, 1% (v/v) Triton X-100, 2.5 mM sodium pyrophosphate, 1 mM β–glycerolphosphate, 1 mM Na_3VO_4, 1 μg/ml leupeptin (#9803, Cell Signaling®). Made by diluting 10X stock with MilliQ H_2O.
3X loading buffer:	50 mM Tris (pH 6.8), 30% (v/v) glycerol, 3% (w/v) SDS, 0.6% (w/v) bromophenol blue and 0.3% (v/v) β-mercaptoethanol.
5X running buffer:	124 mM Tris base, 250 mM glycine and 5% SDS, pH 8.3
1X transfer buffer:	25 mM Tris base, 192 mM glycine, 200 ml methanol, made up to 1 litre with water, pH 8.1-8.4
Stacking Gel:	10% acrylamide:bis (29:1), 0.5 M Tris (pH 6.8), 10% SDS, 10% APS and 100 μl TEMED.
Resolving Gel:	4% acrylamide:bis (29:1), 1.5 M Tris (pH 8.8), 10% SDS, 10% APS and TEMED.

2.3.2 Sample Preparation and Protein Extraction

Fibroblasts were seeded in 100 mm Petri dishes at a density of ~1x10^6 cells/dish and maintained under routine culture conditions for 1-3 days prior to protein extraction. Sub-confluent (~80-90% confluence) cell monolayers were

washed twice with ice-cold, sterile 1X PBS to remove residual media. The PBS was removed and ~100 μl 1X ELISA lysis buffer supplemented with 100 mM PMSF (Sigma®) was added to the dishes. Cells were incubated in lysis buffer on ice for 5 minutes. The cells were then scraped into the 1X ELISA lysis buffer and transferred to an Eppendorf tube. Whole cell extracts (WCEs) were centrifuged at 20,000 rpm for 15 minutes at 4°C in a refrigerated Falcon 6/300 (Sanyo). Following centrifugation, the supernatant was removed, transferred to a fresh Eppendorf tube and stored at -80°C.

2.3.3 Protein Quantification

WCEs lysates were quantified by the Bradford colorimetric method, using the Coomassie® Plus Protein Assay Reagent (Pierce). ELISA lysis buffer, previously used to obtain the WCEs, was diluted 1/10 with sterile water and used to prepare a series of BSA standards with final concentrations in the range of 0-400 μg/ml. A 1/10 dilution of each WCE was prepared by adding 5 μl of WCE to 45 μl H_2O. 40 μl of each WCE and BSA standard were transferred to 1.6 ml plastic cuvettes, to which 1 ml of Coomassie Plus Protein Assay Reagent (Pierce) was added. The OD (at 595 nm) of WCEs and BSA standards was determined using an UltraSpec 31000 PRO (Amersham Biosciences) and linear regression analysis of the BSA standards was used to calculate the concentration of protein (μg/μl) present in each WCE.

2.3.4 SDS-PAGE Electrophoresis and Transfer

A Biorad mini-protean II electrophoresis cell system or Biorad Criterion kit (for larger gels) was used to separate and transfer protein lysates to a 0.45 μm nitrocellulose membrane (Millipore). WCEs were electrophoresed on 10 % (w/v) polyacrylamide, SDS resolving gels. Aliquots containing 20 μg of the soluble WCEs were made up to a final volume of 14 μl with sterile water and 7 μl of 3X loading buffer was added to give a final loading volume of 21 μl. The WCEs were denatured at 100°C for 5 minutes and centrifuged for 30 seconds at 12,000 X g before being loaded into the gel. Precision plus protein dual colour standards

(Biorad, Cat 161-0374) were loaded in parallel to confirm the molecular weight of the protein of interest. Protein extracts were electrophoresed and separated at 100 V for ~ 1 hour (or until the dye front reached the bottom of the gel) in 1X running buffer. Following electrophoresis the SDS-PAGE gel was washed and allowed to equilibrate for several minutes in transfer buffer to prevent shrinkage and to remove any contaminating electrophoresis buffer salts and neutralisation salts.

Immediately prior to protein transfer methanol was added to the transfer buffer. The methanol serves two main purposes: it promotes the dissociation of SDS from the protein and improves absorption of proteins onto the membrane. The nitrocellulose membrane was washed in sterile de-ionised water for ~30 seconds and incubated in transfer buffer prior to use to prevent drying and to facilitate equilibration between the transfer buffer and the membrane. The gel/membrane sandwich was assembled in the transfer cassette by placing a piece of filter paper on top of on a fibre pad, followed by the pre-equilibrated gel, followed by the membrane, another piece of filter paper and another fibre pad. The cassette was then placed into the transfer apparatus and the proteins were transferred to the nitrocellulose membrane at 100 V for 1 hour in 1X transfer buffer with an ice block to prevent over-heating.

2.3.5 Immuno-detection

Following protein transfer, nitrocellulose membranes were incubated in Enhanced chemiluminescence (ECL) Advance Blocking Agent (GE Healthcare, Buckinghamshire, UK) according to the manufacturer's guidelines for 1 hour at room temperature to reduce non-specific antibody binding. Membranes were incubated at 4°C overnight on a roller in primary antibody (Table 2.2) diluted in blocking buffer. The nitrocellulose membrane was washed with 0.1 % (v/v) Tween 20 in PBS at room temperature with gentle agitation for 5 minutes, followed by two 5 minute washes and a 15 minute wash with fresh 0.1 % (v/v) Tween 20 in PBS. The membrane was then incubated with the appropriate HRP-conjugated secondary antibody (Table 2.2) diluted in blocking buffer for 1 hour at room temperature and the wash procedure repeated. The protein-antibody complexes

were detected using the Amersham ECL™ Advance Western Blotting Detection kit (GE Healthcare, Buckinghamshire, UK) according to the manufacturer's recommendations. Briefly, ECL Advance Solution A and B were equilibrated at room temperature prior to use and then mixed in a 1:1 ratio. Residual wash buffer was removed from the nitrocellulose membrane and the combined ECL solutions spread to cover the membrane and then left for 5 minutes at room temperature. Any residual reagent was removed from the membrane and proteins were visualised using an AutoChemi System (UVP, Upland, CA, USA) or by exposing the membrane to autoradiography hyperfilm (Amersham Pharmacia Biotech). In the case of the latter method, following exposure, the autoradiography hyperfilm was developed and fixed using an XOGRAPH Compact X4 Automatic X-ray Film Processor (X-Ograph Imaging System, Ltd., Gloucestershire, UK).

Table 2.2. Antibodies used during Western Blot analysis.

Antibody	Supplier	Source	Dilution	2° antibody	Con
p38 MAPK	Cell Signaling (Cat No. 9212)	Rabbit	1/1000	GAR	1/1000
Phospho-p38 (Thr180/Tyr182)	Cell Signaling (Cat No. 9211)	Rabbit	1/1000	GAR	1/1000
HSP27 (G31)	Cell Signaling (Cat No. 2402)	Mouse mAb	1/1000	RAM	1/1000
Phospho-HSP27 (Ser82)	Cell Signaling (Cat No. 2401)	Rabbit	1/1000	GAR	1/1000
SAPK/JNK	Cell Signaling (Cat No. 9252)	Rabbit	1/1000	GAR	1/1000
Phospho-SAPK/JNK (Thr183/Tyr185)	Cell Signaling (Cat No. 4668)	Rabbit	1/1000	GAR	1/1000
Cofilin	Cell Signaling (Cat No. 3312)	Rabbit	1/1000	GAR	1/1000
Phospho-Cofilin (Ser3)	Cell Signaling (Cat No. 3311)	Rabbit	1/1000	GAR	1/1000

Abbreviations: GAR, goat anti-rabbit; RAM, rabbit anti-mouse.

Secondary antibodies are from Amersham ECL kit and are HRP-linked.

2.4 Detection of telomerase Activity by the Telomeric Repeat Amplification Protocol (TRAP) Assay

The TRAPeze® Gel-Based Telomerase Detection Kit (Millipore, UK), which is based on an improved version of the original method described by (Kim et al. 1994), was used to detect telomerase activity. This assay is a one buffer, two enzyme system that utilises the polymerase chain reaction (PCR). In the first step, telomerase adds a number of telomeric repeats (TTAGGG) on the 3' end of a substrate oligonucleotide (TS). In the second step, the extended products are amplified by PCR using the TS and RP (reverse) primers, generating a ladder of products with 6 base increments starting at 50 nucleotides. Amplification products are resolved on a polyacrylamide gel and detected by fluoro-imaging.

2.4.1 Preparation of cell extracts

Wash Buffer:	10 mM HEPES-KOH (pH 7.5), 1.5 mM $MgCl_2$, 10 mM KCl, 1 mM dithiothreitol (DTT), diethylpyrocarbonate (DEPC) water.
Lysis Buffer:	10 mM Tris-HCl (pH 7.5), 1 mM $MgCl_2$, 1 mM EGTA, 0.1 mM Benzamidine, 5 mM β-mercapto ethanol, 0.5% (v/v) 3-([3-cholamidopropyl]-dimethyl-ammonia)-1-propanesulfonate (CHAPS; Pierce), 10% (v/v) glycerol, DEPC water.
1X reaction buffer:	20 mM Tris-HCl (pH 8.3), 1.5 mM $MgCl_2$, 63 mM KCl, 0.005% Tween 20 (v/v), 1 mM EGTA (pH 8), 50 μM dNTP's (Promega), 0.1 mg/ml bovine serum albumin (BSA; Promega). 1X reaction buffer is made by diluting 10X stock in DEPC water.

Polyacrylamide Protean II gel: 45 ml distilled water, 30 ml 5X TBE buffer (54 g Tris base, 27.5 g boric acid and 20 ml 0.5 M EDTA made up to 1 litre with water), 25 ml 19:1 bis acrylamide (BIO-RAD Laboratories, Inc.), 500 µl 100 mg/ml APS and 100 µl TEMED.

50X dNTP Mix: 2.5 mM each dATP, dTTP, dGTP and dCTP

Primer Mix: RP primer, K1 primer and TSK1 template

Exponentially growing hTert-immortalised fibroblast cultures were trypsinised and resuspended in 8 ml of medium and counted. The cells were centrifuged at 277 X g for 5 minutes at room temperature and the medium was discarded. The cell pellets were resuspended and washed in 10 ml of 1X sterile PBS. The cells were centrifuged at 202 X g for 5 minutes at room temperature and the supernatant was aspirated. The pellets were resuspended in 1 ml of 1X PBS and transferred to a 1.5 ml RNase-free Eppendorf tube. The samples were centrifuged at 15,000 X g for 2 minutes at 4°C and the supernatant was discarded. The pellets were stored at -80°C.

The cells were thawed on ice and resuspended in 1 ml of wash buffer. The cell suspension was centrifuged at 15,000 X g for 2 minutes at 4°C and the supernatant aspirated. Cell pellets were resuspended in 20 µl of fresh lysis buffer and incubated on ice for 30 minutes. Lysates were centrifuged at 12,000 X g for 30 minutes at 4°C and supernatants were aliquoted into fresh tubes. The supernatants were snap frozen on dry ice and stored at -80°C. To prepare negative controls (and destroy telomerase activity), the diluted cell lysates were divided into two equal aliquots. One aliquot from each sample was incubated at 85°C for 10 minutes to destroy telomerase activity, and the other aliquot was placed on ice for 10 minutes. Positive control cell extracts [derived from adenovirus transformed human embryonic kidney cells (HEK 293) (Graham et al. 1977)] were prepared by diluting stock aliquots 1:20 with 1X lysis buffer (2 µl/assay). All cell lysates, were thawed on ice, diluted in lysis buffer to give approximately 5000 cell equivalents/µl.

2.4.2 TRAP assay – Stage 1 (extension of TS primer)

A 'Master Mix' containing 50 µl 1X reaction buffer, 1 µl of 50X dNTP mix, 1 µl TS primer (5'-AATCCGTCGAGCAGAGTT-3'), 1 µl TRAP Primer Mix, 1 µl (2 Units) Taq Polymerase and 39.6 µl dH$_2$O was prepared and incubated on ice. 48 µl of the 'Master Mix' was aliquoted into RNase-free PCR tubes to which 2 µl of either heat-treated and non-heat treated cell extracts were added and incubated on ice. Cell extracts were transferred to a GRI MJ Tetrad Thermocycler, and incubated for 30 minutes at 30°C.

2.4.3 TRAP assay – Stage 2 (PCR amplification)

Following the initial extension, PCR amplification was performed at 94°C in a GRI MJ Tetrad Thermocycler. The amplification conditions were 31 cycles of denaturation (92°C, 30 seconds), annealing (50°C, 30 seconds) and extension (72°C, 90 seconds).

Following amplification, 5 µl of loading dye containing bromophenol blue (Sigma®) and xylene cyanol (Sigma®) (0.25% each in 50% glycerol/50 mM EDTA) was added to each sample. 25 µl of each sample was electrophoresed at 400 V on a 10% polyacrylamide 20 cm Protean II gel in a tank containing 1.5X TBE buffer, for approximately 4 hours or until the bromophenol blue electrophoresed to ~3 cm from the bottom of the gel. The gel was incubated in SYBR® Green (Cambridge Bioscience) diluted 1:10,000 in water for 10 minutes at room temperature with agitation. The gel was washed for 5 minutes in water at room temperature to remove excess SYBR® Green. After washing, the gel was scanned on a STORM imager (Amersham Biosciences), employing the blue fluorescence mode.

2.5 Clonogenic assay

Fibroblasts were seeded at 4x10^3 cells in quadruplicate in 10 cm cell culture dishes and were maintained under routine culture conditions for 10 days. Cells were re-fed every 3 days during this period. Following incubation, cells were washed twice with PBS and fixed for 5 minutes with 70 % (v/v) ethanol, and left to

75

air-dry overnight at room temperature. The plates were subsequently stained in Giemsa's solution (pH 6.8; BDH, Poole, Dorset) diluted 1:10 in water for ~30 minutes or until the colonies were visible. The plates were washed with tap water to remove any residual Giemsa solution and colonies were visualised using a light microscope. Colonies with a minimum of 50 cells were scored and plating efficiency was calculated as a percentage of the number of colonies formed compared to the initial number of cells seeded.

2.6 Cell Survival Determination by Colony Forming Assay

Sub-confluent, exponentially growing human fibroblasts were trypsinised from T75 flasks and 4000 cells were seeded in 10 cm culture dishes and allowed to attach for 24 hours under standard culture conditions. Cells were treated with the following DNA damaging agents for 24 hours: Doxorubicin (DOX) at 2.5, 5, 10 and 20 nM; Cisplatin (CisPt) at 1, 1.5, 2 and 12.5 μM; Camptothecin (CPT) at 2.5, 5, 10 and 20 nM; 4-Nitroquinoline 1-oxide (4NQO) at 5, 10, 15 and 20 nM; Hydrogen Peroxide (H_2O_2) at 10, 20, 40 and 80 μM. Following treatment fibroblasts were washed twice with PBS to remove any residual agent, re-fed with fresh growth medium and maintained under routine culture conditions for 10 days. Cells were re-fed every 3 days during this period. Following incubation, cells were fixed and stained as described in section 2.5. Colonies with a minimum of 50 cells were scored unless otherwise stated. Plating efficiency was calculated as a percentage of the number of colonies formed compared to the initial number of cells seeded.

2.7 Flow Cytometry

2.7.1 Cell Cycle Analysis

The general flow cytometric method has been previously described (Smith et al. 2007). Briefly, cells were seeded at a density of 5×10^5 as a monolayer in T75 flasks and allowed to attach for a minimum of 24 hours. Cell monolayers were detached using trypsin and cell numbers were determined using a Coulter counter (Beckman Coulter Z1). Cells were centrifuged at 90 X g for 5 minutes at room temperature in a Centaur 2 centrifuge (Sanyo) and the pellet was re-suspended in

temperature in a Centaur 2 centrifuge (Sanyo) and the pellet was re-suspended in the appropriate volume of fresh medium to give ~5×10^5 cells/ml. Cells were incubated on ice prior to the addition of RNase A (final concentration of 0.5 mg/ml; SIGMA) and Ethidium Bromide (Eb) in Triton X-100 (final concentration of 50 μg/ml cells at 5×10^5; SIGMA) and cells were analysed within 1 hour. The investigational agent CyTRAK Orange™ (Biostatus, Leicestershire, UK) has been used for nuclear versus cytoplasmic discrimination or as a cell location dye to define the perimeter of the cell (www.biostatus.com/product/cytrak_orange/). CyTRAK Orange™ was supplied as an aqueous stock solution of 5 mM and routinely stored at 4°C without freezing and used at 20 μM for all experiments. The standard protocol was to incubate cells with CyTRAK Orange™ for 10-15 minutes at 37°C prior to direct analysis.

For cell cycle profiling, a FACS Vantage flow cytometer (Becton-Dickinson Immunocytometry Systems, San Jose, CA, USA) equipped with a Coherent Enterprise II laser (Coherent, Inc., Santa Clara, CA, USA) simultaneously emitting at multiline UV (351–355 nm range) and 488-nm wavelengths with the beams made noncolinear using dichroic separators, was used. The laser power was regulated at 30 mW (monitored on the multiline UV output). All parameters were collected using CellQuest software (Beckton-Dickinson Immunocytometry Systems, San Jose, CA, USA). Unless stated otherwise data were collected for 1×10^4 events using the FSC parameter as the master signal. Optics used are listed in (Table 2.3).

Table 2.3. Flow cytometry fluorescence optics

	FACS Vantage	
Probe / drug	Excitation (nm)	Parameter & emission filter (nm)
Eb	488	FL2 585 /42
CyTRAK Orange™	488	FL2 585 /42

Data were analysed using CellQuest software (Beckton-Dickinson Immunocytometry Systems, San Jose, CA, USA) or WinMDI (http://facs.scipps.edu/software.html; authored by Dr. J. Trotter, The Scripps Research Institute, California, USA), with forward scatter (FSC), side scatter (SSC) and pulse width gated to exclude any cell debris and/or doublets. Cell cycle analysis was carried out using Cylchred. (www.cardiff.ac.uk/medicine/haematology/cytonetuk/documents/software.html); authored by Dr. T. Hoy, Department of Haematology, Cardiff University; School of Medicine, Cardiff, UK). Cell cycle distributions were determined using an algorithm for the normal distribution of fluorescence intensity profiles for fluorochrome-stained G1 and G2 cells.) Flow data was then exported into spreadsheets for further analysis.

2.8 Immunofluorescence detection of p38 MAPK

Cells were seeded at a density of 2×10^4 on glass coverslips (No 1.5, Fisher) and allowed to attach for 24 hours prior to treatment. Immunofluorescence was performed according to the Cell Signaling Immunofluorescence protocol (www.cellsignal.com/support/protocols/IF.html). Briefly, the medium was removed and cells were fixed in 4% (w/v) paraformaldehyde [made from stock solution of 16% (w/v) diluted in PBS; Thermo Scientific, Rockford, USA, Cat No. 28908] for 30 minutes at room temperature. Cells were washed three times with PBS to removed residual fixative prior to permeabilisation with 0.2% (v/v) Triton X100 in PBS for 20 minutes at 4°C. Coverslips were washed three times before being incubated with blocking buffer [5% (w/v) BSA/PBS] overnight at 4°C. Coverslips were incubated with primary antibody against p38 MAPK (Cell Signaling, Cat No. 9212) at 1/25 dilution [in 0.6% (w/v) BSA/PBS] for 1 hour at room temperature. Coverslips were washed three times in PBS prior to incubation with secondary antibody [Goat Anti-Rabbit IgG (H+L), F(ab')2 Fragment (Alexa Fluor® 488 Conjugate): Invitrogen A-11034], diluted in 0.6% (w/v) BSA/PBS for 1 hour at room temperature in the dark. Coverslips were rinsed a further three times in PBS. To label the nuclei of these cells, the coverslips were incubated with DRAQ5™ (Biostatus, Leicestershire, UK)

for 10 minutes at room temperature in the dark. DRAQ5™ was supplied as an aqueous stock solution of 5 mM and routinely stored at 4°C without freezing and used at 20 μM for all experiments. Coverslips were mounted on glass slides (Thermo Scientific) with ProLong® Gold Antifade Reagent (Invitrogen, Cat No. P36930), sealed with nail varnish and stored at 4°C in the dark prior to analysis. Imaging was performed as described in section 2.9.1.

2.9 Imaging

2.9.1 Fluorescence imaging

Images from fluorescently stained slides were captured using an Axiovert S100 TV microscope (Carl Zeiss, Inc., Welwyn Garden City, UK) with Hamamatsu camera (model C4742-95-12, Hamamatsu Photonics, Welwyn Garden City, UK), fluorescent lamp (model ebx75 isolated, Carl Zeiss, Inc., Welwyn Garden City, UK) and shutter lambda 10-2 (Kinetic Imaging Ltd, Wirral, UK) using suitable filter blocks (Table 2.4). Image analyses were conducted using MetaMorph Offline Version 7 (Molecular Devices, Downingtown, PA, USA).

Table 2.4. Fluorescence filters

Filter	Excitation (nm)	Emission (nm)
Alexa Fluor 488	480 / 30	535 / 40
DAPI	350 / 50	630 / 60
FITC	480 / 30	460 / 50
DRAQ5™	620 / 60	700 / 75

2.9.2 Time-lapse imaging

For live cell imaging of different cell types or treatments over short or long periods of time, time-lapse imaging was used. A standard multi-well culture dish containing the cells was incubated on a stage of a time-lapse instrument as previously described (Errington et al. 2005a; Marquez et al. 2003) (Figure 2.4).

Specific conditions, including drug treatment, cell type, field numbers and time delay, are described in the relevant chapter material and methods.
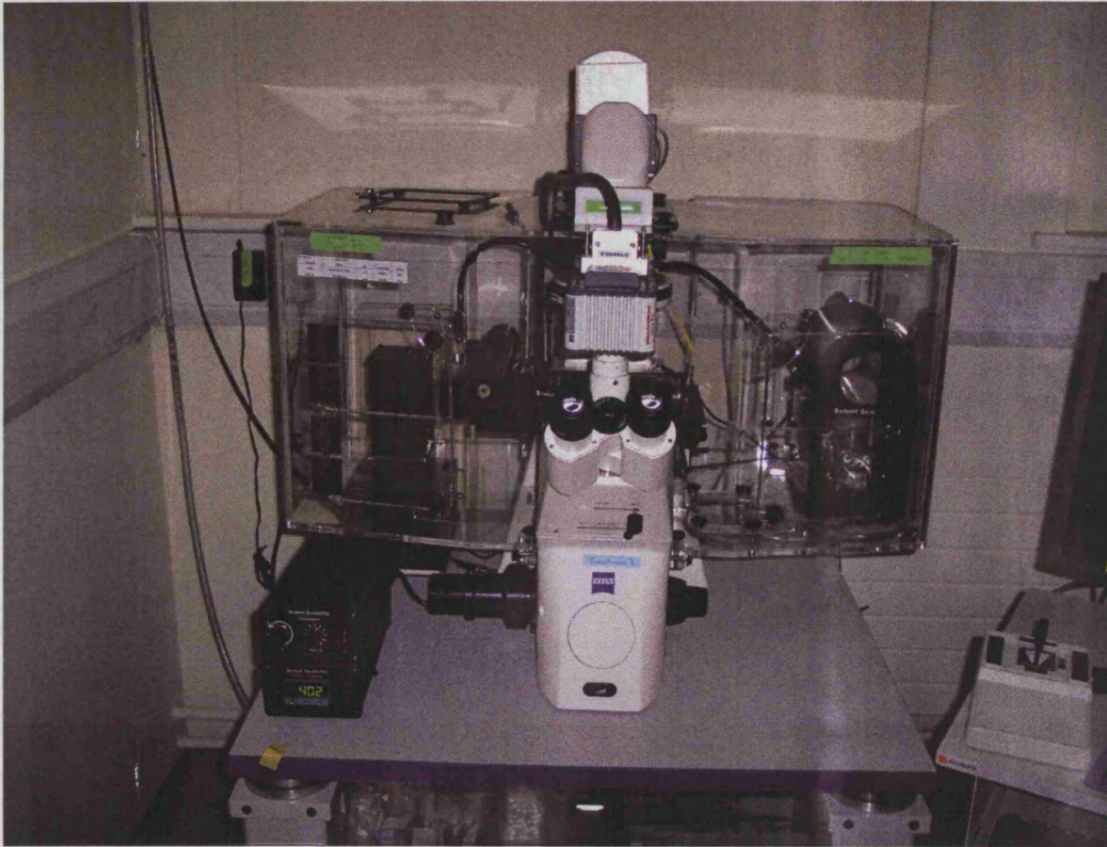
Figure 2.4. Time-lapse instrument

Chapter 3   Replicative Growth Capacity of Adult Dermal Fibroblasts from Normal and GI Syndrome Individuals

3.1 Introduction

Primary mammalian cells have a finite proliferative capacity in culture after which they enter a state of irreversible growth arrest known as senescence (Hayflick 1965; Hayflick and Moorhead 1961). An approach to studying inducers and modifiers of cellular senescence requires the establishment of primary culture models for dermal fibroblasts. It can be considered that senescence of such primary cultures arises from both extrinsic and intrinsic signals, but must eventually be enacted through an exit from the 'normal' cell cycle employing mechanisms of arrest typically realised by cells under different forms of stress (e.g. the appearance and non-resolution of genomic damage). As with all *in vitro* systems it is likely that the culture conditions are suboptimal (e.g. lack of 3-D tissue context) or indeed supra-normal (e.g. frequent use of hyperoxia rather than the limited oxygenation conditions found in tissues). Therefore there is an assumption that cells in culture are attempting to accommodate to *in vitro* conditions and this may be reflected in a degree of engagement of stress response pathways. Further, continual *in vitro* passage characteristically selects for cells with proliferative potential thus imparting heterogeneity to the cell culture at different passage ages. There is mounting evidence that cells also experience considerable levels of endogenous stress (see Introduction) not least a progressive shortening of telomeres realised as a genomic stress response. Telomere attrition is thought to act as a mitotic clock eventually leading to senescence (Harley et al. 1990; Olovnikov 1973) – effectively limiting cellular replicative potential. Several models have been proposed to explain how telomere shortening can lead to cellular senescence. However, it is widely accepted that shortened telomeres are perceived by the cell as DNA damage which triggers a stress response (Vaziri 1997). For example, telomere dysfunction can result in telomeric fusion events that

lead to genomic rearrangements, such as nonreciprocal translocations, thus generating GI (Capper et al. 2007; Gisselsson et al. 2001). In GI syndrome cells it is possible that increased levels of genomic instability also gives rise to replication stress and promotion of senescence. Here the focus is on the growth potential of normal adult dermal fibroblasts against a panel of GI syndromes fibroblasts to identify any unusual growth (kinetic) phenotypes that may be indicative of higher levels of SIPS in these cells.

In the 1970's it was shown that fibroblasts from individuals with WS have a reduced proliferative capacity when compared with control cells from donors of the same age (Martin 1978; Martin et al. 1970). In 1979 Goldstein compared the growth potential of fibroblasts from individuals with WS and progeria (Goldstein 1979). Here the mean lifespan for WS fibroblasts was found to be 6.6 PDs compared to a 50.3 PDs for normal controls (Goldstein 1979). These findings are supported by subsequent studies that also show WS cells to have limited growth potential and reduced growth rates in culture (Faragher et al. 1993; Salk et al. 1981). It has been argued that it is this reduced growth that underlies the accelerated ageing seen in WS (Kipling et al. 2004). Although less is known about the cellular growth potential of the other GI syndromes described here there is evidence to suggest that some display reduced replicative potential. For example, fibroblasts from HGPS are reported to show reduced growth capacity compared to normal controls (Goldstein 1979). Here the mean lifespan of HGPS fibroblasts was shown to be 33 PDs, however there was a large variation between the different strains tested ranging from 6 PDs to 52 PDs (Goldstein 1979). Interestingly, it was also noted that HGPS show increased levels of apoptosis (Bridger and Kill 2004), which may contribute to the shortened lifespan observed in these cells. These data suggest there is marked heterogeneity between different cell strains from the same syndrome and may reflect differences due to individual genetic backgrounds. In addition, it was reported that BS and CSA cultures have shortened lifespans, although only a single strain was used for each syndrome (Thompson and Holliday 1983).

Initial evidence suggested that the accelerated senescence seen in WS was due to increased telomere erosion (Kruk et al. 1995). When analysed, telomeres in WS cells were found to be shorter than those in normal cells (Kruk et al. 1995), and telomere erosion appeared to be accelerated in four WS fibroblast strains (Schulz et al. 1996). However, the erosion rates overlapped with those seen in normal strains and no increase in erosion rate was seen in two further WS strains (Choi et al. 2001). These data were further challenged by the observation that telomeric erosion is not accelerated at the single cell level in WS clones (Baird et al. 2004), suggesting that accelerated telomere erosion is not responsible for the shortened replicative lifespan of WS fibroblasts. An alternative hypothesis was put forward by Davis (Davis et al. 2005) based on the observation that WS fibroblasts in culture resemble cells that are grown under conditions of stress (Wang et al. 2002). This together with the fact that exposure to stressful stimuli, such as H_2O_2 (Huot et al. 1997) or activation of oncogenes (Wang et al. 2002) is known to trigger premature senescence in normal cells, led to the hypothesis that WS may be undergoing SIPS (Davis et al. 2005).

Evidence in the literature shows that oncogenic ras- or arsenite-induced premature senescence of fibroblasts is due to activation of p38 (Guay et al. 1997; Huot et al. 1997) and that constitutive activation of p38 can induce proliferative arrest that is very similar to normal senescence (Haq et al. 2002). The genomic instability and increased levels of replication fork stalling (Rodriguez-Lopez et al. 2002) seen in WS cells provides a plausible trigger for replication stress in WS cells and a possible involvement for p38 signalling in inducing the shortened replicative lifespan (Davis et al. 2005). Support for this theory came from the observation that the growth rate and replicative lifespan of WS cells could be significantly increased by treatment with the potent p38 inhibitor, SB203580 (Davis et al. 2005; Davis et al. 2006) (reference data for AG03141(WS) cells given in Appendix A). Primary AG05229(WS) fibroblasts treated daily with SB203580 showed an increased growth rate from 0.13 to 0.34 PD/day and an extension in lifespan from 18.0 to 43.7 PDs, which is now within the range expected for normal fibroblasts (Davis et al. 2005) . Interestingly, this effect is reversible as removal of

the drug results in a reduction in growth rate to that seen for untreated cells. Furthermore, restoration of the drug supplementation once again increases the growth rate and extends the lifespan of AG05229(WS) cells, although the lifespan extension is less than that seen in cells treated continuously with SB203580 (Davis et al. 2005). In the same study, high levels of p21^{WAF1} were observed in WS cells, suggesting that p38 signalling via p21^{WAF1} may induce a significant degree of cell-cycle arrest in young WS cells, thus causing the slow growth rate of WS cultures.

One of the criticisms of these studies was that long-lived foetal lung cells (MRC5) were used as a control. As the WS cells were short-lived adult dermal cells, it is possible that the effects seen with SB203580 were due to a combination of adult dermal cell-specific effects and a short lifespan. As a result a second study was undertaken using normal adult dermal fibroblasts for comparison. Although the effect of SB203580 was greater in these cells compared to the MRC5 cells, the effect on WS remained significantly higher (Davis and Kipling 2009). Collectively the findings provide strong supporting evidence that the effects of SB203580 on WS cellular lifespan are mainly due to the loss of WRN resulting in SIPS via p38 activation.

The importance of using appropriate control cells is highlighted by the observation that normal human fibroblasts show large variability in proliferative potential (Goldstein et al. 1978; Martin et al. 1970; Schneider and Mitsui 1976). This variability was attributed to differences in donor health status and the conditions and timing of the biopsy (Goldstein et al. 1978). However, in a study of 124 cell cultures established from human skin biopsies, which were explanted using the same experimental technique as part of the Baltimore Longitudinal Study of Aging (BLSA), a high degree of variability in replicative lifespan was also observed (Cristofalo et al. 1998a). This study showed that the lifespan of normal dermal fibroblasts grown under standard conditions ranged from 19-67 PD and no correlation was observed between replicative lifespan and donor age. This variation suggests that there are differences between different normal fibroblast strains that affect their ability to grow in culture. The degree of participation of p38

signalling might be expected to be different in these strains and as such the impact of p38 inhibition may vary between strains. Support for this hypothesis comes from a recent study showing that there is variation in the growth potential of normal adult dermal fibroblasts: four strains of adult dermal fibroblasts had growth rates ranging 0.15-0.35 PDs/Day and replicative lifespans ranging from 24-47.8 PDs (Davis and Kipling 2009). Furthermore, SB203580 had a differential effect on the lifespan of these cells, showing a lifespan extension of between 14.7 and 41%. As a result it is necessary to characterise the growth patterns and impact of p38 inhibition of normal adult dermal fibroblasts in order to use them as a comparison to study and identify any alterations in fibroblast behaviour in the GI syndromes panel.

The aim of this chapter is to characterise the growth rates and lifespans of a panel of normal and GI syndrome fibroblasts in the presence and absence of p38 inhibitors. To address this, a pragmatic screening approach of all syndromes in the presence and absence of p38 inhibitors was undertaken using cumulative PDs to calculate the growth rate and maximum lifespan.

3.2 Specific Materials and Methods

3.2.1 Cell culture

All cells were grown as monolayer cultures in EMEM and were maintained in a humidified incubator at 37°C, 20% O_2 and 5% CO_2. For drug treatments, cells were fed daily with EMEM containing 2.5 μM SB203580, 2.5 μM BIRB796 or 0.5 μM VX745, dissolved in DMSO. Control cells were supplemented with an equivalent volume of DMSO, added to the medium. p38 inhibitor concentrations were chosen based on previous studies (see Appendix B).

3.2.2 Growth curves

Growth curves were constructed for each cell strain using population doublings (PDs) per day. Population doublings were calculated according to the formula: $PD=\log(N_t/N_0)/\log2$, where N_t is the number of cells counted and N_0 is the number of cells seeded. The number of population doublings (PDs) for each

passage (P) was calculated from the cell count by comparing the total cell count following trypsinisation with the initial number of cells seeded. For cumulative PDs, the number of PDs calculated following each subcultivation was added to the previous count.

3.2.3 Calculation of maximum growth rate

Cells in early passage cultures tend to divide more rapidly than do those in late passage cultures. When the cumulative PDs were plotted against the time in culture, a clear decrease in the slope of the resulting line (change in growth rate) was observed. This initial slope over the first 30 days was calculated using linear regression as a measure of maximal growth rate of each cell strain. The R^2 values for each growth curve were > 0.90.

3.2.4 Statistical analysis

Differences in both the replicative lifespan of untreated GI syndrome cells and in the impact of p38 inhibitors on replicative lifespan of GI syndrome cells were compared to the mean for normal cells using a two-tailed z-test. p-values were calculated from the z-value and a significance level of <0.05 was used. This approach was chosen as it allowed comparison of lifespan data on a strain-by-strain basis compared to the mean effect for the three normal strains.

3.3 Results: Altered Growth Kinetics in Normal Dermal and GI Syndrome Fibroblasts Treated with p38 inhibitors

3.3.1 Normal Dermal Fibroblasts

To assess the effect of treatment of primary normal adult dermal fibroblasts with SB203580, BIRB796 and VX745, cells were grown continuously in the presence or absence the drugs until they reached M1 senescence. Three strains of adult dermal fibroblasts were chosen for use in this study. As shown in Figure 3.1A the strain with the shortest lifespan, AG06234(N), has an initial growth rate of 0.28 PD/day and a replicative lifespan of 19.1 PDs. This growth rate increases to 0.40, 0.43 and 0.33 PD/day in the presence of SB203580, BIRB796 and VX745,

respectively. The replicative lifespan of AG06234(N) cells increases to 26.6, 27.8 and 22.8 PDs, which equates to a lifespan extension of 40%, 46% and 20% in the presence of SB20358, BIRB796 and VX745, respectively. The strain with an intermediate lifespan, AG13152(N), has an initial growth rate of 0.20 PDs/day and a replicative lifespan of 22.1 PDs (Figure 3.1B). In the presence of SB203580, BIRB796 and VX745 respectively, these increase to 0.35, 0.37 and 0.29 PDs/day and the replicative lifespan increases to 29.6, 32.3 and 25.7 PDs. This equates to a lifespan extension of 34%, 47% and 17% in the presence of SB20358, BIRB796 and VX745, respectively. These data are consistent with previous reports in the literature for the replicative lifespan of AG13152(N) cells as 26 PDs (Cristofalo et al. 1998a) and 24.0 PDs (Davis and Kipling 2009). Similarly, AG13152(normal) had an initial growth rate of 0.15 PDs/day that increased to 0.18 PDs/day in the presence of SB203580, and the replicative lifespan to 29.5 PDs, which equates to a lifespan extension of ~28% (Davis and Kipling 2009). This strain can therefore be used as a reference to allow comparison of the growth of normal cells observed both in this study and previously in the literature. The longest-lived strain, AG16409(N) has an initial growth rate of 0.45 PDs/day and a replicative lifespan of 50.3 PDs (Figure 3.1C). The initial growth rate of AG16409(N) cells increases to 0.60, 0.68 and 0.53 with continued treatment with SB203580, BIRB796 and VX745, respectively. The lifespan of AG16409(N) cells increases to 56.5 and 63.2 when treated with SB203580 and BIRB796, which equates to a lifespan extension of 12% and 26%. However, VX745 treatment has a marginal effect on the growth rate and lifespan of AG16409(N) cells. These data are summarised in section 3.3.10 and in tables 3.1 and 3.2.

The data presented here represents the experimental lifespans observed for normal cells; however, information provided by the repository shows that AG16409(N), AG06234(N) and AG13152(N) have achieved 4, 15 and 6 PDs, respectively, prior to receipt of the cells. The maximum lifespan of AG16409(N), AG06234(N) and AG13152(N) is therefore 54.3 PDs, 34.1 PDs and 28.1 PDs, respectively. The following data obtained for the GI syndromes represents the experimental data; however, the starting PD is noted for any strains with known

replicative histories and the corrected lifespan data is used for the statistical analysis.

3.3.2 Rothmund Thomson Syndrome (RTS)

The RTS strain with the shortest lifespan, AG18375(RTS), has an initial growth rate of 0.30 PD/day and a replicative lifespan of 10.3 PDs (Figure 3.2A). This growth rate increases to 0.39 and 0.37 PDs/day in the presence of SB203580 and BIRB796 but is unchanged in VX745. The replicative lifespan of AG18375(RTS) cells also increases to 14.3, 17.5 and 10.4 PDs in the presence of SB20358, BIRB796 and VX745, which equates to a lifespan extension of 39%, 70% and 1%, respectively. The strain with an intermediate lifespan, AG17524(RTS), has an initial growth rate of 0.33 PDs/day and a replicative lifespan of 28.8 PDs (Figure 3.2B). In the presence of SB203580, BIRB796 and VX745 respectively, the growth rates increase to 0.47, 0.50 and 0.43 PDs/day and the replicative lifespan increases to 42.0, 46.2 and 36.0 PDs. This equates to a lifespan extension of 46%, 60% and 25% in the presence of SB203580, BIRB796 and VX745, respectively. The longest-lived strain, AG18371(RTS) has an initial growth rate of 0.38 PDs/day and a replicative lifespan of 37.9 PDs (Figure 3.2C). The initial growth rate of AG18371(RTS) cells increases to 0.69, 0.76 and 0.55 with an increase in lifespan to 43.2, 51.5 and 38.6 PDs in continued treatment with SB203580, BIRB796 and VX745, respectively. This equates to a 14%, 36%, 2% extension in lifespan in the presence of SB203580, BIRB796 and VX745.

3.3.3 Bloom Syndrome (BS)

The BS strain with the shortest lifespan, GM02520(BS), has an initial growth rate of 0.18 PDs/day and a replicative lifespan of 19.3 PDs (Figure 3.3A). Treatment with SB203580, BIRB796 and VX745 results in an increase in growth rate to 0.40, 0.43 and 0.30 PDs/day, respectively. The replicative lifespan of GM02520(BS) also increases to 29.3, 34.9 and 28.2 PDs in the presence of SB203580, BIRB796 and VX745, which equates to a lifespan extension of 52%, 81% and 46%, respectively. The strain with the intermediate lifespan, GM02548(BS), has a growth rate of 0.37 PDs/day and a replicative lifespan of 23.8

PDs (Figure 3.3B). With SB203580, BIRB796 and VX745 treatment, the growth rate increases to 0.48, 0.51 and 0.47 PDs/day and the lifespan to 35.5, 41.5 and 37.2 PDs, respectively. This equates to a lifespan extension of 49%, 74% and 57% in drug treated GM02548(BS) cells. Finally, the strain with the longest lifespan, GM02932(BS), has a growth rate of 0.32 PDs/day and a replicative lifespan of 24.5 PDs (Figure 3.3C). Treatment of GM02932(BS) cells with SB203580, BIRB796 and VX745 results in an increase in the growth rate to 0.43, 0.42, and 0.37 PDs/day, and an increase in lifespan to 33.7, 37.8 and 29.5 PDs. This equates to a lifespan extension of 38%, 55% and 21% in SB203580, BIRB796 and VX745 treated GM02932(BS) cells, respectively.

3.3.4 Hutchinson Gilford Progeria Syndrome (HGPS)

The HGPS strain with the shortest lifespan, GM01972(HGPS), has an initial growth rate of 0.13 PDs/day and a replicative lifespan of 3.8 PDs (Figure 3.4A). Treatment of GM01972(HGPS) cells with SB203580, BIRB796 and VX745 results in an increase in the growth rate to 0.18, 0.25 and 0.17 PDs/day and an increase in replicative lifespan to 5.5, 7.7 and 4.7 PDs, respectively. This equates to a lifespan extension of 46%, 102% and 23% in drug treated GM01972(HGPS) cells. The strain with the intermediate lifespan, AG10677(HGPS) has an initial growth rate of 0.29 PDs/day and a replicative lifespan of 14.4 PDs (Figure 3.4B), although was shown previously in the literature to have a replicative lifespan of only 6.3 PDs (Bridger and Kill 2004). With SB203580, BIRB796 and VX745 treatment, the growth rate increases to 0.41, 0.45 and 0.38 PDs/day and the lifespan increases to 20.9, 21.9 and 17.5, respectively. This equates to a lifespan extension of 45%, 52% and 22% in drug treated AG10677(HGPS) cells. Finally, the strain with the longest lifespan, AG11498(HGPS), has an initial growth rate of 0.38 PDs/day and a replicative lifespan of 14.8 PDs (Figure 3.4C). Treatment of AG11498(HGPS) cells with SB203580 and BIRB796 results in an increase in the growth rate to 0.39 and 0.46 PDs/day and a lifespan extension of 49% and 61%. Treatment with VX745 had no effect on the initial growth rate of AG11498(HGPS) cells but extends the lifespan by 13%.

The information provided by the repository shows that AG10677(HGPS) and AG11498(HGPS) have achieved 6 PDs and 10 PDs, respectively, prior to receipt of the cells; however, no information is provided for AG01972(HGPS). The maximum lifespan of AG10677(HGPS) and AG11498(HGPS) is therefore 20.4 PDs and 24.8 PDs, respectively.

3.3.5 Nijmegen-Breakage Syndrome (NBS)

The NBS strain with the shortest lifespan, GM07166(NBS), has an initial growth rate of 0.22 PDs/day and a replicative lifespan of 17.8 PDs (Figure 3.5A). Treatment with SB203580, BIRB796 and VX745 results in an increase in growth rate to 0.41, 0.38 and 0.33 PDs/day, respectively. The replicative lifespan of GM07166 also increases to 39.5, 41.7 and 30.0 PDs in the presence of SB203580, BIRB796 and VX745, which equates to a lifespan extension of 122%, 135% and 69%, respectively. The strain with the intermediate lifespan, RO202(NBS), has an initial growth rate of 0.35 PDs/day and a replicative lifespan of 43.1 PDs (Figure 3.5B). With SB203580 and BIRB796 treatment, the growth rate increases to 0.49, 0.54 and 0.40 PDs/day. The lifespan of RO202 cells increases to 48.8, 53.7 and 46.5 PDs, which equates to a lifespan extension of 13%, 25% and 7% in the presence of SB203580, BIRB796 and VX745, respectively. Finally, the strain with the longest lifespan, RO242(NBS), has an initial growth rate of 0.34 PDs/day and a replicative lifespan of 53.5 PDs (Figure 3.5C). Treatment of RO242(NBS) cells with SB203580 and BIRB796 results in an increase in the growth rate to 0.38 PDs/day; however, VX745 treatment results in a slight reduction in the initial growth rate to 0.32 PD/day. The lifespan of RO242(NBS) cells also increases to 67.9, 65.9 and 62.6 PDs. This equates to a lifespan extension of 27%, 23% and 17% in SB203580, BIRB796 and VX745, respectively.

The information provided by the repository shows that GM07166(NBS) has achieved 5.65 PDs prior to receipt of the cells and therefore have a maximum lifespan of 23.5 PDs; however, no information is provided for the other two NBS strains.

3.3.6 Ligase 4 Syndrome (LIG4)

The LIG4 strain with the shortest lifespan, GM17523(LIG4), has an initial growth rate of 0.23 PDs/day and a lifespan of 11.6 PD (Figure 3.6A). Treatment with SB203580, BIRB796 and VX745 results in an increase in growth rate to 0.37, 0.40 and 0.30 PDs/day and an increase in lifespan to 19.4, 22.5 and 15.7 PD, respectively. This equates to a lifespan extension of 68%, 95% and 36% in drug treated GM17523(LIG4) cells. The strain with the longer lifespan, GM16088(LIG4), has an initial growth rate of 0.25 PDs/day and a lifespan of 15.9 PD (Figure 3.6B). Treatment of GM16088(LIG4) cells with SB203580, BIRB796 and VX745 results in an increase in the growth rate to 0.36, 0.49 and 0.29 PDs/day and an extends the lifespan to 23, 28.3 and 20 PD, respectively. This equates to a lifespan extension of 45%, 79% and 26% in drug treated GM16088(LIG4) cells.

3.3.7 Cockayne Syndrome A (CSA)

Untreated GM01856(CSA) cells have a growth rate of 0.40 PDs/day and a replicative lifespan of 21.1 PDs/day. Treatment of GM01856(CSA) cells with SB203580, BIRB796 and VX745 results in an increase in the growth rate to 0.50, 0.58 and 0.46 PDs/day, and an increase in replicative lifespan to 30.0, 34.5 and 24.3 PDs, respectively (Figure 3.7). This equates to an increase in growth rate of 27%, 46% and 17% and a lifespan extension of 42%, 64% and 15% in the presence of SB203580, BIRB796 and VX745, respectively.

3.3.8 Dyskeratosis Congenita (DKC)

GM01744(DKC) cells have a growth rate of 0.15 PDs/day and a replicative lifespan of 5.9 PDs (Figure 3.8). Treatment of GM01744 cells with SB203580, BIRB796 and VX745 results in an increase in the growth rate to 0.22, 0.27 and 0.17 PDs/day, respectively. The replicative lifespan of GM01744 also increases to 10.4, 11.8 and 8.2 PDs, which equates to a 77%, 100% and 39% lifespan extension when treated with SB203580, BIRB796 and VX745, respectively. The information provided by the repository shows that GM01774(DKC) has achieved

6.74 PDs prior to receipt of the cells and therefore have a maximum lifespan of 12.6 PDs.

3.3.9 Seckel Syndrome (SS)

The SS strain with the shortest lifespan, GM18366(SS), has an initial growth rate of 0.19 PDs/day and a replicative lifespan of 11.2 PDs (Figure 3.9A). Treatment with SB203580, BIRB796 and VX745 increases the initial growth rate of GM18366(SS) cells to 0.31, 0.36 and 0.25 PDs/day, respectively. The replicative lifespan of GM18366(SS) also increases to 21.4, 29.6 and 19.8 PDs in the presence of SB203580, BIRB796 and VX745, which equates to a lifespan extension of 91%, 164% and 77%, respectively. The strain with the longer lifespan, GM09812(SS), has a growth rate of 0.5 PDs/day and a replicative lifespan of 32.9 PDs (Figure 3.9B). With SB203580, BIRB796 and VX745 treatment, the growth rate of GM09812(SS) cells increases to 0.63, 0.73 and 0.60 PDs/day and the lifespan is extended to 39.1, 44.4 and 36.9 PDs, respectively. This equates to a lifespan extension of 19%, 35% and 12% in drug treated GM09812(SS) cells.

3.3.10 Summary of Growth Potential of Normal Dermal and GI Syndrome Fibroblasts

The following section provides a summary of:

1.   The lifespan and growth rate data for untreated normal and GI syndrome cells.

2.   The effect of p38 inhibitors on lifespan and growth rate of normal and GI syndrome cells.

1. Comparison of lifespans

In order to compare the lifespans of GI syndrome and normal cells the replicative history of each strain, as provided by Coriell, is added to the experimental data collected in this study. In cases where the replicative histories are unknown, passage history has been used as an indicator of replicative history.

Consistent with evidence from the literature (Cristofalo et al. 1998a; Davis and Kipling 2009), inter-strain heterogeneity with regard to growth rate and lifespan was observed in normal cells. AG16409(N) had the fastest growth rate (0.45 PDs/day) and longest lifespan (54.3 PDs) of the three normal strains, AG06234(N) had an intermediate growth rate (0.28 PDs/day) and lifespan (34.1 PDs), whereas AG13152(N) had the slowest growth rate (0.20 PDs/day) and shortest lifespan (28.1 PDs). The mean growth rate and lifespan of normal cells was 0.31 PDs/day and ~39 PDs, respectively. These data suggest that there are differences in the growth potential of dermal fibroblasts that have no known defect, and thus provide a baseline against which to compare the growth of GI syndrome fibroblasts.

Figure 3.10 provides a visual representation of the range of growth rates (panel A) and lifespans (panel B) observed for the GI panel, and allows simple observations of trends and differences to be made. The majority of GI syndrome cell strains have growth rates within the normal range with the exception of GM02520(BS), AG01972(HGPS), GM01774(DKC) and GM18366(SS) that have slower than normal growth rates and GM09812(SS) which has a faster than normal growth rate (Figure 3.10A). Given that growth rate will change over time and is therefore dependent on where in the replicative lifespan the measurement is taken, a more in-depth analysis of lifespan was undertaken.

Figure 3.10B shows that the majority of GI syndrome cell strains have lifespans that are at the bottom end of the normal range [AG18371(RTS), AG17524(RTS) and GM09812(SS)] or are below the normal range [AG18375(RTS), all three BS strains, all three HGPS strains, GM07166(NBS), both LIG4 strains, GM01856(CSA), GM01774(DKC) and GM18366(SS)], with the exception of RO202(NBS) and RO242(NBS) which have lifespans that are above the normal mean lifespan. Statistical analysis of the differences in lifespan for each of the GI syndromes fibroblast strains compared to the mean lifespan for the three normal strains was performed using a two-tailed z test. Figure 3.10C shows that AG18375(RTS), AG01972(HGPS), GM17523(LIG4) and GM18366(SS) have a significantly shorter lifespan compared to normal cells, suggesting that these cell

strains are replicatively compromised compared to normal cells, perhaps reflecting an increased commitment to SIPS.

2. Impact of p38 inhibitors

Treatment with p38 inhibitors was shown to increase the growth rate and extend the lifespan of all cells irrespective of their genetic background, suggesting that all cells are undergoing some degree of p38-mediated proliferation restraint. Although inter-strain heterogeneity in the effect of each inhibitor was observed (summarised in Table 3.1), in general BIRB796 was shown to have the greatest, whereas VX745 had the least impact on growth rate and lifespan. Given the issues associated with changing growth rates over time (discussed previously), a more in-depth analysis of the impact of p38 inhibitors on lifespan was performed (Table 3.1 and Figure 3.11).

Statistical analysis of the impact of SB203580, BIRB796 and VX745 on the lifespan of each individual GI syndrome cell strain was compared to the mean effect for normal cells in the presence of each inhibitor. Table 3.1 shows that AG18375(RTS) show a statistically significant lifespan extension in response to BIRB796 (p=0.008). GM02548(BS) and GM02520(BS) show a statistically significant lifespan extension in the presence of BIRB796 and VX745. GM01972(HGPS) shows a significant lifespan extension in response to BIRB796 only (p<0.001). GM07166(NBS) shows a significant lifespan extension in the presence of all three p38 inhibitors (p<0.001 for all). Similarly, GM17523(LIG4) show a significant lifespan extension in response to all p38 inhibitors (p=0.006, p<0.001 and p=0.20, respectively), whereas GM16088(LIG4) only show a significant lifespan extension in response to BIRB796 (p<0.001). GM01856(CSA) shows a significant lifespan extension in response to BIRB796 only (p=0.035), whereas both GM01774(DKC) and GM18366(SS) show a significant lifespan extension in response to all three p38 inhibitors.

The observation was also made that in normal cells there appears to be a correlation between the growth potential and the response to p38 inhibitors. For

example, AG13152(N) cells showed the slowest growth rate and shortest lifespan but showed the greatest response to p38 inhibitors, whereas AG16409(N) had the fastest growth rate, the longest lifespan but showed the smallest response to p38 inhibitors. The data suggest that AG13152(N) cells are undergoing a greater degree of p38-restraint on growth potential compared to the other two normal strains. The same pattern is observed in GI syndrome cells, in that the strains with the slowest growth rate and shortest lifespan show the greatest response to p38 inhibitors. For example, GM07166(NBS) has a much reduced growth rate and lifespan compared to the other two NBS strains and show a far greater response to p38 inhibitors. Figure 3.12 shows that there is a negative correlation between lifespan extension in BIRB796 and the maximum lifespan of untreated cells, suggesting that the cells with the shortest lifespan have the greatest response to BIRB796 and that this is not weighted by the presence of normal cells. A similar effect was seen for SB203580 and VX745 (data not shown).

3.4 Discussion

Given the extensive number of strains, the pragmatic option was taken of an unbiased screen of growth potential in all of the cells using the standard technique described. This approach was critical for valid comparisons in such extended longitudinal studies. The maximum growth rate of each culture was calculated by linear regression at early growth stages while maximum lifespan represents an endpoint and is not as affected by passage fluctuations in growth rate.

Heterogeneity in growth potential and in p38 inhibitor responses were observed between normal strains and between strains from the same GI syndrome. p38 inhibitors extended the lifespan and increased the growth rate of all cell strains irrespective of their genetic background, suggesting that all cells strains undergo some degree of p38-mediated proliferation restraint. Whilst the observed heterogeneity in growth potential between cell strains could indicate differences in the level of commitment to SIPS, it is possible that it could also reflect differences in progression towards replicative senescence due simply to differences in replicative histories. Given the uncertainties in replicative history for the majority of

strains used, the passage history was used to give some indication of replicative history. Typically the passage history of the strains, as provided by the repository, is 2-15; however, this is not provided for all of the strains used.

Other factors that could contribute to inter-strain heterogeneity include differences in the micro-anatomical localisations from which the cells are explanted. For example, it has been reported that cultured fibroblasts isolated from the upper and deeper dermis, at the same anatomical site, exhibit differences in proliferative potential (Azzarone and Macieira-Coelho 1982). These areas are subject to current collaborations to investigate the age-related modifications of distinct dermal fibroblast populations (Dr. Terence Davis unpublished data). Controversies over the impact of donor age on the growth potential of primary cells remain (Cristofalo et al. 1998a; Pignolo et al. 1992). The current data set does not have the power to resolve this issue, however, the relationship between donor age and replicative lifespan of the panel are shown for illustrative purposes (Figure 3.13). Here, no correlation between donor age and lifespan is observed and this does not appear to be weighted by the presence of normal cells. To further assess impact of donor age in primary cells with different genetic backgrounds, a wider screen using more strains would be required. Finally, uncertainties in disease status for some cell strains could also contribute to inter-strain differences. For example, the disease status of RO242(NBS), RO202(NBS) and GM09812(SS) was determined by clinical diagnosis and to date the mutation status of these cells have not been characterised. Moreover, evidence in the literature suggests that RO242(NBS) cells are derived from a patient that represents a possible variant of NBS that shows some differences in clinical presentation and some unusual cytogenetic features compared to other NBS patients (Der Kaloustian et al. 1996). Therefore, it is possible that the inter-strain heterogeneity in growth potential observed for NBS and SS cells is due to fact that these represent different disorders with different growth characteristics.

The observation that some strains such as AG01972(HGPS) and GM01774(DKC) have very short experimental lifespans suggest that these strains

may be close to replicative senescence. This gives rise to the issue that small differences in growth parameters will be translated into large percentage differences in these strains. Furthermore, it is known that telomeres are very short in all forms of DKC (Gupta and Kumar 2010; Vulliamy et al. 2001b), therefore the increase in stress signals that arise due to telomere attrition in DKC may cause the increased response to p38 inhibitors observed here.

Despite the known caveats of this approach, the main findings presented in this chapter are as follows:

- AG18375(RTS), all three HGPS strains, GM07166(NBS), both LIG4 strains, GM01774(DKC) and GM18366(SS) have truncated lifespans compared to normal cells

- Of these AG18375(RTS), AG01972(HGPS), GM17523(LIG4) and GM18366(SS) were shown to have a statistically shorter lifespan compared to normal cells, suggesting that these strains are replicatively compromised.

- Treatment with p38 inhibitors consistently increases the growth rate and extends the lifespan of all cell strains, irrespective of their genetic background, suggesting that all of these cell strains are undergoing some degree of p38-mediated proliferation restraint.

- The following cell strains showed a significant lifespan extension in response to at least one p38 inhibitor, suggesting that these strains are undergoing a higher level of p38-mediated proliferation restraint (or SIPS) compared to normal cells: AG18375(RTS), GM02548(BS), GM02520(BS), GM01972(HGPS), GM07166(NBS), GM16088(LIG4), GM17523(LIG4), GM01856(CSA), GM01774(DKC) and GM18366(SS).

Whilst, the current screen has provided valuable information regarding the heterogeneity in growth potential of both normal and GI syndrome fibroblasts, the findings underline the need to clarify several issues: The need to identify the target cells for p38 inhibitor action, the potential contribution of cells induced to re-enter

the cell cycle, the difficulty in identifying degrees of commitment in primary systems for progression to cell cycle exit/senescence, the complication of ongoing proliferation of cells – perhaps not affected by p38 inhibitors – resulting in an effective dilution of responding cells as the culture progresses and the difficulty of comparing GI panel strains that may have different degrees of commitment to senescence due to telomere attrition. These issues are addressed in the subsequent chapters.
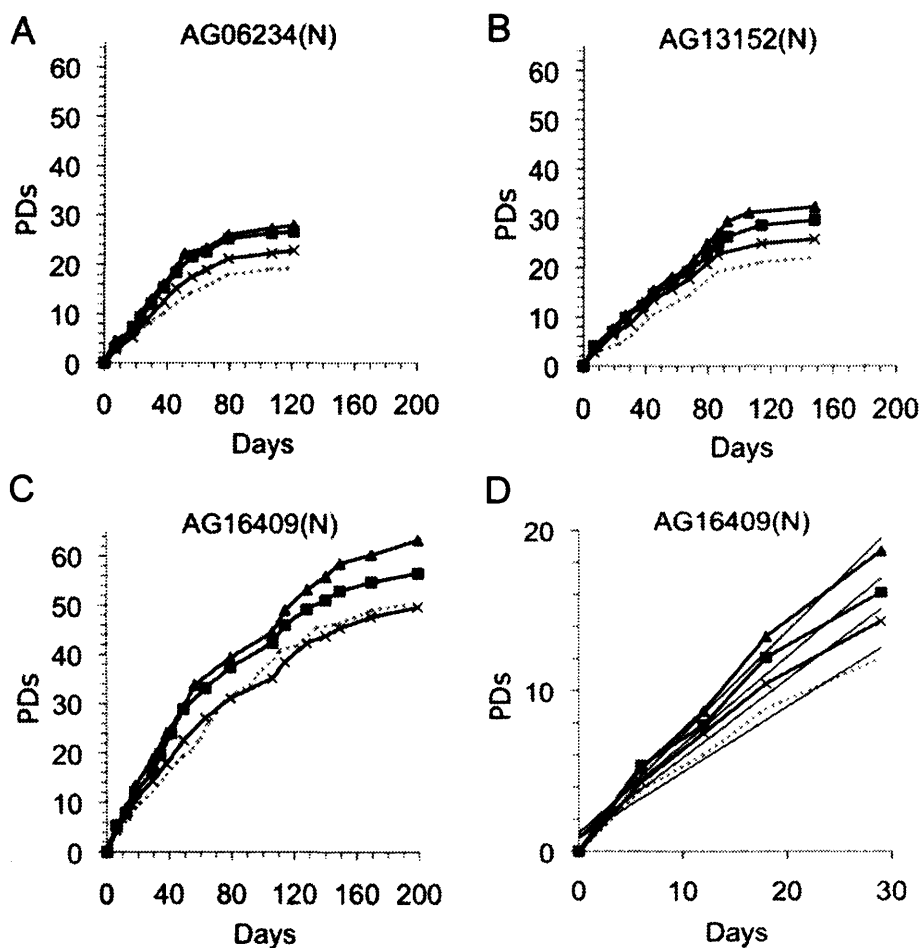
Figure 3.1. Growth (cumulative population doublings) of normal adult dermal fibroblasts with SB20580, BIRB796 and VX745.

Fibroblasts AG06234(N) (panel A), AG13152(N) (panel B) and AG16409(N) (panel c) were grown in standard EMEM with no supplementation (dotted line), or with continuous daily supplementation with SB203580 (-■-), BIRB796 (-▲-), or VX745 (-✗-). Growth is measured as population doubling (PDs) versus days. Panel D shows an example of the linear regression used to calculate the maximum growth rate of the cultures. The R^2 values for each was > 0.9.
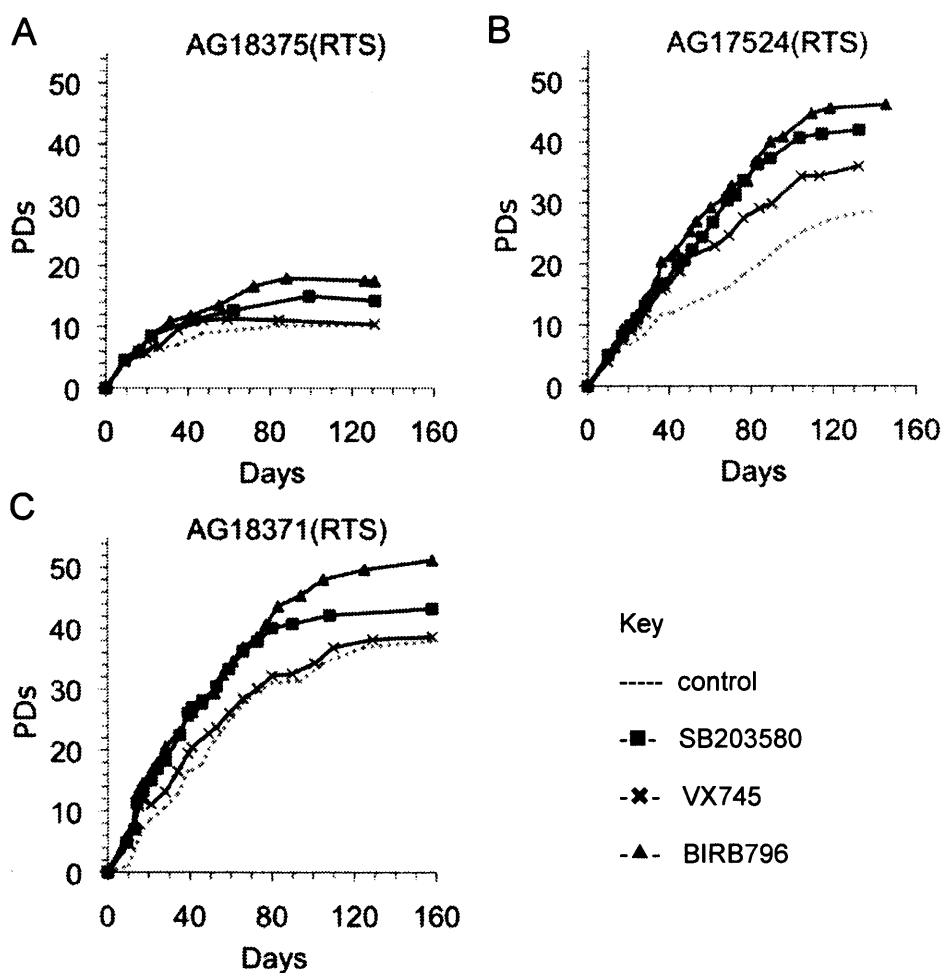
Figure 3.2. Growth (cumulative population doublings) of RTS fibroblasts with SB20580, BIRB796 and VX745.

Fibroblasts AG18375(RTS) (panel A), AG17524(RTS) (panel B) and AG18371(RTS) (panel c) were grown as in 3.1.
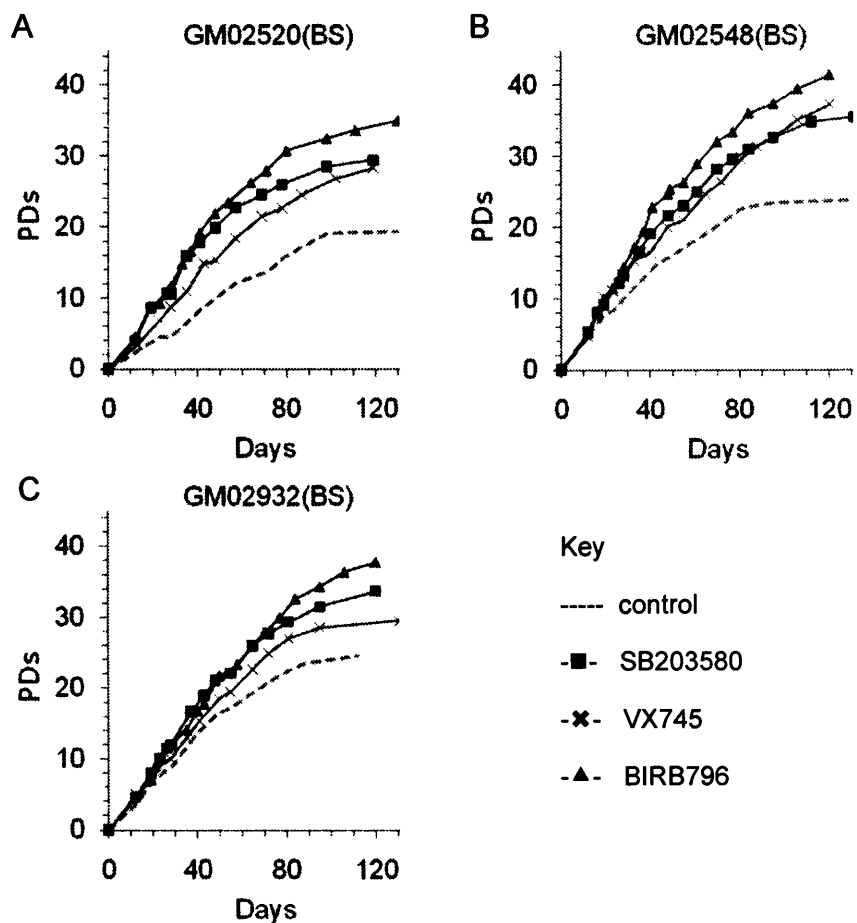
Figure 3.3. Growth (cumulative population doublings) of Bloom syndrome (BS) fibroblasts with SB20580, BIRB796 and VX745.

Fibroblasts GM02520(BS) (panel A), GM02548(BS) (panel B) and GM02932(BS) (panel c) were grown as in 3.1.
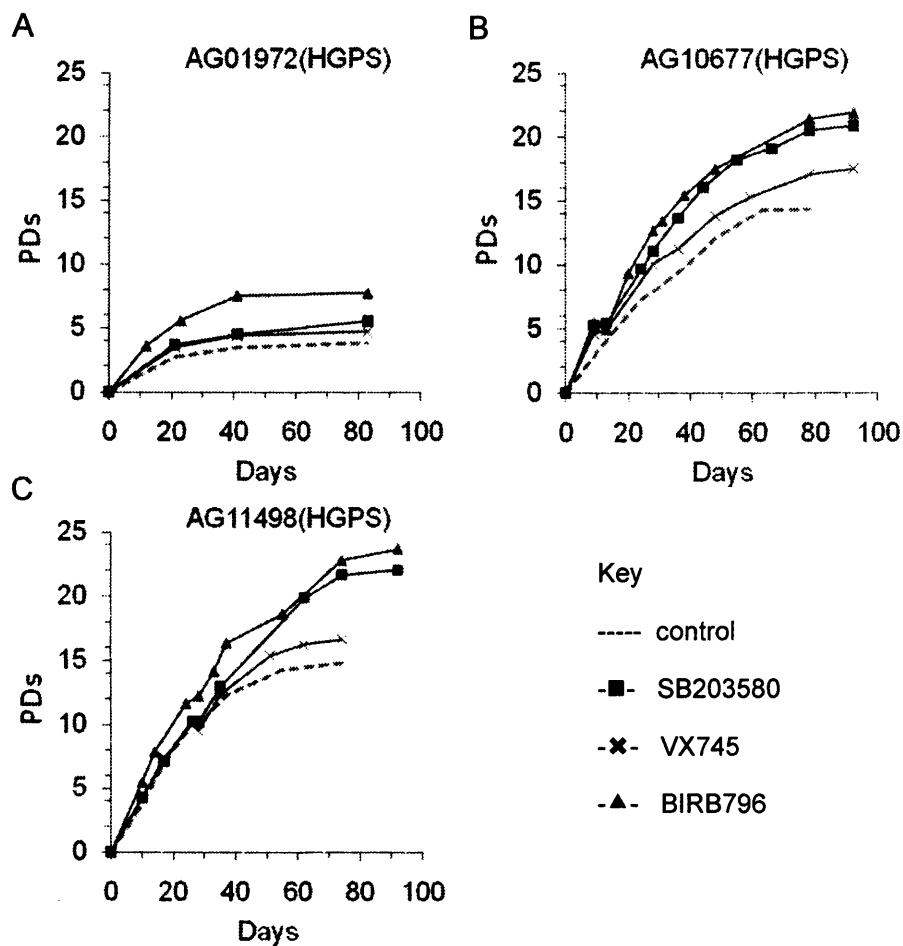
Figure 3.4. Growth (cumulative population doublings) of Hutchinson-Gilford Progeria syndrome (HGPS) fibroblasts with SB20580, BIRB796 and VX745.

Fibroblasts AG01972(HGPS) (panel A), AG10677(HGPS) (panel B) and AG11498(HGPS) (panel c) were grown as in 3.1.
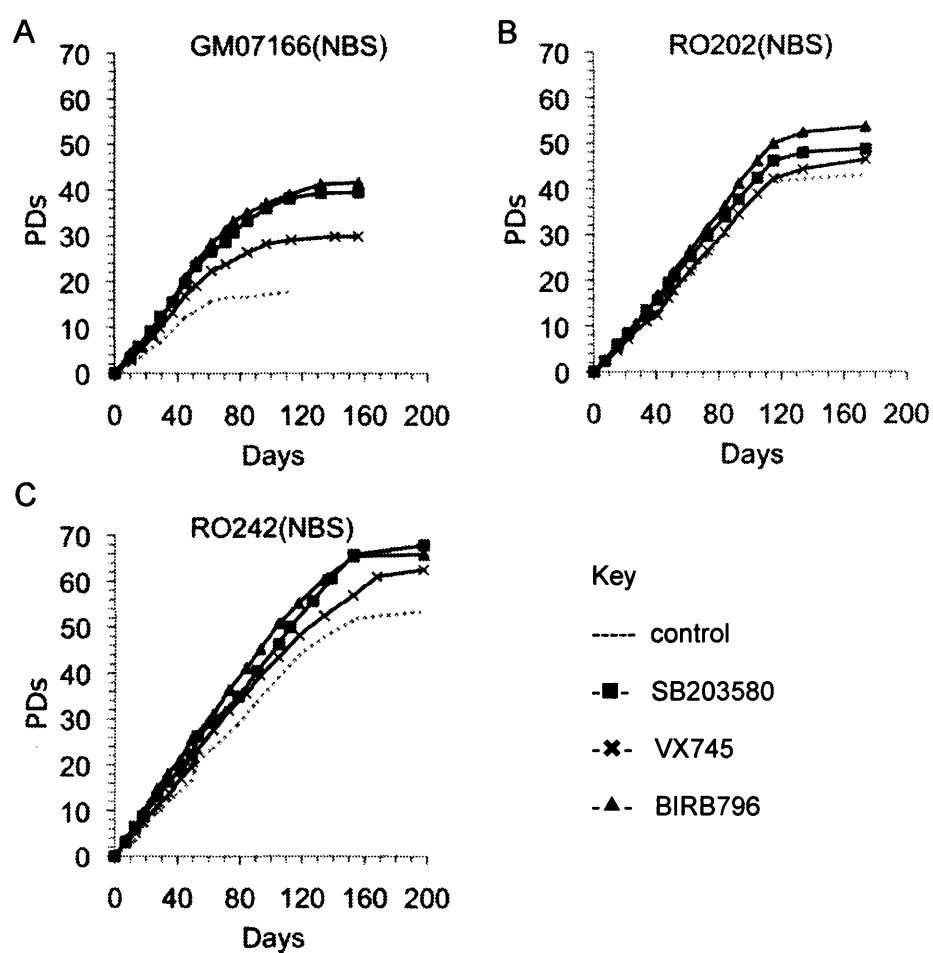
Figure 3.5. Growth (cumulative population doublings) of Nijmegen Breakage syndrome (NBS) fibroblasts with SB20580, BIRB796 and VX745.

Fibroblasts GM07166(NBS) (panel A), RO202(NBS) (panel B) and RO242(NBS) (panel c) were grown as in 3.1.
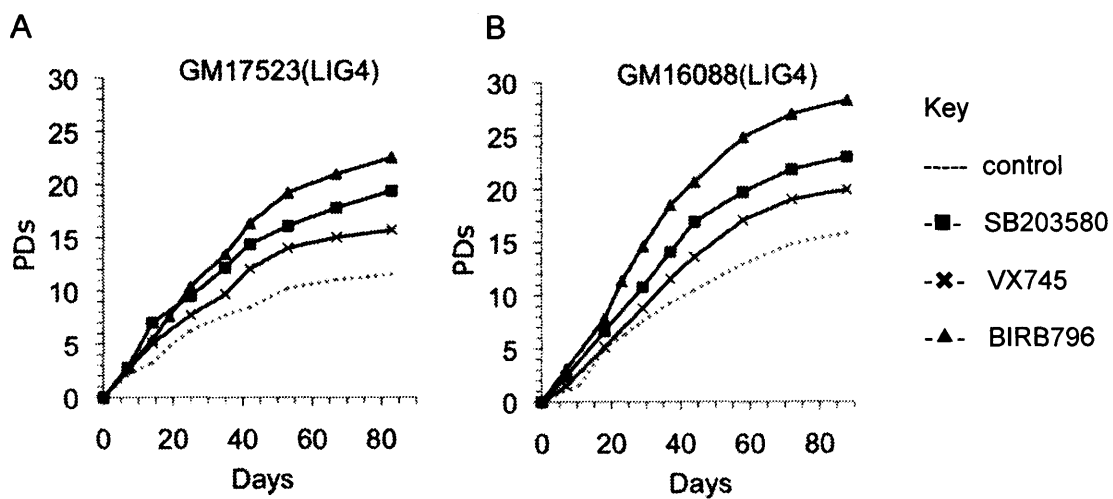
Figure 3.6. Growth (cumulative population doublings) of Ligase 4 syndrome (LIG4) fibroblasts with SB20580, BIRB796 and VX745.

Fibroblasts GM17523(LIG4) (panel A) and GM16088(LIG4) (panel B) were grown in were grown as in 3.1.

104
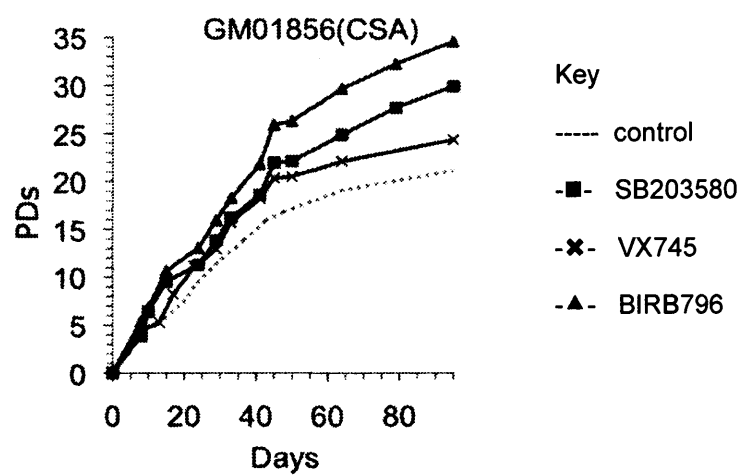
Figure 3.7. Growth (cumulative population doublings) of Cockayne Syndrome A (CSA) fibroblasts with SB20580, BIRB796 and VX745.

Fibroblasts GM01856(CSA) were grown as in 3.1.
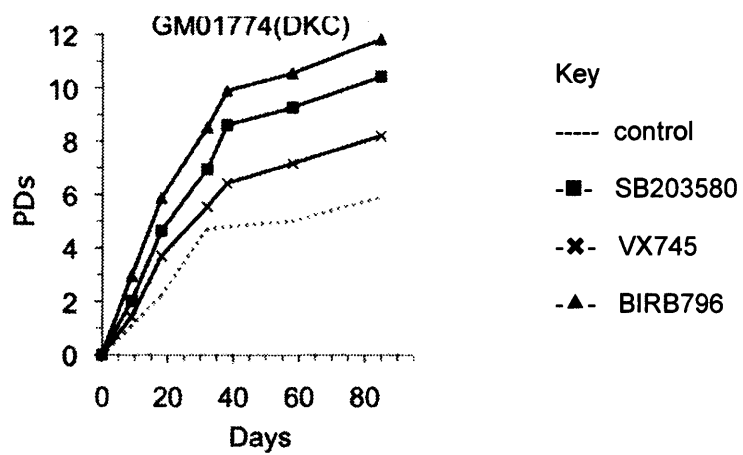
Figure 3.8. Growth (cumulative population doublings) of Dyskeratosis Congenita (DKC) fibroblasts with SB20580, BIRB796 and VX745.

Fibroblasts GM01774(DKC) were grown as in 3.1.
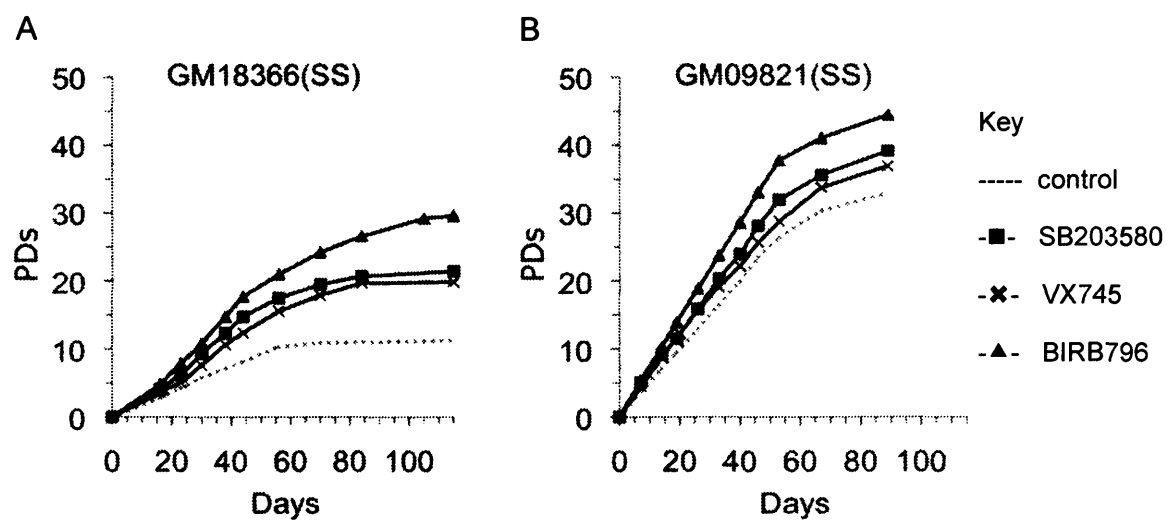
Figure 3.9. Growth (cumulative population doublings) of Seckel Syndrome (SS) fibroblasts with SB20580, BIRB796 and VX745.

Fibroblasts GM18366(SS) (panel A) and GM01982(SS) (panel B) were grown as in 3.1.

A

Maximum growth rate (PD/Day): 0.60, 0.40, 0.20, 0.00

(plotted across: Normal, RTS, BS, HGPS, NBS, LIG4, CSA, DKC, SS)

B

Maximum Lifespan (PDs): 60, 50, 40, 30, 20, 10, 0

(plotted across: Normal, RTS, BS, HGPS, NBS, LIG4, CSA, DKC, SS)

Syndrome

Key

	◆	■	▲
Normal	AG16409	AG13152	AG06234
RTS	AG18371	AG17524	AG18375
BS	GM02932	GM02548	GM02520
HGPS	AG11498	AG10677	AG01972
NBS	RO242	RO202	GM07166
LIG4	GM16088	GM17523	
CSA	GM01856		
DKC	GM01774		
SS	GM09812	GM18366	

C

Cell strain	Replicatve Lifespan (PDs)	z value[a]	p value[b]
AG16409(Normal)	54.26		
AG13152(Normal)	28.05		
AG06234(Normal)	34.05		
AG18375(RTS)	10.26	-2.08	0.038
AG17524(RTS)	28.77	-0.73	0.465
AG18371(RTS)	37.92	-0.06	0.952
GM02932(BS)	24.45	-1.04	0.298
GM02548(BS)	23.78	-1.09	0.276
GM02520(BS)	19.29	-1.42	0.156
AG11498(HGPS)	24.77	-1.02	0.308
AG10677(HGPS)	20.36	-1.34	0.180
GM01972(HGPS)	3.8	-2.55	0.011
RO242(NBS)	43.05	0.31	0.757
RO202(NBS)	53.51	1.07	0.285
GM01766(NBS)	23.43	-1.12	0.263
GM16088(LIG4)	15.86	-1.67	0.095
GM17523(LIG4)	11.56	-1.98	0.048
GM18366(SS)	11.22	-2.01	0.044
GM09812(SS)	32.9	-0.43	0.667
GM01856(CSA)	21.1	-1.29	0.197
GM01774(DKC)	12.60	-1.91	0.056

[a] two-tailed z-test

[b] p value calculated from z value. A significance level of 0.05 is given.

Figure 3.10. Summary of growth rates and lifespans of GI syndrome and normal fibroblasts.

Panel A and B provide a graphical representation of the range of growth rates and lifespans observed for GI syndrome and normal fibroblast cell strains. The mean growth rate and lifespan for each syndrome is indicated by ✕. The shaded regions represent the range of growth rates (panel A) and lifespans (panel B) observed for normal dermal fibroblasts. The dotted line in panel B represents the significance level as tested by Z-test: any strains that are on or below this line are considered to have statistically shorter lifespans compared with normal cells. Panel C shows the results for the statistical analysis of GI syndrome cell lifespans compared to normal cells. Individual GI cell strains were compared to the normal mean using a two-tailed z-test and any strains with a significantly shorter lifespan compared to normal cells are highlighted in red.

108

Table 3.1. Impact of p38 inhibitors on growth rate and lifespan of GI syndrome and normal fibroblasts.

Cell strain	Drug Treatment	Maximum growth rate (PDs/Day)[a]	Increase in growth rate (%)[b]	Replicatve Lifespan (PDs)	Lifespan extension (%)[b]	z value[c]	P value for lifespan extension[d]
AG16409(Normal)	-	0.45		50.3			
	SB203580	0.60	33.3	56.5	12.3		
	BIRB796	0.68	51.1	63.2	25.6		
	VX745	0.53	17.8	50.3	0.0		
AG13152(Normal)	-	0.20		22.1			
	SB203580	0.35	75.0	29.6	33.9		
	BIRB796	0.37	83.3	32.3	46.2		
	VX745	0.29	43.3	25.7	16.3		
AG06234(Normal)	-	0.28		19.1			
	SB203580	0.40	42.4	26.6	39.3		
	BIRB796	0.43	52.9	27.8	45.5		
	VX745	0.33	17.6	22.8	19.4		
AG18375(RTS)	-	0.30		10.26			
	SB203580	0.39	31.3	14.27	39.1	0.74	0.460
	BIRB796	0.37	24.8	17.47	70.3	2.67	0.008
	VX745	0.29	-2.9	10.38	1.2	-1.03	0.303
AG17524(RTS)	-	0.33		28.77			
	SB203580	0.47	40.7	42.02	46.1	1.23	0.219
	BIRB796	0.50	49.9	46.16	60.4	1.83	0.067
	VX745	0.43	27.5	36.03	25.2	1.28	0.201
AG18371(RTS)	-	0.38		37.92			
	SB203580	0.69	82.3	43.24	14.0	-1.01	0.313
	BIRB796	0.76	101.3	51.51	35.8	-0.28	0.780
	VX745	0.55	44.8	38.63	1.9	-0.96	0.337
GM02932(BS)	-	0.32		24.45			
	SB203580	0.43	34.8	33.69	37.8	0.65	0.516
	BIRB796	0.42	33.5	37.79	54.6	1.32	0.187
	VX745	0.37	17.3	29.46	20.5	0.83	0.407
GM02548(BS)	-	0.37		23.78			
	SB203580	0.48	29.4	35.45	49.1	1.44	0.150
	BIRB796	0.51	39.2	41.45	74.3	3.02	0.003
	VX745	0.47	28.7	37.23	56.6	4.29	<0.001
GM02520(BS)	-	0.18		19.29			
	SB203580	0.40	126.5	29.34	52.1	1.65	0.099
	BIRB796	0.43	144.5	34.91	81.0	3.59	<0.001
	VX745	0.30	71.5	28.17	46.0	3.28	0.001
AG11498(HGPS)	-	0.38		14.8			
	SB203580	0.39	3.1	22.03	48.9	1.43	0.153
	BIRB796	0.46	21.7	23.70	60.1	1.80	0.072
	VX745	0.38	0.1	16.65	12.5	0.06	0.952
AG10677(HGPS)	-	0.29		14.4			
	SB203580	0.41	40.2	20.9	45.1	1.17	0.242
	BIRB796	0.45	53.1	21.9	52.1	1.11	0.267
	VX745	0.38	28.3	17.5	21.5	0.93	0.352
GM01972(HGPS)	-	0.13		3.80			
	SB203580	0.18	34.6	5.53	45.5	1.19	0.234
	BIRB796	0.25	95.3	7.69	102.4	5.42	<0.001
	VX745	0.17	27.4	4.69	23.4	1.11	0.267

Table 3.1 continued

Cell strain	Drug Treatment	Maximum growth rate (PDs/Day)[a]	Increase in growth rate (%)[b]	Replicatve Lifespan (PDs)	Lifespan extension (%)[b]	z value[c]	P value for lifespan extension[d]
RO202(NBS)	-	0.35		43.05			
	SB203580	0.49	40.3	48.81	13.4	-1.06	0.289
	BIRB796	0.54	54.8	53.67	24.7	-1.24	0.215
	VX745	0.40	16.8	46.49	8.0	-0.37	0.711
RO242(NBS)	-	0.34		53.51			
	SB203580	0.38	12.6	67.91	26.9	-0.11	0.912
	BIRB796	0.38	12.9	65.91	23.2	-1.37	0.171
	VX745	0.32	-5.5	62.56	16.9	0.48	0.631
GM07166(NBS)	-	0.22		17.8			
	SB203580	0.41	81.2	39.5	121.9	6.55	<0.001
	BIRB796	0.38	67.1	41.7	134.3	8.15	<0.001
	VX745	0.33	47.3	30	68.5	5.44	<0.001
GM16088(LIG4)	-	0.25		15.86			
	SB203580	0.36	42.1	22.99	45.0	1.15	0.250
	BIRB796	0.49	92.1	28.33	78.6	3.39	<0.001
	VX745	0.29	15.8	19.96	25.9	1.34	0.180
GM17523(LIG4)	-	0.23		11.56			
	SB203580	0.37	57.1	19.42	68.0	2.77	0.006
	BIRB796	0.40	72.9	22.53	94.9	4.78	<0.001
	VX745	0.30	27.1	15.73	36.1	2.32	0.020
GM01856(CSA)	-	0.40		21.1			
	SB203580	0.50	27.0	29.88	41.6	0.92	0.358
	BIRB796	0.58	46.1	34.54	63.7	2.11	0.035
	VX745	0.46	16.5	24.32	15.3	0.32	0.749
GM01774(DKC)	-	0.15		5.9			
	SB203580	0.22	46.7	10.4	76.3	3.35	<0.001
	BIRB796	0.27	82.2	11.8	100.0	5.22	<0.001
	VX745	0.17	15.6	8.2	39.0	2.60	0.009
GM18366(SS)	-	0.19		11.22			
	SB203580	0.36	87.8	21.4	90.7	4.36	<0.001
	BIRB796	0.31	61.9	29.57	163.5	10.66	<0.001
	VX745	0.25	32.0	19.82	76.6	6.22	<0.001
GM09812(SS)	-	0.50		32.9			
	SB203580	0.62	24.7	39.11	18.9	-0.68	0.497
	BIRB796	0.73	45.3	44.42	35.0	-0.35	0.726
	VX745	0.60	19.3	36.87	12.1	0.02	0.984

[a] The maximum growth rate is based on the linear regression part of the curve at early growth stages (30 days in culture) and is calculated by linear regression.

[b] The increase in growth rate and lifespan following treatment with SB203580, BIRB796 and VX745 is calculated as a percentage increase compared to the untreated control.

[c] Two-tailed z-test

[d] p-value is calculated based on the z-value. A significance level of 0.05 is given and any strains showing a significantly different response to p38 inhibitors compared with the normal mean are highlighted in red.
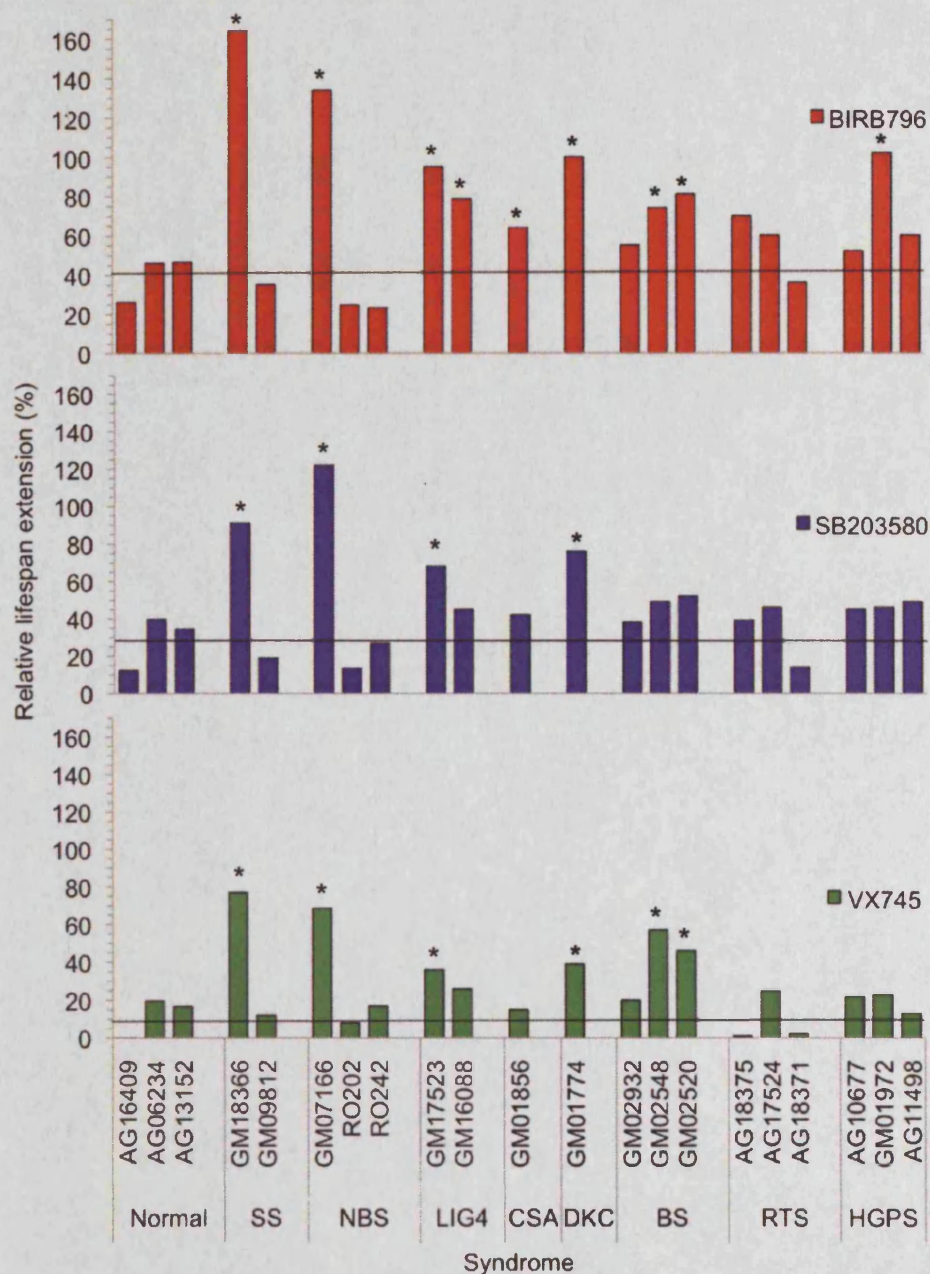
Figure 3.11. Relative lifespan extension in SB203580-, BIRB796- and VX745-treated cells.

The lifespan extension is given as the percentage increase compared to untreated controls. The black line indicates the mean lifespan extension for each drug. A two-tailed z-test was performed to assess the impact of SB203580, BIRB796 and VX745 on the lifespan of GI syndrome cell strains compared to the mean lifespan extension for normal cells (see table 3.1). Those strains that were shown to have a statistically different response to p38 inhibitors compared to the normal mean are indicated by *.
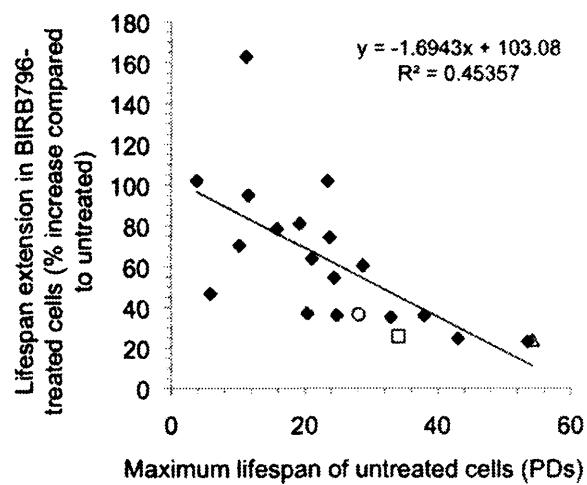
Figure 3.12. Relationship between *in vitro* lifespan extension in BIRB796-treated cells and maximum lifespan of untreated cells.

A regression line (R^2=0.45) is shown. Normal strains AG16409, AG06234 and AG13152 are represented by (△), (□) and (○), respectively, and GI syndrome fibroblasts are represented by (◆).
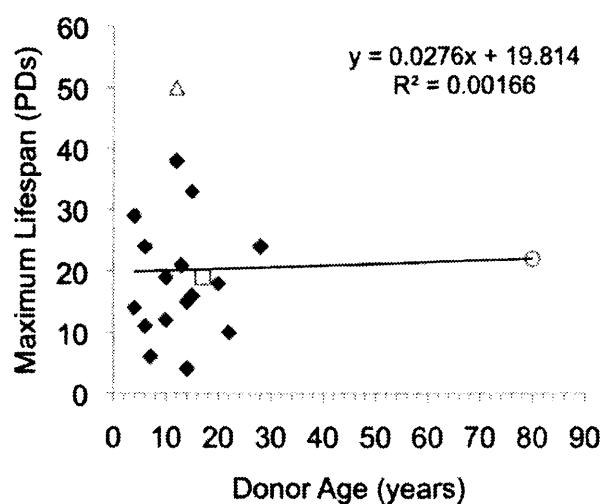
Figure 3.13. Relationship between *in vitro* proliferative capacity of adult dermal fibroblasts and donor age (years).

A regression line (R=0.002) is shown. Normal strains AG16409, AG06234 and AG13152 are represented by (△), (□) and (O), respectively, and GI syndrome fibroblasts are represented by (◆).

Chapter 4   Cellular Morphology of Dermal Fibroblasts from Normal and GI Syndrome Individuals and the effects of p38 inhibitors

4.1 Introduction

There is a growing consensus that the senescent cellular phenotype correlates with cells that are enlarged, flattened and granular (Burton 2009; Campisi 1997b; Campisi and d'Adda di Fagagna 2007; Rubin 1997). Although morphological change is associated with the senescent phenotype the mechanisms underlying such changes have not been well studied. It has been reported that WS fibroblasts early in their replicative lifespan show an altered, enlarged cellular morphology with extensive networks of F-actin stress fibres (Davis et al. 2005), and resemble normal fibroblasts that have undergone stress-induced premature senescence (SIPS) as a result of oncogenic ras expression or arsenite treatment (Deng et al. 2004; Guay et al. 1997; Huot et al. 1997; Wang et al. 2002). These observations support the hypothesis that WS cells may be undergoing SIPS triggered by increased levels of replication stress (Davis et al. 2005). The aim of this section of work was to determine if morphological changes, possibly indicative of SIPS, could be consistently observed in a panel of other GI syndrome cells.

According to current definition, stress fibres are bundles of numerous contractile acto-myosin filaments that are involved in adhesion, motility and morphogenesis (Naumanen et al. 2008). These transient structures form in response to tension and disappear when tension is released (Naumanen et al. 2008; Pellegrin and Mellor 2007). It has been suggested that the formation of stress fibres is a protective mechanism in which stabilisation of actin filaments results in increased resistance to stresses (Landry et al. 1989; Mehlen et al. 1996). Stress fibres have been reported in cells that have undergone SIPS, for example in

response to H_2O_2 (Chen et al. 1998; Toussaint et al. 2002); however, the usefulness of stress fibre presentation as a predictive marker of cells that have undergone SIPS remains unclear. A link between stress fibre presentation and entry into a senescence phenotype would therefore provide a valuable biomarker approach to investigating of the induction of SIPS.

The small heat-shock protein 27 (HSP27) is constitutively expressed in a variety of mammalian cell types (Benndorf et al. 1994) and its expression has been shown to increase in response to sub-lethal stresses including heat shock, toxins, and oxidative stress (Landry et al. 1989; Lavoie et al. 1995). Activation of HSP27 is therefore widely accepted to be a protective mechanism that allows a cell to respond to stressful stimuli (Franklin et al. 2005; Jaattela and Wissing 1992; Stetler et al. 2009). Evidence in the literature suggests that HSP27 phosphorylation is involved in the regulation of microfilament dynamics, modifying the actin response to physiological agonists and stabilising the actin cytoskeleton under stressful conditions (Huot et al. 1996; Huot et al. 1995; Lavoie et al. 1995). Furthermore, phosphorylation of HSP27 has been shown to be regulated by MK2 via p38 MAPK (Guay et al. 1997; Huot et al. 1997; Shi et al. 2003) leading to the hypothesis that the altered morphology, including increased level of stress fibres, in WS cells, reflects the increased activation of p38 and its downstream target HSP27. Support for this theory comes from the observation that treatment of young WS cells with the p38 inhibitor SB203580 reduced the appearance of stress fibres, reverted the cellular morphology to that resembling young normal cells, and reduced the phosphorylation of HSP27 seen in these cells (Davis et al. 2005).

The aim of this chapter is to assess whether there are any differences in cellular morphology and stress fibre presentation in GI syndromes cells compared to normal cells. To address this a semi-quantitative examination of cellular morphology of the GI syndrome panel members in the presence and absence of p38 inhibitors was undertaken. Furthermore, the impact of p38 inhibitors on a known downstream target of p38, HSP27, was assessed.

4.2 Materials and Methods

4.2.1 Cell culture conditions

All cells were grown as monolayer cultures in EMEM and were maintained in a humidified incubator at 37°C, 20% O_2 and 5% CO_2. For drug treatments, cells were fed daily with EMEM containing 2.5μM SB203580, 2.5μM BIRB796 or 0.5μM VX745, dissolved in DMSO. Control cells were supplemented with an equivalent volume of DMSO added to the medium. All cells were photographed under a phase contrast microscope (using 10X eyepiece and 10X objective).

4.2.2 Visualisation of stress fibres

Actin staining for fluorescence microscopy was performed essentially as previously described (Huot et al. 1997). Cells were plated onto glass coverslips in EMEM and allowed to settle for 48 hours at 37°C. The cells were washed in PBS, fixed in 3.7% (w/v) paraformaldehyde for 20 minutes, and permeabilised with 0.1% (v/v) Triton X-100 for 20 minutes. F-actin was detected using fluorescein isothyocynate-conjugated phalloidin (33μg/ml), diluted 1:50 in PBS for 20 minutes in the dark. Cells were then washed with PBS and the coverslips mounted onto glass slides using ProLong Gold Antifade reagent.

4.2.3 Semi-quantitative analysis of stress fibres presentation and morphological features

Careful observations were made of each cell strain throughout their lifespans. Pictures were taken at early growth stages (approximately 30 days in culture) to provide semi-quantitative analysis of the differences in cellular morphology and stress fibre presentation in each strain. An attempt was made to describe the inter- and intra-strain heterogeneity with regard to cell morphology and visual estimates of the proportions of different cellular morphologies present were made. The term majority refers to a feature that was shown in > 50% of the cells, and the term minority refers to a feature shared by < 10% of cells.

116

4.2.4 Analysis of activation of HSP27 by ELISA

The following reagents are provided as part of the PathScan™ Sandwich ELISA kit (Cell Signaling, NEB UK).

1X ELISA lysis buffer:	20 mM Tris (pH7.5), 150 mM NaCl, 1 mM EDTA, 1 mM EGTA, 1% (v/v) Triton X-100, 2.5 mM sodium pyrophosphate, 1 mM β–glycerolphosphate, 1 mM Na_3VO_4, 1 µg/ml leupeptin (#9803, Cell Signaling®). Made by diluting 10X stock with MilliQ H_2O.
1X Wash Buffer:	Made by diluting 20X Wash Buffer [1% (v/v) Tween-20 , 0.5% (v/v) Kathon® (CAS# 55965-84-9) in 20X PBS] in MilliQ H_2O.
Sample Diluents:	0.1% (v/v) Tween-20, <0.1% (w/v) sodium azide in 20X PBS.
TMB Substrate:	0.05% (w/v) 3,3',5,5' tetramethylbenzidine, 0.1% (v/v) H_2O_2, complex polypeptides.
STOP Solution:	0.05% (w/v) α and β unsaturated carbonyl compound.

Sample preparation, protein extraction and quantification were performed as previously described in Methods section 2.3.2 and 2.3.3. The level of total and phosphorylated HSP27 was assessed using the PathScan® Total HSP27 Sandwich ELISA (Cat No. #7295, Cell Signaling) and PathScan® Phospho-HSP27 (Ser78) Sandwich ELISA (Cat No. #7290, Cell Signaling) according to the manufacturers guidelines. Briefly, microwell strips were allowed to reach room temperature prior to use. WCE were diluted 1:1 in Sample Diluent and vortexed to mix thoroughly. 100 µl of each diluted WCE was added to the appropriate well, sealed with tape and incubated overnight at 4°C to allow for best detection of the target protein. 100 µl of Sample Diluent alone was added to one well as a negative control for the background detection levels for each ELISA. Following incubation, the contents of the plate was discarded and wells were washed four times with 1X

Wash Buffer. Following each wash the plates were tapped firmly on paper towels to remove any residual solution from the wells. Care was taken not to allow the wells to completely dry at any time and the underside of the plate was wiped to remove any solution that may affect the later analyses. 100 µl of Detection Antibody was added to each well and incubated for 1 hour at 37°C. Plates were washed as previously described before 100 µl of HRP-linked secondary antibody was added to each well and incubated for 1 hour at 37°C. Plates were washed again as previously described before 100 µl of TMB Substrate was added to each well for 30 minutes at room temperature and a blue colour was observed. 100 µl of STOP Solution was added to quench the reaction and plates were shaken gently to ensure the solutions were mixed. A colour change from blue to yellow was observed. Spectrophotometric analysis of samples was performed at 450 nm within 30 minutes of the STOP Solution being added. The data generated was transferred into Excel for further analysis. The background signal for each ELISA, given as the OD for the Sample Diluent alone, was subtracted from all experimental values and the activation of HSP27 was calculated as a ratio of the phospho-HSP27 signal: Total-HSP27 levels.

4.3 Results

To assess whether GI syndrome cells show any features of cells undergoing stress the cellular morphology and degree of stress fibre presentation for the GI panel members were compared to normal adult dermal fibroblasts. Furthermore, to assess whether p38 inhibitors can modulate cellular morphology, the pragmatic approach was taken to simultaneously grow these cells in a range of different p38 inhibitors and perform a semi-quantitative analysis of changes in cellular morphology and stress-fibre presentation. Comments are made on cell size, cell shape and on other aspects of cellular morphology including granularity and stress fibre presentation; however, quantitative measurements of these features were not made in this chapter. Note that for the GI panel, only cells that show some notable differences compared to normal cells have been described in detail in this chapter, full details of the cellular morphologies and stress-fibre presentation are provided

118

on the accompanying disk. This chapter thus serves as a screen to identify any cell strains that show obvious morphological changes associated with SIPS. The results are summarised in section 4.3.10

4.3.1 Normal Dermal Fibroblasts

Given the variation in morphology of normal dermal fibroblasts reported in the literature, the cellular morphology of three strains of normal dermal fibroblasts was examined to provide a view of how normal cells appear in culture. In a population of AG16409(N) cells there is a spectrum of morphological types including small spindle-like cells, larger irregular-shaped cells, and enlarged, flattened cells that are granular in appearance (Figure 4.1b). The majority of AG16409(N) cells are small and spindle-like or small irregular-shaped cells (>95%) and the enlarged, granular cells are relatively infrequent (~2%). When stained with phalloidin-FITC, the majority of cells lack F-actin stress fibres; however, some stress fibres are observed in the enlarged cells (indicated by arrow in Figure 4.1a). Treatment with SB203580 has a minor effect on the size distribution of AG16049(N) cells, with the enlarged cells remaining in the population (Figure 4.1d). When stained with phalloidin-FITC, the SB203580-treated cells resemble their untreated counterparts (Figure 4.1c). A similar response is observed using VX745 (Figure 4.1 g, h). BIRB796 has the biggest effect on AG16409(N) cells (Figure 4.1f), with the majority of cells appearing less granular and very few enlarged cells remaining. This change is confirmed when stained with phalloidin-FITC as nearly all cells are small and lack stress fibres (Figure 4.1e).

A similar result is seen for the normal strain AG06234(N), although more enlarged cells are observed (~15%) compared to AG16409(N) cells. Some small spindle-like cells are also observed (indicated by arrow in Figure 4.2b). When stained with phalloidin-FITC, stress fibres are observed in some of the enlarged cells but these are not extensive and do not tend to be seen in the small cells (Figure 4.2a). Treatment with p38 inhibitors has a minor effect on the size distribution and cellular morphology of AG06234(N) cells, with SB203580- (Figure

4.2 c, d), BIRB796- (Figure 4.2 e, f) and VX745- (Figure 4.2 g, h) treated populations showing a reduction in the number of enlarged cells.

In the third normal strain, AG13152(N),the majority of cells are enlarged and granular (~60%) (Figure 4.3b). Some stress fibres can be seen in the enlarged cells even in the bright-field images, but not in the small cells (Figure 4.3b), and these are oriented mostly parallel to the long axis of the cell (Figure 4.3a). Treatment with p38 inhibitors has a greater effect on the cellular morphology of AG13132(N) cells than was seen for the previous two strains, reducing the proportion of enlarged cells to ~10%.

In summary, inter-strain heterogeneity is observed in normal cells with regard to the proportion of enlarged cells. Stress fibres are observed in all three strains but these only occur in enlarged cells. p38 inhibitors have a minor effect on all three strains, reducing the proportion, but not completely removing, enlarged cells from the population. A consistent pattern of response to each inhibitor is observed, with BIRB796 having the greatest impact on cellular morphology and VX745 having the least effect. These observations provide a view on how normal adult fibroblasts appear in culture, and provide a baseline against which to compare the morphologies and responses to p38 inhibitors in the GI panel members.

4.3.2 Rothmund Thomson Syndrome

Young AG17524(RTS) cells resemble AG06234(N) cells, with the majority of cells being small and spindle-like or with an irregular shape (~90%), although some enlarged, granular cells (~10%) are observed (Figure 4.4b). As seen in normal cells, stress fibres are only observed in the enlarged cells (Figure 4.4a). A characteristic feature of AG17524(RTS) appears to be the presence of granular structures resembling abnormal Golgi structures and short, multi-directional stress fibres around the nuclei of some of the enlarged cells that are visible under bright-field microscopy (indicated by inset in Figure 4.4b). Treatment with p38 inhibitors has a minor effect on the morphology of AG17524(RTS) cells, similar to that seen for AG06234(N) cells. Some enlarged cells remain following treatment with p38

inhibitors and these retain their stress fibre phenotype and characteristic granular structures around the nucleus (See accompanying disk).

AG18371(RTS) cells are more similar to AG13152(N) cells in that the cells are more enlarged compared to AG17524(RTS) cells. However, AG18371(RTS) cells also display granular structures around the nucleus (Figure 4.4d), similar to those observed in AG17524(RTS) cells. In addition, prominent stress fibres that extend across the long-axis of the cell are observed in the enlarged cells in AG18371(RTS) (as indicated by arrows Figure 4.4c). p38 inhibitors appear to have a slightly greater effect on AG18371(RTS) cells compared to AG17524(RTS) cells but is similar to the response seen for AG13152(N) cells (See accompanying disk).

The third strain, AG18375(RTS), differs from the previous two RTS strains, with ~50% of cells having an unusual polygonal shape with lamellipodial-like or filopodial-like extensions (Figure 4.5a). Some of the enlarged AG18375(RTS) cells have a granular region surrounding the nucleus, similar to that seen in AG18371(RTS) cells, although this is more pronounced (indicated by inset in Figure 4.5b). Stress fibres were observed in enlarged cells but not in the smaller cells (Figure 4.5a). Treatment of AG18375(RTS) cells with SB203580 and VX745 has a similar effect as seen for AG13152(N) cells; however, BIRB796 appears to have a greater effect, reducing cell size and granularity of AG18375(RTS) cells compared to normal cells (Figure 4.5 e and f).

4.3.3 Bloom Syndrome

Young GM02932(BS) and GM02520(BS) cells resemble AG16409(N) or AG06234(N) cells, with the majority of cells being small with a spindle-like or irregular shape and only a few enlarged cells present (Figure 4.6 b and d). As seen in normal cells, stress fibres are only observed in the enlarged cells (Figure 4.6 a and c). GM02548(BS) cells contain a higher proportion of enlarged cells (~20%) compared to the other two BS strains, and have a similar morphology to AG13152(N) cells (Figure 4.6e and f). Treatment with p38 inhibitors has a similar effect on all three BS strains as was observed for normal cells, with a reduction in

the proportion of enlarged cells but those that remain retaining their stress fibre phenotype (See accompanying disk).

4.3.4 Hutchinson-Gilford Progeria Syndrome

Young AG11498(HGPS) cells have a similar morphology to AG06234(N), with some enlarged cells present but the majority of cells are small and irregularly shaped (Figure 4.7b). The second strain AG10677(HGPS) also resembles AG06234(N) cells and is relatively indistinguishable from the AG11498(HGPS) strain (Figure 4.7d). The third strain AG01972(HGPS) shows some differences compared to the previous two strains in that it contains more enlarged cells (~35%). In addition, some cells that are very enlarged compared to normal cells, with an unusual cytoplasmic patterning are observed in AG01972(HGPS) cells (indicated by arrow in Figure 4.7f). When stained with phalloidin-FITC, extensive stress fibre networks are observed only in the very enlarged cells in all three strains (Figure 4.7 a, c and e). Treatment with p38 inhibitors had a minor effect on the morphology of both AG11498(HGPS) and AG10677(HGPS) cells, similar to that observed for AG06234(N) cells but a slightly greater impact on AG01972(HGPS), similar to that observed for AG13152(N) cells (See accompanying disk).

4.3.5 Nijmegen-Breakage Syndrome

Young RO202(NBS) and RO242(NBS) cells have a similar morphology to AG16049(N) cells, with the majority of cells being small (~90%) with only a few enlarged cells with stress fibres present (~10%) (Figure 4.8 a-d). Treatment with p38 inhibitors has a minor effect on the morphology of RO202(NBS) and RO242(NBS) cells, reducing the proportion of enlarged cells to <5% in each case, with only minor differences being observed between the different inhibitors used (See accompanying disk).

However, the third strain GM07166(NBS) has a strikingly different morphology to the previous two strains. Although some small spindle-like cells are observed, in young GM07166(NBS) cells the majority of cells are enlarged and

granular (~85%) with extensive stress fibre networks that are visible under bright field microscopy (Figure 4.9b). GM07166(NBS) cells have a characteristic cytoplasmic pattern similar to that seen in RTS cells; however, these patterns appear to occur throughout the cytoplasm rather than be focussed around the nucleus as was seen in RTS cells (Figure 4.4 and Figure 4.5 a and b) and are more prominent in the enlarged cells (indicated by inset in Figure 4.9b). When stained with phalloidin-FITC, extensive stress fibres are observed only in the enlarged cells (Figure 4.9a), with the majority of stress fibres oriented parallel to the long axis of the cell but some being more irregularly oriented in other cells. Treatment with all three p38 inhibitors has a striking effect on the cellular morphology of GM07166(NBS) cells, reducing the proportion of enlarged cells in the population (Figure 4.9 c-h). In particular, BIRB796 reduces the proportion of enlarged cells in the population to <5% (Figure 4.9f).

4.3.6 Ligase 4 Syndrome

Young GM17523(LIG4) and GM10688(LIG4) cells resemble AG06234(N) cells, with the majority of cells being small and spindle-like or irregularly shaped and only a few enlarged cells with stress fibres (<5%) present (Figure 4.10 a-d). Treatment with p38 inhibitors has a minor effect on the morphology of both GM17523(LIG4) and GM10688(LIG4) cells, similar to that observed for normal cells (See accompanying disk).

4.3.7 Cockayne Syndrome A

Young GM01856(CSA) cells resemble AG06234(N) or AG16409(N) cells, with the majority of cells being small and spindle-like or irregularly shaped (~90%) (Figure 4.11b) and only a few enlarged cells with stress fibres being observed (~10%) (Figure 4.11a). Treatment with p38 inhibitors has a minor effect on the morphology of GM01856(CSA) cells (See accompanying disk), similar to that observed in normal cells.

4.3.8 Dyskeratosis Congenita

In a young population of GM01774(DKC) the majority of cells are enlarged, flattened and granular (Figure 4.11d). Stress fibres are present in all enlarged cells and can be seen even in the bright-field images (Figure 4.11c and d). Staining with phalloidin-FITC shows that the F-actin stress fibres are mostly oriented along the long axis of the cell (indicated by arrows in Figure 4.11c). Treatment with p38 inhibitors has a minor effect on cellular morphology, with cells having a less granular appearance overall; however, the proportion of enlarged cells in the population is relatively unchanged and these still have stress fibres (See accompanying disk).

4.3.9 Seckel Syndrome

Young GM09812(SS) cells are reminiscent of AG16409(N) and AG06234(N) cells, with the majority of cells being small (>95%) with only very few enlarged cells observed (<5%) (Figure 4.11f). When stained with phalloidin-FITC, stress fibres are observed only in the few enlarged cells (Figure 4.11e). Treatment with p38 inhibitors has a minor effect on the morphology of GM09812(SS) cells (See accompanying disk).

In contrast, the GM18366(SS) strain has a strikingly different morphology to that observed for GM09812(SS) cells, with ~50% of cells being enlarged and granular with few small spindle-like cells observed (<5%) (Figure 4.12b). Stress fibres are only observed in the enlarged cells (Figure 4.12a) and although the majority of GM18366(SS) cells are enlarged with stress fibres these do not appear to be as extensive as seen in other strains, such as GM07166(NBS) cells (Figure 4.9a). Treatment with p38 inhibitors has a striking effect on GM18366(SS) cells, reducing the proportion of enlarged cells with stress fibres and increasing the proportion of small cells (Figure 4.12 c-h). In particular, BIRB796 reduces the proportion of enlarged cells with stress fibres to <10% (Figure 4.12e and f).

4.3.10 Summary of stress fibre presentation and cellular morphology

Given that stress fibre presentation appears to be related to cell size, a semi-quantitative analysis of the proportion of enlarged cells in GI syndromes and normal cells was undertaken and the results are summarised in Table 4.1. The following comparison of cellular morphologies was undertaken at early growth stages (approximately 30 days in culture). The proportion of enlarged cells in AG16409(N) is relatively low (~5%), with the majority of cells being small and spindle-like. In contrast, AG13152(N) cells show a higher proportion of enlarged cells (~45%), whereas AG06234(N) have an intermediate morphology. These data suggest that heterogeneity in cell morphology can be detected between different primary fibroblast strains that have no known defect. It is therefore expected that GI syndrome cells may have an added level of heterogeneity as a result of the underlying molecular defect. When comparing the morphology of GI syndrome cells, the range of morphologies observed for normal cell strains were taken into account.

The following section provides a summary of:

1. The cellular morphology of young untreated normal and GI syndrome cells.

2. The effect of p38 inhibitors on cellular morphology.

1. Comparison of cellular morphology

AG17524(RTS) cells were shown to have a relatively normal appearance with low numbers of enlarged cells. AG18371(RTS) cells had a higher proportion of enlarged cells than seen for AG17524 but these were estimated to be a similar size to those observed in AG13152(N) cells. The AG18375(RTS) strain showed some differences compared to the other two RTS strains in that the enlarged cells had an unusual polygonal shape and were present in higher numbers than observed in the other RTS strains; however, again these were estimated to be of a similar size to those observed in AG13152(N) cells. GM02520(BS) and GM02932(BS) had a similar morphology to AG06234(N), although the proportion of enlarged cells was

slightly higher in these strains compared to AG06234(N) cells. GM02548(BS) cells also resembled normal cells, but had a higher proportion of enlarged cells compared to the other two BS strains. The proportion of enlarged cells in all three HGPS strains was at the top end of the normal spectrum, with AG10677(HGPS) and AG11498(HGPS) cells resembling AG13152(N) cells. AG01972(HGPS) cells also had a similar appearance to AG13152(N) cells; however, some very enlarged cells with unusual cytoplasmic patterning and prominent stress fibres were observed. In NBS, the RO202(NBS) and RO242(NBS) strains resembled AG16409(N) cells, with very few enlarged cells present. In contrast, GM07166(NBS) cells had a strikingly different morphology, with a much higher proportion of enlarged cells (~85%) with prominent stress fibres compared to all of the normal strains. GM01856(CSA) cells have a similar appearance to AG16409(N) or AG06234(N) cells with the majority of cells being small and spindle-like; however, the enlarged cells present appear to be larger than those observed in normal cells. Both GM17523(LIG4) and GM16088(LIG4) have a similar morphology to AG06234(N) cells, with the majority of cells being small and only a few enlarged cells observed. DKC cells show an altered morphology to normal cells, with a much higher proportion of enlarged cells (~60%) and prominent stress fibres. GM18366(SS) have a similar morphology to that observed for GM01774(DKC) cells, with a higher proportion of enlarged cells (~50%) than normal cells, whereas GM09812(SS) cells resemble AG06234(N) cells, with few enlarged cells observed.

To further assess the usefulness of changes in morphology as a biomarker of commitment to senescence, a correlative study of the proportion of enlarged cells versus the maximum lifespan of each of the cell strains was undertaken. Figure 4.13 shows a negative correlation between the proportion of enlarged cells and lifespan, suggesting that the strains that contain the greatest number of enlarged cells tend to have the shortest lifespan. Therefore, the proportion of enlarged cells appears to be a relatively reliable marker of commitment to senescence.

2. Effects of p38 inhibitors

The effects of p38 inhibitors on cellular morphology are summarised in Table 4.2. In general, treatment with p38 inhibitors reduced the proportion of enlarged cells in both normal and GI syndrome cells, with BIRB796 having the greatest impact and VX745 the least impact on morphology. p38 inhibitors have a minor effect on AG16409(N) cells with the proportion of enlarged cells being relatively unchanged. AG13152(N) cells show the greatest response, with the proportion of enlarged cells being reduced from ~45% to ~10% in response to all three inhibitors, and AG06234(N) cells have an intermediate response. Given the problems associated with this interstrain heterogeneity, the responses to p38 inhibitors in the GI panel members were assessed on a strain-by-strain basis using a two-tailed z-test. Although some cell strains, such as GM07166(NBS), showed a marked change in cellular morphology in response to p38 inhibitors, none of the differences observed were found to be statistical significant. It is likely that this is due to the heterogeneity in cellular morphologies observed for the three normal strains.

4.3.11 Activation of HSP27: A downstream target of p38

To assess the activation of p38-mediated stress pathways, the activation of a downstream target of p38, HSP27, was examined. These data show that p-HSP27 can be detected in all cells and that p38 inhibitors reduce the level of p-HSP27 (Figure 4.14). In general, BIRB796 was seen to have the greatest impact on p-HSP27 levels, whereas VX745 had the least effect. This is consistent with the pattern of effect of these inhibitors on both the morphology and growth potential (Chapter 3) of these cells. Inter-strain differences in p-HSP27 levels are observed in normal cells. AG16409(N) shows the lowest level of p-HSP27, AG06234(N) shows the intermediate level and AG13152(N) cells show the highest level of p-HSP27. Treatment with p38 inhibitors has the greatest effect on AG13152(N) cells and the least effect on AG16409(N) cells, reducing the levels of p-HSP27 to similar levels in all three strains. When compared to normal cells, GM01856(CSA) cells show a similar level of p-HSP27 to AG13152(N) cells, however, p38 inhibitors have

a reduced effect on GM01856(CSA) cells compared to normal cells. GM09812(SS) cells have a low level of p-HSP27 and p38 inhibitors only have a minor effect on this, whereas GM18366(SS) cells have a higher level of p-HSP27, similar to that seen in AG13152(N) cells. Although, p38 inhibitors reduce the level of p-HSP27 in GM18366(SS) cells the effect is not as great as seen for normal cells. In NBS, RO202(NBS) and RO242(NBS) show low levels of p-HSP27, comparable to AG06234(N) cells, and have a normal response to p38 inhibitors; however, GM07166(NBS) cells show a higher than normal level of p-HSP27. Treatment of GM07166(NBS) has a larger impact on the level of p-HSP27 than seen for the other two NBS strains but is comparable to those seen for AG13152(N) cells. GM02520(BS) and GM02932(BS) show a normal level of p-HSP27, similar to the level observed for AG06234(N), and show a normal response to p38 inhibitors. Although the level of p-HSP27 in GM02548(BS) was higher than seen in the other two BS strains, it was still within the normal range. Treatment of GM02548(BS) with p38 inhibitors had a larger impact than seen for the other two BS strains but is comparable to those seen for normal cells. In RTS cells, inter-strain heterogeneity in p-HSP27 levels are observed, with AG17524(RTS) showing the lowest level of p-HSP27 and AG18375(RTS) showing the highest level, similar to that observed for AG13152(N) cells. AG11498(HGPS) and AG01972(HGPS) cells have a similar level of p-HSP27 to AG13152(N) cells, whereas AG10677(HGPS) has a lower level of p-HSP27, similar to that seen in AG06234(N) cells. Treatment with p38 inhibitors reduces the level of p-HSP27 to a similar level in all three HGPS strains, therefore having the largest effect on AG11498(HGPS) and AG01972(HGPS) cells. Both strains of LIG4 cells and DKC show a low level of p-HSP27 and p38 inhibitors have a minor effect on these cells.

Overall there appears to be a correlation between the level of p-HSP27 and cellular morphology in these cells. In general the strains that show an enlarged morphology also show increased levels of p-HSP27. For example, GM18366(SS) cells have an enlarged morphology and show increased levels of p-HSP27 compared to GM09812(SS) cells. Similarly, GM7166(NBS) cells show an enlarged morphology and increased p-HSP27 levels compared to the other two NBS strains.

In RTS cells, AG18375 has the highest proportion of enlarged cells and the highest level of p-HSP27, AG18371 has the intermediate morphology and p-HSP27 levels and AG17524 has the smallest proportion of enlarged cells and the lowest levels of p-HSP27. A similar pattern is observed for HGPS cells, in which GM09172 cells have the highest proportion of enlarged cells and the highest p-HSP27 levels. However, DKC show an unexpectedly low level of p-HSP27 given the high proportion of enlarged cells observed in this strain. In addition, those strains that show the highest level of p-HSP27 tend to show the greatest response to p38 inhibitors, for example GM7166(NBS), AG18375(RTS) and AG01972(HGPS).

4.4 Discussion

A full morphological characterisation of these cells has proved problematic considering the inter-strain heterogeneity in cellular morphology observed within the same syndrome and the difficulty in providing quantitative analysis of morphological characteristics. Another complication for the study was the uncertain passage history of the cell strains used as discussed in the previous chapter. The data presented here therefore provide a cross section of morphological changes that could arise from time in culture. Given the extensive number of strains, the pragmatic option was taken of an unbiased screen of cellular morphology and stress fibre presentation in all of the cells using the standard technique (summarised in Table 4.1).

Examination of the morphology of normal cells revealed inter-strain differences in the proportion of enlarged cells that was thought to be indicative of differences in the level of commitment to senescence. Given the uncertain replicative histories for some of these strains, it is also possible that the differences in morphology reflect differences in the level of replicative senescence since it is widely accepted that cells undergo morphological changes as they progress towards replicative senescence (Campisi 1999). Support for this theory came from the observation that the proportion of enlarged cells appears to correlate to the lifespan. For example, the AG13152(N) strain has the shortest lifespan and highest proportion of enlarged cells, whereas the AG16409(N) strain has the longest

lifespan and lowest proportion of enlarged cells. The findings underline the complexity associated with morphological characterisation of primary fibroblasts with uncertain replicative histories

Despite the known caveats, the findings suggest that differences in morphology, given as the proportion of enlarged cells, correlates with p-HSP27 levels. For example, the AG13152(N) strain show the highest level of p-HSP27, whereas the AG16409(N) strain show the lowest level. Moreover, the impact of p38 inhibitors appears to correlate with changes in morphology, with AG16409(N) cells showing a minor response to p38 inhibitors, whereas AG13152(N) cells show the greatest response. Overall, the findings support the view that primary cell populations consist of a subset of cells that are undergoing replicative senescence and a subset of cells that are undergoing SIPS. The working hypothesis here is that primary GI syndrome cell populations will also contain a subset of cells that are undergoing replicative senescence but may also contain a higher proportion of cells that are undergoing SIPS due to ongoing replicative stress.

As expected inter-strain heterogeneity in cellular morphology was observed in the GI syndrome panel. Overall, the majority of GI syndrome cell strains had a similar morphology to normal cells, with the exception of GM07166(NBS), GM01774(DKC), GM18366(SS) and AG18375(RTS), which had a higher proportion of enlarged cells that were granular and contained numerous stress fibres. The ratio of p-HSP27:HSP27 is higher than normal in both GM07166(NBS) and GM18366(SS), but is unexpectedly low in GM01774(DKC) given the enlarged morphology of DKC cells and impact of the inhibitors on growth potential of these cells. Analysis of the contribution of SIPS to DKC cells is complicated by the fact that DKC is caused by mutations in components of telomerase, suggesting that the truncated lifespan of DKC cells is due to the presence of very short telomeres. The observation that p38 inhibitors have a minor effect on the morphology of GM01774(DKC) cells suggests that these cells are indeed simply closer to the end of their replicative lifespan. In contrast, treatment of both GM07166(NBS) and GM18366(SS) with p38 inhibitors has a striking effect on both their morphology

and on the level of p-HSP27, suggesting a role for p38-mediated SIPS in these cells.

In conclusion, the main findings of this chapter are:

- Stress fibre presentation appears to be related to cell size rather than differences in underlying stress signalling, therefore cell size rather than stress fibre presentation appears to be more reliable marker of differences in replicative potential.

- GM07166(NBS), GM18366(SS), AG18375(RTS) and GM01774(DKC) show an altered cellular morphology, including a higher proportion of cells that are enlarged and granular, indicating a potential increase in the degree of SIPS occurring in these cells.

- Treatment with p38 inhibitors consistently reduces the proportion of enlarged, granular cells, with BIRB796 having the greatest effect.

- GM07166(NBS) and GM18366(SS) show the change in cellular morphology (reduction in proportion of enlarged cells) following treatment with p38 inhibitors.

- Differences in morphology, given as the proportion of enlarged cells, appears to correlate with the ratio of p-HSP27:HSP27, with GM07166(NBS) having the highest proportion of enlarged cells and the highest p-HSP27 levels.

This chapter raises issues associated with qualitative assessment of cellular morphology in heterogeneous populations and the need for quantitative methods of measuring cell enlargement, as an indicator of proliferation restraint. These issues are addressed in chapter 8.
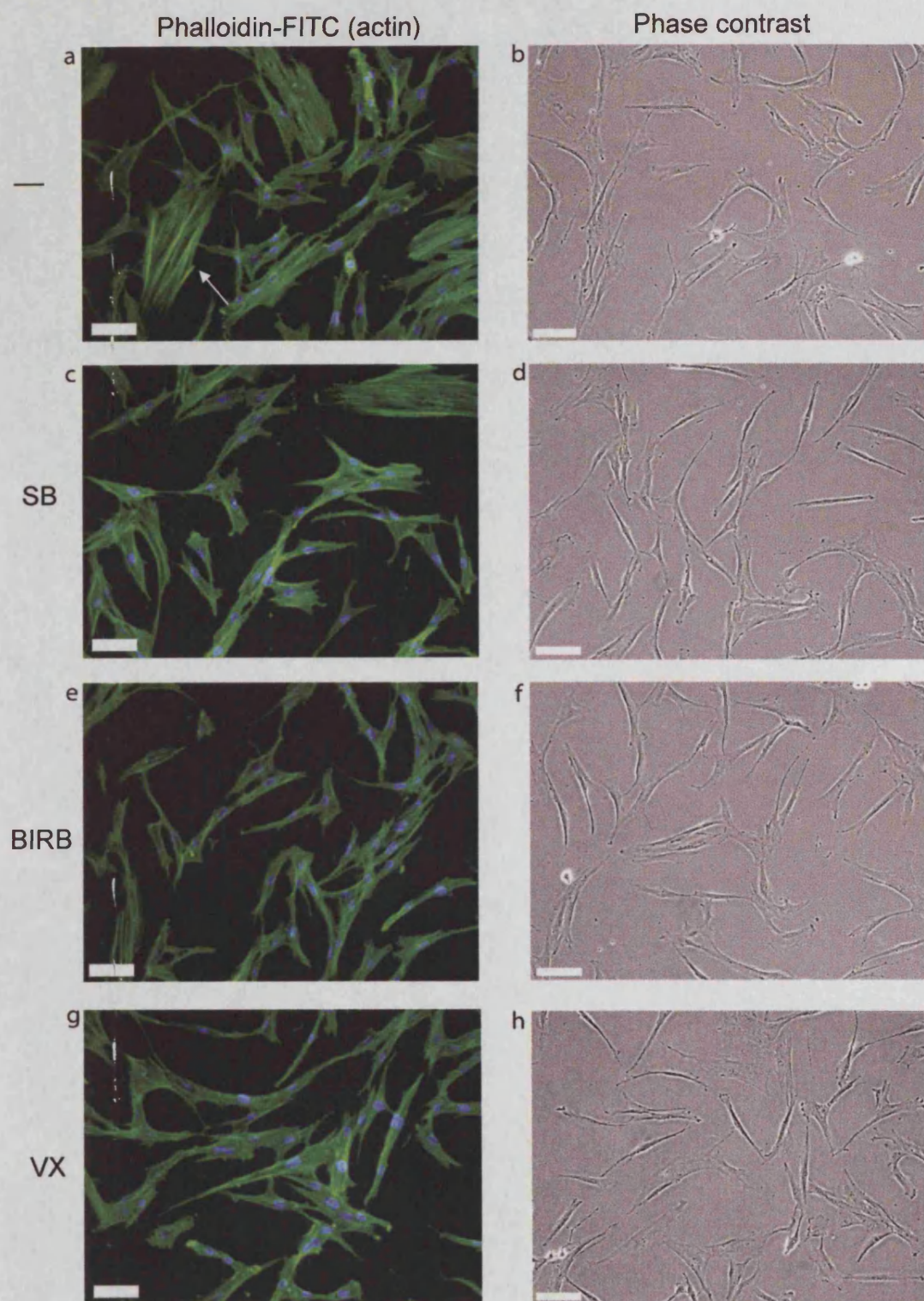
Figure 4.1. Cellular morphology and stress fibre presentation in AG16409(N) fibroblasts.

Cells were grown in the absence (a and b) or presence of SB203580 (c and d), BIRB796 (e and f) or VX745 (g and h). Panels a, c, e and g show visualisation of F-actin stress fibres stained with phalloidin-FITC and DAPI staining of the nuclei. Panels b, d, f and h show phase contrast pictures. White bar represents 100 μm.

132

Phalloidin-FITC (actin) Phase contrast
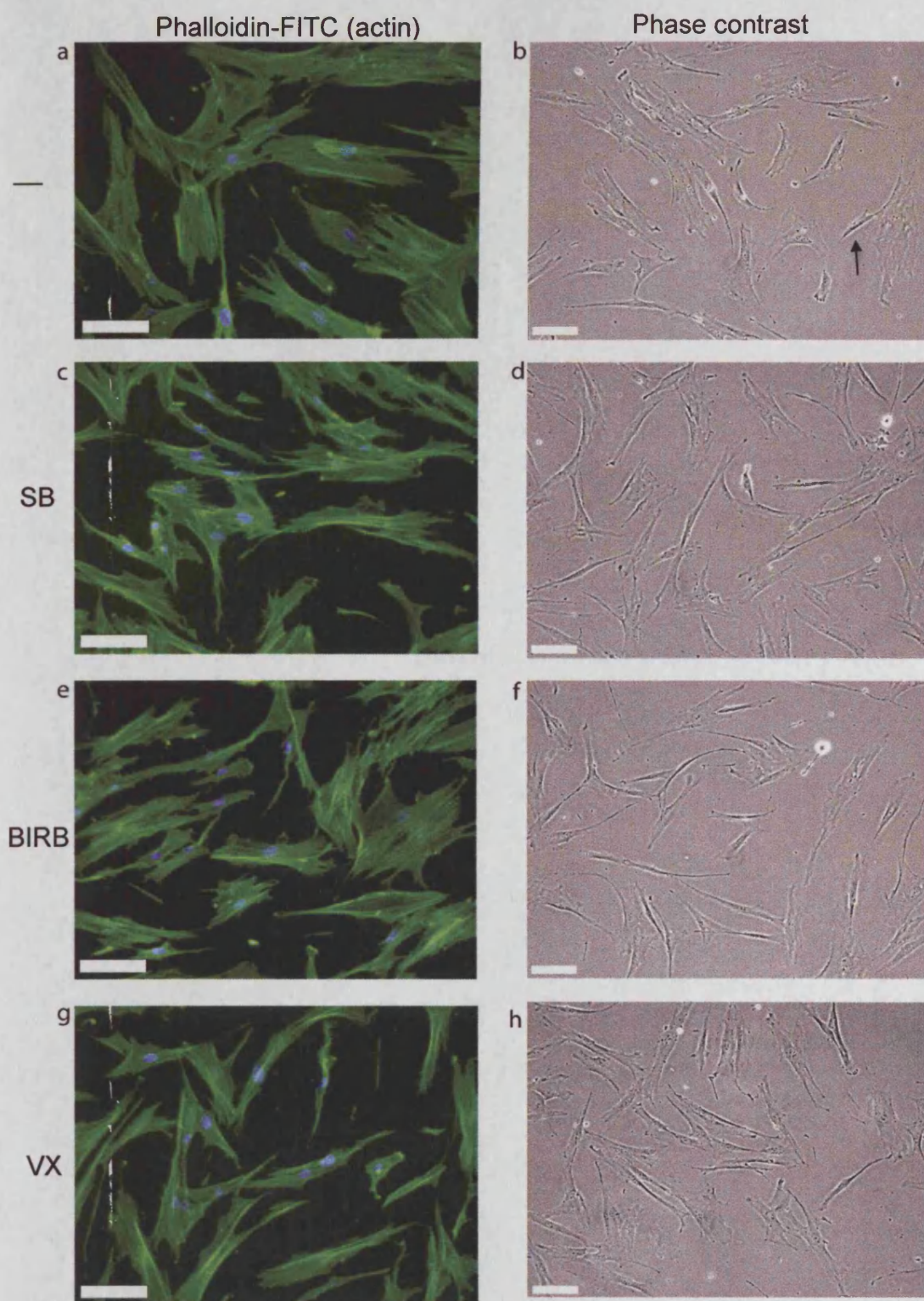
Figure 4.2. Cellular morphology and stress fibre presentation in AG06234(N) fibroblasts.

Panels are as in Figure 4.1 White bar represents 100 μm. Arrow in (b) indicates small spindle-like cell.

133

Phalloidin-FITC (actin)   Phase contrast
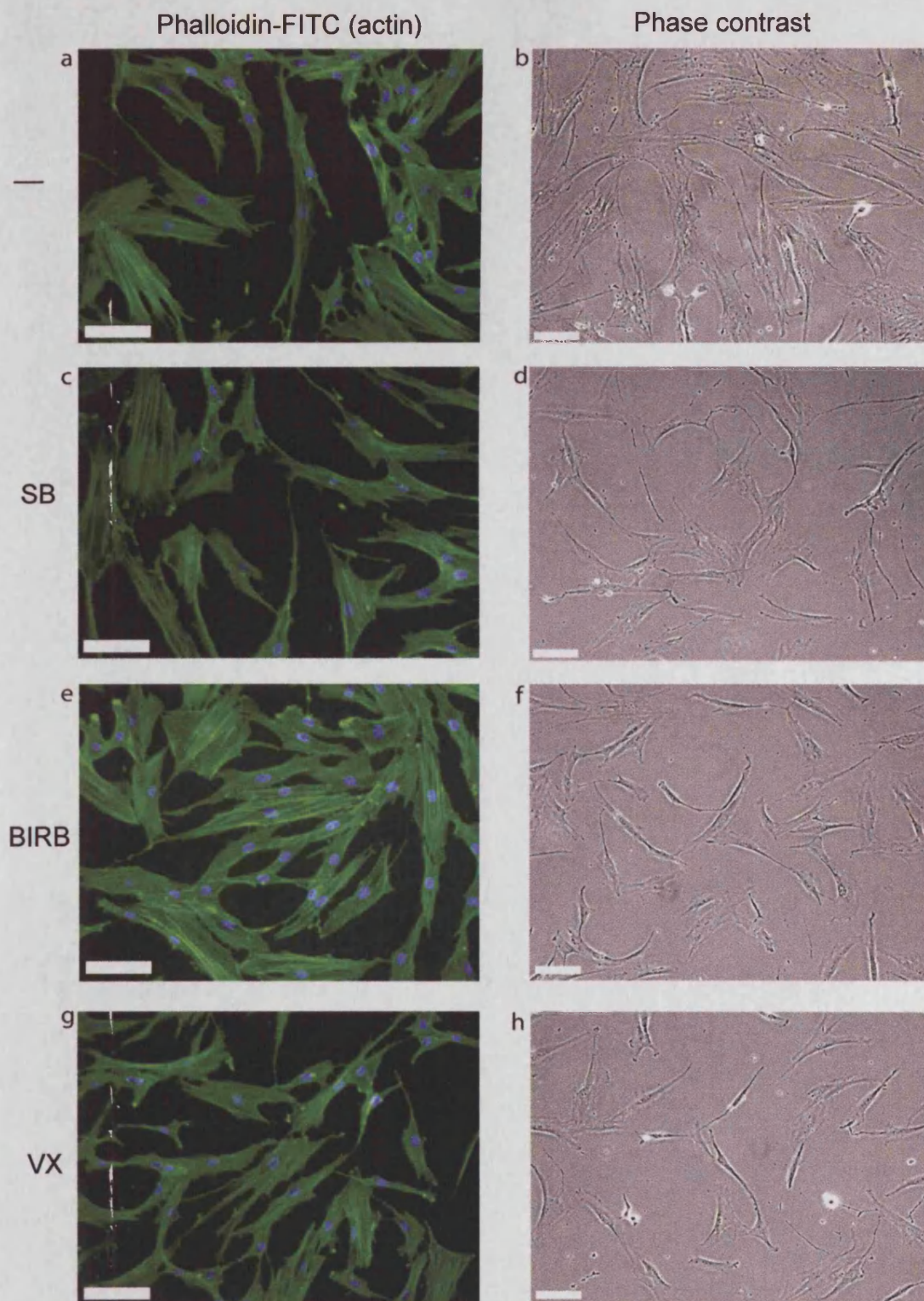
Figure 4.3. Cellular morphology and stress fibre presentation in AG13152(N) fibroblasts.

Panels are as in Figure 4.1. White bar represents 100 μm.

134

Phalloidin-FITC (actin) **Phase contrast**

a — AG17524(RTS)

b

c — AG18371(RTS)

d
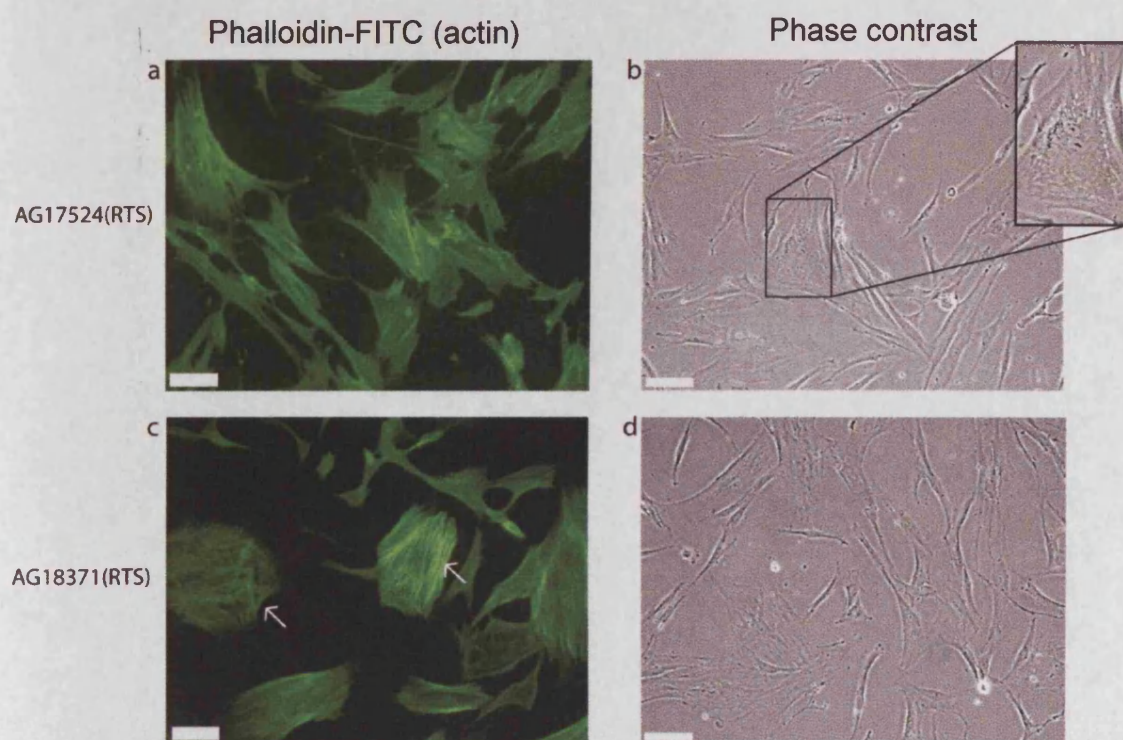
Figure 4.4. Cellular morphology and stress fibre presentation in untreated AG17524(RTS) and AG18371(RTS) fibroblasts.

Panels (a) and (c) show visualisation of F-actin stress fibres in AG17524(RTS) and AG18371(RTS) cells stained with phalloidin-FITC, respectively. Panels (b) and (d) show phase contrast pictures of AG17542(RTS) and AG18371(RTS), respectively. White bar represents 100 μm.

Phalloidin-FITC (actin)   **Phase contrast**
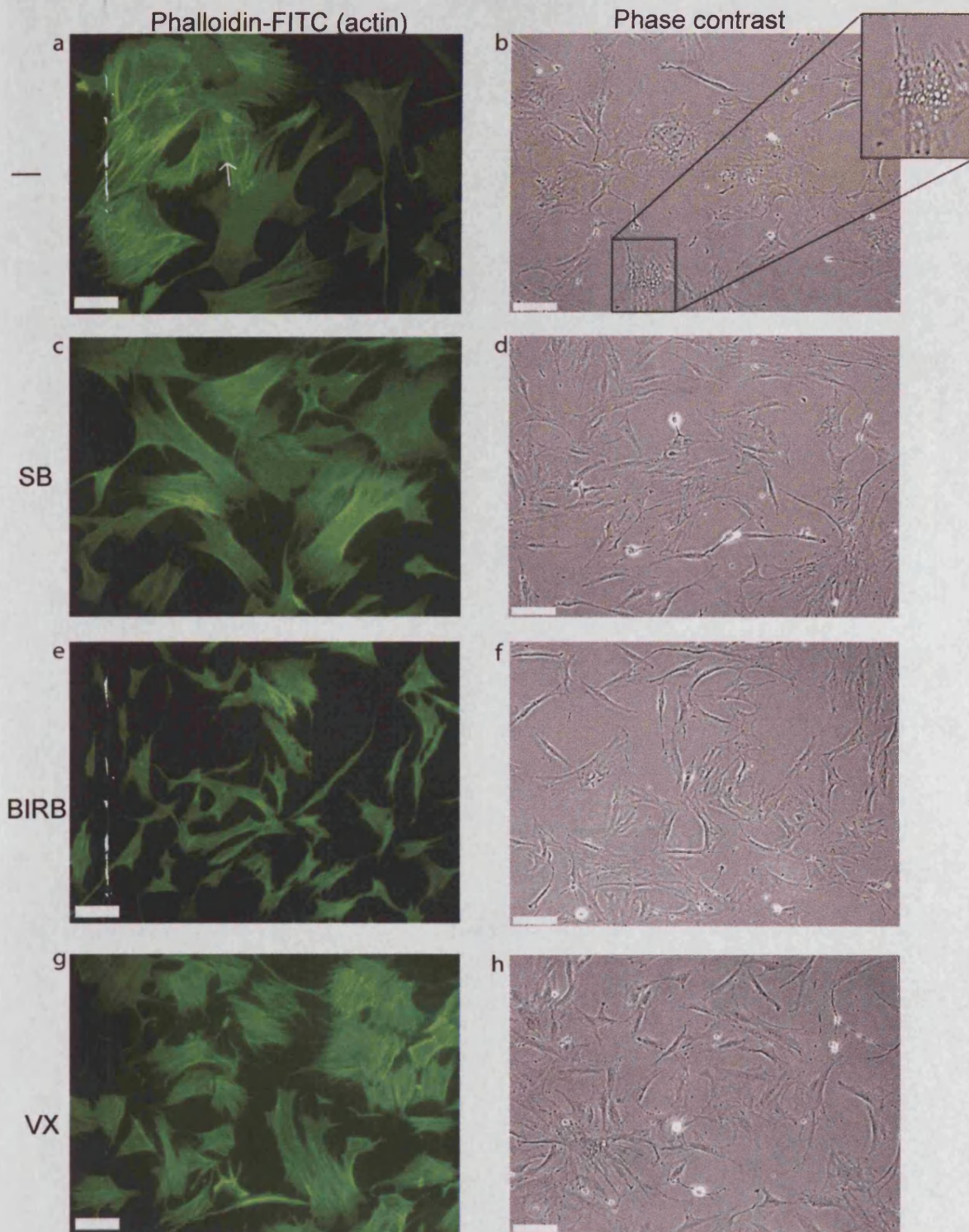
Figure 4.5. Cellular morphology and stress fibre presentation in AG18375(RTS) fibroblasts.

Panels are as in Figure 4.1. Inset in (b) shows a magnified image of an enlarged cell.

Phalloidin-FITC (actin)   Phase contrast

GM02932(BS)

GM02520(BS)
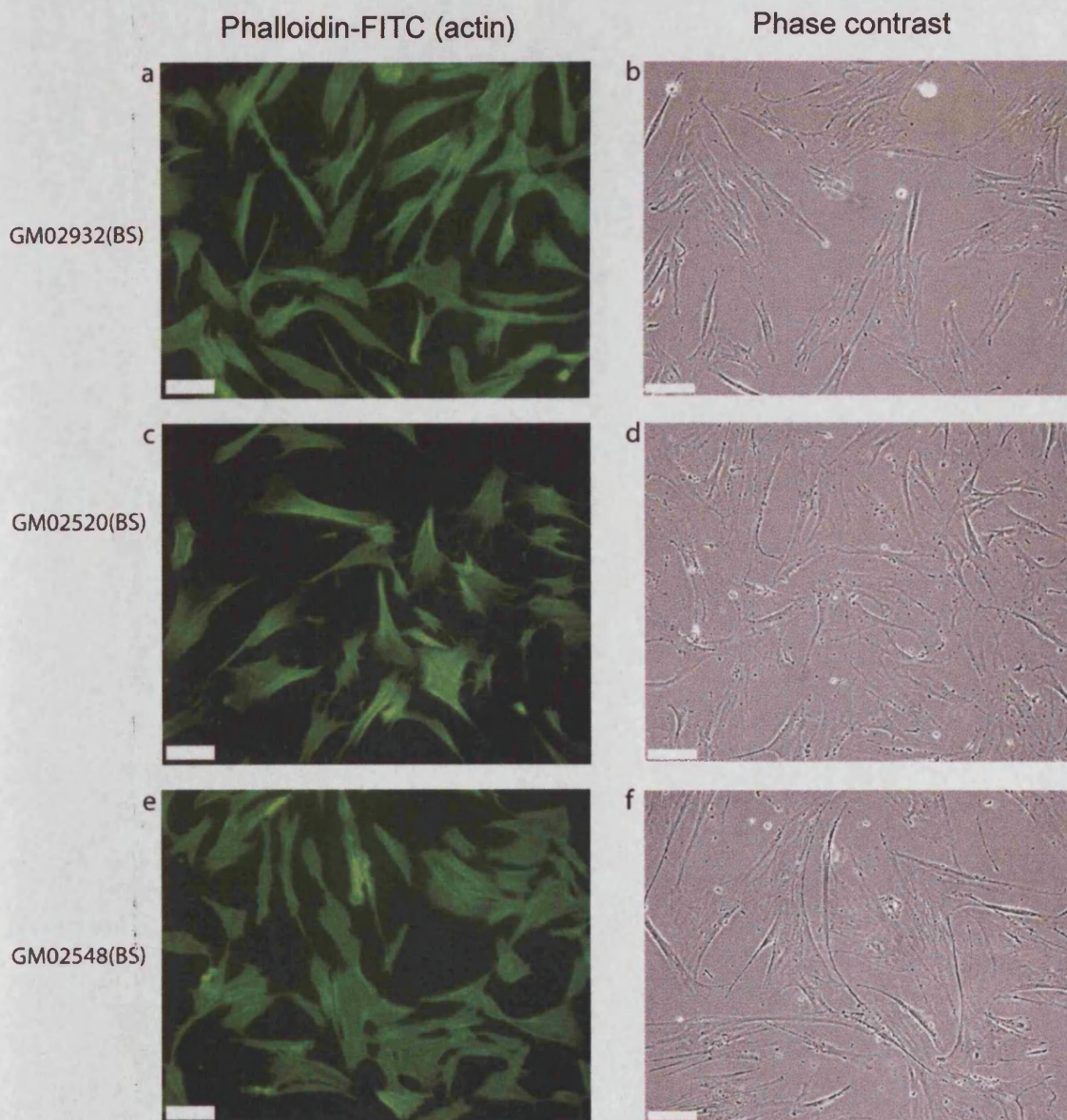
GM02548(BS)

Figure 4.6. Cellular morphology and stress fibre presentation in untreated GM02932(BS), GM02520(BS) and GM02548(BS) fibroblasts.

Panels (a) and (c) show visualisation of F-actin stress fibres in GM02932(BS), GM02520(BS) and GM02548(BS) cells stained with phalloidin-FITC, respectively. Panels (b) and (d) show phase contrast pictures of GM02932(BS), GM02520(BS) and GM02548(BS), respectively. White bar represents 100 μm.

Phalloidin-FITC (actin)   Phase contrast

AG11498(HGPS)

AG10677(HGPS)
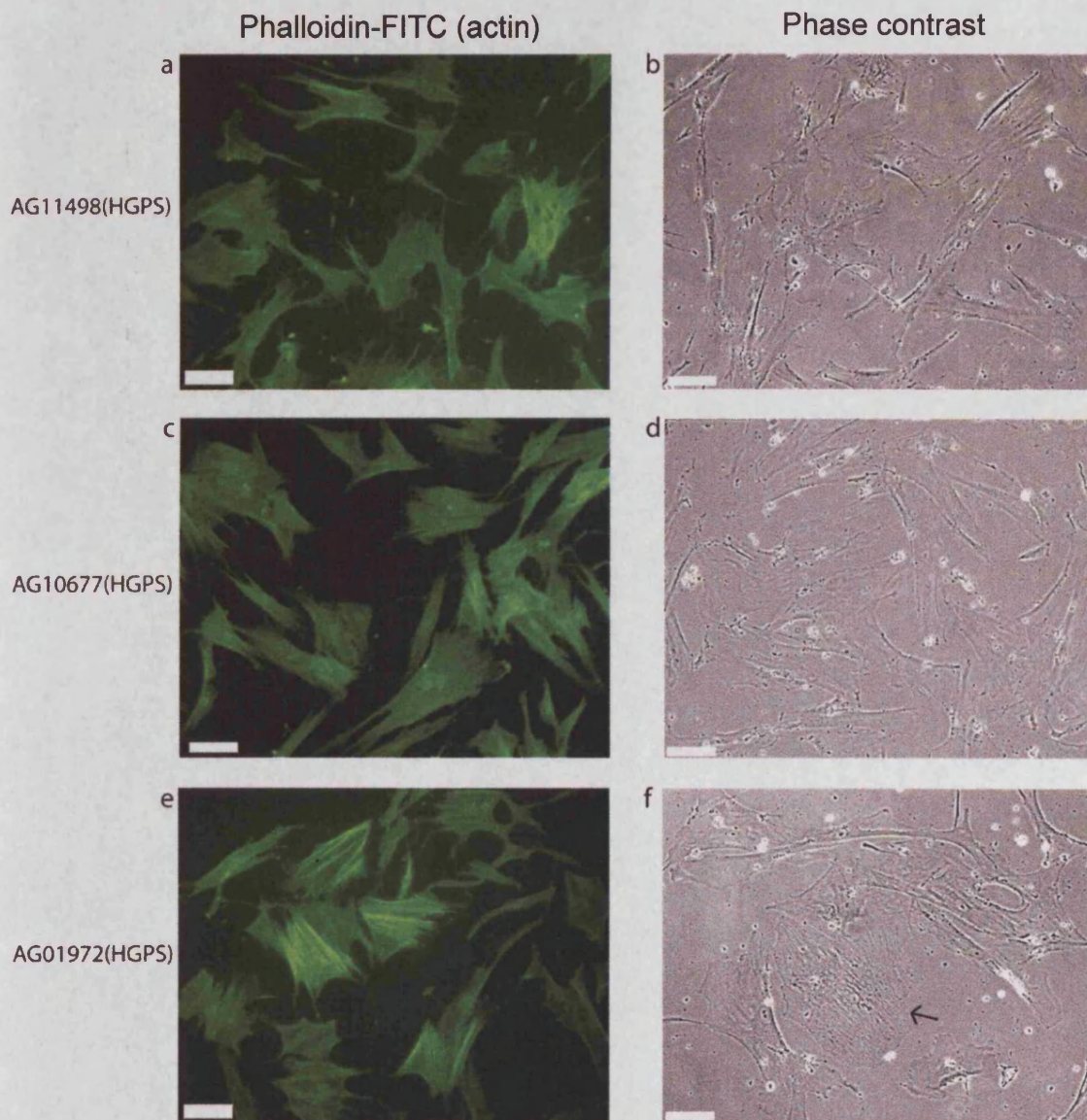
AG01972(HGPS)

Figure 4.7. Cellular morphology and stress fibre presentation in untreated AG11498(HGPS), AG10677(HGPS) and AG01972(HGPS) fibroblasts.

Panels (a, c and e) show visualisation of F-actin stress fibres in AG11498(HGPS), AG10677(HGPS) and AG01972(HGPS) cells stained with phalloidin-FITC, respectively. Panels (b, d and f) show phase contrast pictures of AG11498(HGPS), AG10677(HGPS) and AG01972(HGPS), respectively. White bar represents 100 μm. Arrow in (f) indicates presence of enlarged cell will unusual cytoplasmic patterning in AG01972(HGPS) cells.

138

Phalloidin-FITC (actin)   Phase contrast
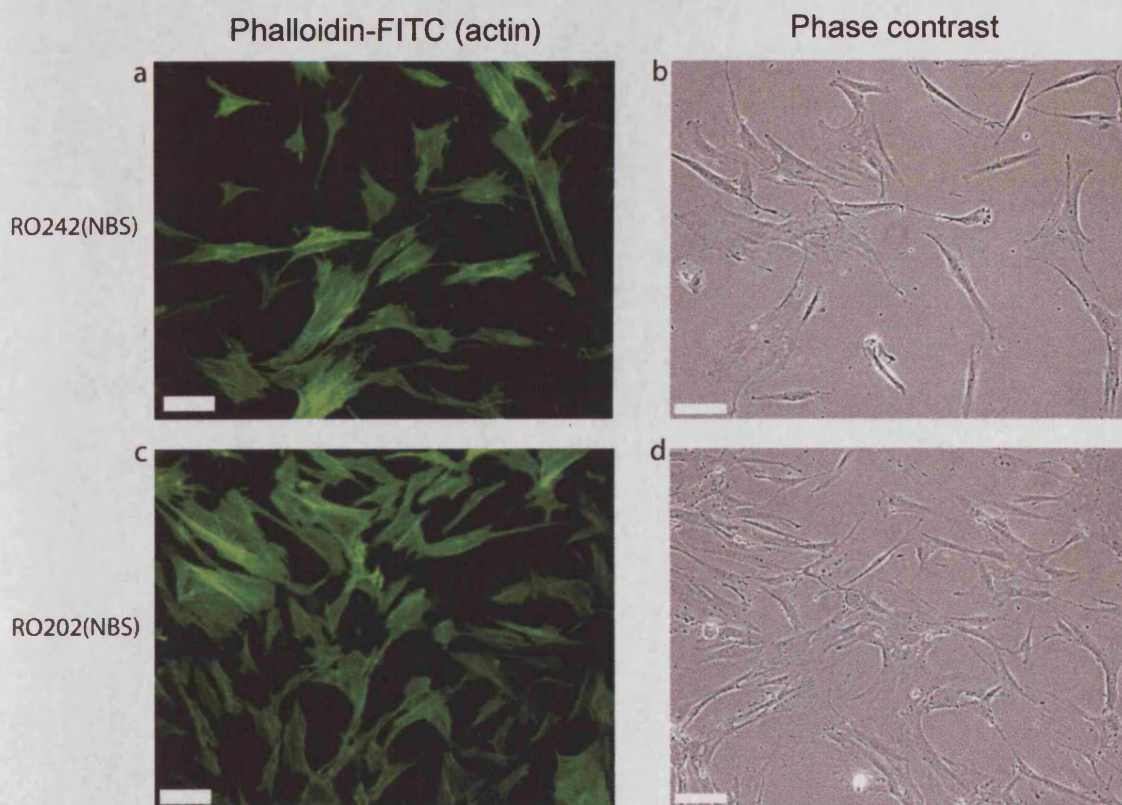
RO242(NBS)

RO202(NBS)

Figure 4.8. Cellular morphology and stress fibre presentation in untreated RO242(NBS) and RO202(NBS) fibroblasts.

Panels (a) and (c) show visualisation of F-actin stress fibres in RO242(NBS) and RO202(NBS) cells stained with phalloidin-FITC, respectively. Panels (b) and (d) show phase contrast pictures of RO242(NBS) and RO202(NBS), respectively. White bar represents 100 μm.

139
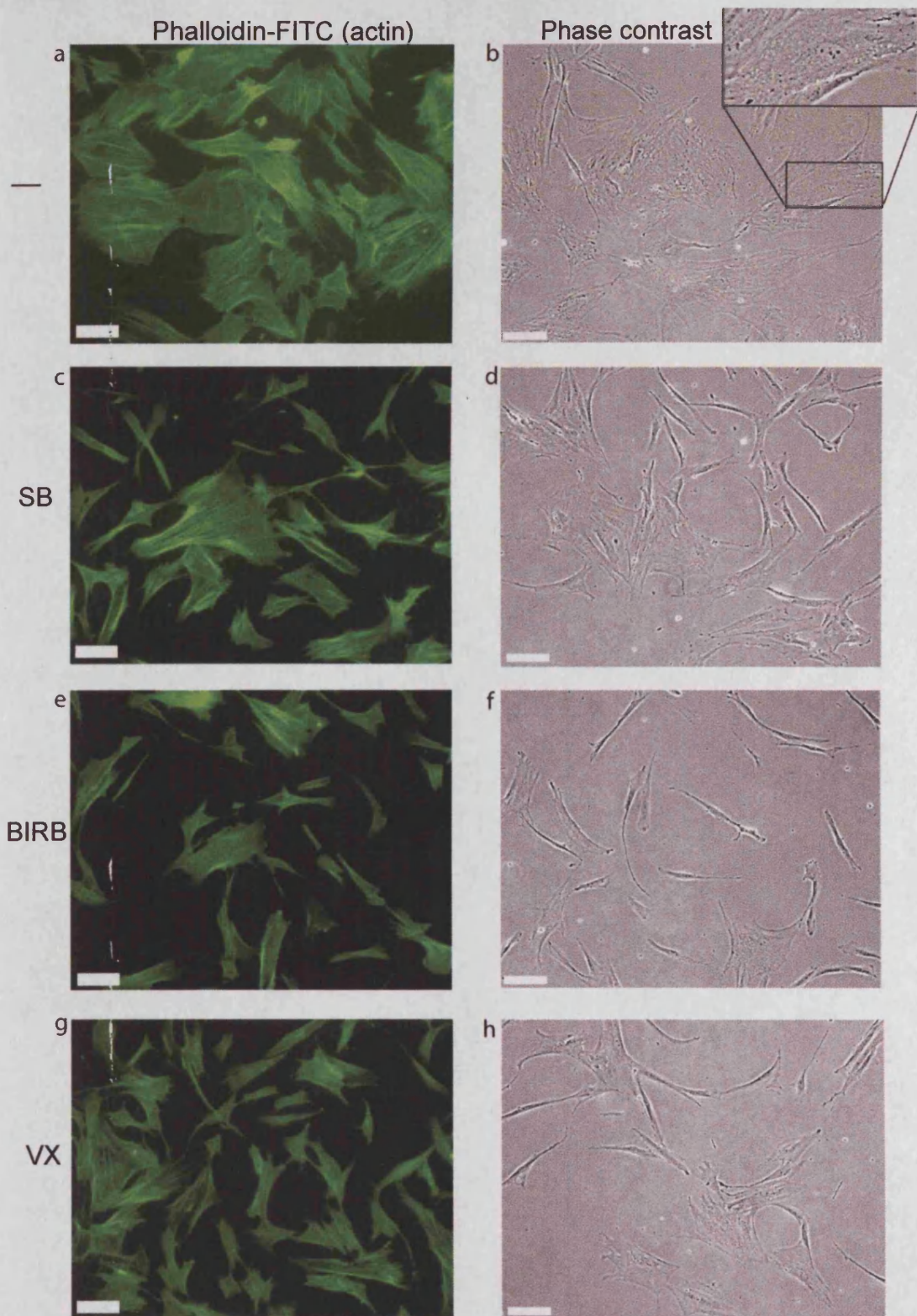
Figure 4.9. Cellular morphology and stress fibre presentation in GM07166(NBS) fibroblasts.

Panels are as in Figure 4.1 Inset in (b) shows a magnified image of an enlarged cell.

140

Phalloidin-FITC (actin)   **Phase contrast**
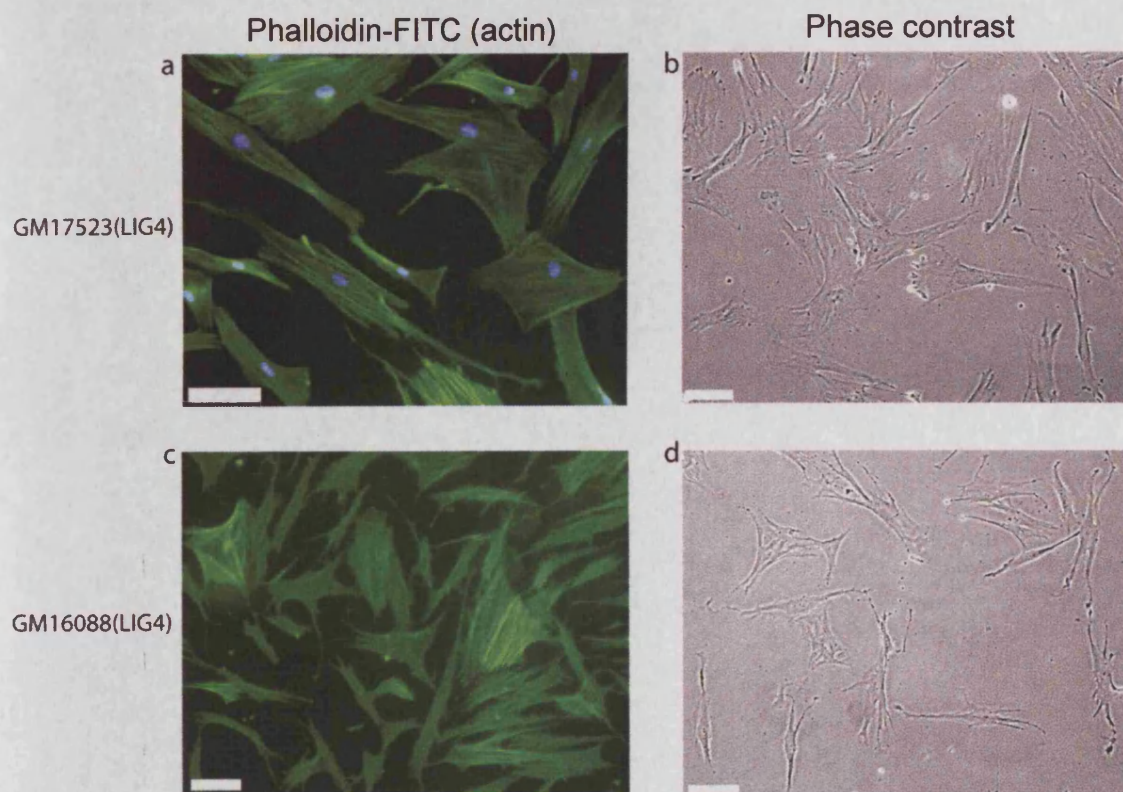
Figure 4.10. Cellular morphology and stress fibre presentation in untreated GM17523(LIG4) and GM16088(LIG4) fibroblasts.

Panels (a) and (c) show visualisation of F-actin stress fibres in GM17523(LIG4) and GM16088(LIG4) cells stained with phalloidin-FITC, respectively. Note that GM17523(LIG4) cells are also stained with DAPI. Panels (b) and (d) show phase contrast pictures of GM17523(LIG4) and GM16088(LIG4), respectively. White bar represents 100 μm.

141

Phalloidin-FITC (actin)   **Phase contrast**

GM01856(CSA)

GM01774(DKC)
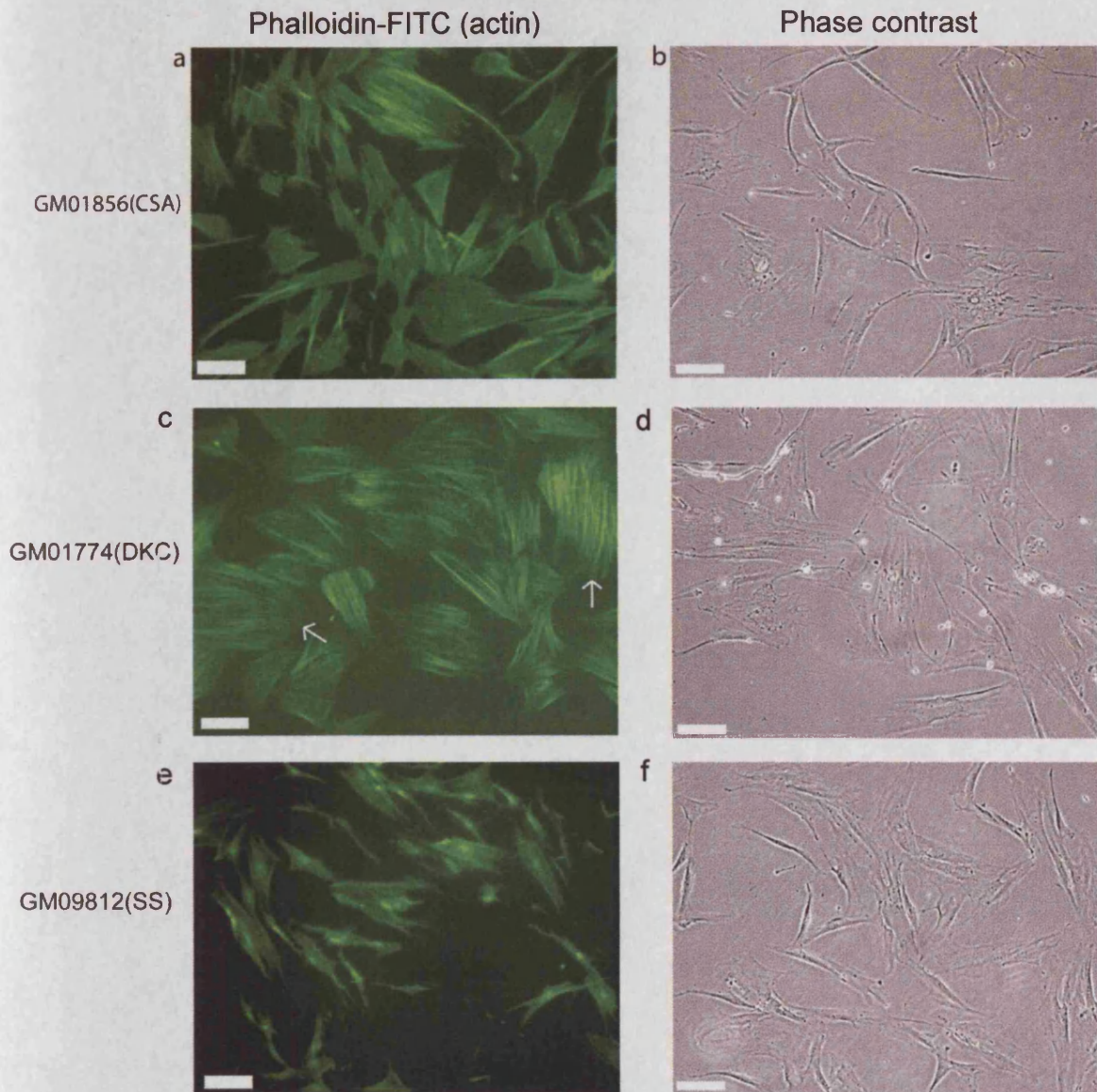
GM09812(SS)

Figure 4.11. Stress fibre presentation and cellular morphology in untreated GM01856(CSA) (a and b), GM01774(DKC) (c and d) and GM09812(SS) (e and f) fibroblasts.

White bar represents 100 μm.

Phalloidin-FITC (actin)   Phase contrast
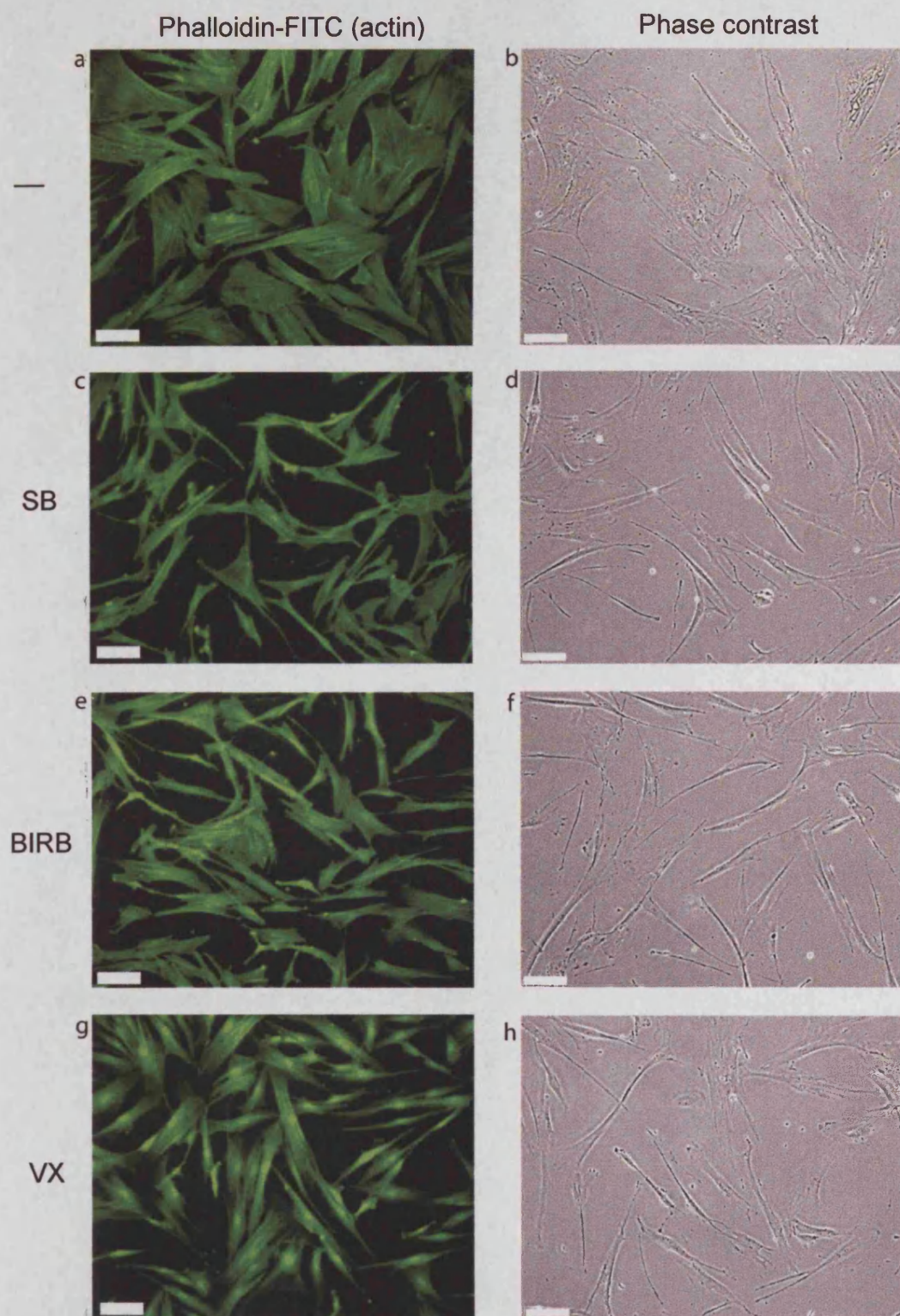
Figure 4.12. Cellular morphology and stress fibre presentation in GM18366(SS) fibroblasts.

Cells were grown in the absence (a and b) or presence of SB203580 (c and d), BIRB796 (e and f) or VX745 (g and h). Panels are as in Figure 4.1

143

Table 4.1. Summary of stress fibre phenotype of adult dermal fibroblasts from normal and GI individuals

Syndrome	Proportion of enlarged cells in the popn (%) *	Stress fibre phenotype
Normal	5-45%	Stress fibres only observed in the enlarged cells in the population.
RTS	10-30%	Stress fibres only observed in enlarged cells, but not all enlarged cells possess stress fibres. Most stress fibres are oriented parallel to long axis of the cell but in some cells stress fibres are shorter and their directionality is less regular. In some cells these irregularly orientated stress fibres are present throughout the cytoplasm but in others are concentrated around the nucleus.
BS	10-20%	Resemble normal cells, with stress fibres only being observed in the few enlarged cells in the population.
HGPS	30-40%	Inter-strain heterogeneity observed for stress fibre presentation. Some enlarged cells contain extensive stress fibres whereas others contain relatively few. Most stress fibres are oriented parallel to long axis of the cell.
NBS	5-85%	Inter-strain heterogeneity observed for stress fibre presentation. Stress fibres only observed in enlarged cells and these are oriented parallel to long axis of the cell.
LIG4	~10%	Resemble normal cells, with stress fibres only being observed in the few enlarged cells in the population.
CSA	~10%	Resemble normal cells, with stress fibres only being observed in the few enlarged cells in the population.
DKC	~60%	The majority of cells are enlarged with extensive stress fibres. Differences in the number of stress fibres in cells of similar sizes are observed. Most stress fibres are oriented parallel to the long axis of the cell.
SS	5-50%	Inter-strain heterogeneity observed for stress fibre presentation. Stress fibres only present in enlarged cells but these are not as extensive as seen in RTS or NBS cells.

* % of enlarged cells estimated from three fields each containing >30 cells quoting to an accuracy of +/- 5%.
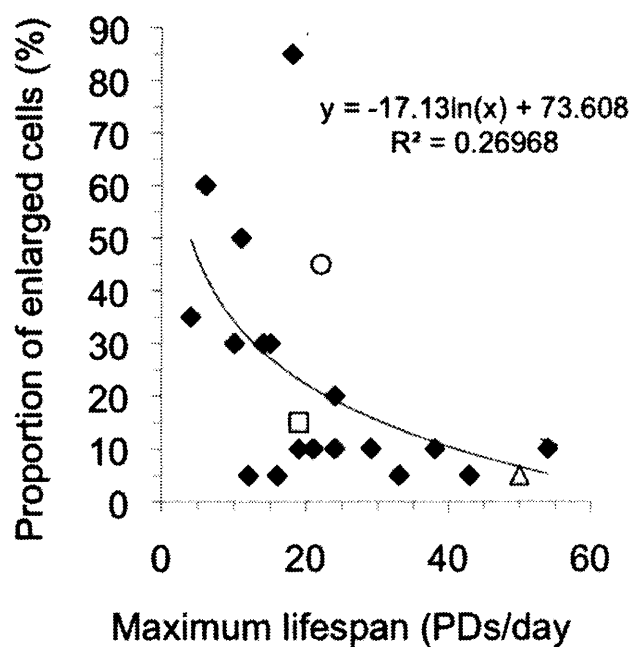
Figure 4.13. Correlation between cellular morphology and maximum lifespan.

The proportion of enlarged cells is estimated from single fields containing >50 cells quoting to an accuracy of +/- 5% and is used as a semi-quantitative measure of cellular morphology. The three normal strains are indicated by open symbols: AG16409 ($\triangle$), donor age 12 years; AG06234 ($\square$), donor age 17 years; AG13152 (O), donor age 80 years. The trendline represents the logarithmic regression of these data and shows that there is a negative correlation between the proportion of enlarged cells and maximum lifespan. The form of this regression and the R^2 value are given.

Table 4.2. Summary of the impact of p38 inhibitors on the morphology of normal and GI syndrome fibroblasts

Cell strain	Drug Treatment	Proportion of enlarged cells in pop[n] (%) [a]	Change in proportion of enlarged cells (%)	z value	P-value [b]
AG16409(N)	-	5			
	SB203580	5	0		
	BIRB796	5	0		
	VX745	5	0		
AG13152(N)	-	45			
	SB203580	10	-78		
	BIRB796	10	-78		
	VX745	10	-78		
AG06234(N)	-	15			
	SB203580	5	-67		
	BIRB796	10	-33		
	VX745	10	-33		
AG18375(RTS)	-	30			
	SB203580	10	-67	-0.440	0.66
	BIRB796	10	-67	-0.759	0.45
	VX745	15	-50	-0.332	0.74
AG17524(RTS)	-	10			
	SB203580	5	-50	-0.044	0.97
	BIRB796	5	-50	-0.332	0.74
	VX745	5	-50	-0.332	0.74
AG18371(RTS)	-	20			
	SB203580	5	-75	-0.638	0.52
	BIRB796	5	-75	-0.973	0.33
	VX745	10	-50	-0.332	0.74
GM02932(BS)	-	15			
	SB203580	5	-67	-0.440	0.66
	BIRB796	5	-67	-0.759	0.45
	VX745	15	0	0.949	0.34
GM02548(BS)	-	20			
	SB203580	5	-75	-0.638	0.52
	BIRB796	5	-75	-0.973	0.33
	VX745	10	-50	-0.332	0.74
GM02520(BS)	-	10			
	SB203580	10	0	1.145	0.25
	BIRB796	10	0	0.949	0.34
	VX745	10	0	0.949	0.34
AG11498(HGPS)	-	30			
	SB203580	20	-33	0.352	0.73
	BIRB796	25	-17	0.522	0.60
	VX745	30	0	0.949	0.34
AG10677(HGPS)	-	30			
	SB203580	10	-67	-0.440	0.66
	BIRB796	10	-67	-0.759	0.45
	VX745	20	-33	0.095	0.92
GM01972(HGPS)	-	40			
	SB203580	15	-63	-0.341	0.73
	BIRB796	5	-88	-1.293	0.20
	VX745	10	-75	-0.973	0.33

146

Table 4.2 continued

Cell strain	Drug Treatment	Proportion of enlarged cells In pop^n (%) [a]	Change in proportion of enlarged cells (%)	z value	P-value [b]
RO202(NBS)	-	5			
	SB203580	5	0	1.145	0.25
	BIRB796	5	0	0.949	0.34
	VX745	5	0	0.949	0.34
RO242(NBS)	-	10			
	SB203580	5	-50	-0.044	0.97
	BIRB796	5	-50	-0.332	0.74
	VX745	5	-50	-0.332	0.74
GM07166(NBS)	-	85			
	SB203580	15	-82	-0.813	0.42
	BIRB796	5	-94	-1.463	0.14
	VX745	25	-71	-0.860	0.39
GM16088(LIG4)	-	10			
	SB203580	5	-50	-0.044	0.97
	BIRB796	5	-50	-0.332	0.74
	VX745	5	-50	-0.332	0.74
GM17523(LIG4)	-	10			
	SB203580	5	-50	-0.044	0.97
	BIRB796	5	-50	-0.332	0.74
	VX745	5	-50	-0.332	0.74
GM01856(CSA)	-	10			
	SB203580	10	0	1.145	0.25
	BIRB796	5	-50	-0.332	0.74
	VX745	10	0	0.949	0.34
GM01744(DKC)	-	60			
	SB203580	40	-33	0.352	0.73
	BIRB796	40	-33	0.095	0.92
	VX745	30	-50	-0.332	0.74
GM18366(SS)	-	50			
	SB203580	35	-30	0.431	0.67
	BIRB796	0	-100	-1.614	0.11
	VX745	10	-80	-1.101	0.27
GM09812(SS)	-	5			
	SB203580	5	0	1.145	0.25
	BIRB796	5	0	0.949	0.34
	VX745	5	0	0.949	0.34

[a]The proportion of enlarged cells is estimated from three fields each containing >30 cells. Enlargement is a subjective measurement and was not quantitatively measured.

[b] two-tailed z-test. A significance level of <0.05 is used.
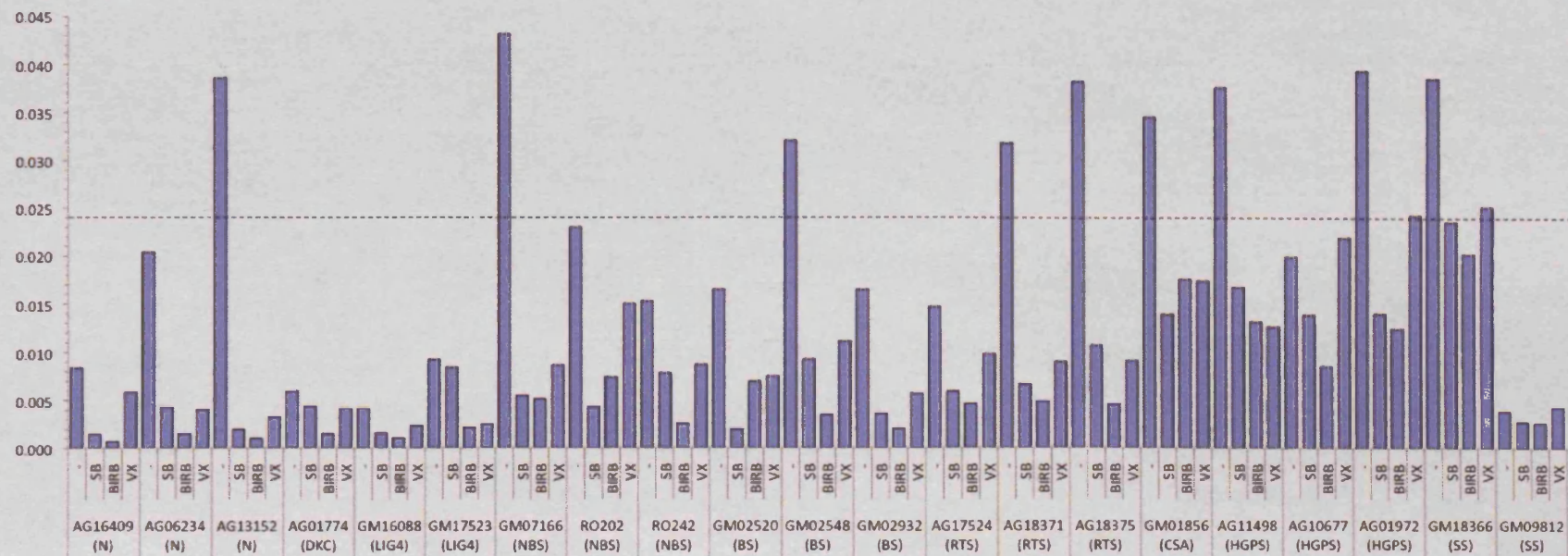
Figure 4.14. Activation of HSP27 in normal and GI syndrome fibroblasts.

Cells were grown in the presence and absence of SB203580, BIRB796 and VX745. Activation of HSP27 in each strain is given as the ratio of phospho-HSP27/Total-HSP27 as measured by ELISA (OD measured at 450 nm). The dotted line indicates the mean HSP27 ratio for untreated normal cells.

Chapter 5 Immortalisation of primary fibroblasts: model systems not limited by in vitro lifespan

5.1 Introduction

The current model for primary somatic cell senescence is entry into an irreversible block in G_1 and or G_2/M phase, effectively representing an exit from the cell cycle that is realised as senescence (Hayflick 1965; Hayflick and Moorhead 1961). Senescence as a phenomenon can be induced either by progressive shortening of telomeres during ongoing cell division (Harley et al. 1990; Olovnikov 1973), or by exposure to stress (Chen et al. 2007). The finding that senescence can be induced in a telomere-independent manner has raised speculations about the existence of multiple 'senescence clocks' and ensuing lively debates about alternative explanations (Drayton and Peters 2002). Analysis of senescence mechanisms have been further complicated by recent reports that *in vitro* cultures of human dermal fibroblasts are not homogeneous but in fact appear to be mosaics of cells under going different mechanisms of senescence induction that progress in parallel (Beausejour et al. 2003; Itahana et al. 2003). To disassemble this complexity and the inherent heterogeneity of primary cell systems here it is proposed that removal of a primary senescence trigger, telomere attrition, will allow for a coherent comparison to be made between the GI panel members without the prejudice associated with this origin of stress signalling. This would allow comparison of cells undergoing telomere attrition and those relieved of that origin of stress. Although this approach would remove the ability to study replicative senescence in these cells, it would allow comparison of cell cycle exit influences that is independent of stress signals arising from telomere shortening i.e. those that give rise to SIPS. Further, it would permit a more rational comparison of cell cycle dynamics and differences in constitutive levels of p38 activation associated with a given genetic background.

In WS, it is hypothesised that while the shortening of telomeres may be the main driving force for senescence, ongoing replication stress could trigger SIPS in

a subset of WS cells. Support for this theory comes from the finding that ectopic expression of hTert prevents the accelerated senescence seen in WS fibroblasts (Choi et al. 2001; Ouellette et al. 2000; Wyllie et al. 2000), without correcting the slow growth and senescent-like morphology seen in their primary counterparts (Davis et al. 2005; Davis et al. 2006). In addition, a reduction, but not removal, of p38 activation is observed in hTert immortalised WS cells (Davis et al. 2005), consistent with the lack of telomere shortening that is expected in a telomerase-expressing culture. The role of SIPS in other GI syndromes is relatively unknown; however, evidence from the literature shows that ectopic expression of hTert can immortalise cells from other GI syndrome cells without altering their phenotypic characteristics (Ouellette et al. 2000), suggesting a possible role for telomere-independent mechanisms of senescence induction in these cells.

Recent evidence has suggested that in addition to telomere shortening, stress signalling via p38 may play a role in establishing M1 senescence in normal cells. For example, activated p38 is present in normal WI38 and MRC5 cells at M1 but not in young cells (Iwasa et al. 2003). Late passage WS cells have also been shown to have activated p38 (Davis et al. 2005), suggesting that the pathways leading to M1 in WS cells resemble those in normal cells. The finding that the rate of telomere erosion per cell division is not increased in WS cultures (Baird et al. 2004) suggests that telomere-independent mechanisms of senescence may contribute to the shortened replicative lifespan seen in WS cultures. The finding that activation of p38 plays a significant role in SIPS (Guay et al. 1997; Huot et al. 1997), together with the observation that WS cells show features of cells undergoing stress (Davis et al. 2005), lead to the hypothesis that WS cells are subject to SIPS. Indeed, p38 was found to be activated in young WS cells as shown by presence of phosphorylated p38, associated with high levels of p21^{WAF1} and phosphorylated HSP27 (Davis et al. 2005). To date, less is known about the activation status of p38 in other GI syndrome cells. However, recently, Davis et al described low levels of phosphorylated p38 and its downstream target HSP27 in AT cells, comparable to those observed for normal controls (Davis and Kipling 2009). These data strongly suggest that the p38 pathway is not significantly

activated in AT cells. The same study also assessed the activation of the JNKs in AT cells, since these are known to be activated in response to stress (Davis 2000), and showed that in AT fibroblasts activated JNK1/2 is barely detectable (Davis and Kipling 2009). Together these data suggest that the relative involvement of p38 to SIPS may differ between GI syndromes.

Given the difficulties of comparing GI syndrome fibroblasts that display differences in the degree of commitment to cell cycle exit/senescence the primary aim of this chapter is to generate a panel for more extensive studies in which lifespan is not limited. Conceptually, this provides a model in which the stress signals that may arise from telomere attrition are removed to allow further investigation into the level of commitment to SIPS in GI syndrome cells. Furthermore, since there is no evidence in the literature that RTS cells can be immortalised by ectopic expression of hTert, this study will provide novel information on the ability of RTS cells to be immortalised. The experimental objectives of this chapter are therefore to generate hTert immortalised cultures for each panel member and to assess the p38 activation status of these cells compared to their primary counterparts.

5.2 Materials and Methods

5.2.1 Retroviral gene transfer

All manipulations during the retroviral infection procedure were undertaken with significant caution and in accordance with the Advisory committee on Genetic Modification (ACGM) guidelines.

Amphotropic retrovirus vectors expressing the HPV16 E6 oncoprotein from a pLXSN construct, packaged in PA317 cells (Halbert et al. 1991), were kindly provided by Dr. Denise Galloway (Seattle, Washington). pBABE-hTert (Wyllie et al. 2000) is an amphotropic retrovirus expressing the catalytic protein subunit of human telomerase (hTert) constructed by cloning the EcoRI insert of pGRN121 (Nakamura et al. 1997) into a pBABE-puro vector (Morgenstern and Land 1990).

For control infections pBABE-puro vectors packaged in ψCRIP cells were used (Wyllie et al. 2000).

Gene transfer was carried out as described previously (Bond et al. 1994). 100,000 cells were plated onto 100 mm culture dishes in EMEM and left to settle for 48 hrs at 37°C after which polybrene was added to a final concentration of 8 µg/ml for 1 hour. The medium was then replaced with 5 ml viral supernatant in growth medium (either pBABE-hTert-puro or pBABE-puro at approximately 10^5 viral particles per ml) and the cells incubated at 37°C for 24 hrs. For each gene transfer the retroviral infections were done twice. 24 hrs after the second infection, fibroblast cultures were passed into EMEM containing puromycin (2.5 µg/ml) and surviving cells after five days were transferred to T75 culture vessels and cultured in EMEM containing puromycin. Telomerase activity was subsequently confirmed by TRAP assay (as described in section 2.4) and immortality was determined by growth of the cells beyond the known replicative senescence limit for the primary cells.

5.3 Results

5.3.1 Ectopic expression of the catalytic subunit of telomerase, hTert, in RTS primary adult dermal fibroblasts results in the reconstitution of telomerase activity

AG18371(RTS) fibroblasts were transduced with an amphotropic pBABE retroviral vector co-expressing hTert cDNA, and the puromycin resistance gene. In parallel, primary AG18371(RTS) fibroblasts were also infected with an empty pBABE-puro (control) vector. RTS cells transduced with both the pBABE-hTert-puro or the empty control vector were designated as 0 PD post-transfection and were assayed for telomerase activity using the TRAP assay (Kim et al. 1994). Negative controls were prepared for each lysate by incubating an aliquot of each sample at 85°C for 10 minutes to destroy telomerase activity as previously described in section 2.4.1. In addition, cell extracts prepared from the adenovirus 5-transformed 293 cell line, derived from HEK cells and known to express

telomerase, were used as a positive control. TRAP reaction products appear as a ladder of bands with a periodicity corresponding to the size of the tandem telomeric repeats and indicate reconstitution of telomerase activity following ectopic expression of hTert.

The retroviral infection of primary RTS fibroblasts with the empty pBABE-puro vector did not confer telomerase activity (Figure 5.1, lanes 1 and 2). Similarly, telomerase activity was not detected in the heat-treated samples (Figure 5.1, lanes 2, 4 and 6). Conversely, telomerase activity was detected in the non-heat treated samples prepared from primary RTS fibroblasts infected with pBABE- hTert-puro (Figure 5.1, lane 3). These data suggest that the ectopic expression of hTert is sufficient to restore telomerase activity *in vitro* in RTS primary fibroblasts.

5.3.2 Ectopic expression of hTert in primary RTS dermal fibroblasts extends proliferative lifespan

Following retroviral infection, AG18371(RTS) fibroblast populations were propagated under routine culture conditions (see section 2.1). Primary AG18371(RTS) cells, infected with an empty pBABE-puro (control) vector, were propagated as polyclonal populations and passaged continuously following puromycin selection until the cultures ceased proliferation. Primary AG18371(RTS) cells, transduced with an empty pBABE-puro vector, ceased proliferation at 33.8 PDs and 189 days in culture post retroviral infection. Between days 137 and 189 no population doublings were achieved. Conversely, the polyclonal population of RTS cells infected with pBABE-hTert-puro, was propagated for 456 days in culture and achieved ~93 PDs. This culture displayed a logarithmic growth pattern with a growth rate of 0.23 PDs/Day.

5.3.3 Ectopic expression of hTert in GI syndrome fibroblasts results in the reconstitution of telomerase activity

From the panel of GI syndrome fibroblasts previously characterised in chapters 3 and 4, one strain from each syndrome was chosen for immortalisation by hTert. The criteria for selection of the GI syndrome strains were based on

observations of alterations in cellular morphology and/or growth potential that are indicative of SIPS in these cells. As such, the following strains were infected with an amphotropic retrovirus encoding hTert: GM02548(BS), GM01856(CSA), GM07166(NBS), GM17523(LIG4), AG18371(RTS), and AG11498(HGPS). The decision not to include DKC in this panel was made based on the fact that DKC has a known defect in hTert, therefore restoration of telomerase activity may confound the study. All cells were subsequently assayed for telomerase activity using the TRAP assay as previously described. Negative controls were prepared for each lysate (as previously described), by incubating an aliquot of each sample at 85°C for 10 minutes to destroy telomerase activity. Telomerase activity was detected in all of the non heat-treated samples (Figure 5.3, lanes 1, 3, 5, 7, 9, 11 and 13), whereas telomerase activity was not detected in heat-treated samples (Figure 5.3, lanes 2, 4, 6, 8, 10, 12 and 14). These data suggest that the ectopic expression of hTert is sufficient to restore telomerase activity *in vitro* in primary GI panel fibroblasts.

5.3.4 Ectopic expression of hTert in primary GI syndrome fibroblasts extends proliferative lifespan

Following retroviral infection, GI syndrome fibroblast populations were propagated under routine culture conditions (see section 2.1) in media containing puromycin. Cultures, infected with an empty pBABE-puro (control) vector, were propagated as polyclonal populations and passaged continuously following puromycin selection until the cultures ceased proliferation.

Primary GM01856(CSA) cells ceased proliferation at 21 PDs and 95 days in culture after which no further lifespan extension was observed. Conversely, the GM01856(CSA) fibroblasts infected with pBABE-hTert-puro, were propagated for 202 days and achieved 76 PDs (Figure 5.4). This culture displayed a logarithmic pattern and displayed no decline in growth rate. A similar pattern was observed for the other cell strains tested and these are given in Table 5.1.

5.3.5 Characterisation of stress signalling pathways in primary fibroblasts

The p38 and JNK pathways are known to be activated in response to stress [reviewed by (Kyriakis and Avruch 2001)]. Therefore, the level of phosphorylated p38 and JNK in normal and GI syndrome cells were compared by Western blot. Two sets of immunoblots are provided for primary fibroblasts (Figure 5.5 A and B). These were generated at different times but they both have a common control strain, AG16409(N) that acts as an internal marker enabling cross-comparison of the two series of blots. AG16409(N) cells (Figure 5.5A) and HCA2 cells (Figure 5.5B) treated with anisomycin were used as internal controls so as to confirm the identity of the phosphorylated-p38 and phosphorylated-JNK1/2 proteins.

Anisomycin is an antibiotic that binds to the 60S ribosomal subunit and inhibits the peptidyl-transferase reaction, thus blocking translation. In addition, independently of its ability to inhibit protein synthesis, anisomycin is known to activate both JNK- and p38-pathways and is used widely in the literature as a positive control for p38 activation (Cano et al. 1994; Hazzalin et al. 1997; Iordanov et al. 1997; Shifrin and Anderson 1999; Torocsik and Szeberenyi 2000; Xiong et al. 2006). As expected, both AG16409(N) and HCA2 cells that have been stimulated with anisomycin show high levels of phosphorylated p38 and JNK1/2 (Figure 5.5A, lanes 1 and 2; B lanes 1and 2).

When Figure 5.5B is analysed, it is seen that GI strains GM01774(DKC), GM18366(SS) and GM16088(LIG4) have a similar level of p-p38 (Figure 5.5B, lanes 5, 7, and 8) as that found in HCA2 cells and the normal dermal strains AG16409(N) and AG06234(N) (Figure 5.5B, lanes 1, 3 and 4). A much elevated level of p-p38 is observed for GM17523(LIG4) (Figure 5.5B, lane 9), suggesting these cells show activation of p38; however, this is most likely due to overloading of this lane as indicated by the high levels of JNK1/2 seen in this strain. Conversely, a much-reduced level of p-p38 is observed for GM09812(SS) (Figure 5.5B lane 6) that may be due to under loading as indicated by the low levels on

JNK1/2 seen in this strain. Alternatively, it is possible that p38 is activated to a lower extent in GM09812(SS). These data suggest that overall there is no activation of p38 in these syndromes above that seen in normal cells.

A similar pattern is seen in GI strains AG18375(RTS), AG17524(RTS), GM02932(BS), GM07166(NBS) and AG10677(HGPS) (Figure 5.5A, lanes 4, 5, 6, 12 and 13), indicating that there is little activation of p38 in these syndromes beyond that seen in the normal strain AG16409(N) (Figure 5.5A, lane 2). For GI strains AG18371(RTS), GM02548(BS), GM02520(BS), GM01856(CSA), RO202(NBS), RO242(NBS), AG11498(HGPS) and AG01972(HGPS) a reduced level of p-p38 is seen (Figure 5.5A, lanes 3, 7-11, 14 and 15). As the levels of p-p38 appear to correlate with the levels of p38 across the gel, it is possible that the low levels of p38 seen in these samples simply reflects the degree of protein loading in these lanes, thus suggesting that the level of p38 activation in these cells may be similar to that observed in normal cells. Alternatively, p38 may be activated to a lower extent in these strains that would show considerable intra-GI syndrome differences.

In summary the data shown in Figure 5.5A and B suggest that the majority of primary GI syndrome cells have p-p38 levels comparable with those observed for normal cells, although some strains appear to show a reduced p38 activation.

When the immunoblots were examined for the activation of JNK1/2, p-JNK1/2 is barely detectable in any of the normal or GI strains (Figure 5.5A, lane 2, Figure 5.5B, lanes 1, 3 and 4). However, activated JNK1/2 (p-JNK1/2) can be detected in AG16409(N) and HCA2 cells that have been treated with anisomycin (Figure 5.5A, lane1 and B, lane 2, respectively). In general, the level of p-JNK1/2 detected is roughly proportional to the level of JNK1/2 seen in these cells, suggesting that any variation seen is due to differences in protein loading. The exceptions appear to be the RO202(NBS) and RO242(NBS) (Figure 5.5A, lanes 10 and 11), AG11498(HGPS) (Figure 5.5A, lane 14) and GM01774(DKC) strains (Figure 5.5B, lane 5) which show low levels of JNK1/2 activation.

Differences are observed in the JNK1/2 isoforms that are activated in some strains. For example, in DKC, it is the p46 isoforms of JNK1/2, which refer to the JNK1α1 and JNK2α1 isoforms (Liu et al. 2004), that are activated (Figure 5.5B lane 5), whereas RO202(NBS), RO242(NBS) and AG11498(HGPS) show low levels of activation of both p54 and p46 isoforms. Given the different roles of JNK isoforms in cell proliferation (Bode and Dong 2007) it was questioned as to whether the differences in JNK activation correlate with the growth rates of these cells; however, no clear correlation between growth rate and JNK activation was observed.

5.3.6 p38 activation status in hTert-immortalised fibroblasts

To assess the p38 activation status of the newly generated hTert panel, protein lysates from hTert cells soon after transfection (designated early passage hTert cells) were assessed for total p38 levels and its activating phosphorylation by western blot. Each syndrome strain has been analysed separately and compared with AG16409(N)^{hTert} cells treated with and without anisomycin as positive and negative controls, respectively. As expected both p-p38 and p-JNK1/2 are detected in AG16409(N)^{hTert} cells treated with anisomycin (Figure 5.5C, lanes 1, 4, 7, 10, 14, 17 and 20); however, little p-p38 or p-JNK1/2 is detected in untreated AG16409(N)^{hTert} cells (Figure 5.5C lanes 2, 5, 8, 11, 15, 18 and 21). This appears to suggest that immortalisation with hTert has reduced the activation of p38 seen in primary AG16409(N) cells (Figure 5.5C), although this has not been compared directly. In contrast, p-p38 is detected in hTert-immortalised AG18371(RTS)^{hTert}, GM01856(CSA)^{hTert}, GM07166(NBS)^{hTert} and GM17523(LIG4)^{hTert} cells, with particularly high levels of p-p38 in the latter two strains (Figure 5.5C lanes 3, 9,12 and 19). Very low levels of p38 activation are seen in GM02548(BS)^{hTert} or AG11498(HGPS)^{hTert} (Figure 5.5, lanes 6 and 16). This agrees with the apparent low levels of p38 activation seen in the corresponding primary cells (Figure 5A, lanes 7 and 14), suggesting that p38 may indeed be activated at low levels in these strains. For comparison, AG03141(WS)^{hTert} cells that are known to express activated p38 are shown in lane 22 (Davis et al. 2006). These data suggest that

hTert immortalisation does not prevent activation of p38 in GI syndrome cells but does reduce the level of p-p38 in normal cells.

When these hTert-immortalised strains are analysed for the activation of JNK1/2, no p-JNK1/2 is found in any of the GI syndrome cells used (Figure 5.5, lanes 2, 3, 6, 9, 12, 16, 19 and 22), supporting the observation of little JNK1/2 activation seen in primary cells (see figure 5).

The apparent decline in p-p38 seen in AG16409(N)^{hTert} cells prompted the question as to whether hTert populations gradually underwent an element of *in vitro* selection in which levels of p38 phosphorylation were seen to decline in accordance with increasing passage. Preliminary data on late passage (>30 passages) hTert cells suggest that p-p38 levels were indeed decreased in GI cells indicating the need to track passage age for hTert cultures (data not shown). All subsequent studies were thus performed on early passage hTert cells to remove this element of *in vitro* selection.

5.4 Discussion

This chapter shows the successful generation of an hTert-immortalised panel of GI syndrome cells that can be used for further analysis of SIPS in these cells. In addition it has been shown that hTert is able to extend the lifespan of RTS cells beyond their normal senescence point, data that was not previously available.

An analysis of stress-signalling pathways in both primary and hTert systems give rise to three main conclusions:

Firstly, the Western Blot analysis of primary cells suggests that the level of p38 phosphorylation in GI syndrome cells may be similar to that observed for normal cells, although some inter-strain (and intra-GI syndrome) variation is observed. If it is assumed that the biological outcomes observed for growth in p38 inhibitors is driven by changes in p38 phosphorylation, the observation that p38 inhibitors have very similar effects on the growth of primary cells from all syndromes despite the variations of p-p38 observed, suggests that only low levels

of p38 activity are necessary to affect the replicative potential of cell cultures. Thus, it is possible that relatively small changes in p38 activation are translatable into significant changes in growth potential when assayed over long periods of time. If this is the case such changes may be beyond the resolution of the detection systems used. Alternatively, it is possible that the small changes in replicative potential observed for most cultures are not due to changes in p38 activation and that the inhibitors are having their effects due to off-target issues. This may be supported by the observation that VX745, which is very highly specific for p38 (Lee and Dominguez 2005), consistently shows the smallest effects on cell proliferation and lifespan.

Secondly, the level of p-p38 appears to be reduced following hTert-immortalisation in normal cells, but not in GI syndrome cells. This suggests that in normal cells the major stress signals giving rise to growth restraint may be removed by ectopic expression of hTert, whereas GI syndrome cells retain some degree of p38 stress signalling that could reflect ongoing SIPS in these cells i.e. GI syndrome cells have the added burden of telomere independent senescence. The hypothesis therefore is that hTert-immortalised GI cells should be a target for inhibitor action, whereas hTert-immortalised normal cells are likely to show a reduced response to p38 inhibitors compared to their primary counterparts. These data also indicate that the hTert system can be used to further study the role of SIPS in GI syndrome cells with the stipulation that early passage cells are used, a hypothesis supported by the observation that SIPS can still occur in hTert-immortalised Ataxia Telangiectasia cells (Naka et al. 2004).

Finally, it is clear that JNK1/2 are not activated to any significant extent in any primary or hTert-immortalised GI fibroblast strain, suggesting that any underlying stress signalling occurring in these cells does not significantly activate JNK1/2 and similarly, it is likely that any off-target effects of the p38 inhibitors towards JNK1/2 are unlikely to impact upon growth potential.

In summary, the main conclusions of this chapter are:

159

- hTert-immortalisation can extend the lifespan of AG8371(RTS), GM17523(LIG4), GM01856(CSA), GM02548(BS), GM07166(NBS), AG11498(HGPS) and AG16409(N) cells beyond their normal senescence barriers, suggesting that senescence in these cell strains is driven by telomere shortening.

- Generation of the hTert panel can be used for further studies of SIPS in GI sydrome cells.

- GI syndrome cells have low levels of p-p38, similar to those observed for normal cells.

- The level of p-p38 appears to be reduced in hTert-immortalised GI syndrome cells but not normal cells, suggesting that GI syndrome cells have an added burden of stress signalling that is telomere-independent.

Table 5.1. Growth potential of primary versus hTert-expressing cultures

Syndrome	1° /hTert	Days in culture	PD	Senescence?
Normal	1°	170	49.6	✓
	hTert	212	85.7	✗
BS	1°	95	21.0	✓
	hTert	154	56.8	✗
NBS	1°	154	21.6	✓
	hTert	192	41.4	✗
LIG4	1°	95	13.9	✓
	hTert	185	35.1	✗
HGPS	1°	55	10.3	✓
	hTert	109	28.2	✗
RTS	1°	189	33.8	✓
	hTert	456	93	✗

Figure 5.1. Reconstitution of telomerase activity in primary RTS fibroblasts (AG18371) transfected with hTert.

Retroviral infection with pBABE-hTert-puro vector (Lanes 3, 4) or the empty pBABE-puro vector (Lanes 1, 2). HEK 293 cells were used as a positive control (Lanes 5, 6). TRAP assays were performed using the TRAPeze® Kit (Millipore) according to the manufacturer's guidelines. The arrow indicates the position of the internal telomerase amplification standard as a control for the PCR inhibition. Each sample was assayed with (+) or without (-) prior heat treatment to destroy telomerase activity.
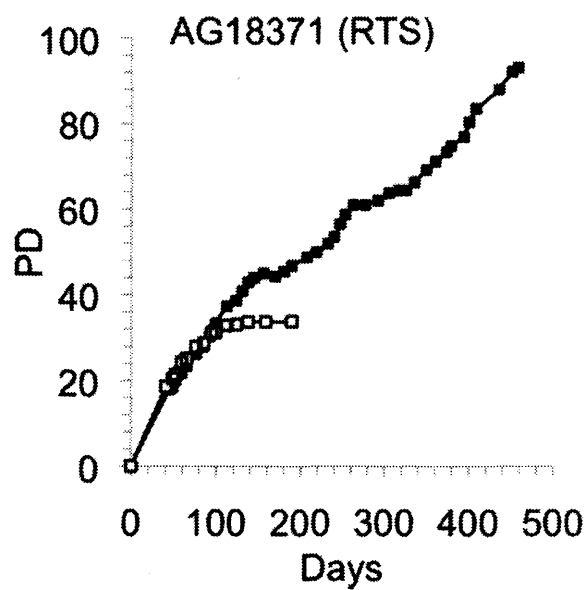
Figure 5.2. Extension of proliferative lifespan of polyclonal population of RTS (AG18371) fibroblasts transfected with hTert.

Cells infected with pBABE-hTert-puro (closed squares) or an empty pBABE-puro vector (open squares). All cells were propagated under routine culture conditions in selective media.
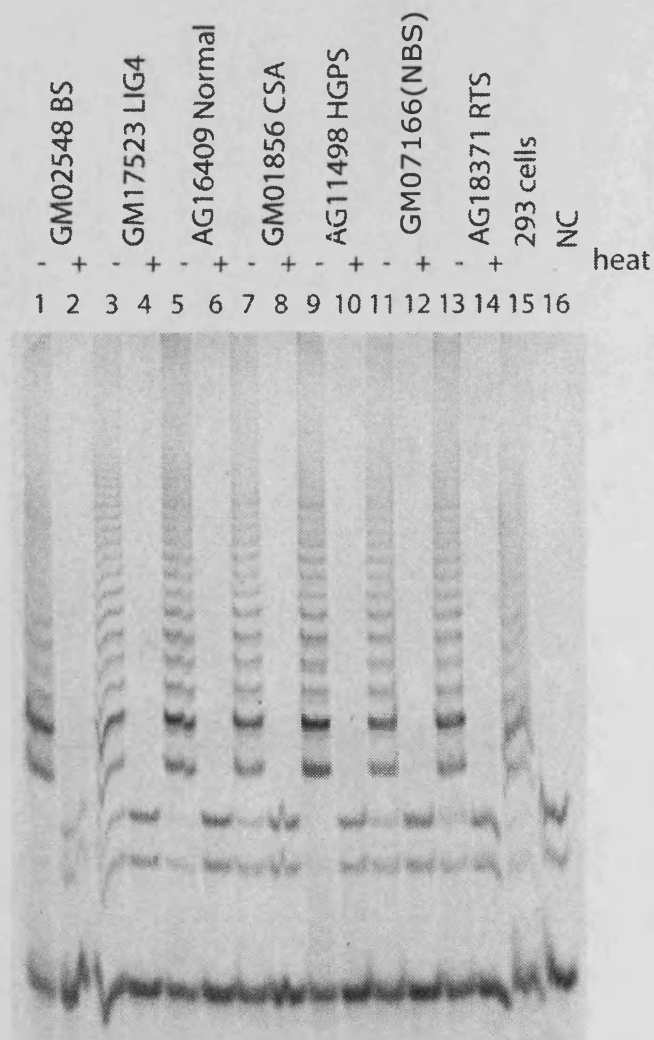
Figure 5.3. Reconstitution of telomerase activity in fibroblasts derived from normal (AG16409) and GI syndrome individuals transfected with hTert.

Retroviral infection with pBABE-hTert-puro vector. TRAP assays were performed as previously described (Kim et al. 1994). The arrow indicates the position of the internal telomerase amplification standard as a control for the PCR inhibition. Each sample was assayed with (+) or without (-) prior heat treatment to destroy telomerase activity. HEK 293 cells were used as a positive control. Abbreviations: NC negative control.
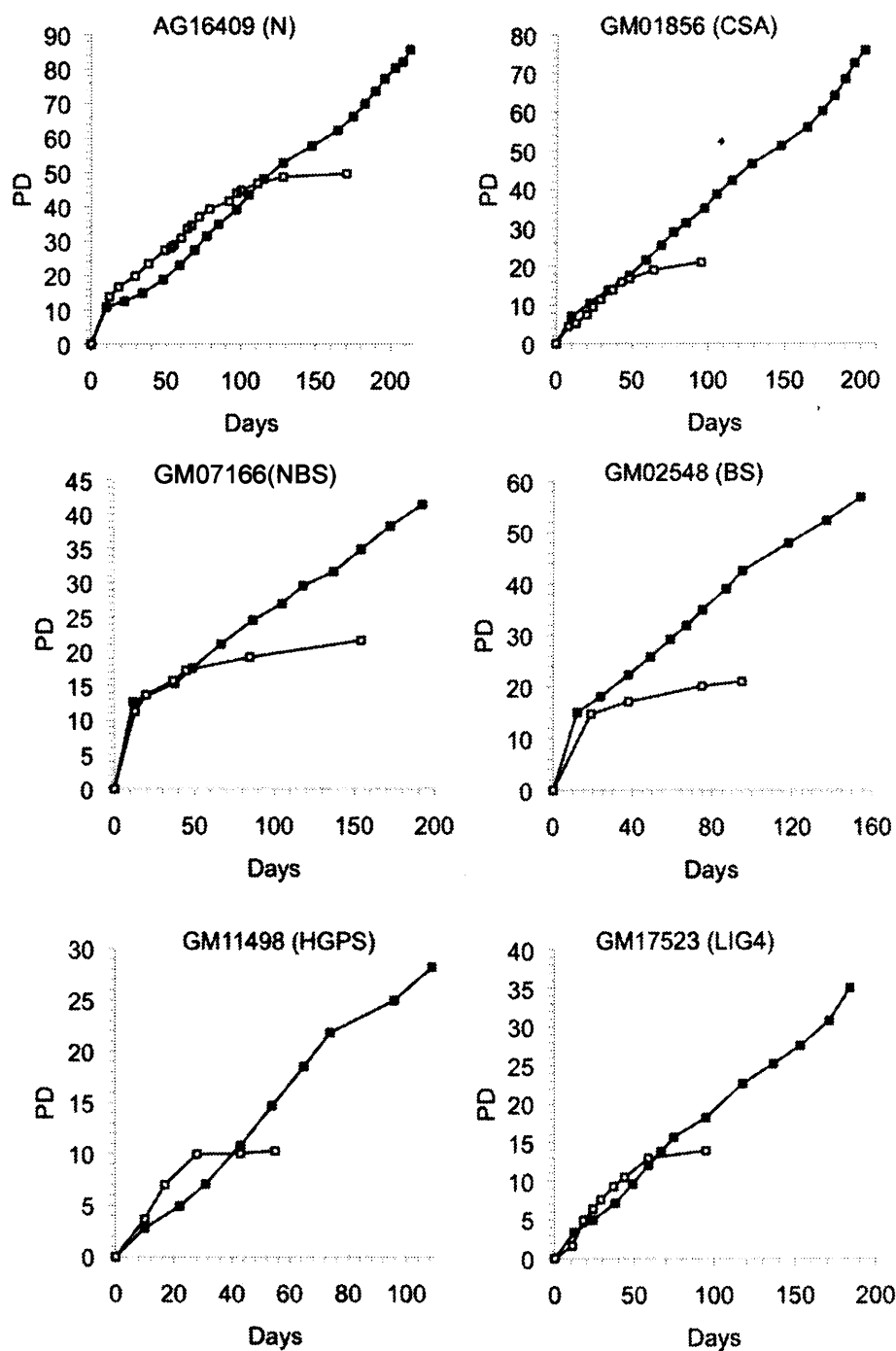
Figure 5.4. Extension of proliferative lifespan of polyclonal populations transfected with hTert.

Primary (open squares) and hTert-expressing (closed squares) fibroblasts from normal and GI syndrome individuals were propagated under routine culture conditions and growth curves generated from cumulative population doublings.

165
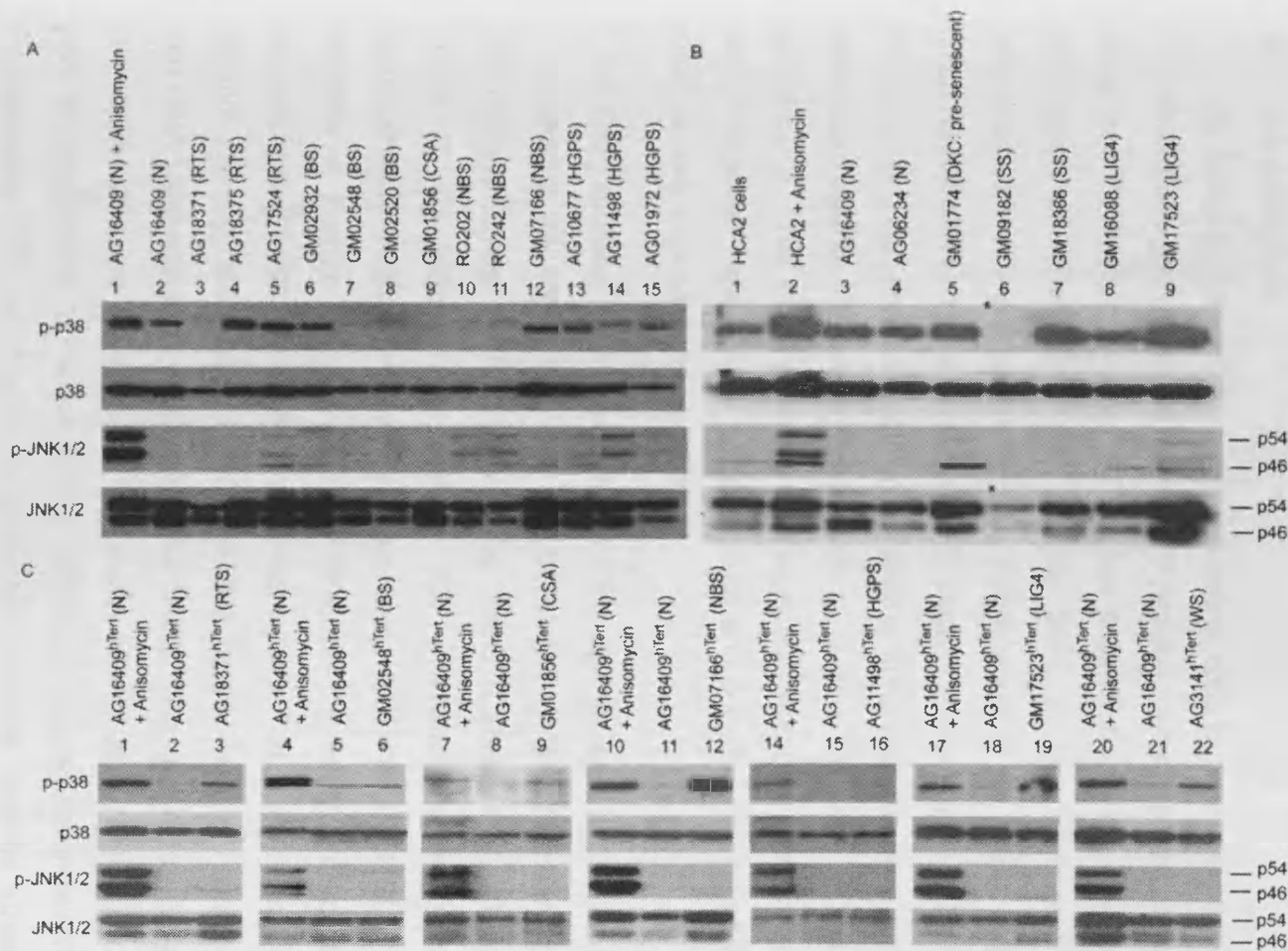
Figure 5.5. Immunoblot analysis of stress signalling proteins in GI syndromes fibroblasts.

For Panels A and B protein lysates were prepared from primary fibroblasts grown under standard conditions. For Panels C protein lysates were prepared from hTert-immortalised fibroblasts grown under standard conditions. * in lane 6 of panel B indicates an under-loading of GM09182(SS). Expression levels for phosphorylated p38 (p-p38), p38, phosphorylated JNK1/2 (p-JNK1/2) and JNK1/2 were assessed. For JNK1/2 the p46 and p54 kDa versions are indicated. For each blot an equal amount (10µg) of protein was loaded per sample.

Chapter 6   Impact of p38 Inhibition on Response to

DNA Damage

6.1 Introduction

As noted in the Introduction exposure of cells to genotoxic agents such as UV and chemotherapy drugs, such as DOX, cause multiple types of cell damage and have been shown to induce SIPS (see below). Evidence in the literature that expression of hTert does not prevent SIPS in normal human fibroblasts in response to UV, γ-irradiation or H_2O_2 (Gorbunova et al. 2002), suggests that the hTert model can be used to study SIPS. Here, the proposal is to test the propensity for SIPS in hTert-immortalised GI syndrome fibroblasts using a range of different genotoxic agents. These agents have a known capacity to induce cell cycle arrest/SIPS. This study provides a unique opportunity to determine the extent to which GI panel cells have a compromised and possibly shared ability to deal with exogenously imposed genomic stress.

The rationale for the selection of the agents was based on their accepted mechanisms of action and the nature of the genomic lesion generated. The approach is similar to that adopted by others (Cabral et al. 2008; Fan and Luo 2008) in the selection of agents (UV irradiation, 4-nitroquinoline 1-oxide, camptothecin, etoposide, hydroxyurea, and H_2O_2) for RECQL4 helicase gene function in human cells including Rothmund-Thomson syndrome. The agents studied here fall into two categories. First, *agents that interfere with the modulation of DNA topology* including inhibitors of DNA topoisomerase I (camptothecin; CPT) and DNA topoisomerase II (doxorubicin; DOX). Changes in topology are intimately connected with the assembly of chromatin during DNA replication, its packaging prior to progression to mitosis and decatenation prior to chromosome segregation. Furthermore, CPT is thought to generate S-phase specific stress through the generation of strand interruptions following replicon collision with trapped ternary complexes. The Topo II targeting agent DOX shows less cell cycle specificity and a

167

potential for multiple modes of action associated with DNA intercalation and inhibition of macromolecular biosynthesis. Second, *agents that disrupt DNA integrity* (e.g. base damage, SSBs/DSBs) potentially arising from radical induction (e.g. induced by H_2O_2). Third, those *agents that induce more discrete forms* of DNA damage at specific residues and require nucleotide removal processes and associated repair pathways [e.g. purine adducts induced by 4-nitroquinoline 1-oxide (4NQO)] or those that have the ability to generate lesions over long time periods and provide a chronic form of stress and disrupt cell cycle traverse [e.g. DNA cross-link formation by cisplatin (CisPt)].

Here the selected agents are overviewed in terms of their mechanism of action and induction of cellular senescence pathways:

1. CPT is a naturally occurring cytotoxic quinoline alkaloid with strong anti-tumour activity that was first isolated from the bark and stem of *Camptotheca acuminata*, a tree native in China. In eukaryotes CPT specifically inhibits DNA topoisomerase (Topo) I (Hsiang and Liu 1988) and is widely used as a tool in assessing the role(s) of the enzyme. CPT and its analogues form stable ternary complexes with DNA and the Topo I molecule (termed 'cleavable complexes' due to their ability to yield DNA strand breaks upon treatment with alkali). Analyses of CPT-induced DNA breaks show that Topo I is covalently linked to the 3' end of the broken DNA. CPT acts by blocking the rejoining step of the breakage-reunion reaction (Hsiang et al. 1985) and this 'trapping' results in the accumulation of cleavable complexes which resemble the transient intermediates proposed for eukaryotic DNA Topo I. Toxicity of CPT is primarily attributed to the conversion of single-strand breaks into double-strand breaks during the S-phase when the replication fork collides with the cleavage complexes formed by DNA and CPT (Pommier et al. 2003).

Differences in the response to CPT have been reported depending on the dose and p53 status of the cell types studied. Evidence suggests that high doses of CPT induce apoptosis in both p53 functional and non-functional human colon cancer cell lines (Han et al. 2002). However, low doses of CPT induce cell cycle arrest and senescence in p53 functional cells, but apoptosis in p53 nonfunctional

168

cells (Han et al. 2002). In contrast to these observations, a robust SIPS response to CPT has been reported in non-small cell lung carcinoma (H1299) cells that are p53 nonfunctional (Roberson et al. 2005).

2. CisPt (Cisplatin; cis-diamminedichloroplatinum(II) (CDDP) is a fully synthetic platinum-based chemotherapy, being the first member of a group of related drugs used widely to treat various types of cancer, including sarcomas, small cell lung carcinoma and lymphomas. The cytotoxic action of CisPt requires activation of CisPt by aquation involving the sequential replacement of the cis-chloro ligands of CisPt with water molecules (el-Khateeb et al. 1999; Kelland 2000). The major forms of DNA adducts induced by CisPt are 1,2-intra-strand cross-links with purine bases, accounting for 85-90% of total lesions (Kelland 1993). Although often referred to as an alkylating agent, the co-ordination complex has no alkyl group and so cannot carry out alkylating reactions.

CisPt-induced DNA damage is known to activate a number of pathways, including activation of cell cycle checkpoints, which temporally induce a transient S-phase arrest, followed by a durable G_2/M arrest (Shapiro and Harper 1999; Siddik 2003). Since the inhibitory effect of DNA adducts of CisPt on the G_1-phase cyclin-dependent kinases is a later event in the sequence of checkpoint activation (Siddik 2002), cells remain trapped in G_2/M and accumulation of cells in G_1 is rarely seen (Siddik 2003). Available data suggest that the primary responses to CisPt-induced DNA damage are induction of long-term growth arrest (premature cell senescence) and mitotic catastrophe, whereas acute apoptosis may be due to "off-target effects" not necessarily involving DNA damage (Havelka et al. 2007). The involvement of p53 in CisPt-induced senescence is inconclusive, as senescence has been observed in cells both with and without functional p53 (Chang et al. 1999; Roberson et al. 2005; Wang et al. 1998).

3. DOX (DOX; Adriamycin™; also known as hydroxydaunorubicin) is an anthracycline antibiotic, closely related to the natural product daunomycin isolated from *Streptomyces peucetius*. DOX is used as a chemotherapeutic agent in the treatment of a wide range of cancers, including Hodgkin's and Non-Hodgkin's

lymphoma, multiple carcinomas and soft tissue sarcomas (Carter 1975). Though not completely elucidated, the anti-tumour activity of DOX is thought to be exerted in two ways: firstly by intercalating between base pairs leading to distortion of the helix (Momparler et al. 1976), which disrupts DNA synthesis and transcription, and secondly by inhibiting DNA Topo II, which is critical to DNA function. DOX stabilises the Topo II complex after it has broken the DNA chain for replication, thus preventing the DNA double helix from being resealed and generating breaks in genomic DNA. Both of these mechanisms result in DNA disruption that ultimately can lead to cell cycle arrest and death signalling.

Topo inhibitors such as DOX induce DNA damage in tumour cells, subsequently activating p53 and leading to cell cycle arrest or apoptosis (Lowe et al. 1994; Pommier et al. 1994). For example, it has been reported that breast tumour cells (MCF-7 cells) treated with DOX undergo SIPS that is dependent on functional p53 (Elmore et al. 2005; Elmore et al. 2002). It has also been shown that DOX is a potent inducer of a reversible senescent-like state in normal human fibroblasts (Michishita et al. 1998). Evidence suggests that the cytotoxic activity of DOX occurs predominantly in G_2 (Potter et al. 2002).

4. 4NQO is a quinoline derivative. The exact mechanism of action of 4NQO is not clear, but it is known to be metabolically activated to 4-hydroxyaminoquinoline-1-oxide. The latter reacts with DNA to form purine adducts. Similar to UV photolesions, 4NQO DNA adducts are removed by the NER pathway in normal human cells (Zelle and Bootsma 1980). 4NQO also generates substantial amounts of ROS in the cell, thereby producing DNA strand breaks and alkali-labile sites (Nunoshiba and Demple 1993). In addition, it induces formation of irreversible topoisomerase cleavage complexes (Top1cc) that are converted into DNA breaks, similar to CPT (Miao et al. 2006).

Evidence suggests that treatment with 4NQO consistently reduces the levels of cyclin D1 in a dose-dependent manner in mouse embryonic fibroblasts (NIH 3T3), human osteosarcoma (U2OS) cells and normal human fibroblast (WI38) cells (Suwaki et al. 2010) that is reminiscent of the rapid cyclin D1 degradation observed

170

in cells treated with other DNA damaging agents such as IR and UV (Agami and Bernards 2000; Hiyama et al. 1997). Furthermore, following low doses of 4NQO, cells accumulated in S-phase and G_2/M phases of cell cycle, indicating that low doses of 4NQO caused proliferative arrest, with no notable accumulation of cells with a sub-G_1 content of DNA, suggesting that exposure to a low dose of 4NQO does not trigger apoptotic cell death (Suwaki et al. 2010). However, medium-high doses of 4NQO have been reported to trigger a strong G_1 arrest that may be accompanied by apoptotic cell death (Suwaki et al. 2010).

5. H_2O_2 is naturally produced in organisms as a by-product of oxidative metabolism. Hydrogen peroxide can be converted to the highly damaging hydroxyl radical and can generate singlet oxygen, which is not itself a free radical, but acts as a catalyst for free radical formation. Reactive oxygen species (ROS) are known to damage proteins, nucleic acids and cell membranes. The most abundant DNA lesion caused by H_2O_2 is a base modification to 7,8-dihydro-8-oxoguanine (8-oxoG) (Chatgilialoglu and O'Neill 2001). Conversion of 8-oxoG causes selective mis-incorporation of adenine opposite to 8-oxoG that can lead to a G-T transversion in the DNA (Wood et al. 1990; Wood et al. 1992). H_2O_2 is a ROS that is known to cause oxidative damage primarily through the hydroxyl radical that results from the Fenton reaction (Buda et al. 2003; Imlay et al. 1988).

Cytotoxic doses of H_2O_2 have been reported to induce necrosis or apoptosis (Frippiat et al. 2002), whereas sub-lethal H_2O_2 treatment induces senescence-like growth arrest of human fibroblasts (Duan et al. 2005; Frippiat et al. 2001; Frippiat et al. 2002). This cell cycle arrest has been shown to be associated with down regulation of cyclin D1 (Barnouin et al. 2002; Hiyama et al. 1997), which predominantly results in an immediate G_1 arrest, allowing the damage to be repaired prior to further DNA replication. Furthermore, prolonged low doses of H_2O_2 induce senescent-like morphological changes, irreversible G_1 cell cycle arrest and a significant increase in SA-β-gal in young human diploid fibroblasts (Dimri et al. 1995; Frippiat et al. 2002).

The sensitivities of the GI panel members to CPT, DOX, 4NQO, CisPt and H_2O_2, along with the experimental methods used to determine sensitivity, are summarised in Table 6.1.

The p38 pathway has been implicated in the DNA damage response and is reported to be activated in response to various DNA damage-inducing agents (Boldt et al. 2002; Bragado et al. 2007; Coffer et al. 1995; Kool et al. 2003; Lee et al. 2002; Wilhelm et al. 1997). Evidence suggests that p38 can be potently activated by drugs that induce DNA damage by either promoting the formation of DNA adducts (e.g. by CisPt) or inhibiting Topo II (e.g. by DOX), but not by therapeutically relevant doses of γ-irradiation (Sanchez-Prieto et al. 2000). Further evidence suggests that apoptosis induced by CisPt requires the onset of a p53-mediated p38α pathway through the generation of ROS (Bragado et al. 2007). Oxidative stress, such as that caused by H_2O_2, is widely known to activate the p38 pathway via ASK1 (Matsukawa et al. 2004; Pan et al. 2010). Similarly, p38 activation has been reported in response to CPT, where it is involved in CPT-induced cell death (Lee et al. 2002). p38 also regulates cell cycle checkpoints in response to DNA damage induced by UV radiation, including the G1/S and the early G2/M checkpoints (Bulavin et al. 2001; Manke et al. 2005). Although the importance of p38 in cell cycle checkpoints induced by IR is less well understood, MEK6 and p38 have been implicated in the IR-induced G2/M checkpoint (Wang et al. 2000b).

The working hypothesis is that different forms of genomic stress may result in common pathways for stress signalling, namely the p38 pathway, and in their impact on the probability of cell cycle exit. The approach was to screen all of the GI panel members to identify hallmarks of cell cycle arrest (either of accumulation in G_2/M or restricted exit from G_1) as hallmarks of a stress response. The dose range for each drug was chosen based on previous evidence from the literature with the aim of inducing low-levels of stress for a prolonged period of time so that the frequency of arrest can report on sensitivity.

6.2 Results

6.2.1 Sensitivity of hTert-immortalised genomic instability syndrome fibroblasts to genotoxic agents

Clonogenic survival assays are commonly used to determine the sensitivity of cells to cytotoxic agents (Franken et al. 2006); however, these assays require cells to form discernible colonies that are subjectively defined. To assess the plating efficiency (PE) for each of the GI panel members, colonies of ≥ 50 cells were counted in the absence of genotoxic agents. Figure 6.1 shows that the PE for normal cells is ~11%, which is consistent with reports in the literature (Franken et al. 2006). CSA and BS cells show a similar PE to that observed for normal cells; however, the PE observed for NBS, LIG4, RTS and HGPS is much lower. Based on these observations the syndromes were grouped into those with normal PE (normal, BS and CSA) and those with sub-normal PE (NBS, LIG4, RTS and HGPS). Comparison of the PE by one tailed t-test showed that the PE for each group was significantly different (p=0.001).

Clonogenic survival was determined by counting the number of colonies of ≥ 50 cells. Differences in sensitivity to each of the agents for each of the GI panel members were examined by comparing the shapes of the dose-response curves and IC_{50} values. IC_{50} values were defined as the dose at which 50% survival was achieved, and were retrieved graphically to avoid curve-fitting anomalies. In cases in which a 50% survival level was not achieved the dose at which 80% survival was achieved (IC_{20}) value was compared.

No correlation was observed between intrinsic sensitivity and PE when IC_{50} values were analysed on a drug-by-drug basis. Furthermore, by comparing the IC_{50} values for each agent between the normal PE and sub-normal PE group, the difference in the inherent sensitivity of the two groups to the panel of agents could be analysed. Using a 1 tailed t-test, no significant difference in IC_{50} values for CTP (p=0.35), DOX (p=0.42), 4NQO (p=0.10), CisPt (p=0.24) and H_2O_2 (p=0.36), was observed between the two groups. These data suggest that any inherent

differences in replicative potential in these cells do not contribute to their sensitivity to the panel of genotoxic agents.

The sensitivity of each of the GI panel members to each of the agents was compared to the response observed for normal cells. The IC_{50} values for normal cells in response to CPT, DOX, 4NQO and H_2O_2 were 7 nM, 4 nM, 5 μM and 53 μM, respectively (Table 6.2). An IC_{50} value was not obtained for normal cells in response to CisPt; however, an IC_{20} value of 1.2 μM was recorded (Table 6.2). Using the same criteria the relative survival of GI syndrome cells were studied and details of the pattern of responses observed are described. Table 6.2 shows a comparison of the IC_{50} (or 20% killing in the case of CisPt) values for each GI syndrome relative to normal cells.

Survival curves are shown in Figures 6.2-6.8 where responses are compared to the normal strain AG16409(N)^{hTert}. As expected, CSA cells showed a slight to moderate increase in sensitivity to CPT (Figure 6.2A) (Squires et al. 1993), DOX (Figure 6.2B) and 4NQO (Figure 6.2C) but normal responses to H_2O_2 (Figure 6.2E). In contrast, CSA cells show relative resistance to CisPt compared to normal cells (Figure 6.2D) although absolute toxicity levels were insufficient for a definitive determination.

As expected BS cells were hypersensitive to CPT (Figure 6.3A) (Mao et al. 2010) and to a much lesser degree 4NQO (Figure 6.3C) (Prince et al. 1999). BS cells showed pronounced hypersensitivity to DOX (Figure 6.3B). The literature suggests that BS cells are also hypersensitive to CisPt (Mao et al. 2010), while the data shown in Figure 6.3D are unable to confirm that observation due to the low levels of drug toxicity achieved. Similarly, BS cells showed essentially normal response to H_2O_2 at low doses (Figure 6.3E). Overall, BS cells show the same pattern of responses as those observed for CSA.

Contrary to findings in the literature that NBS cells are hypersensitive to CPT (Kraakman-van der Zwet et al. 1999), Figure 6.4A shows that NBS cells respond normally to CPT. A similar response was observed in response to H_2O_2

(Figure 6.4E), whereas NBS cells show evidence of increased sensitivity to 4NQO (Figure 6.4C) and show relative resistance to CisPt (Figure 6.4D). NBS cells show slight resistance to DOX at low doses (2.5-10 nM) (Figure 6.4B).

LIG4 show a normal response to CPT at low doses (2.5-10 nM) but some evidence of increased sensitivity at a higher dose (20 nM) (Figure 6.5A). LIG4 cells show pronounced hypersensitivity to DOX (Figure 6.5B) but are relatively resistant to 4NQO (Figure 6.5C), CisPt (Figure 6.5D) and H_2O_2 (Figure 6.5E).

Consistent with recent findings in the literature, Figure 6.6A shows that RTS cells are hypersensitive to high dose CPT (Jin et al. 2008). Contrary to findings in the literature that the RTS cells showed pronounced hypersensitivity to DOX (Jin et al. 2008) similar in extent to that shown by BS cells, Figure 6.6B shows that RTS cells show a normal response to DOX. Figure 6.6D shows RTS cells are hypersensitive to CisPt, however, this conflicts with previous reports in the literature that RTS cells show normal to moderate sensitivity to this agent (Cabral et al. 2008). RTS cells show moderate resistance to H_2O_2 at low doses (10-40 μM) but are hypersensitive to this agent at higher doses (40-80 μM) (Figure 6.6E). Consistent with previous reports, RTS cells also show relative resistance to 4NQO (Jin et al. 2008) (Figure 6.6C).

HGPS cells show pronounced hypersensitivity to CPT (Figure 6.7A) and DOX (Figure 6.7B) and moderate hypersensitivity to CisPt (Figure 6.7D) but a normal response to 4NQO (Figure 6.7C) and H_2O_2 at low doses (10-20 μM) (Figure 6.7E).

As expected, WS cells showed hypersensitivity to CPT (Figure 6.8A) (Mao et al. 2010; Poot et al. 1999) but showed a normal response to DOX, 4NQO and H_2O_2 (Figure 6.8B, C and E). Contrary to previous findings (Mao et al. 2010; Poot et al. 2001), WS cells were relatively resistant to CisPt (Figure 6.8D).

In an attempt to identify patterns of response to the genotoxic panel in GI syndrome fibroblasts these data are summarised in the form of a heatmap (Figure 6.9). Overall, all cells are hypersensitive to CPT even at low doses, with the

exception of NBS, which shows a normal response to the agent. All cells are also hypersensitive to DOX at higher doses (20 nM), although RTS and NBS cells are relatively resistant at lower doses and WS shows a normal response at lower doses. CSA, BS and NBS are hypersensitive to 4NQO at all doses, whereas WS are only hypersensitive at higher doses (15-20 μM). In contrast, LIG4, RTS and HGPS are relatively resistant to 4NQO. RTS and HGPS show pronounced hypersensitivity to CisPt, whereas all other cells are relatively resistant to CisPt. The response of GI syndromes to H_2O_2 is more variable: CSA, NBS and WS show a normal response to H_2O_2; BS and HGPS show a normal response at lower doses but are hypersensitive at higher doses; LIG4 and RTS are relatively resistant to H_2O_2, although RTS is hypersensitive at the highest dose (80 μM).

6.2.2 Cell cycle dynamics in response to DNA damage in hTert-immortalised genomic instability syndrome fibroblasts

To assess the short-term impact of the genotoxic panel on cell cycle exit, a single dose for each agent was selected for flow cytometric analysis based on the previous survival data. The following doses were used: CPT 10nM, DOX 10nM, 4NQO 15 μM, CisPt 2.5 μM and H_2O_2 80 μM representing clonogenic survival levels of ~40%, ~20%, ~15%, ~70% and ~30% respectively for normal cells. Bright field imaging was used to review the cellular morphology and to allow simple observation of changes in growth parameters. To assess the impact of the drugs on population growth, the increase in cell number for each cell strain in the presence and absence of each drug was assessed.

In normal cells, cell cycle arrest in G_2/M was observed following CPT and DOX (Figure 6.10C). However, treatment with 4NQO, CisPt and H_2O_2 had no effect on the percentage of cells in G_2/M in normal cells (Figure 6.10C). In contrast, no cell cycle arrest in G_1 is observed for normal cells in response to any agent (Figure 6.10D). No differences were observed in the morphology of normal cells following treatment with these agents, suggesting that cell cycle arrest is not necessarily associated with clear morphology changes or commitment to loss of viability (Figure 6.10B). The cell cycle arrest observed following CPT and DOX treatment

was associated with a slight reduction in population growth; however, this effect was relatively minor (Figure 6.10E).

Using the same approach, certain patterns were observed for the impact of the panel of genotoxic agents on G_2/M and G_1 arrest on GI syndrome cells when compared to normal cells. Note that only cells that show differences in their response to the genotoxic panel have been described in detail in this chapter, full details of all GI panel members are provided on the accompanying disk. Firstly, CPT and DOX consistently induce G_2/M arrest in all cells irrespective of their genetic backgrounds. Secondly, a similar level of G_2/M arrest (~3-fold) is induced by CPT and DOX in all cells, with the exception of BS and RTS cells, which show an increased level of G_2/M arrest (7-fold and 5-fold for BS and 5-fold and 4.5-fold for RTS in response to CPT and DOX, respectively), suggesting that BS and RTS cells are hypersensitive to these agents (Figure 6.11C and Figure 6.14C). Thirdly, treatment with 4NQO, CisPt and H_2O_2 generally had little effect on the cell cycle dynamics of all cells compared to that seen for CPT and DOX, although there are some exceptions. These include, BS cells, which also show increased G_2/M arrest in response to 4NQO (~2-fold) (Figure 6.11C), LIG4 that also show increased G_2/M arrest in response to 4NQO and H_2O_2 (~2fold) (Figure 6.13C) and finally RTS cells that show increased G_2/M arrest in response to all of the agents (Figure 6.14C). Fourthly, treatment with each of the agents did not induce G_1 arrest in the majority of cell strains; however, some exceptions were observed. These include RTS, which shows an increase in G_1 arrest in response to CPT, DOX and CisPt (Figure 6.14D) and HGPS, which shows an increase in G_1 arrest in response to all agents (Figure 6.12D).

6.2.3 Does BIRB796 alter post-treatment recovery from CPT?

To establish whether BIRB796 can overcome an arrest associated with DNA damage, the proportion of cells that accumulate in G_2/M following CPT treatment was assessed in the presence and absence of BIRB796. Furthermore, the impact of BIRB796 on the longer-term viability of these cells following CPT treatment was assessed. Here, the working hypothesis is that cells undergoing low levels of DNA

damage will show p38-restrained cell cycle exit. To test this, cells were treated with a single dose of CPT (10 nM) as previously described, washed and incubated with and without BIRB796 for a further 72 hours for short-term flow cytometric analysis or incubated for 10 days for clonogenic survival. The decision to temporally separate the addition of the CPT and BIRB796 was made in an attempt to reduce the issue of cross-reaction of the two agents. Three strains (normal, BS and CSA) were selected for analysis based on the previous observations that these cells showed the greatest response to CPT. Moreover, these cells were shown to consistently have the fastest growth rate therefore giving the best opportunity to observe significant shifts in cell cycle distribution over short periods for recovery from drug-induced cycle arrest.

Preliminary observations indicated that all three strains were in cycle at the start of the experiment, as reflected in the growth curves (Figure 6.15B). There was evidence of changes in the G_2/M content to a minor extent in normal and BS cells, but evidence of synchronisation in CSA, which may be expected in short term cultures such as these. Despite any changes in cell cycle dynamics of control cells BIRB796 treatment alone consistently increased the growth rate and increased the proportion of cells in cycle (designated as G_2+S) in all three strains (data not shown). As expected treatment with CPT induced accumulation in the proportion of cells in G_2/M in all three strains; however, differences were observed between three strains in their response to CPT. Although these differences may reflect inherent differences in the sensitivity of these strains to CPT, it is possible that these differences simply reflect the proportion of cells that were available for CPT action (i.e. those traversing S-phase) during the course of the experiment. T=0 data showed that there were differences in the proportion of actively dividing cells in the three strains, with CSA cells showing a reduced proportion of cells in S-phase (7%) compared to normal (31.7%) and BS cells (51.5%). The observation that CSA cells also show a reduced accumulation of cells in G_2/M compared with normal and BS cells when treated with CPT (Figure 6.15A) and relative resistance to CPT when assessed for clonogenic potential (Figure 6.16), suggests that the observed differences in sensitivity between strains are due to differences in the cell

cycle phase distribution at the time of addition of CPT and therefore the inter-strain differences were not assessed further.

As shown in Figure 6.15A, both normal and BS cells show early and sustained accumulation of cells in G_2/M, suggesting a long-lived block to cell cycle progression. In keeping with this, the growth curves for both normal and BS cells show a sustained growth arrest following CPT treatment, although there is some evidence of recovery at T=96 in normal cells (Figure 6.15B). Addition of BIRB796 reduced retention of cells in G_2/M in normal cells at both early and later times post treatment. The sustained retention of cells in G_2/M in BS was only affected by BIRB796 at later times (T=96) (Figure 6.15A), during which other effects of BIRB796 on cells that escaped CPT treatment could be occurring. CSA cells show a reduced accumulation of cells into G_2/M compared to normal and BS cells following CPT treatment (Figure 6.15A). In keeping with this, the growth curve for CSA cells indicate continued proliferation following CPT, although this was reduced compared to their untreated counterparts (Figure 6.15B). In CSA, progressive recruitment of cells into G_2 following CPT treatment occurs up to T=72 hours, after which there is evidence of recovery (confirmed by the increase in culture growth) (Figure 6.15). The recovery of CSA cells following CPT was demonstrably enhanced by BIRB796 treatment, shown by both a reduction in the G_2/M proportion and an increase in growth rate compared to normal cells (Figure 6.15). Overall these data show that BIRB796 has the ability to reduce the G_2/M accumulation in all three strains studied but the kinetics of that recovery may differ according to cell type.

As shown in Figure 6.16A, large differences in the clonogenic potential (given by the number of colonies of ≥50 cells) for the three strains are observed, with BS cells having a higher clonogenic potential compared to normal and CSA cells. Despite these differences, the sensitivity of the three strains to CPT does not appear to correlate with clonogenic potential *per se* (Figure 6.16B). Similarly, there does not appear to be a relationship between the overall clonogenic potential of untreated cells and the impact of BIRB796. As a result the differences in

clonogenic potential were assumed not to alter the analysis although it was appreciated that a different proportion of the entire population is being analysed between strains.

As expected, pre-treatment with 10 nM CPT for 24 hours reduces the clonogenic potential of GM01856(CSA)^{hTert}, AG16409(N)^{hTert} and GM02548(BS)^{hTert} cells compared to their untreated counterparts (Figure 6.16A). Conversely, treatment with BIRB796 alone increases the clonogenic potential of GM01856(CSA)^{hTert}, AG16409(N)^{hTert} and GM02548(BS)^{hTert} cells compared with untreated cells (Figure 6.16A). This suggests that BIRB796 stimulates cells that were previously non-clonogenic to re-enter cycle so that they now report as being clonogenic. BIRB796 also increases the clonogenic potential of cells that were pre-treated with CPT compared to CPT treatment alone, suggesting that BIRB796 increases recovery of cells following CPT treatment; however, the clonogenic potential of cells treated with CPT+BIRB796 is lower than those treated with BIRB796 alone (Figure 6.16A). These data suggest that there are a proportion of cells that are BIRB796-recoverable (BR) and that pre-treatment with CPT reduces the proportion of BR-cells.

6.3 Discussion

Inconsistencies in the reported sensitivity of GI syndrome cells to genotoxic agents in the literature suggest that the issues associated with using different experimental techniques or in the cell type studied (e.g. fibroblast or lymphoblast, primary or transformed) still stand. Therefore this study provided the opportunity to compare the drug sensitivities of each of these syndromes using a standard technique. The screen was undertaken with certain known limitations (e.g. pragmatically trying to assay all of the lines at the same time to reduce errors due to differences in conditions). In addition, differences in the PE of the different cell strains were observed. Although these differences were shown not to affect the sensitivity of each of the GI panel members to the panel of genotoxic agents, clearly the informative population in this analysis is restricted to cells that have the potential to undergo at least 6 PDs (to give rise to colonies of ≥50 cells). In the

case of NBS, for example, the PE is <1%, therefore >99% of the population cannot be analysed using this method.

Despite the differences in PE, the results indicate that some cell lines show hypersensitivity to major classes of damage, such as those induced by CPT and DOX. The screen has revealed high levels of sensitivity in BS, RTS, HGPS and LIG4 in response to DOX and similarly in RTS in response to CisPt. Moreover, RTS cells have previously been reported to show a normal response to CisPt (Cabral et al. 2008); however, different cell strains were studied, suggesting that there may be inter-strain heterogeneity amongst RTS cells in their response to genotoxic agents. In general, all of the GI syndrome fibroblasts showed a normal response to H_2O_2. This is consistent with the finding in the literature that only prolonged treatment with low doses of H_2O_2 induce senescence (Duan et al. 2005), therefore a 24 hour treatment may not be sufficient to induce long-term arrest in these cells. These data also suggest that the molecular defect in these cells does not sensitise to low levels of oxidative stress. Clearly further investigation is required to fully profile the sensitivity of these cells to genotoxic agents and may provide an insight into the molecular defect or pathways that are defective in these cells.

When analysed by flow cytometry, both CPT and DOX consistently induced a G_2/M arrest in all cells, whereas the impact of 4NQO, CisPt and H_2O_2 on the cell cycle dynamics of all strains was slight. Agents that act across the cell cycle may result in 'freezing' of the DNA content distributions and therefore recruitment into arrest being less apparent. Given the differences in the populations available for clonogenic and flow cytometric analysis, concordance between early measures of drug response, for example cell cycle arrest was not expected to necessarily relate to clonogenic data. Despite these differences, the results showed that in general, those strains that showed an early drug response (i.e. arrest within 24 hours) also showed a reduction in clonogenic potential in the longer term. However, some exceptions were observed, for example, LIG4 cells showed a reduction in clonogenic potential in response to DOX but did not show an early cell cycle arrest.

These results indicate that in LIG4 the cell cycle arrest induced by DOX cells takes longer than 24 hours to be realised. The results also identify an inherent problem when analysing fibroblasts from some of these syndromes. For example, using the standard cell cycle fitting approach, possible anomalies in cell cycle phase assignment were identified in some samples including WS cells. These issues include the presence of split peaks, possibly representing subpopulations with different cell cycle properties that cannot be analysed efficiently using the standard cell cycle fitting approach. This raises the need for alternative approaches of identifying cell cycle phases and as such region analysis was used in other studies.

Flow cytometric analysis of GM01856(CSA)^{hTert}, AG16409(N)^{hTert} and GM02548(BS)^{hTert} cells that had been pre-treated with CPT and subsequently incubated in BIRB796 indicated that BIRB796 increased recovery, although the timing of this recovery appeared to differ between strains. It was also shown that BIRB796 increases the clonogenic potential of CPT pre-treated GM01856(CSA)^{hTert}, AG16409(N)^{hTert} and GM02548(BS)^{hTert} cells compared to those incubated in CPT alone. This suggests that BIRB796 does indeed increase the recovery of GM01856(CSA)^{hTert}, AG16409(N)^{hTert} and GM02548(BS)^{hTert} cells following exposure to CPT. However, the observation that BIRB796 alone also increases the clonogenicity of GM01856(CSA)^{hTert}, AG16409(N)^{hTert} and GM02548(BS)^{hTert} cells, suggets that the increase in clonogenicity seen in CPT-treated cells may be due to the action of BIRB796 on cells that escaped the initial CPT treatment.

In summary, the main findings from this chapter are:

• GI syndrome and normal cells show a reduction in clonogenic potential, reflecting long-term cell cycle arrest (potentially SIPS), in response to at least one of the genotoxic agents used here. This suggests that the hTert panel remain susceptible to SIPS and therefore provide a feasible model to study differences in endogenous levels of SIPS in these cells.

- The study revealed hypersensitivity of some strains to genotoxic agents (e.g. BS, RTS, HGPS and LIG4 are hypersensitive to DOX and RTS is hypersensitive to CisPt).

- 24 hour incubation with 10 nM CPT and 10 nM DOX consistently induces G_2/M arrest in all cell strains tested.

- BIRB796 increases the clonogenic potential of hTert-immortalised CSA, BS and normal cells.

- BIRB796 increases the clonogenic potential of CPT pre-treated hTert-immortalised CSA, BS and normal cells. It is therefore possible that BIRB796 increases the recovery of these cells following CPT treatment; however, it is also possible that the increase in clonogenicity is due to the action of BIRB796 on cells that escaped the initial CPT treatment.

Table 6.1. Summary of the sensitivity profiles for GI panel members to genotoxic stress.

Syndrome	Agent	Cell type	Assay	Findings	Ref
WS	CPT	SV40-transformed GM639 and U2 OS cells	WRN depletion by shRNA knockdown and treated with 6-12 nM CPT for 24 hours and colonies allowed to grow for 8 days prior to analysis. Colonies of ≥6 cells were counted to determine survival.	Hypersensitivity	Mao et al 2010
	CPT	Lymphoblastoid	Cells were treated with 10-50 nM CPT for 24 hours prior to flow cytometric analysis of cell survival and level of apoptosis.	Hypersensitivity (Higher levels of apoptosis)	Poot et al 1999
	CPT	ES cells	Cells were treated for 1 hour with 0.1-0.5 μM CPT and colonies allowed to form for 7 days prior to analysis.	Hypersensitivity	Leder et al 1998
	DOX	Lymphoblastoid	Cells were analysed for cell survival, cell cycle and entry to apoptosis by flow cytometry (cells treated with 100-400 nM DOX for 24 hours prior to analysis) and proliferative survival by BrdU (cells exposed to 100-400 nM DOX for 72 hours prior to analysis)	Normal sensitivity	Poot et al 2001
	4NQO	Primary fibroblasts from WS individuals and WRN-/- and WRN +/+ lymphoblastoid cells	Cells were treated with 0.3-1.0 μM 4NQO for 24 hours and 60 minutes, respectively. Proliferative survival and apoptosis rate was measured by BrdU and flow cytometry.	Hypersensitivity	Poot et al 2002
	4NQO	SV40-transformed WRN fibroblast cell lines	Cells were treated with 0.1-0.8 mg/ml for 24 hours. Cells were trypsinised and replated for colony formation and left to grow for 10 days prior to analysis. Colonies of >50 cells were counted to determine survival.	Hypersensitivity	Prince et al 1999
	CisPt	Lymphoblastoid	Cells treated with 0-2 μM CisPt for 24 hours prior to flow analysis and 72 hours prior to proliferative survival assay	Hypersensitivity (1.5 fold)	Poot et al 2001
	CisPt	SV40-transformed GM639 and U2 OS cells	Cells treated with 1-2 μM for 24 hours	Hypersensitivity	Mao et al 2010
	H₂O₂	Primary fibroblasts from WS individuals and WRN-/- and WRN +/+ lymphoblastoid cells	Cells treated with 10-80 μM for 24 hours	Normal sensitivity	Prince et al 1999
	H₂O₂	Primary WI-38 and IMR-90.	Cells were depleted of WRN by siRNA. Cells were treated with 10-150 μM H2O2 for 45 minutes.	Hypersensitivity	Szekely et al 2005
	H₂O₂	Primary WS cells	Cells were treated with 50-200 μM H2O2 for 1 hour.	Resistance	Cabral et al 2008

Table 6.1 continued

Syndrome	Agent	Cell type	Assay	Findings	Ref
RTS	CPT	Primary RTS fibroblasts	Cells were treated with 0.25-15 nM CPT for 72 hours. Colonies of >50 cells (or for slow growing strains >16 cells) were scored after 10-14 days.	Hypersensitivity	Jin et al 2008
	DOX	Primary RTS fibroblasts	Cells were treated with 0.1-1 µM DOX for 30 minutes.	Hypersensitivity	Jin et al 2008
	4NQO	Primary RTS fibroblasts	Cells were treated with 0.2-1 µM 4NQO for 1	Normal sensitivity	Cabral et al 2008
	4NQO	Primary RTS fibroblasts	Cells were treated with 20-80 nM 4NQO for 24 hours.	Resistance	Jin et al 2008
	CisPt	Primary RTS fibroblasts	Cells were treated with 1-8 mM CisPt for 4 hours.	Normal sensitivity	Cabral et al 2008
	CisPt	Primary RTS fibroblasts	Cells were treated with 0.5-2.5 µM CisPt for 24 hours.	Modest sensitivity	Jin et al 2008
	H_2O_2	Primary RTS (AG18371)	Cells were treated with 0.1-1 mM H2O2 for 15 minutes. Cell proliferation was measured to assess recovery.	Hypersensitivity	Werner et al 2006
	H_2O_2	Primary RTS fibroblasts	Cells were treated with 50-200 µM H2O2 for 1 hour.	Normal sensitivity	Cabral et al 2008
BS	CPT	SV40-transformed GM639 and U2 OS cells	Cells were depleted of BLM by shRNA knockdown and treated with 6-12 nM CPT for 24 hours and colonies allowed to grow for 8 days prior to analysis	Hypersensitivity	Mao et al 2010
	DOX	Lymphoblastoids	Cell viability was monitored at 4, 8, and 24 h following treatment with 5-25 mg/ml DOX	Resistance	Wang et al 2001
	4NQO	SV40-transformed WRN fibroblast cell lines	Cells were treated with 0.1-0.8 mg/ml for 24 hours.	Hypersensitivity	Prince et al 1999
	CisPt	SV40-transformed GM639 and U2 OS cells	Cells treated with 1-2 µM for 24 hours	Hypersensitivity	Mao et al 2010
CSA	CPT	Primary and SV40-transformed human fibroblasts.	Cells were treated with 0.13-2 µM CPT for 1 hour. Colonies were allowed to form for 8-14 days.	Hypersensitivity	Squires et al 1993
	4NQO	CSA fibroblasts	Cells were treated with 1 nm-1 µM 4NQO for 90 minutes. Colonies were scored after 14-21 days.	Hypersensitivity	Wade and Chu 1979
NBS	CPT	SV40-transormed NBS fibroblasts.		Hypersensitivity (3-fold)	Kraakman-van der Zwet et al 1999
HGPS	CPT	Spontaneously immortalised Zmpste24-deficient MEFs	Cells were treated with 1-6 µM for 1 hour and assessed by colony forming assay.	Hypersensitivity	Liu et al 2005
LIG4	CisPt	Lig4-/- MEFs	Cells were treated with 2.5-15 µM CisPt for 3 hours and assessed by colony forming assay.	Hypersensitivity	Kondo et al 2010

Table 6.2. Sensitivity of GI syndrome and normal fibroblasts to the panel of genotoxic agents.

| Cell line | IC_{50} | | | | IC_{20} |
	nM CPT	nM DOX	μM 4NQO	μM H_2O_2	μM CisPt
Normal	7	4	5	52.5	1.2
CSA	6	2	4.5	52.5	2.05
BS	4.5	2	4	40	2.1
NBS	7	5	3	40	2.5
LIG4	10.5	1.2	19	80	-
RTS	7	2	13	55	0.54
HGPS	2	1.5	6	35	0.6
WS	1.5	3	8	53	2.5

Sensitivity of cells to genotoxic agents as indicated by the IC_{50} values (or IC_{20} values for CisPt).
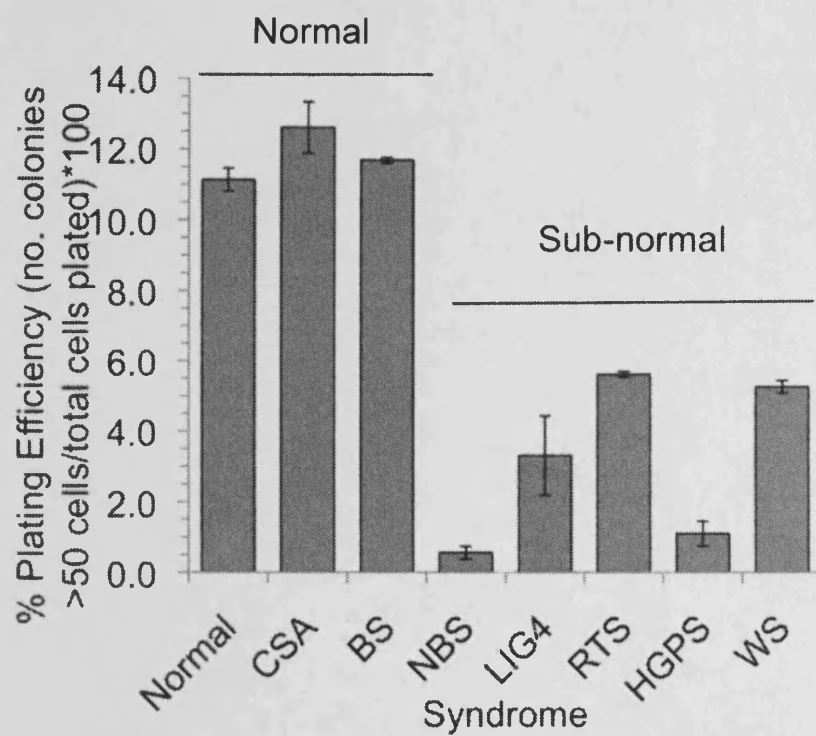
Figure 6.1. PE of GI syndrome cells.

PE was calculated as a percentage of the number of colonies of >50 cells/number of cells plated, and plotted as a mean of duplicate plates. Error bars represent the range of data obtained (n=2).
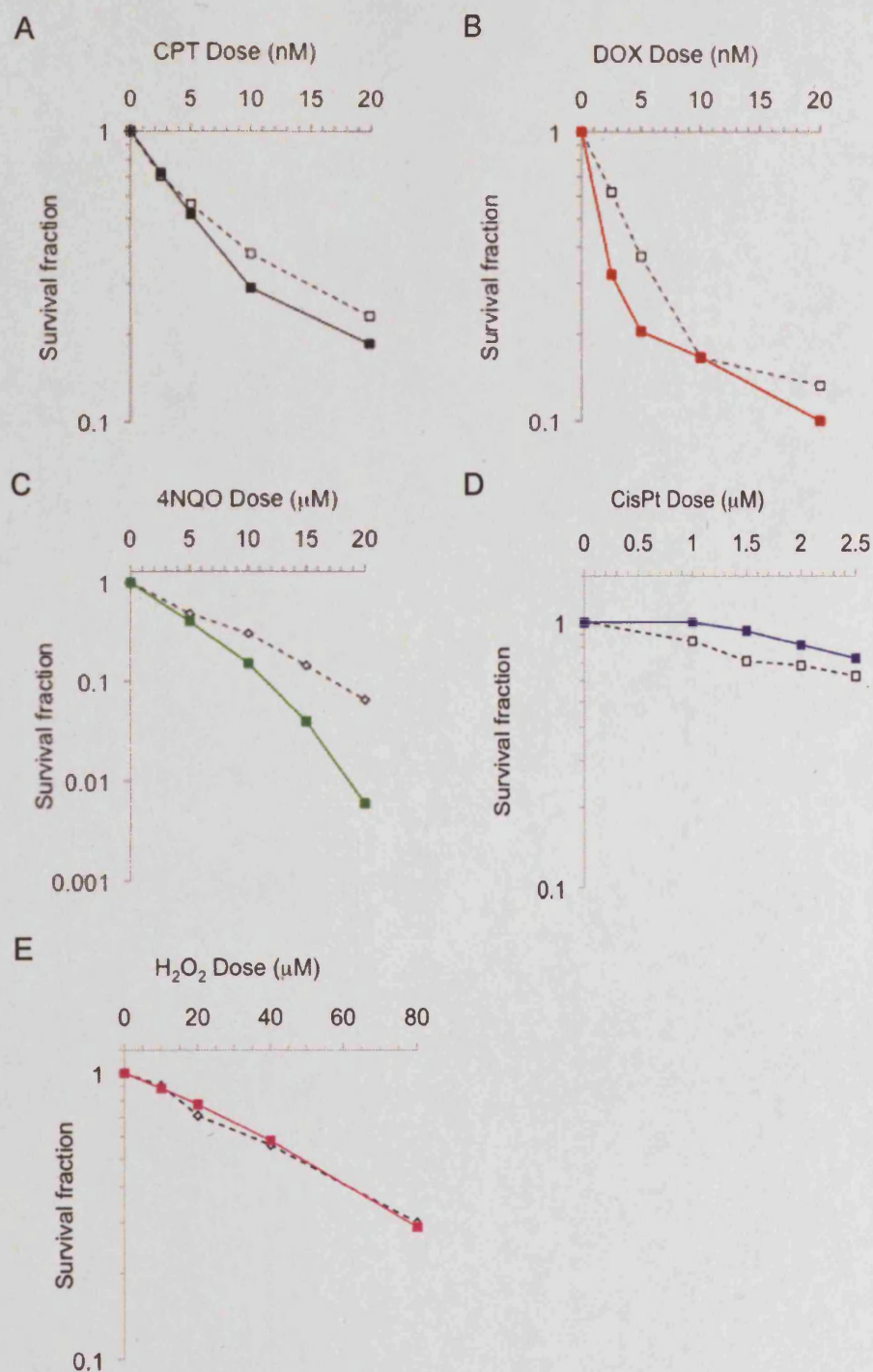
Figure 6.2. Analysis of clonogenic survival of GM01856(CSA)[hTert] fibroblasts following exposure to DNA damaging agents.

Panels A-E show responses to CPT, DOX, 4NQO, CisPt and H_2O_2 for CSA (solid lines) compared to AG16409[hTert] (N) (dotted line). Survival was determined by counting colonies >50 cells. Data derived from a single experimental screen, n=2.
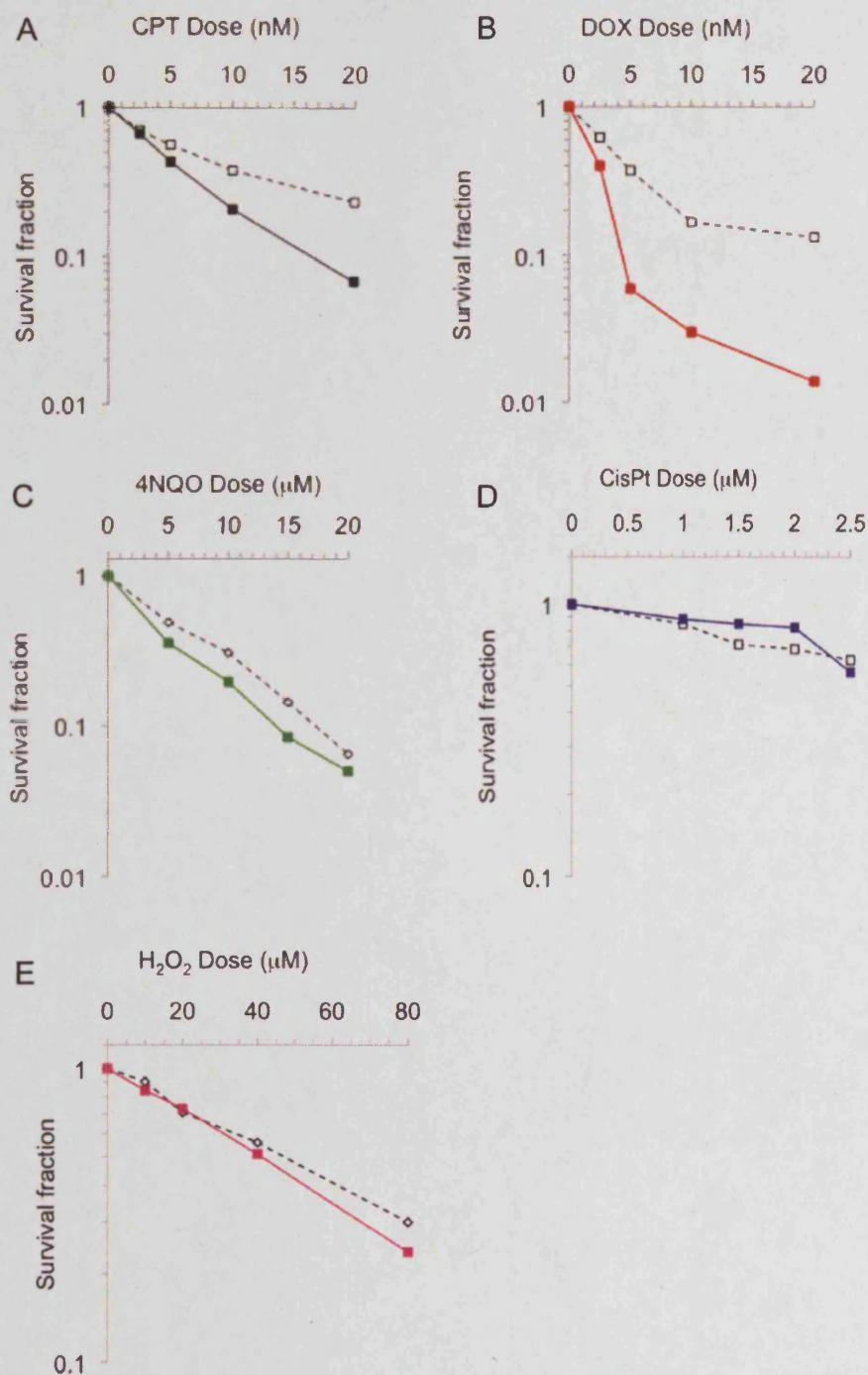
Figure 6.3. Analysis of clonogenic survival of GM2548(BS)[hTert] fibroblasts following exposure to DNA damaging agents.

Panels A-E show responses to CPT, DOX, 4NQO, CisPt and H_2O_2 for BS (solid lines) compared to AG16409[hTert] (N) (dotted line). Survival was determined by counting colonies >50 cells. Data derived from a single experimental screen, n=2.

189
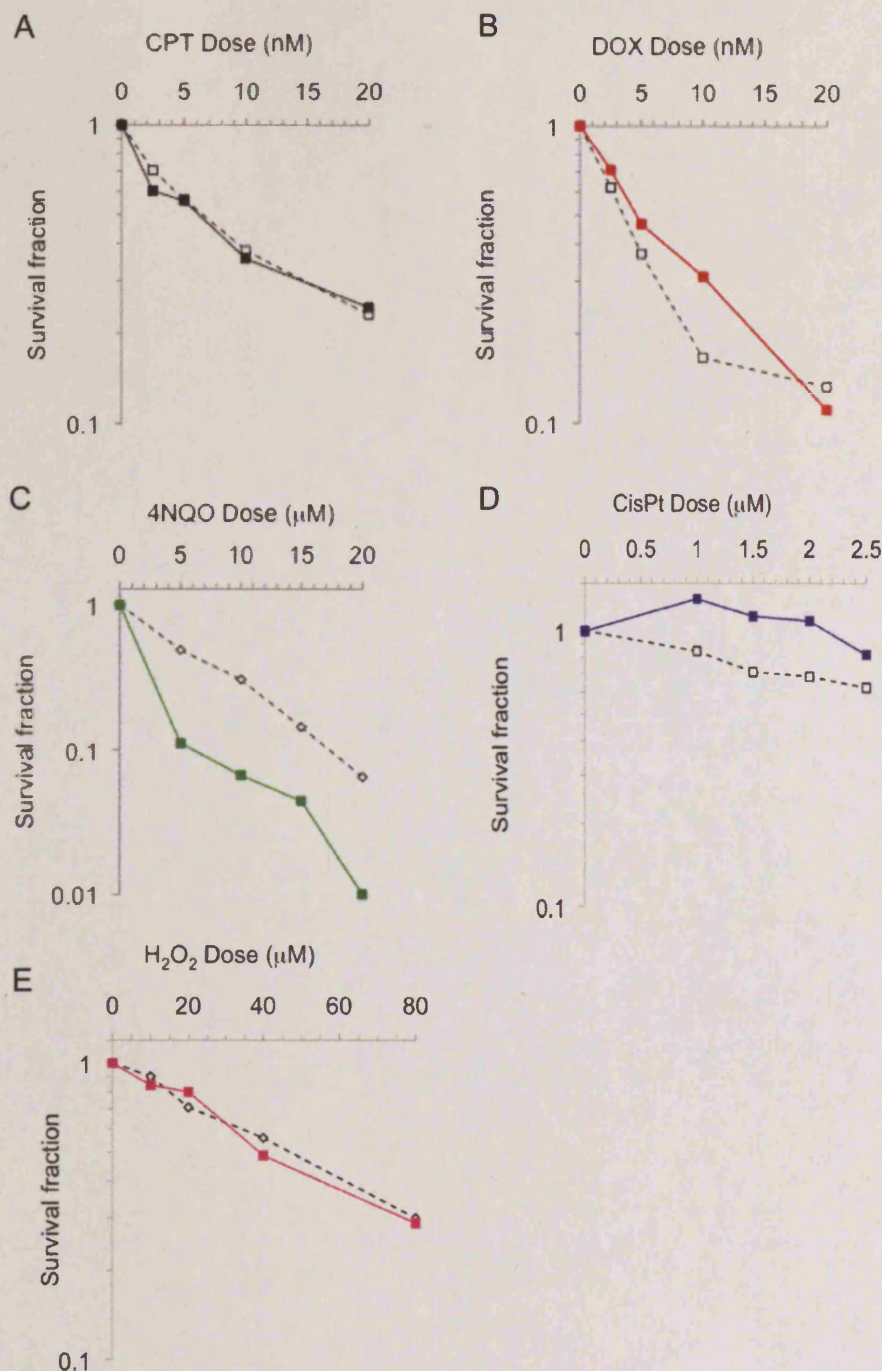
Figure 6.4. Analysis of clonogenic survival of GM07166(NBS)[hTert] fibroblasts following exposure to DNA damaging agents.

Panels A-E show responses to CPT, DOX, 4NQO, CisPt and H_2O_2 for NBS (solid lines) compared to AG16409[hTert] (N) (dotted line). Survival was determined by counting colonies >50 cells. Data derived from a single experimental screen, n=2.
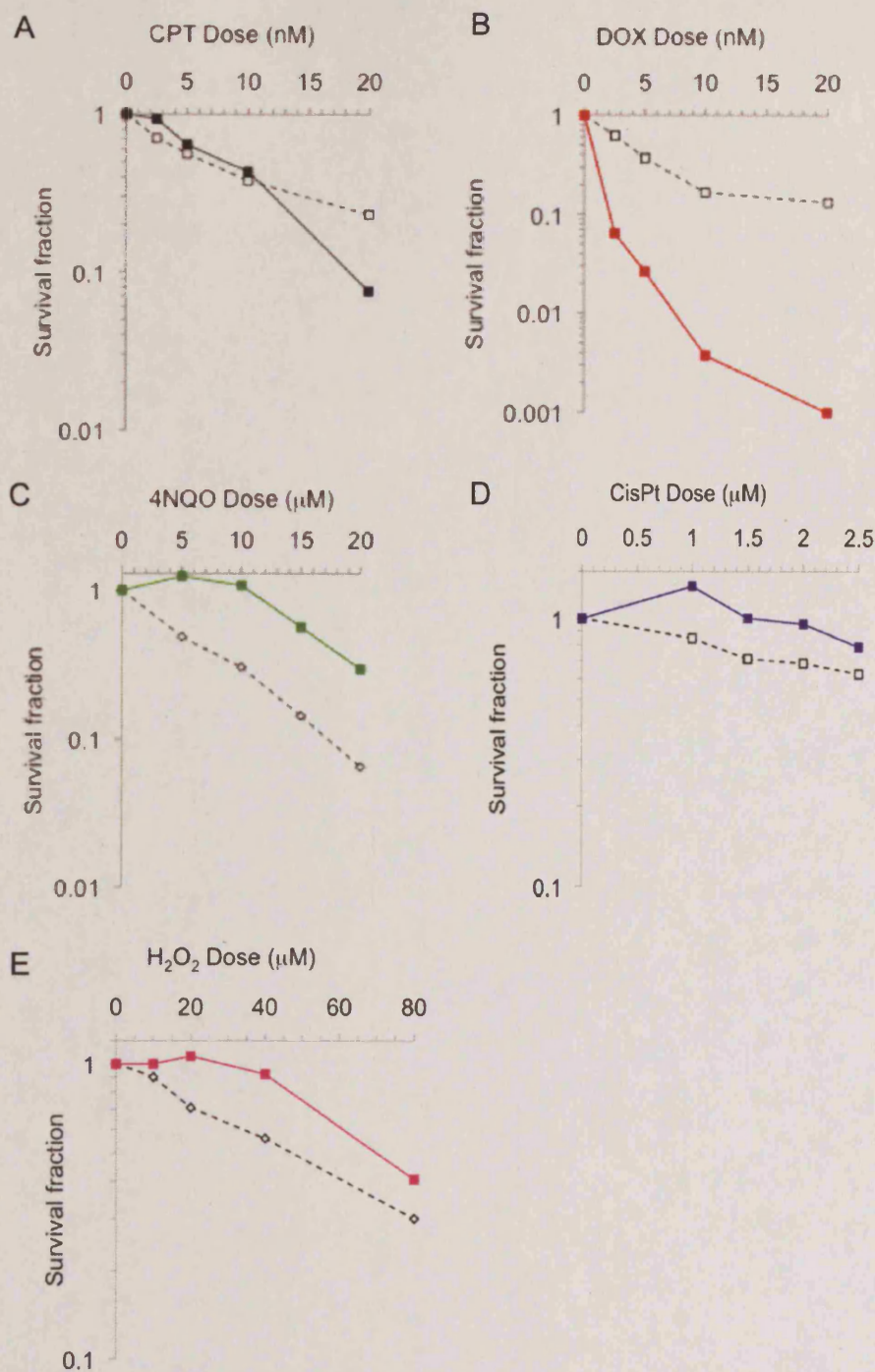
Figure 6.5. Analysis of clonogenic survival of GM17523(LIG4)^{hTert} fibroblasts following exposure to DNA damaging agents.

Panels A-E show responses to CPT, DOX, 4NQO, CisPt and H_2O_2 for LIG4 (solid lines) compared to AG16409^{hTert} (N) (dotted line). Survival was determined by counting colonies >50 cells. Data derived from a single experimental screen, n=2.

191
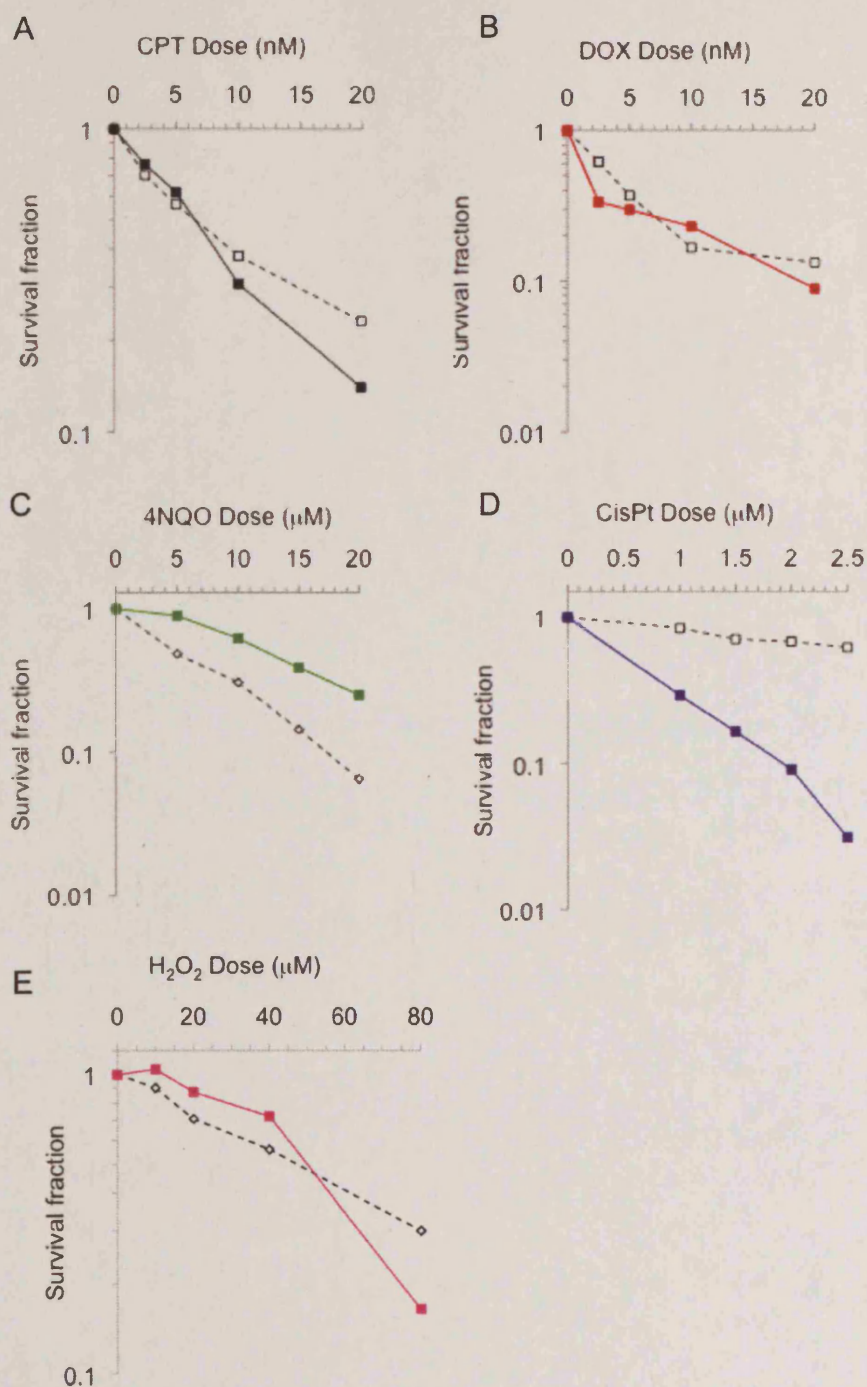
Figure 6.6. Analysis of clonogenic survival of AG18371(RTS)[hTert] fibroblasts following exposure to DNA damaging agents.

Panels A-E show responses to CPT, DOX, 4NQO, CisPt and H_2O_2 for RTS (solid lines) compared to AG16409[hTert] (N) (dotted line). Survival was determined by counting colonies >50 cells. Data derived from a single experimental screen, n=2.
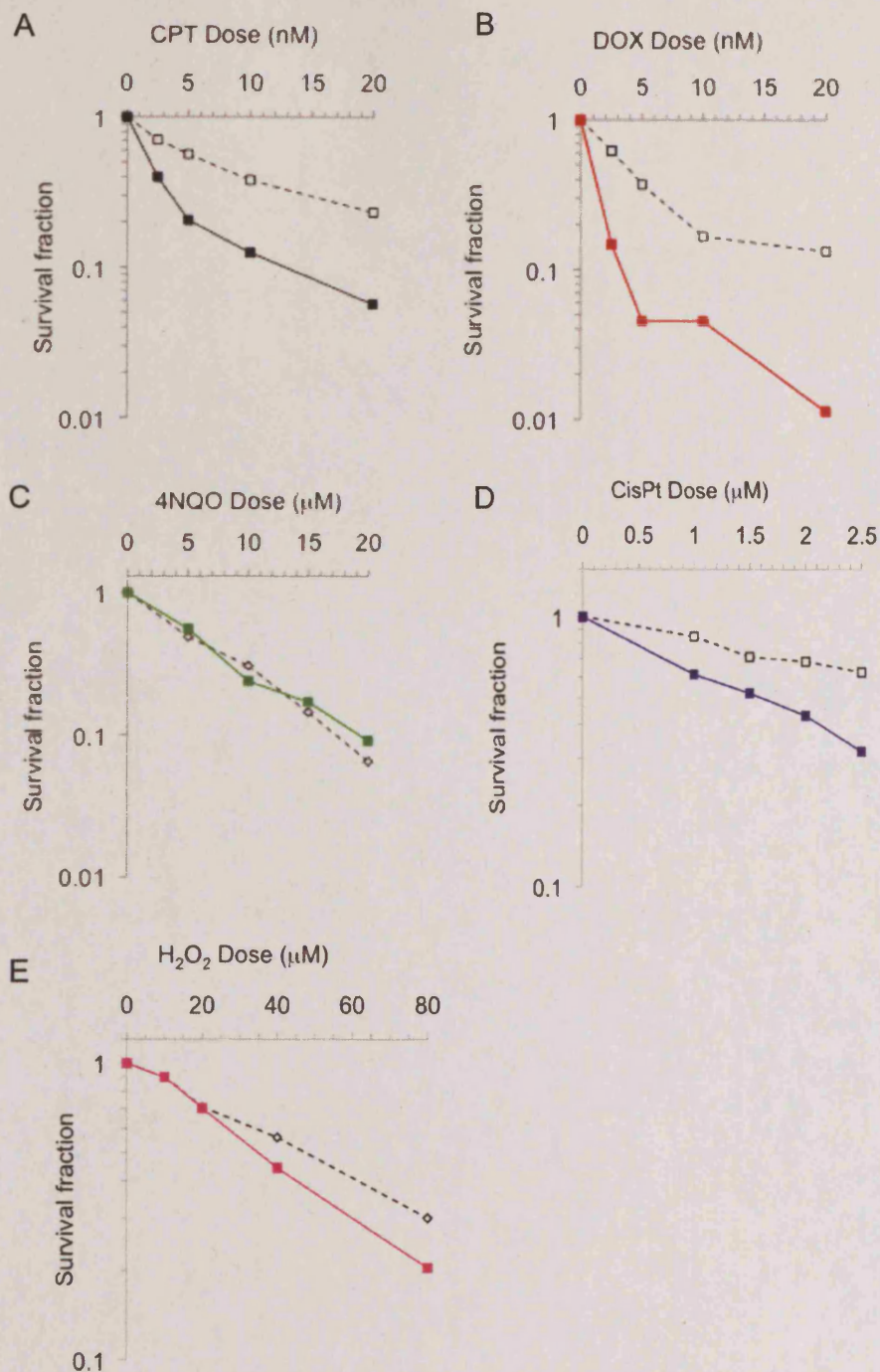
Figure 6.7. Analysis of clonogenic survival of AG11498(HGPS)^{hTert} fibroblasts following exposure to DNA damaging agents.

Panels A-E show responses to CPT, DOX, 4NQO, CisPt and H$_2$O$_2$ for HGPS (solid lines) compared to AG16409^{hTert} (N) (dotted line). Survival was determined by counting colonies >50 cells. Data derived from a single experimental screen, n=2.
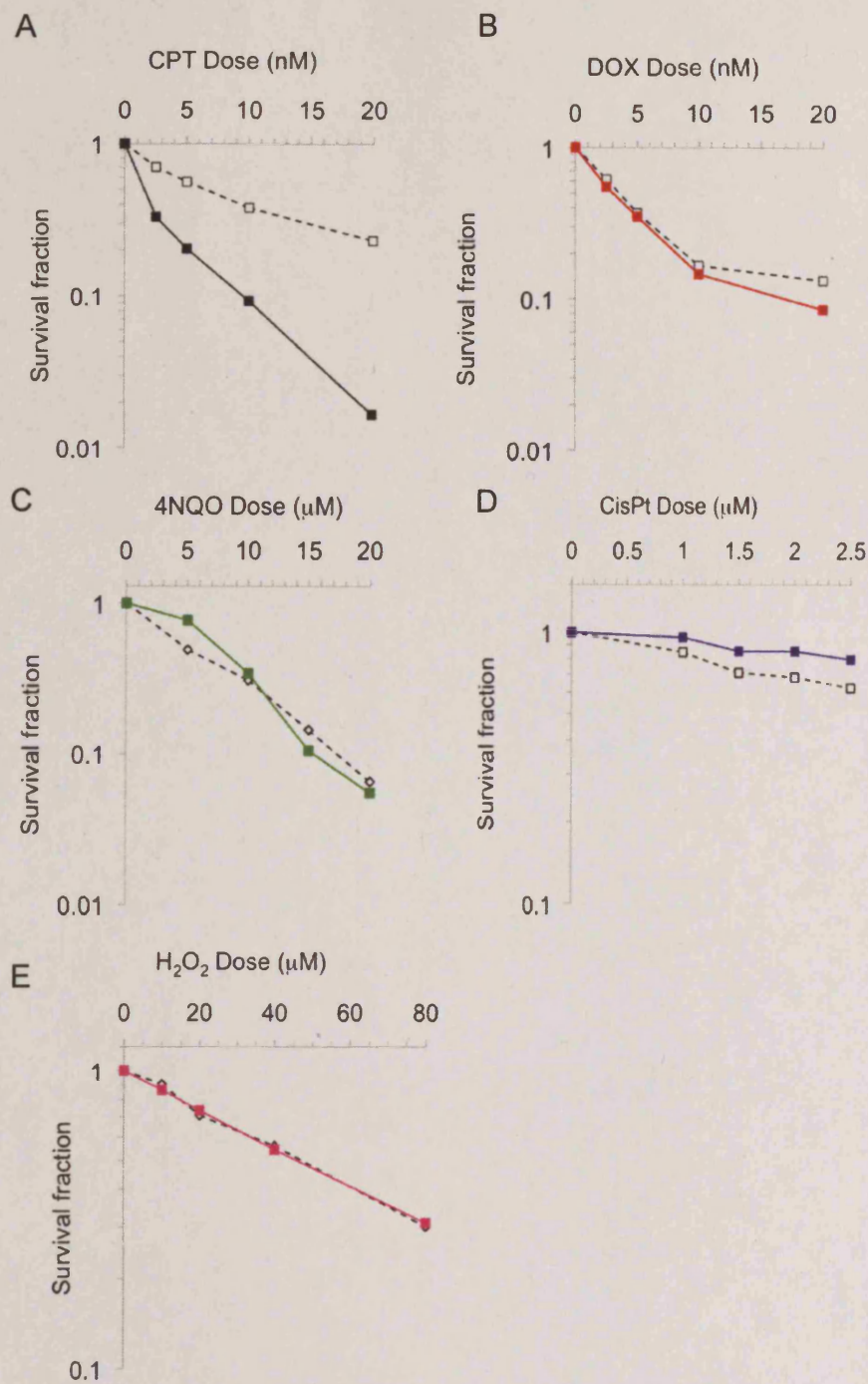
Figure 6.8. Analysis of clonogenic survival of AG03141(WS)[hTert] fibroblasts following exposure to DNA damaging agents.

Panels A-E show responses to CPT, DOX, 4NQO, CisPt and H_2O_2 for WS (solid lines) compared to AG16409[hTert] (N) (dotted line). Survival was determined by counting colonies >50 cells. Data derived from a single experimental screen, n=2.

Syndrome	Drug																		
	CPT (nM)				DOX (nM)				4NQO (µM)				CisPt (µM)				H$_2$O$_2$ (µM)			
	2.5	5	10	20	2.5	5	10	20	5	10	15	20	1	1.5	2	2.5	10	20	40	80
CSA																				
BS																				
NBS																				
LIG4																				
RTS																				
HGPS																				
WS																				
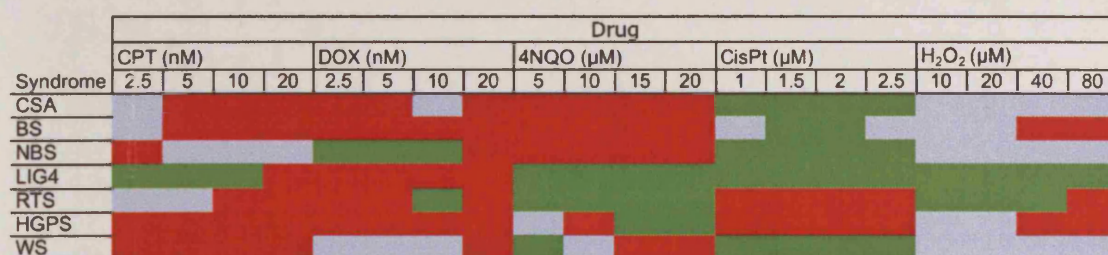
Figure 6.9. Heatmap summarising the responses of GI panel to genotoxic agents.

Red indicates that cells show hypersensitivity compared to normal, green indicates cells show relative resistance and blue indicates that cells show an equivalent response. Results are based on a comparison of the IC$_{50}$ for all drugs with the exception of CisPt in which IC$_{20}$ values were compared.
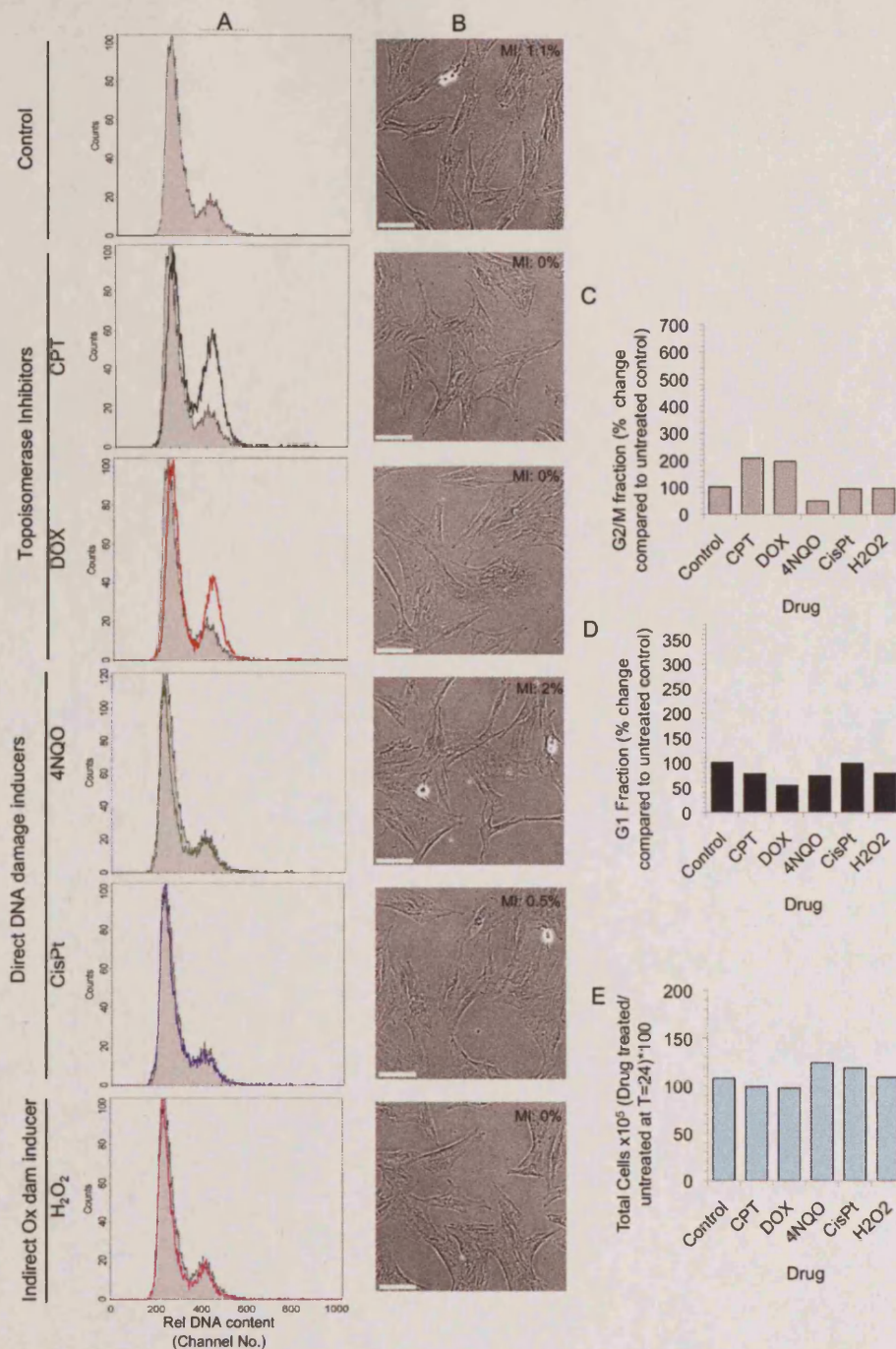
Figure 6.10. Analysis of the impact of DNA damaging agents (24 h exposure) on cell cycle progression, cell morphology and proliferation for AG16409(N)^{hTert} fibroblasts.

Panels A show changes in relative DNA content distributions, compared with an untreated control (grey shaded), following exposure to CPT (10 nM x 24h, black line); DOX (10 nM x 24 h, red line), 4NQO (15 µM x 24 h, green line), CisPt (2.5 µM x 24 h, blue line) and H_2O_2 (80 µM x 24 h, pink line). Panels B show the corresponding appearance of cultures at 24 h (bar = 100 µm) by phase contrast microscopy. Panel C and D show relative changes in G_2/M and G_1 for each drug treatment, respectively. Panel E shows the total cell number in the presence or absence of each drug treatment. 10,000 events were analysed and data was gated to remove cell debris. Mitotic index (MI) is calculated based on the number of mitosis events observed in three fields.

196
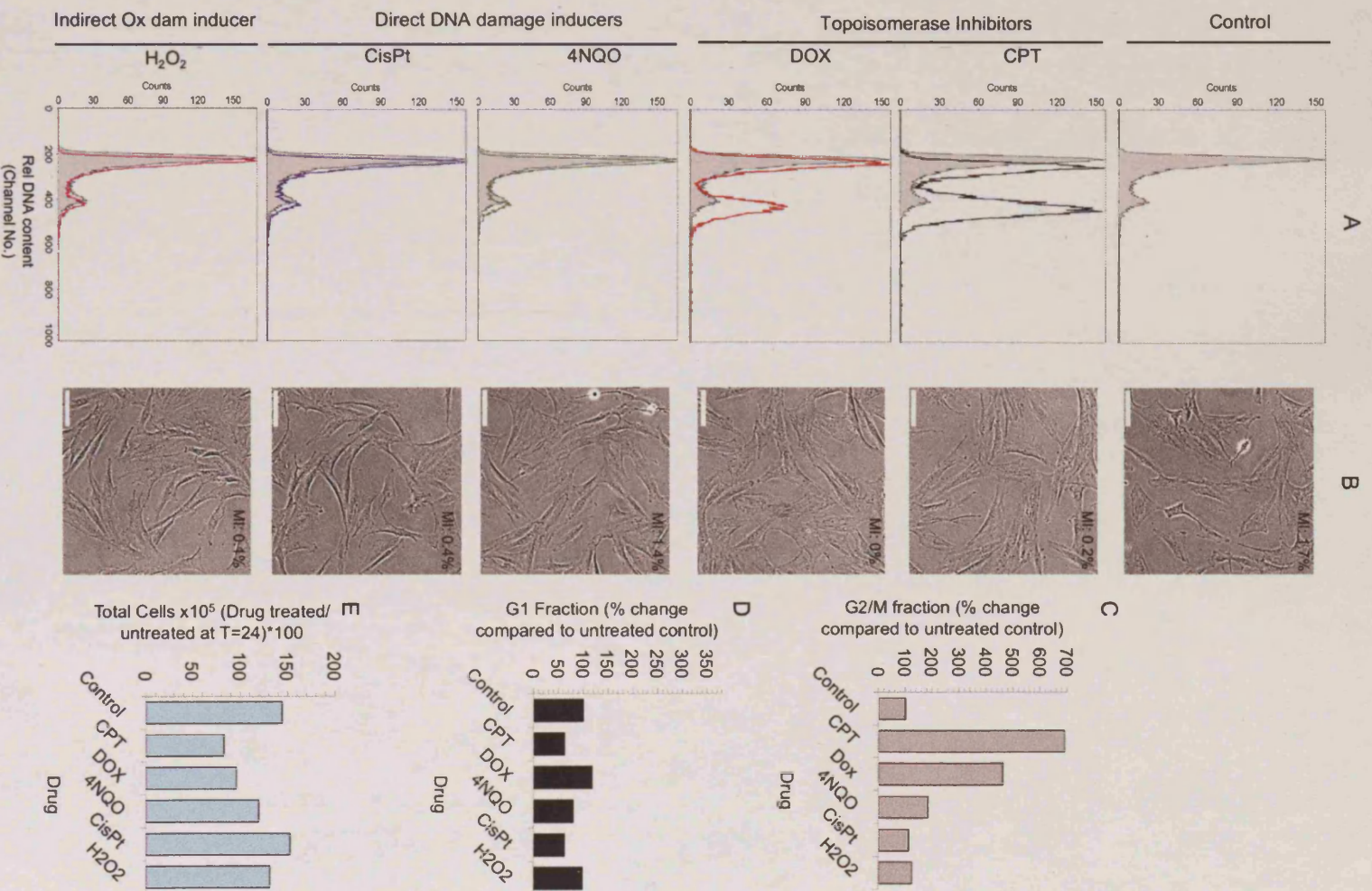
Figure 6.11. Analysis of the impact of DNA damaging agents (24 h exposure) on cell cycle progression, cell morphology and proliferation for GM02548(BS)^hTert fibroblasts.

Panel details given in legend to Figure 6.10.

197
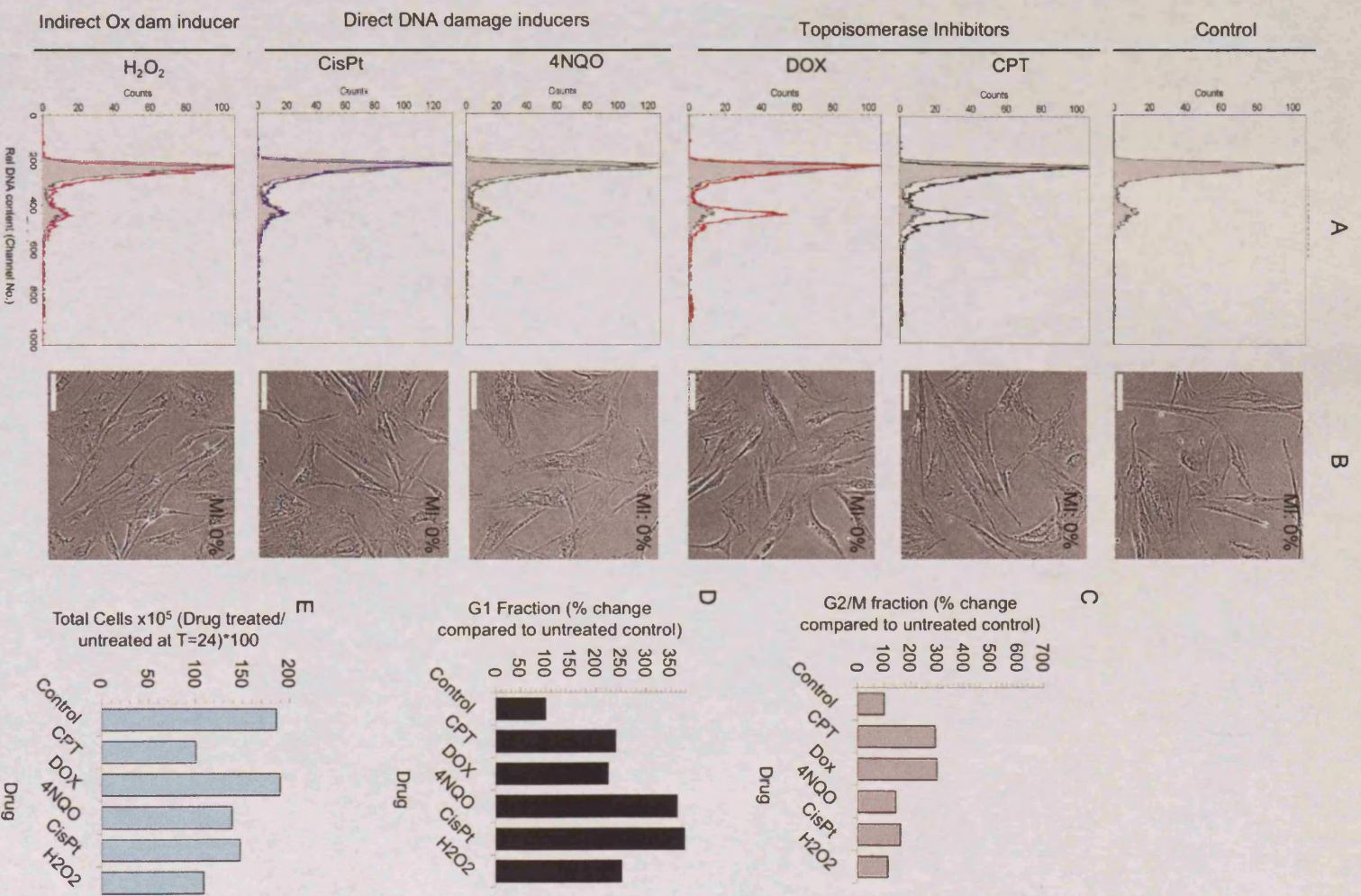
Figure 6.12. Analysis of the impact of DNA damaging agents (24 h exposure) on cell cycle progression, cell morphology and proliferation for AG11498(HGPS)[hTert] fibroblasts.

Panel details given in legend to Figure 6.10
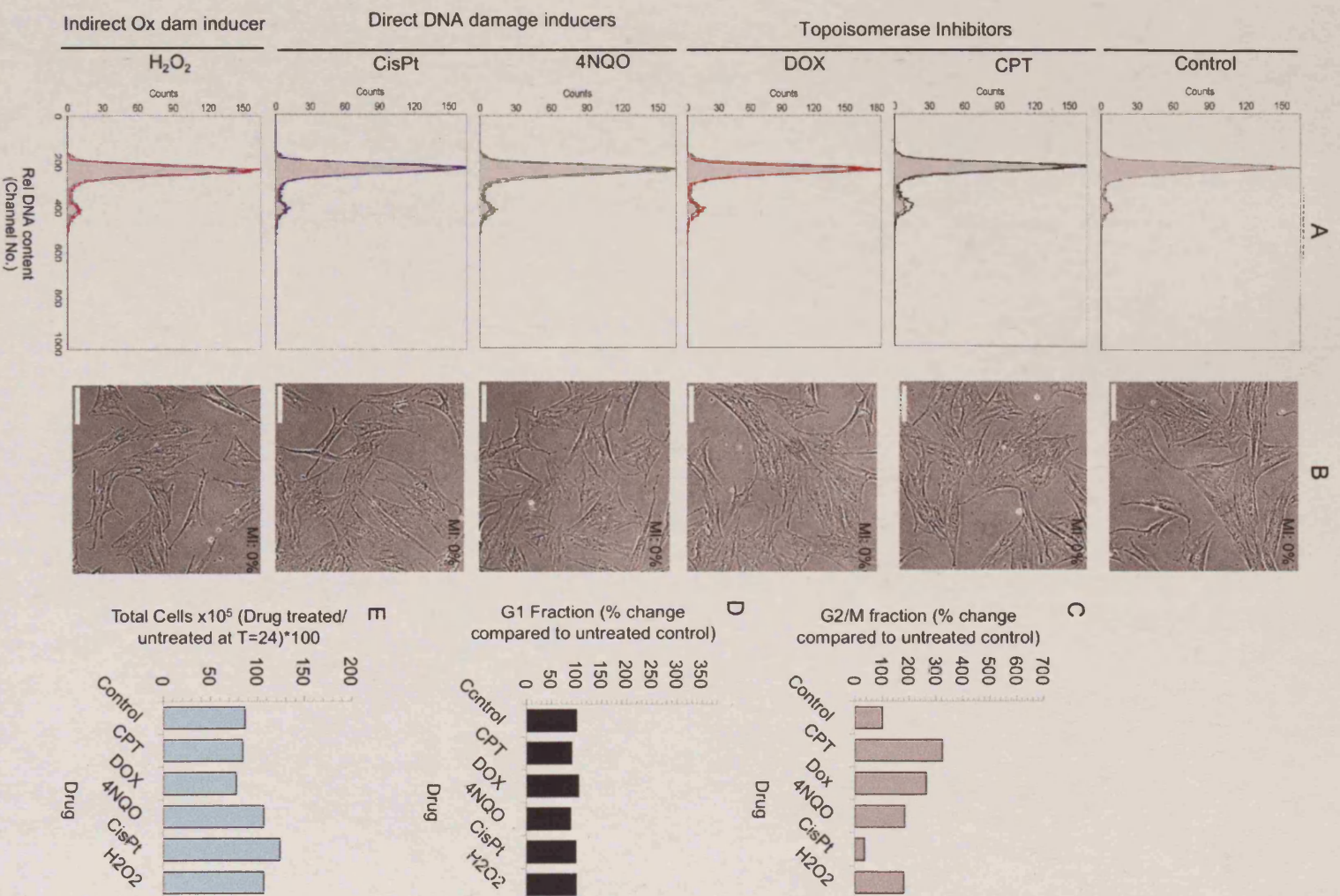
Figure 6.13. Analysis of the impact of DNA damaging agents (24 h exposure) on cell cycle progression, cell morphology and proliferation for GM17523(LIG4)^{hTert} fibroblasts.

Panel details given in legend to Figure 6.10

199
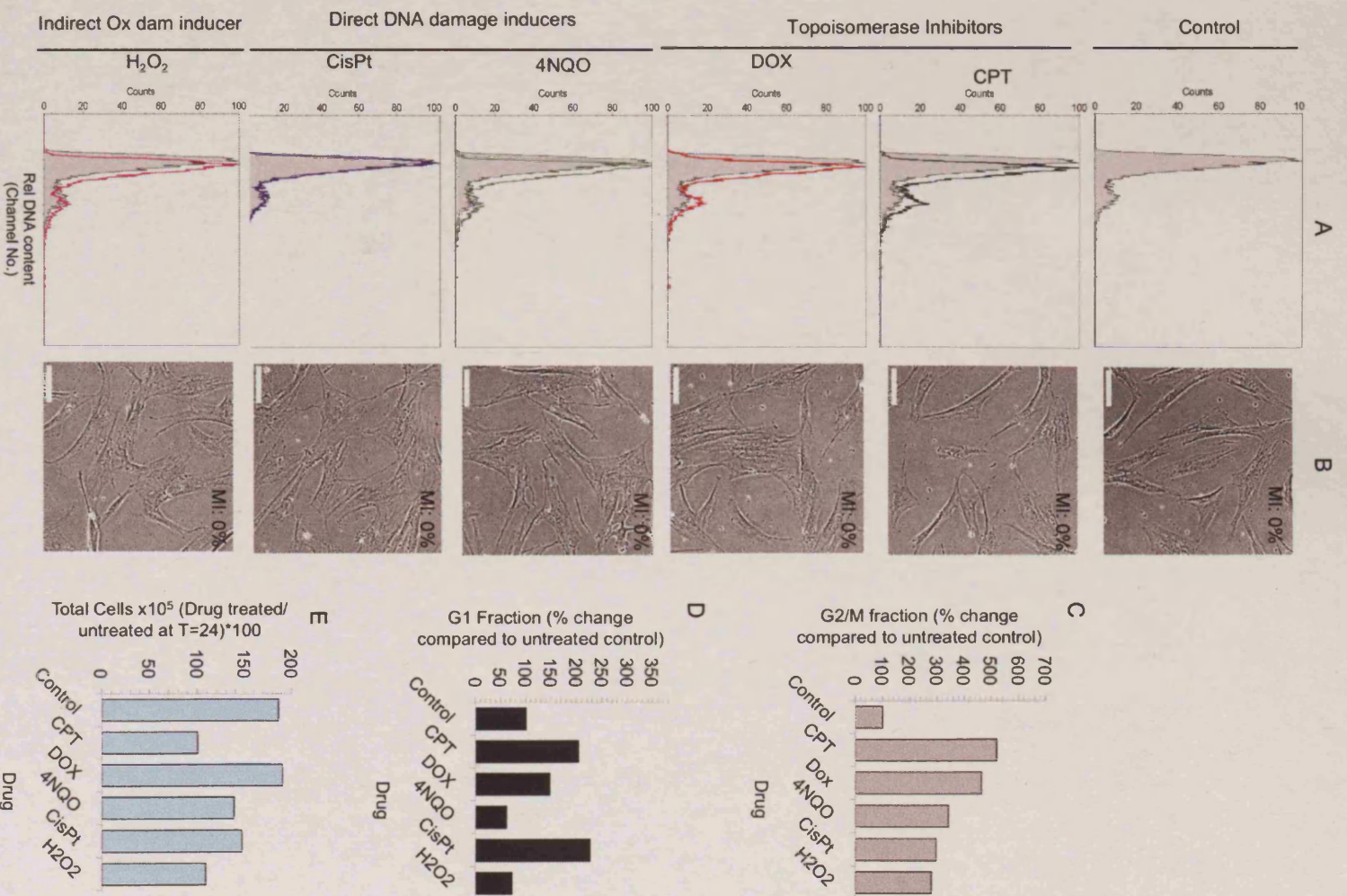
Figure 6.14. Analysis of the impact of DNA damaging agents (24 h exposure) on cell cycle progression, cell morphology and proliferation for AG18371(RTS)^{hTert} fibroblasts. Panel details given in legend to Figure 6.10

200
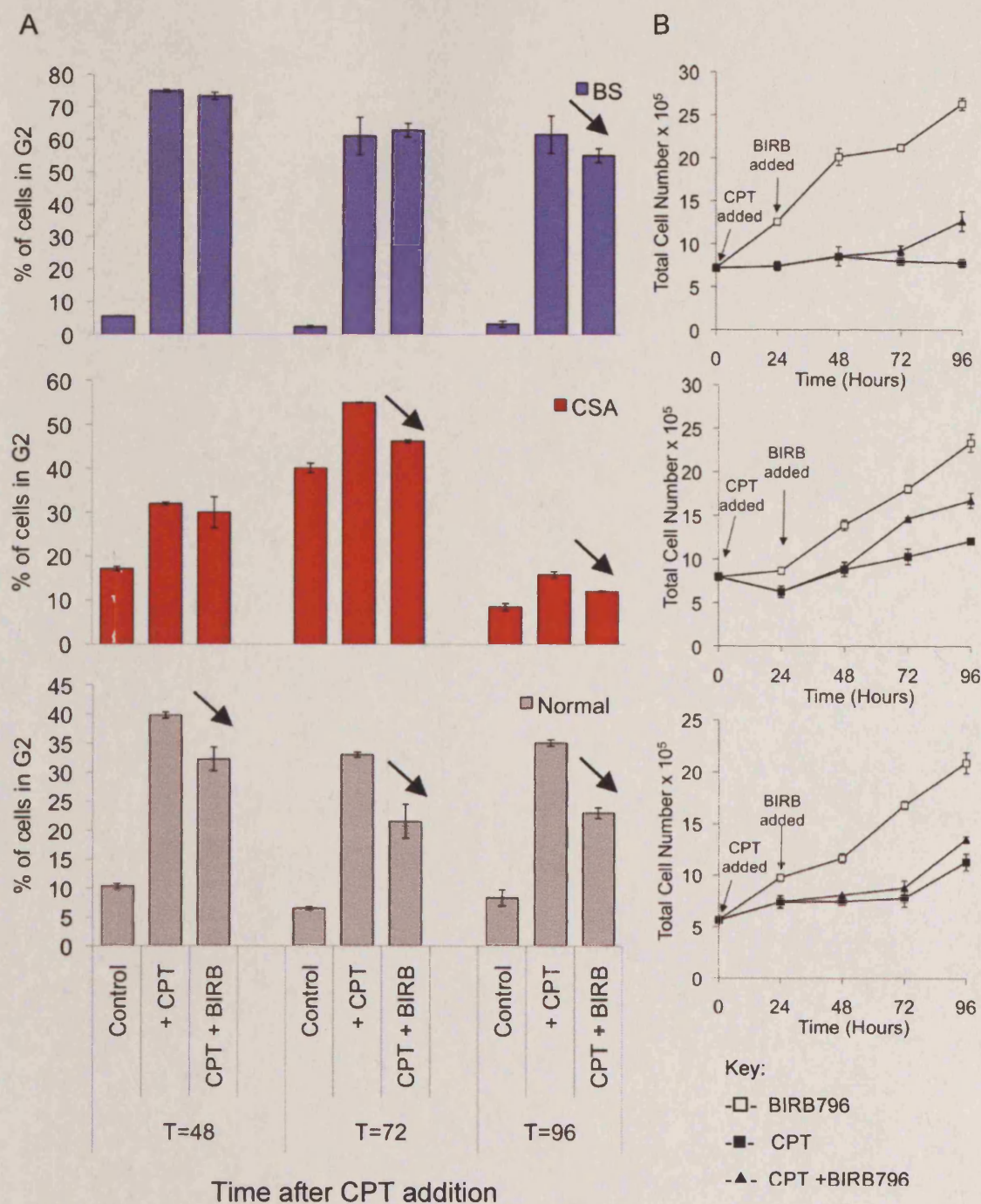
Figure 6.15. Impact of BIRB796 on recovery of cells following CPT pre-treatment.

AG16409(N)[hTert], GM02548(BS)[hTert] and GM01856(CSA)[hTert] cells were seeded (5×10^5) and allowed to attach for 24 hours prior to treatment. Cells were treated with CPT (10 nM; T=0) for 24 hours (T=24), washed and incubated in media with or without BIRB796 for a further 72 hours. The cell cycle distributions of cells were analysed at T=48, T=72 and T=96 hours. Panel A shows flow cytometric analysis of the proportion of cells in G_2/M and panel B shows the increase in cell number over the course of the experiment. The data represents the mean of 2 samples analysed in parallel and error bars represent the range of these values.
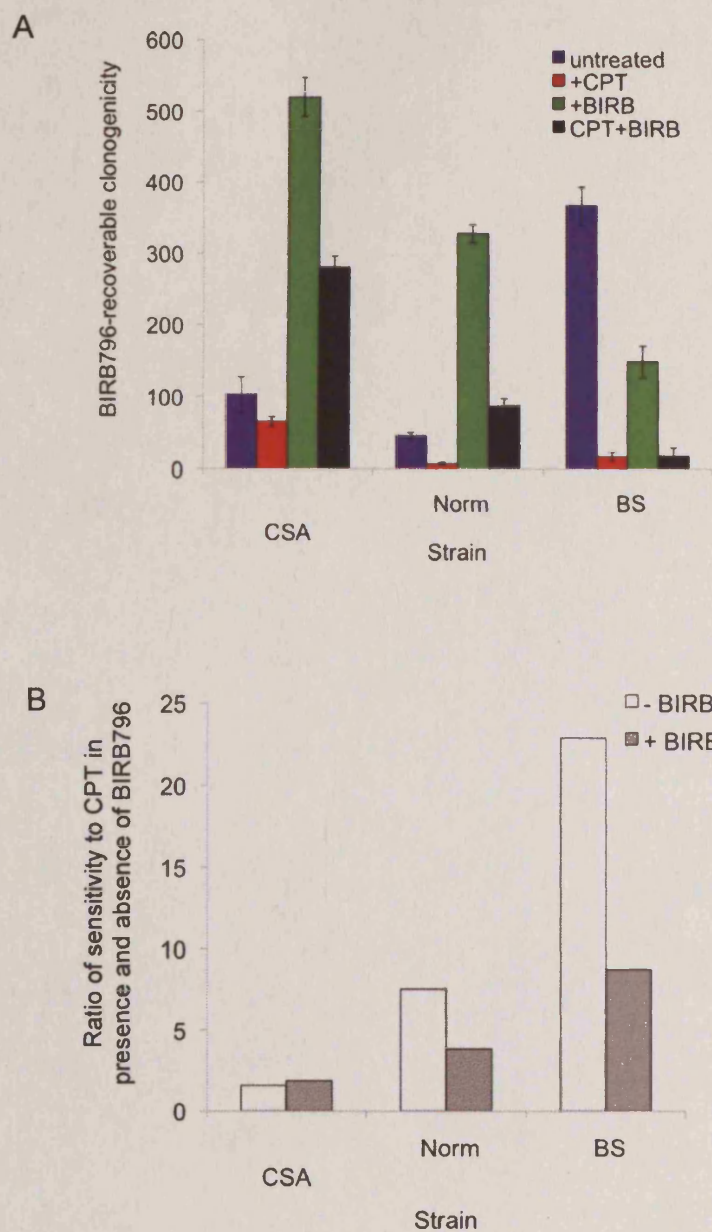
Figure 6.16. Impact of BIRB796 on the clonogenic potential of CPT pre-treated normal, CSA and BS cells

AG16409(N)[hTert], GM02548(BS)[hTert] and GM01856(CSA)[hTert] cells were pre-treated with CPT (10 nM) for 24 hours and washed prior to incubation in the presence or absence of BIRB796 for 10 days. Clonogenicity was measured by the number of colonies ≥50 cells. Panel A shows the shows the absolute number of colonies generated in untreated, CPT-treated, BIRB796-treated and CPT+BIRB796-treated cells. Panel B shows the sensitivity of the three strains to CPT, given as a ratio of the number of colonies in untreated:CPT-treated cells in the presence and absence of BIRB796. n= 4 ± SD.

Chapter 7 BIRB796 Inhibitor Effects: Cell Cycle Dynamics and Clonogenic Potential of hTert Immortalised fibroblasts

7.1 Introduction

The generation of the hTert panel in Chapter 5 provides the opportunity to determine whether there are differences in the level of commitment to cell cycle exit in cells derived from individuals with defined genetically determined conditions associated with genomic instability. Furthermore, the finding in Chapter 6 that hTert-immortalised cells remain susceptible to cell cycle arrest in response to genotoxic agents suggests that this is a feasible approach. Clearly replicative potential is determined by cell cycle alterations and the working hypothesis is that differences in the limitation of replicative potential reflect the degrees of commitment to long-term exit from the cell cycle. It is proposed that constitutive levels of endogenous stress (e.g. arising from the appearance and incomplete resolution of genomic damage) can affect the probability of transition between out of cycle and subsequent re-entry. It is plausible that GI syndrome cells will show subtle differences in cell cycle dynamics as a result of endogenous stress.

Support for this hypothesis comes from the finding that WS cells show cell cycle alterations that may be associated with their slow growth and reduced replicative lifespan (Poot et al. 1992). Specifically, WS lymphoid cell lines displayed a 2.4 hour prolongation in the minimum duration of the S-phase. Moreover, the fraction of proliferating cells irreversibly arrested in S-phase was shown to be significantly elevated in WS (5.4 % versus 1.4 % in normal controls), although other cell cycle compartments were not significantly affected (Poot et al. 1992). Some evidence also exists to suggest that BS cells have altered cell cycle progression; however, these data are limited and variations in cell types used are common (Bamezai and Shiraishi 1986).

In recent years, the p38 MAPK pathway has been shown to be involved in the induction of both the G_1/S and G_2/M checkpoints [reviewed by (Ambrosino and Nebreda 2001; Thornton and Rincon 2009; Wilkinson and Millar 2000)], although its role in the G_2/M checkpoint is better established. p38 is activated in response to DNA DSBs, induced by exposure to UV, γ-irradiation and chemotherapeutic drugs such as etoposide, leading to the establishment of a G_2/M cell cycle checkpoint (Bulavin et al. 2002; Mikhailov et al. 2004) (Figure 1.4A). Although the mechanism of activation of p38 in response to DNA DSBs is not completely clear, it has been reported to be dependent on the activation of ATM and ATR that serve as DNA damage sensors (Reinhardt et al. 2007). While the activation of ATM is required for activation of p38, it does not appear to be able to directly phosphorylate p38. Instead, activation of p38 appears to be mediated by the Thousand and one (Tao) kinases, which activate p38 via MKK3/6 (Raman et al. 2007). The observation that activation of p38 can occur in the presence of the ATM inhibitor caffeine and in ATM knockout cell lines in response to topoisomerase II inhibitors an UV (Mikhailov et al. 2004; Reinhardt et al. 2007), suggest that there are other not yet established mechanisms that activate p38 in response to DNA damage.

Two main pathways have been described for the involvement of p38 in the induction of the G_2/M checkpoint (Figure 1.4A). The first involves phosphorylation and activation of p53 by p38 and subsequent induction of a p53-dependent G_2/M checkpoint (Bulavin et al. 1999; She et al. 2000; Thornton and Rincon 2009). The activation and stabilisation of p53 by p38 leads to the transcription of p53-target genes such as Growth arrest and DNA damage inducible 45α (GADD45α), p21[CDKN1] and 14-3-3 (el-Deiry et al. 1993; Hermeking et al. 1997; Zhan et al. 1999). p38 also associates with GADD45α proteins and promotes their association with p53, further increasing p53 stability (Bulavin et al. 2003). These proteins enforce a G_2/M checkpoint by either directly or indirectly inactivating the cdk1/cyclinB complex, which is the major engine driving the transition from G_2 to M-phase (Taylor and Stark 2001). The second mechanism by which p38 induces a G_2/M checkpoint is through the phosphorylation and inhibition of the phosphatase Cdc25B (Bulavin et al. 2001). Cdc25B dephosphorylates cdk1 and activates the

cyclin/cdk1 complex driving progression of the cell cycle. It has been proposed that phosphorylation of Cdc25B inhibits its activity by promoting its association with 14-3-3 proteins and sequestering it in the cytoplasm (Lopez-Girona et al. 1999; Morris et al. 2000). While it was initially reported that p38 could directly phosphorylate Cdc25B *in vitro*, more recent studies have shown that p38 promotes the phosphorylation of Cdc25B indirectly through activation of MK2 (Lemaire et al. 2006; Manke et al. 2005). More recently, however, the role of p38 in G_2 delay has been challenged. Contrary to prior reports, a new study suggests that although p38 activation is strongly induced by DNA damage, its activity is not required to induce a G_2/M checkpoint in human cancer cells (Phong et al. 2010).

p38 activation can also contribute to the induction of a G_1/S checkpoint in response to osmotic stress, ROS and DNA damage (Figure 1.4B) [reviewed by (Ambrosino and Nebreda 2001; Thornton and Rincon 2009; Wilkinson and Millar 2000)]. Similar to G_2/M checkpoint regulation, several mechanisms by which p38 mediates a G_1/S checkpoint have been described. Firstly, p38 can induce a G_1/S checkpoint through the activation of p53 resulting in the accumulation of p21 (Kim et al. 2002; Kishi et al. 2001). p21 is thought to induce a G_1/S checkpoint by inactivating Cdk2 (Brugarolas et al. 1999; Poon et al. 1996). Recent evidence also suggests that p21 can inhibit Cdk1 in the absence of Cdk2 to establish a G_1/S checkpoint in response to DNA damage (Satyanarayana et al. 2008). Secondly, p38 can induce a G_1/S checkpoint by reducing the levels of cyclin D1, which is known to form complexes with Cdk4/6 and is essential for the transition to S-phase. p38 has been shown to reduce the levels of cyclin D1 by two independent mechanisms: either at a transcriptional level by phosphorylation and stabilisation of HMG-box protein 1 (HBP1), which subsequently inhibits cyclin D1 gene expression (Yee et al. 2004); or by directly phosphorylating cyclin D1 and targeting it for ubiquitination and proteosomal degradation (Casanovas et al. 2000). Thirdly, p38 can phosphorylate and promote degradation of Cdc25A and thus contribute to establishment of a G_1/S checkpoint (Goloudina et al. 2003). Fourthly, p38 can mediate a G_1/S checkpoint by upregulating expression of p16[INK4A], which inhibits Cdk4/6 activation (Roussel 1999), and p19[ARF], which regulates p53 (Tao and

Levine 1999). Overall, p38 can play a significant a role in cell cycle arrest. It is highly plausible, therefore, that cells that show chronic activation of p38, such as WS cells, will show abnormal cell cycle dynamics.

Conceptually one model for progression to 'senescence' is that a cell in a given population has a small but finite probability of exiting the cell cycle following each division. Once a cell is arrested there are two possibilities, either that cell can re-enter the cell cycle or it can remain in an arrested state. The model in figure 1.6 suggests that the probability of re-entry decreases with time spent out of cycle. It is possible that during a period of cell cycle exit a cell acquires further features that act to reduce the probability of re-entry and the cell therefore appears to be irreversibly arrested. Therefore the replicative potential of a cell or a population is dependent on the rate of exit from the cell cycle and the probability of re-entry. Given the potential role of p38 in cell cycle regulation and the observed effect of p38 inhibitors on relieving growth limitation (chapters 3 and 6), this simple model proposes that the probability of re-entering the cell cycle is limited by increased p38 expression.

Previously, it has been proposed that increased replicative stress in WS cells leads to increased numbers of senescent cells at each division compared to normal cells (Faragher et al. 1993; Kill et al. 1994). The model shown in Figure 1.6 can be used to suggest how a slightly increased exit rate could contribute to the reduced replicative potential of WS cells. An issue for compromised WS cell populations could be that elevated telomere erosion rates may reflect the capacity of cells with replicative potential effectively dividing more frequently to attain an overall population doubling – i.e. a single PD requires the dividing cells to divide more than once. As shown in this model, the long-term effect of this increased exit from cell cycle provides a plausible mechanism for the reduced proliferative capacity of WS cells in culture.

Here it is proposed that the replicative potential of cells is determined by cell cycle dynamics, including the transition between in and out of cycle and that this can be affected by changes in endogenous levels of stress. The primary aim of this

chapter is to examine the cell cycle dynamics of a panel of cells that show different levels of putative endogenous 'replication stress'. The approach was to determine whether altered cell cycle dynamics could be distinguished in populations of GI panel cells over relatively short time periods representing 1-3 cell cycle traverse events. Studies include examination of the transition between in and out of cycle and the effects of p38 inhibitor exposure. There is the possibility that differences in the rate of exit from cell cycle in the GI panel will not be seen in a short-term analysis, therefore, the longer-term replicative potential of GI syndrome cells will be assessed by colony forming assays.

7.2 Results

7.2.1 Impact of BIRB796 on cell cycle dynamics and on exit/re-entry

The previous studies suggest that the greatest opportunity to identify p38 impact over a limited number of cell cycle transits would require the most potent inhibitor, namely BIRB796. Preliminary experiments were also undertaken to determine suitable timing of the experiment and to address issues such as optimal cell density to ensure that cells had the opportunity to undergo cell divisions and providing sufficient sample size for event detection. Cell quality of the informative populations analysed by flow cytometry were defined using conventional light scatter characteristics that differentiate between intact cells and cell debris. A significant range of side scatter signal was observed for G_1 cells suggesting that differences in nuclear structure (and extent of dye intercalation) could reflect the presence of quiescent cells.

To assess the ability of BIRB796 to change cell cycle distribution, for example reduction in cells in G_1, flow cytometric analysis was performed on hTert-immortalised fibroblasts grown continuously in the presence or absence of BIRB796 for a period of 72 hours. There was evidence of culture-mediated cell density issues at 72 hours; therefore data from the 24 hour time-point was used. The proportion of cells that were in cycle as designated as $G_2/M+S$ versus the proportion of cells that were out of cycle in G_0 or traversing G_1 are shown in Figure

7.1B. The majority of strains show a similar cell cycle distribution with >60% of cells being in G_1/G_0. RTS cells appear to show a reduction in the proportion of cells in cycle (18%) compared to the other strains, suggesting that RTS cells may contain a higher proportion of quiescent cells. The observation that a 24 hour BIRB796 treatment consistently reduces the percentage of cells in G_1 across the board suggests that BIRB796 can promote cells to re-enter the cell cycle within one cell cycle transit. The reduction in the G_1 fraction was on average in the order of <5% of the entire population in all cell strains.

Cell cycle analyses depend upon a correlation between fluorescence intensity (as determined by the area of the nominated fluorescence pulse signal; e.g. FL2-A) and cellular DNA content. DNA content distributions using the ethidium bromide (Eb) technique can be compromised by variations in the size and form of nuclei presented to the laser during the FACS analysis. One approach to analysing such variation is to determine the time of flight (TOF; e.g. FL2-W) of the object during its passage through the laser beam. Accordingly, an increase in TOF not matched by an increase in total fluorescence, as given by the integration of the height (FL2-H) and width (FL2-W) measurements of the pulses providing an area measurement (FL2-A), would indicate non-spherical nuclear structure. This analytical approach revealed an increased frequency (at ~5%) of cells with extended TOF values in both G_1 and G_2 compartments in RTS and WS compared to normal cells, suggesting a burden of quiescent or arrested cells (Figure 7.2). The possibility that this extended TOF was due to cell doublets (with abnormally long TOF values) was excluded by our analysis.

7.2.2 Impact of BIRB796 on clonogenic potential

To assess the medium-term impact of increased SIPS on replicative capacity and the role of p38 in this, the clonogenic potential of the GI panel was assessed using a standard colony forming assay. Colonies arising from single cells were counted and plating efficiency (PE) was initially calculated for each as described in section 2.5. However, using this approach the PE of all strains was low (<10%), particularly for RTS in which no colonies containing >50 cells were

colonies containing >50 cells were observed. It was therefore considered that calculation of PE using a threshold of >50 cells/colony following a fixed incubation period was problematic for the slower growing strains. Therefore a new definition that divides the population into cells that have minimal clonogenic potential (MCP), full clonogenic potential (FCP) or are non-clonogenic (NC) was proposed. The functional definition of a cell with MCP is one that must have divided at least twice during the time of the experiment and thus gives rise to a colony of ≥ 4 (but <50) cells. A cell with FCP is designated as one that gives rise to a colony of ≥ 50 cells. The NC fraction are seen as single cells or those that give rise to colonies of <4 cells and are estimated from the proportion of MCP and FCP cells in the population (data not shown). Given this new functional definition, the PE for each strain based on colonies containing ≥ 4 cells was shown to be between ~4-20% for these cells (Figure 7.3B). The differences in PE observed between GI panel members may reflect differences in the level of commitment to senescence in these cells over the clonogenic period.

To assess the impact of BIRB796 on the clonogenic potential, cells were grown continuously in the presence or absence of BIRB796 and the PE for each strain was calculated. These data show that continuous treatment with BIRB796 consistently increases the PE of all strains, with the possible exception of BS cells, suggesting there is a commonality of response to p38 inhibition in these cells (Figure 7.3B). Furthermore, these data suggest that BIRB796 stimulates cells that were previously non-clonogenic to divide so that they are now counted as having MCP and are included in the calculation of PE. There are two possible explanations for this. Firstly, BIRB796 may act on the division competent cells and cause them to divide more often thus resulting in an increase in colony sizes that is perceived as an increase in the proportion of cells with MCP and/or FCP. Secondly, BIRB796 may act on the subset of cells within a candidate colony that would normally have exited the cell cycle and cause them to remain in cycle so that they contribute to colony growth again resulting in an increase in the proportion of cells with FCP and/or causing cells that were previously non-clonogenic to re-enter resulting in an increase in the MCP fraction.

Analysis of the clonogenic fraction was undertaken to identify the target population for BIRB796 action. To address this, the question of whether BIRB796 changes the relative proportions of MCP or FCP cells in each strain was asked. In all cell strains, the percentage of cells showing FCP was increased following BIRB796 treatment, suggesting that BIRB796 increases the clonogenic potential of those cells that previously showed MCP so that they now report as having FCP. In WS, RTS, HGPS, NBS and LIG4 the percentage of cells showing MCP also increases (Figure 7.3A), suggesting that BIRB796 stimulates cells that were previously non-clonogenic to re-enter cycle so that they now report as having MCP. The observation that in these cell strains the increase in the proportion of cells that show FCP is relatively small suggests that there is a subpopulation of cells that are non-responsive to BIRB796 over the time course of the experiment. In normal, CSA and BS cells, the proportion of cells showing FCP is increased, again suggesting that BIRB796 increases the clonogenic potential of cells that previously showed MCP so that they now show FCP. However, the proportion of cells showing MCP is decreased following treatment with BIRB796 in these strains. Given the assumption that any cell that previously showed FCP would also show FCP in the BIRB treated sample, there are two possible explanations for this: firstly, that BIRB796 stimulates cells that previously showed MCP so that they all now report as having FCP; or secondly BIRB796 also stimulates cells that were previously non-clonogenic so that they both now report as having FCP.

To further assess the target population for BIRB796 action, a full distribution of colony sizes in a chosen syndrome, namely WS, in the presence and absence of BIRB796 was undertaken. These data revealed that the distribution of WS proliferative potential was weighted towards the generation of small colonies, with the majority of cells being designated as NC, ~40% showing MCP and relatively few cells (<10%) showing FCP (Figure 7.4). The data clearly show BIRB796 not only increases the total number of colonies (i.e. PE), it also results in a shift in colony size towards larger colonies, perceived as a greater proportion of cells showing FCP and fewer cells showing MCP (Figure 7.4; right panel). This suggests that the main action of BIRB796 is to increase the likelihood of a cell reporting as

'clonogenic' when defined at a specific colony size (e.g. FCP). These data also show that BIRB796 did not increase the maximum colony size observed (130 cells), suggesting that there is a limit on the maximal population doubling rate observed in WS populations and that this is not affected by exposure to BIRB796.

7.3 Discussion

The proportion of cells in cycle was <40% for all cells, suggesting that the majority of cells are either in transit in G_1 or are quiescent in dermal fibroblasts. Inter-syndrome differences were observed, for example RTS cells have a higher proportion of cells in G_1 (>80%) compared to all other strains (>60%), suggesting that RTS cells have a fundamentally compromised ability to progress through the cell cycle.

The overall observation that BIRB796 consistently reduces the proportion of cells in G_1, suggests that BIRB796 can trigger cells to re-enter the cell cycle within one cell cycle transit. Furthermore, it suggests that that there is a common mechanism of restraint and cells may differ from each other on the basis of the proportion of cells available for such modulation. The studies do not, however, address whether there are intrinsic differences in p38 inhibitor sensitive pathways operating in the different GI syndrome strains. The finding that the reduction in the G_1 fraction was in the order of <5% of the entire population in all cell strains suggests that whole population analyses do not have the resolution to assess the early effect of BIRB796 on cell cycle dynamics and therefore small differences in BIRB796 effect between syndromes may not have been observed using this approach.

The observation that there are differences in PE between GI panel members suggests that there may be differences in the level of commitment to cell cycle exit in these cells that subsequently impacts on their clonogenic potential. For example, compared to normal cells, RTS, NBS, LIG4, WS and HGPS syndromes had a lower PE suggesting that these cells show a greater proportion of cells in which restraint operates. Given the functional definition of NC, MCP and FCP, it was

shown that the majority of cells (<80%) in all cell strains were NC. The simplest explanation for this is that the conditions for clonogenic analysis require cells to be seeded sparsely which is known to reduce the growth potential of these cells. However, these findings are consistent with the observation that the majority of cells were seen to be in G_1 when analysed by flow cytometry.

The observation here that BIRB796 increases the PE of all cells is consistent with the findings from the flow cytometric analysis that BIRB796 reduces the percentage of cells in G_1. These findings suggest that there is a common mechanism that limits retention in or re-entry into cycle in all cells that it is dependent, at least in part, on p38. Furthermore the findings suggest that the target population for BIRB796 action include cells that are both non-clonogenic and those that show MCP. However, there appear to be subpopulations of cells within each cell strain that are non-responsive to BIRB796 and the proportion of these subpopulations appear to differ between syndromes. The differences in the effect of BIRB796 on different cell strains suggest that there are inter-strain differences in the target population for BIRB796 action and in the presence of non-responsive subpopulations; however, it is also possible that these differences are due to differences in growth rate of cells between strains.

Further analysis of WS revealed that the main action of BIRB796 is to increase the likelihood of a cell reporting as 'clonogenic' when defined at a specific colony size (e.g. FCP). The observation that BIRB796 did not increase the maximum colony size suggests that there is a limit on the maximal population doubling rate observed in WS populations and that this is not affected by exposure to BIRB796. The population doubling rate is a function of cell cycle transit time (e.g. inter-mitotic time or IMT) and the probability of cell division (asymmetry). Distinction between these factors would require single cell tracking analysis. Overall the data suggest that subfractions of WS populations should be capable of presenting a normal population doubling rate (at least over a period of 10 days) and that such subfractions might be refractory to BIRB796. These findings would

warrant further investigation using single cell tracking analysis to test this hypothesis.

To further assess the role of increased levels of SIPS on the clonogenic potential of cells it may be possible to use a known biomarker, such as SA-βgal, to identify the proportion of senescent cells within each colony in an attempt to identify whether there is a relationship between the level of SIPS and colony size. As a preliminary study, simple observation of the differences in cellular morphology of MCP and FCP colonies was undertaken, and appears to suggest that the majority of cells in MCP colonies are enlarged, which is suggestive of early senescence compromising the clonogenic lineage, whereas the majority of cells in the larger colonies are small and spindle-like (data not shown). These data suggest that a more in depth analysis of cell lineages could be informative.

A

BIRB796	-	+	-	+	-	+	-	+	-	+	-	+	-	+	-	+
□ %G2	19	22	23	22	19	26	23	24	25	25	14	16	16	20	16	18
▨ %S	14	13	12	14	11	13	9	8	13	15	4	6	11	14	9	11
■ %G1	67	65	66	64	71	61	69	67	61	60	82	78	72	66	75	71

(Groups: Normal, CSA, BS, NBS, LIG4, RTS, WS, HGPS)

B

Syndrome	BIRB796	% cells in cycle (G2+S)
Normal	-	33
	+	35
CSA	-	34
	+	36
BS	-	29
	+	39
NBS	-	31
	+	33
LIG4	-	39
	+	40
RTS	-	18
	+	22
WS	-	28
	+	34
HGPS	-	25
	+	29
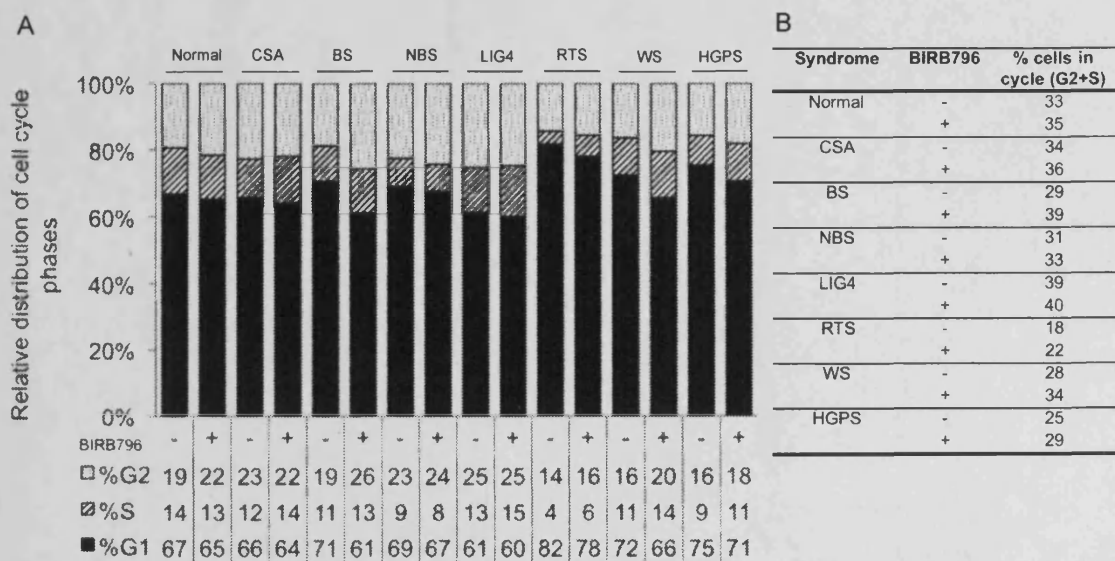
Figure 7.1. Impact of BIRB796 on cell cycle dynamics of hTert-immortalised GI syndrome cells.

Cells were grown continuously in the presence (+) or absence (-) of BIRB796 for 24 hours prior to analysis. (A) shows the full cell cycle analysis, (B) shows the proportion of cells in cycle (designated as G_2+S). Data obtained from a single experiment analysing >9000 gated events with a sampling error of <5%.
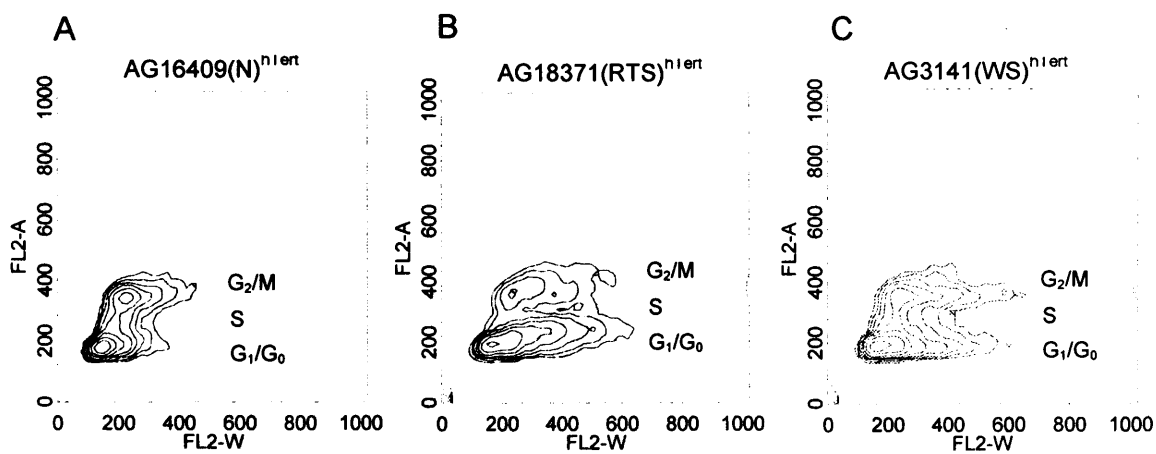
Figure 7.2. Time of flight (TOF) for normal, RTS and WS cells.

TOF (FL2-A) versus total cellular fluorescence associated with DNA (FL2-A) of A) AG16409(N)[hTert], B) AG18371(RTS)[hTert] and C) AG3141(WS)[hTert] cells. Cells were plated 24 hours prior to the experiment start time to allow time for attachment and grown for 24 hours prior to analysis.

A

Clonogenic Fractions (%)

20
15
10
5
0

BIRB: - + | - + | - + | - + | - + | - + | - + | - +

Normal | WS | RTS | HGPS | NBS | LIG4 | CSA | BS

	Normal		WS		RTS		HGPS		NBS		LIG4		CSA		BS	
☐ FCP	1.1	9.8	0.1	1.0	0.0	1.3	0.0	0.0	0.6	1.2	0.0	1.6	2.5	15.	9.1	13.
■ MCP	5.6	4.8	7.9	8.4	3.8	7.1	6.3	16.	11.	16.	13.	15.	6.8	0.1	10.	6.0

B

Syndrome	BIRB796	PE (%)
Normal	-	6.8
	+	14.7
WS	-	8.1
	+	9.5
RTS	-	3.8
	+	8.5
HGPS	-	6.3
	+	16.5
NBS	-	12.1
	+	17.5
LIG4	-	13.5
	+	16.7
CSA	-	9.4
	+	15.7
BS	-	19.9
	+	19.8
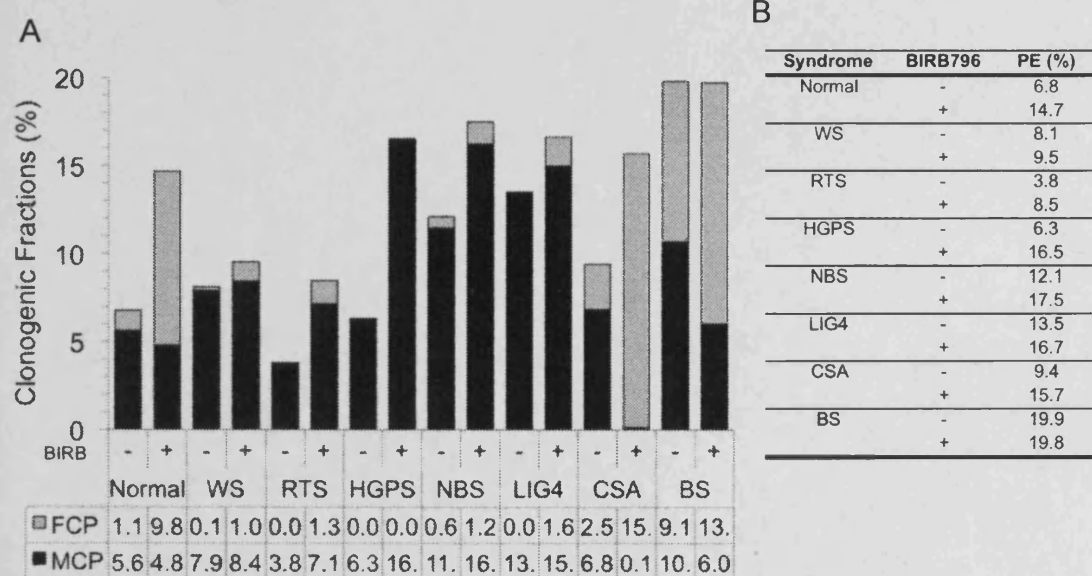
Figure 7.3. Impact of BIRB796 on the clonogenic potential of hTert-immortalised GI cells.

A) shows the proportion of cells showing MCP [$\geq$4(but $\leq$50 cells)] and FCP (>50 cells) in the presence (+) and absence (-) of BIRB796, calculated as a percentage of the total cells seeded (4000 cells). B) shows the plating efficiency (PE), given as the percentage of colonies containing $\geq$4 cells out of the total cells seeded. n=4 ±SD; single experiment.

A

B
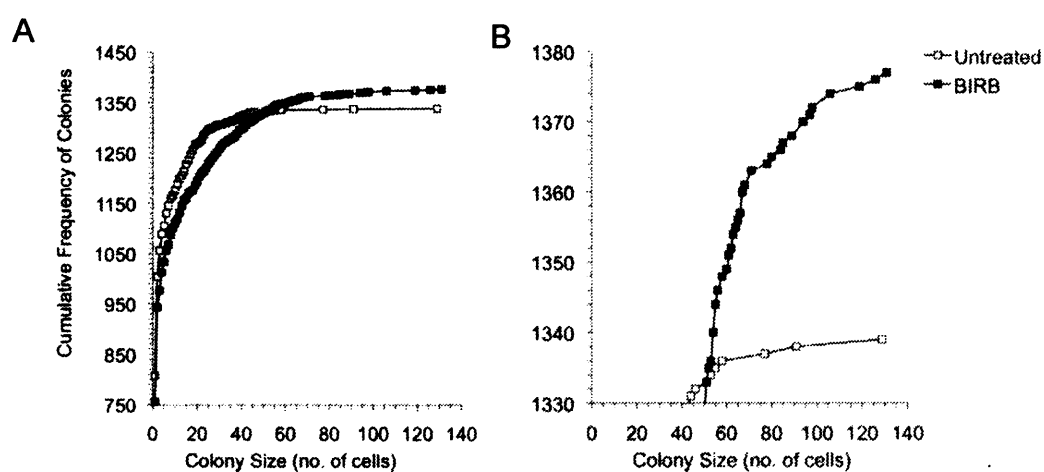
Figure 7.4. Impact of BIRB796 on colony size distribution for hTert-immortalised WS cells.

WS cells were grown continuously in the presence (closed squares) or absence (open squares) of BIRB796 as previously described for clonogenic assays. The number of cells in every colony in the dish was counted and the cumulative frequency of colonies of each size was plotted. Panel B shows the same data as panel A on an expanded axis showing that treatment with BIRB796 results in an excess of colonies of approximately >50 cells. Data represent an average for 4 dishes.

Chapter 8   *Single cell analysis*

8.1 Introduction

The thesis so far has revealed the problems for interpretation associated with studying heterogeneous cell cultures at a whole population level. The findings have shown that some GI syndrome cells have a reduced replicative potential compared to normal cells, however, these studies are complicated by inter-strain heterogeneity. Despite the known caveats of the previous studies, the findings support the hypothesis that a given population of cells in culture comprises cells with different replicative capacities and the relative proportions of these contribute to the replicative capacity of the population as a whole. Furthermore, the findings suggest that the reduced replicative potential observed for some of the GI syndromes is due to a reduction in the proportion of cells that have clonogenic potential (Chapter 7). BIRB796 has been shown to increase the clonogenic potential of all cell strains and appears to act by allowing cells to re-enter the cell cycle. However, the extent of the differences in the proportions of these subpopulations in GI syndrome cells compared to normal cells remains unclear. A solution addressed in this chapter is to study the GI syndrome populations at a cell-by-cell level to assess the differences in the proportion of subpopulations with different division capacities.

Time-lapse microscopy can be described as the repeated collection of a field of view from a microscope at discrete time intervals (Allen 1985). The duration of the time interval defines the temporal resolution, which in turn characterises the type of event detected. Dynamic *in vitro* cell-based assays derived from high-content time-lapse microscopy, where time is the quality parameter, allow interrogation of spatio-temporal cellular events in a population context to be analysed (Khan et al. 2007; Marquez et al. 2003). Time-lapse has been used extensively to study the division capacity of single cells within heterogeneous populations (Errington et al. 2010; Errington et al. 2005b; Forrester et al. 2000;

Marquez et al. 2003). Transmission phase time-lapse offers a relatively non-perturbing method that allows individual cells to be tracked and cellular events such as mitosis to be recorded. Furthermore, this approach provides information on cell morphology (essentially cell shape and cell size) and cell motility and changes in these basic features can be used to indicate cell behaviour interacting on a two-dimensional substrate. By tracking sequential events on a cell-by-cell basis, time-lapse microscopy provides high-content, multi-level descriptors of cell dynamics that can be mined through bioinformatics tools (Khan et al. 2007). Pragmatically, time-lapse also provides a means of independently tracking highly informative (often minority) subpopulations using only relatively small populations. Given the limited access to and reduced replicative potential of many of the GI syndrome cells, the application of such techniques was deemed to be critical to the further study of these cells. Therefore, a subsidiary aim was to assess the feasibility of application of this technique to the study of GI syndrome cells.

Here an extensive study of GI syndrome fibroblasts at the single cell level has been undertaken using time-lapse. The banked images provide a future resource for additional hypothesis testing, while the data gathered here were used to address the focus of the thesis. The study provides extensive information regarding the division capacity and motility of these cells. However, the data analysis in this chapter aims to answer three fundamental questions that have been brought into focus by previous findings in the thesis using selected cell strains. These are outlined below.

8.2 Materials and Methods

8.2.1 Time-lapse imaging

The objective of this study is to track mitosis events for every cell in the start field. Images were taken at 30-minute intervals to satisfy the Nyquist sampling criteria for ensuring that all of the mitotic events are captured in the analysis. Given the recent observation that cells tend to show a Gumbel distribution (used to model extreme values) of inter-mitotic times (IMTs) (Errington et al. 2010), with some outliers that have elongated cell cycle transit times, cells were imaged over a 72

hour period for hTert-immortalised cells, and 96 hours for primary cells to provide the best opportunity to track multiple mitotic events. Images were collected for four independent fields for hTert-immortalised cells and for six independent fields for primary cells. Time-lapse images were stacked and saved as *.stk or *.AVI format. MetaMorph software (Molecular Devices) was used to view the stacked image as a sequence of images that were then were analysed manually.

8.3 Aims

The aims address three fundamental questions (Figure 8.1).

1. Is there a difference in the probability of entering mitosis in RTS and WS cells compared to normal cells? Is this affected by BIRB796?

2. Is there a difference in the time taken to traverse the cell cycle (nominally the range of IMT values) in RTS and WS compared to normal cells? Is this affected by BIRB796?

3. What are the lineage characteristics of RTS and WS cells compared to normal cells? For example is there a difference in the proportion of cells that are capable of 2 or more divisions, reflecting how many cells show MCP. Is this affected by BIRB796?

The strategy here is to use time-lapse imaging to: 1, determine the proportion of dividing and non-dividing cells in RTS, WS and normal cell populations; 2, determine the IMT of dividing cells and 3, investigate the long-term division potential of single-cells using a lineage-based approach. This technique also
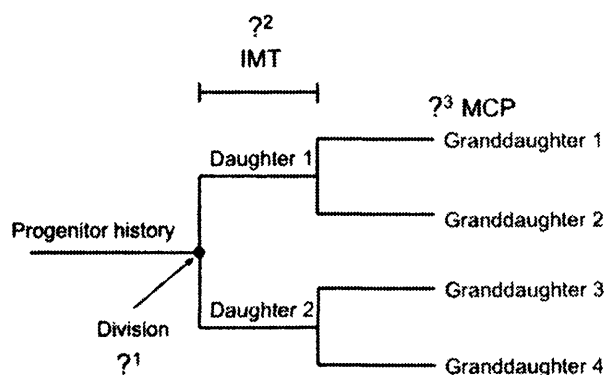
Figure 8.1. Schematic representation of a lineage arising from a progenitor cell and spanning two generations. Question marks indicate the three aspects that are studied in this chapter. Abbreviations: IMT=Inter-mitotic time; MCP=minimal clonogenic potential.

allows a more thorough characterisation of cellular morphology in these heterogeneous cultures and allows a correlative investigation of cell size and division capacity.

8.4 Results

8.4.1 WS and RTS fibroblasts show a higher probability of cell cycle exit compared to normal fibroblasts.

To investigate the potential differences in commitment to division in RTS, WS and normal cells, the proportion of dividing and non-dividing cells in both primary and hTert-immortalised cultures was assessed. AG18371(RTS) and AG03141(WS) were chosen as examples of cell strains that show consistent differences in morphology and growth potential compared to normal cells. This study also provides a unique opportunity to investigate the cellular responses to a *RECQL4* mutation, something that has not previously been studied. The approach was to use a standard plating regime resulting in a range of cell densities for the start field (160-597 cells) according to cell strain. Table 8.1 shows that primary AG18371(RTS) and AG03141(WS) cells contain a higher proportion of non-dividing cells compared to AG16409(N) cells. These data suggest that both AG18371(RTS) and AG03141(WS) cells have a higher propensity for senescence compared to normal cells; however, it is not clear whether this is due to replicative senescence (induced by telomere shortening) or due to SIPS. To investigate this, the proportion of dividing and non-dividing cells in hTert-immortalised cells was assessed. These data show that hTert-immortalised cells consistently show a lower proportion of non-dividing cells than their primary counterparts (Table 8.1), suggesting that some of the non-dividing cells in primary cultures from all three strains represent cells that are undergoing replicative senescence. Although the overall proportion of non-dividing cells is lower in hTert cells, the pattern across the three cell strains is the same, with both AG18371(RTS)^{hTert} and AG03141(WS)^{hTert} cells containing higher proportions of non-dividing cells compared to AG16409(N)^{hTert} cells. Here it is postulated that the difference in the proportion of non-dividing cells in the hTert-immortalised cells compared to primary cells is due

to the removal of one set of stress signals (i.e. those arising from shortened telomeres) so that that non-dividing cells in hTert populations could be subject to ongoing SIPS. Accordingly, the findings suggest that both AG18371(RTS)^{hTert} and AG03141(WS)^{hTert} cells contain a higher proportion of cells that are undergoing SIPS compared to AG16409(N)^{hTert} cells.

Treatment with BIRB796 consistently reduces the proportion of enlarged cells in both primary and hTert cells; however, the effect of BIRB796 is greater in primary cells (Figure 8.2). In primary AG16409(N) cells treatment with BIRB796 results in a reduction in the proportion of non-dividing cells, although this effect is minor. The proportion of non-dividing cells in AG16409(N)^{hTert} cells following BIRB796 treatment is relatively unchanged. Both primary AG18371(RTS) and AG03141(WS) cells show a greater reduction in the proportion of non-dividing cells following BIRB796 treatment when compared to normal cells. Although the effect of BIRB796 in hTert cells is reduced compared to primary cells, both AG18371(RTS)^{hTert} and AG03141(WS)^{hTert} cells show a greater reduction in the proportion of non-dividing cells following BIRB796 treatment when compared to AG16409(N)^{hTert} cells.

Given the issues associated with characterising cellular morphologies that may be indicative of differences in the level of SIPS in GI syndrome cells (Chapter 3), this study provided the opportunity to undertake a quantitative assessment of cell size in the three cell strains. Although not one of the primary objectives of this analysis, the method of data recording trialled here permitted a preliminary analysis of the relationship between proliferative potential and progenitor cell size with indications that this approach could have sufficient resolution to profile dividing and non-dividing subpopulations. Figure 8.3 shows that WS and RTS cell populations consist of some cells that are with the normal size range; however, there appear to be other cells that are much larger than those observed in normal cells. Overall, the mean cell size is greater in RTS and WS cells compared to normal cells, suggesting that these cells contain more arrested/senescent cells compared to normal cells. Differences in the shape of the cell also appears to relate to division

222

potential, for example, some cells have a large area due to their elongated morphology, whereas other cells are polygonal in shape. Preliminary studies show that it is the enlarged, polygonal-shaped cells that tend to be non-dividing (data not shown).

8.4.2 WS traverse the cell cycle more slowly than normal cells.

To determine the IMT of AG16409(N)^{hTert}, AG18371(RTS)^{hTert} and AG03141(WS)^{hTert} cells, only progenitor cells that committed to at least one mitosis qualified for analysis. These were manually tracked and the time between subsequent mitoses were calculated. By definition, only those cells that underwent a second division were informative for this study. Therefore the IMT given for the three cell strains does not take into account those cells that divided once but failed to divide again over the course of the experiment. To avoid any issues associated with changing IMT in successive generations, the IMT of first generation events alone were studied. Figure 8.4 shows that AG16409(N)^{hTert} and AG18371(RTS)^{hTert} cells have a similar IMT (~20 hours), whereas AG03141(WS)^{hTert} cells have an extended IMT of ~28 hours (Rodriguez-Lopez et al. 2002; Rodriguez-Lopez et al. 2003). Treatment with BIRB796 has a very minor effect on the IMT of both AG16409(N)^{hTert} and AG18371(RTS)^{hTert} cells, but has a greater effect on the IMT of AG03141(WS)^{hTert}, reducing it to ~24 hours. These data suggest that the progression of AG03141(WS)^{hTert} cells, but not AG18371(RTS)^{hTert} cells, through the cell cycle are restrained in some way by p38-dependent processes.

8.4.3 Proliferative success of WS cells

Given that there is a higher proportion of non-dividing cells in WS, the cells must have exited the cell cycle at a greater rate (higher probability). Therefore the question arises – can a signature of loss of proliferative potential be seen in cells that initially show proliferative capacity? More importantly can this be examined under normal culture conditions and not the challenging low densities required for conventional clonogenic assays? Lineage tracking allows this to be achieved providing an 'in situ' clonogenic assay. Given that the mean IMT for AG03141(WS)^{hTert} was found to be ~28 hours, it was decided that a 72 hour time

course would be sufficient to see two subsequent mitoses (28 + 28 = 56 plus a 14 hour buffer). Pragmatically, the decision was made to extend the analysis to a more in depth lineage analysis to study the proliferative potential of AG03141(WS)^{hTert} cells over a short period of time. To qualify for this analysis a cell must divide at least once. Consistent with this, Table 8.2 shows that all cells undergo one division, designated generation 1. These data also show that ~80% of both AG03141(WS)^{hTert} and AG16409(N)^{hTert} cells divide a second time, designated as generation 2. Treatment with BIRB796 increases the proportion of progenitor cells that undergo two divisions in both AG03141(WS)^{hTert} and AG16409(N)^{hTert} (Table 8.2). Figure 8.5 shows the impact of BIRB796 on the clonal potential of AG03141(WS)^{hTert} and AG16409(N)^{hTert} cells given by the number of progeny produced from a single progenitor cell. In AG16409(N)^{hTert} cells the majority of progenitor cells give rise to small numbers of progeny (2-4). As expected there is a decline in the proportion of progenitor cells that give rise to larger numbers of progeny, with a maximum of 15 progeny being generated from a single progenitor cell (Figure 8.5A). A similar pattern is observed for AG03141(WS)^{hTert} cells in which the majority of progenitor cells generate small numbers of progeny (2-3) (Figure 8.5B); however, a maximum of only 10 progeny are produced from a single progenitor in AG03141(WS)^{hTert} cells, suggesting that the maximal clonal expansion potential of AG03141(WS)^{hTert} cells is restrained. In general, BIRB796 reduces the proportion of progenitor cells that generate highly restricted progeny numbers (2-3) but increases the proportion of progenitor cells that generate larger numbers of progeny in AG16409(N)^{hTert} cells; however, BIRB796 does not increase the maximum number of progeny produced from a single progenitor (having already qualified as having proliferative potential). A similar effect is observed for the impact of BIRB796 on AG03141(WS)^{hTert} cells, although the BIRB796 does increase the maximum number of progeny produced from a single progenitor from 10 to 11 progeny.

8.5 Discussion

Previous findings in the thesis suggest that the reduced clonogenic potential of RTS and WS cells is due to the dual effects of an increase in the proportion of

cells that are non-clonogenic and a reduced clonal expansion potential of cells that have clonogenic potential. The data presented in this chapter demonstrate the extent to which WS and RTS populations consist of dividing and non-dividing cells compared to normal cells (aim 1). Indeed, primary RTS and WS cultures show a significant increase in the proportion of non-dividing cells. The observation that the proportion of non-dividing cells is reduced in all hTert-immortalised cultures compared to their primary counterparts suggests that replicative senescence contributes to the reduced replicative capacity of all three strains. Despite the known caveats associated with differences in the fraction of cells from which the hTert populations are drawn from, it was assumed that the non-dividing cells in hTert-immortalised cultures represented those that were undergoing SIPS. Given this assumption, the findings that both AG18371(RTS)^{hTert} and AG03141(WS)^{hTert} cultures contained a higher proportion of such non-dividing cells suggest that RTS and WS cultures contain more cells that are undergoing SIPS compared to normal cells. Clearly, the proportions of and progression within these states contribute to overall replicative capacity.

The observation that BIRB796 consistently increases the number of dividing cells in normal, RTS and WS cells suggests that all three strains contain a fraction of cells that are "out of cycle" and whose re-entry into the cell cycle is restrained by p38. This is consistent with earlier observations made in chapter 7 that BIRB796 can increase clonogenic potential by recruiting a subpopulation of cells that were previously non-clonogenic. These findings also suggest that BIRB796 has the same effect on normal cells as it does on RTS and WS at the single cell level; but because there is a greater proportion of cells that are available for BIRB796 action (i.e. a greater number of non-dividing cells) in RTS and WS cultures, BIRB796 has a greater apparent effect at the population level.

The second major finding was that WS cells appear to have an elongated cell cycle transit time as indicated by a longer average IMT compared to normal cells, whereas RTS cells have an IMT comparable to that of the normal reference. The limited comparison with a single 'normal' stain is noted. BIRB796 was shown to

reduce the IMT of WS cells but did not affect the IMT of normal or RTS cells, suggesting that WS cells, but not RTS cells, show some degree of p38 restraint on their progression through the cell cycle.

Lineage analysis allowed clonal expansion to be tracked. Once a cell has been identified as being capable of division, the number of progeny produced from a single progenitor cell is similar in both WS and normal cells. However, there is some evidence that the maximum number of progeny produced from a single progenitor cell is reduced in WS compared to normal cells. These findings suggest that the reduced replicative potential of WS cells may be due to the dual effects of a greater proportion of non-dividing cells and a reduced clonal expansion potential for cells having residual division capacity. However, it is possible that the reduction in the maximum number of progeny generated from a single progenitor cell in WS may simply reflect the extended IMT and given more time the same number of progeny would be generated as seen for normal cells. Extended time-lapse studies could address this point. For example, in order to generate 15 progeny in a 72 hour period, a lineage must be highly branched, synchronised and have a relatively short IMT. Therefore, it is not clear as to whether the reduction in clonal potential for some progenitor cells is due to increased asymmetry in the division potential of sister cells in subsequent generations or an increasing IMT. Data recording of extended lineage analysis would allow a bioinformatics approach to study such complexity.

Overall, these data suggest that the reduced replicative potential observed for WS cells is due to a slightly extended cell cycle traverse time and a higher propensity for cell cycle exit due to SIPS. Similarly, a higher rate of SIPS is shown to occur in RTS cells, however, these cells traverse the cell cycle normally. These findings suggest that analysis of population growth of WS should take into account the impact of the increased drop out rate, since the division-competent cells are required to undergo more divisions for the population to double, therefore it is likely that replicative senescence of the division-competent subpopulation is realised

226

more quickly and therefore appear to increase when viewed at the whole population level versus passage age.

Clearly, models that account of the abnormal growth WS cells need to take into account the dual impact of the increased probability of cell cycle exit and compromised cell cycle traverse. In such models, the impact of p38 inhibition appears to have a greater impact on recruitment of cells into cycle rather than on regularising any underlying defect in cell cycle traverse. This leads to a model in which p38 restraint has selective effects in cell cultures with underlying differences in endogenous stress signalling. These aspects are discussed below.

In summary the main findings of this chapter are:

- AG03141(WS)^{hTert} and primary AG03141(WS) cells show an increased proportion of non-dividing cells compared to primary and hTert-immortalised AG16409(N) cells.

- Similarly, AG18371(RTS)^{hTert} and primary AG18371(RTS) cells show an increased proportion of non-dividing cells compared to primary and hTert-immortalised AG16409(N) cells, although the proportions on non-dividing cells are not as high as those seen in AG03141(WS) cells.

- hTert-immortalisation reduces the proportion of non-dividing cells in RTS and WS cells suggesting that telomere-independent senescence (i.e. SIPS) may contribute to the reduced division capacity of these strains.

- AG18371(RTS)^{hTert} cells have a normal IMT (~20 hours) but AG03141(WS)^{hTert} cells have an elongated IMT (~28 hours), suggesting that WS AG03141(WS)^{hTert} cells traverse the cell cycle slower than normal.

- AG03141(WS)^{hTert} cells show a reduced clonogenic potential as assessed by lineage analysis compared to AG16409(N)^{hTert} cells.

- BIRB796 consistently reduces the proportion of non-dividing cells in both hTert-immortalised and primary AG03141(WS), AG18371(RTS) and

AG16409(N) cells, suggesting that BIRB796 stimulates cells to re-enter the cell cycle.

- BIRB796 reduces the IMT of AG03141(WS)^{hTert} cells but has little effect on the IMT of AG18371(RTS) and AG16409(N) cells, suggesting that AG03141(WS)^{hTert} cells show some degree of p38-mediated restraint on cell cycle progression.

Table 8.1. Proportion of dividing and non-dividing cells in normal, RTS and WS cells.

Cell strain	No. cells in start field*	% Dividing	% Non-dividing
AG16409(N)	597	71.7	28.3
AG16409(N)[hTERT]	267	81.0	12.4
AG18371(RTS)	398	55.0	45.0
AG18371(RTS)[hTERT]	160	57.5	42.5
AG03141(WS)	315	39.0	61.0
AG03141WS)[hTERT]	173	45.7	53.8

* Pooled data were obtained from 6 independent fields for primary cells and 4 independent fields for hTert-immortalised cells. The number of cells in the nominal start field is given as the sum of all fields minus the number of cells lost from the field during the analysis.

Table 8.2. Proportion of progenitor cells that undergo one or two divisions in 72 hours.

Cell strain	n*	BIRB	% progenitor cells that give rise to:	
			gen 1	gen 2
Normal	42	-	100	79
	23	+	100	91
WS	23	-	100	78
	21	+	100	86

*n= number of lineages analysed.

Gen1 represent progenitor cells that undergo one division, and gen 2 represent progenitor cells that undergo two divisions.

A

	AG16409 (N)		AG18371 (RTS)		AG03141 (WS)	
	-	+	-	+	-	+
☐ % Non-div	28.3	20.8	45.0	20.4	61.0	46.8
▨ % Dividing	71.7	79.2	55.0	79.6	39.0	53.2

B

	AG16409(N) hTERT		AG18371 (RTS)hTERT		AG03141WS) hTERT	
	-	+	-	+	-	+
☐ % Non-div	12.4	12.8	42.5	30.0	53.8	42.3
▨ % Dividing	81.0	83.5	57.5	70.0	45.7	54.0
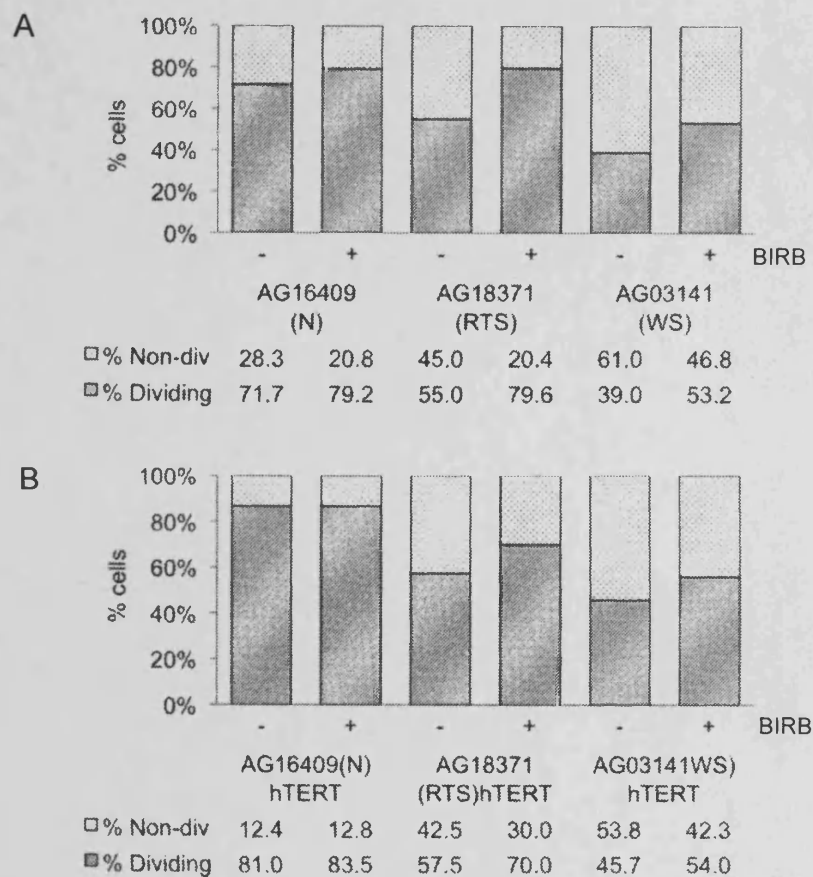
Figure 8.2. Impact of BIRB796 on commitment to division.

Panel A shows the proportion of dividing and non-dividing cells in primary normal, RTS and WS cells, Panel B shows the same for hTert-immortalised cells. Data were obtained from 6 independent fields for primary cells and 4 independent fields for hTert-immortalised cells.

A

B

Cell strain	No. progenitor cells (n=)	Mean cell size	Max cell size	Min cell size
AG16409(N)	625	4022	22896	1200
AG16409(N)hTERT	267	3634	24656	1008
AG18371(RTS)	490	5860	43280	1520
AG18371(RTS)hTERT	197	8611	23968	1792
AG03141(WS)	321	9997	48720	1776
AG03141(WS)hTERT	260	7784	28413	1392
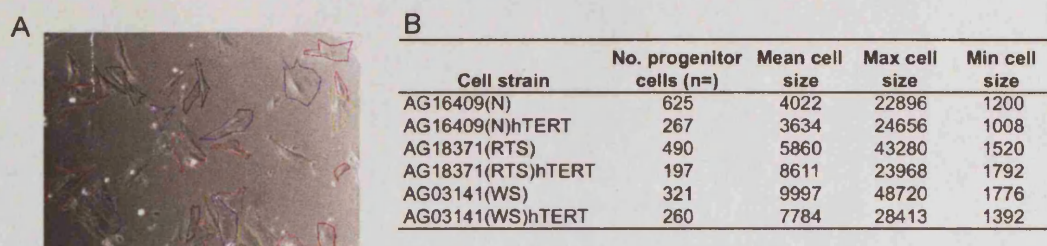
Figure 8.3. Quantitative analysis of cell size in 2D culture.

Panel A shows a typical field with regions traced to identify individual cell size of the progenitor cells. Panel B shows a table of the mean cell size, given as the mean of all of the cells in all of the fields, and of the maximum and minimum sizes observed in each population.

A

B

Cell strain	BIRB	Mean IMT ± SD
AG16409(N)[hTERT]	-	20.63 ± 3.6
AG16409(N)[hTERT]	+	20.71 ± 6.3
AG8371(RTS)[hTERT]	-	19.49 ± 5.5
AG8371(RTS)[hTERT]	+	19.21 ± 3.0
AG03141(WS)[hTERT]	-	26.78 ± 13.2
AG03141(WS)[hTERT]	+	23.61 ± 10.5
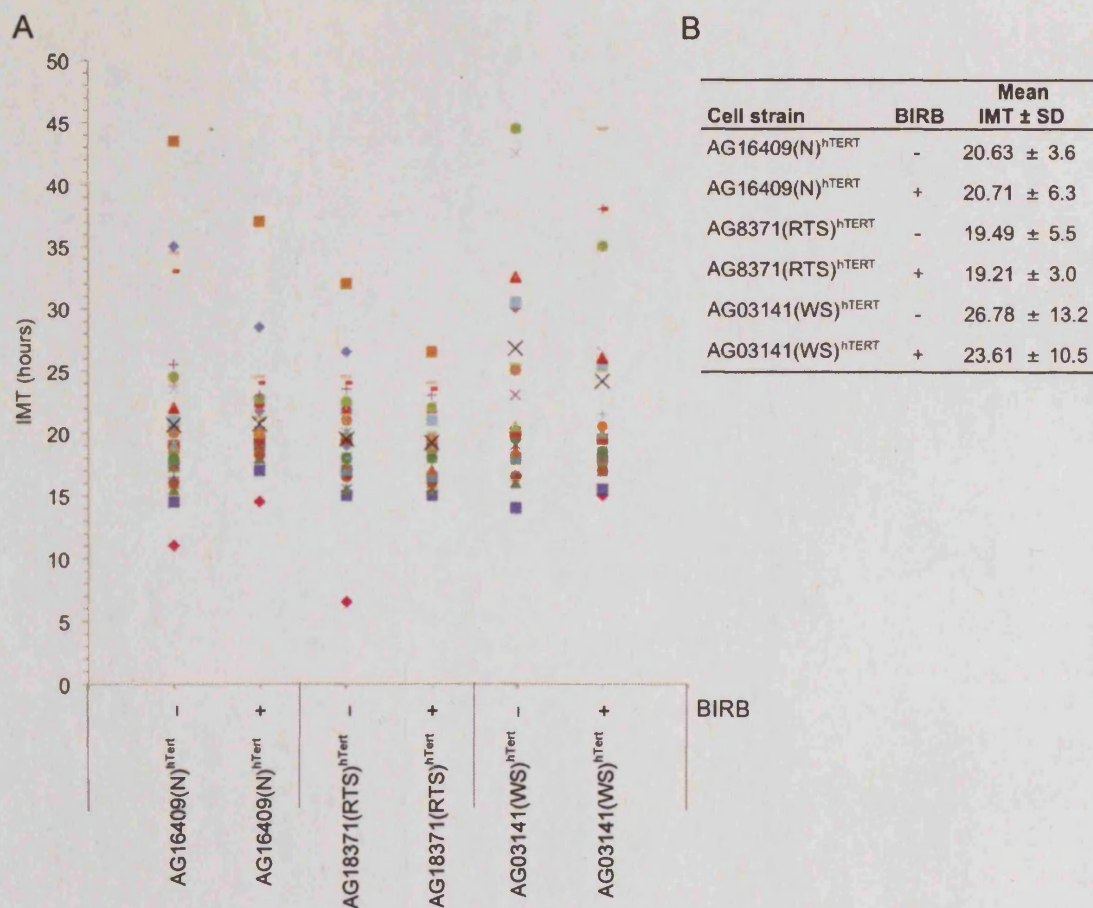
Figure 8.4. Impact of BIRB796 on inter-mitotic time for normal, RTS and WS fibroblasts.

Cells are grown in the presence or absence of BIRB796 and imaged using time-lapse microscopy. A: Range of IMTs observed, mean is indicated by large black cross. B: Mean IMT ± SD. Data obtained from 4 independent fields. Inter-mitotic times are calculated based on 1st generation events.

233
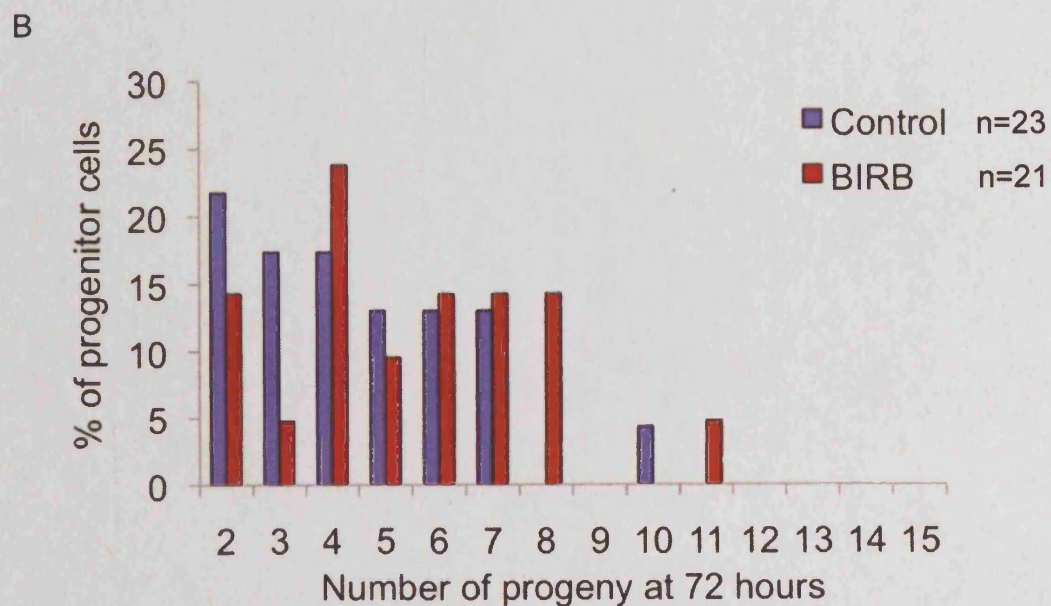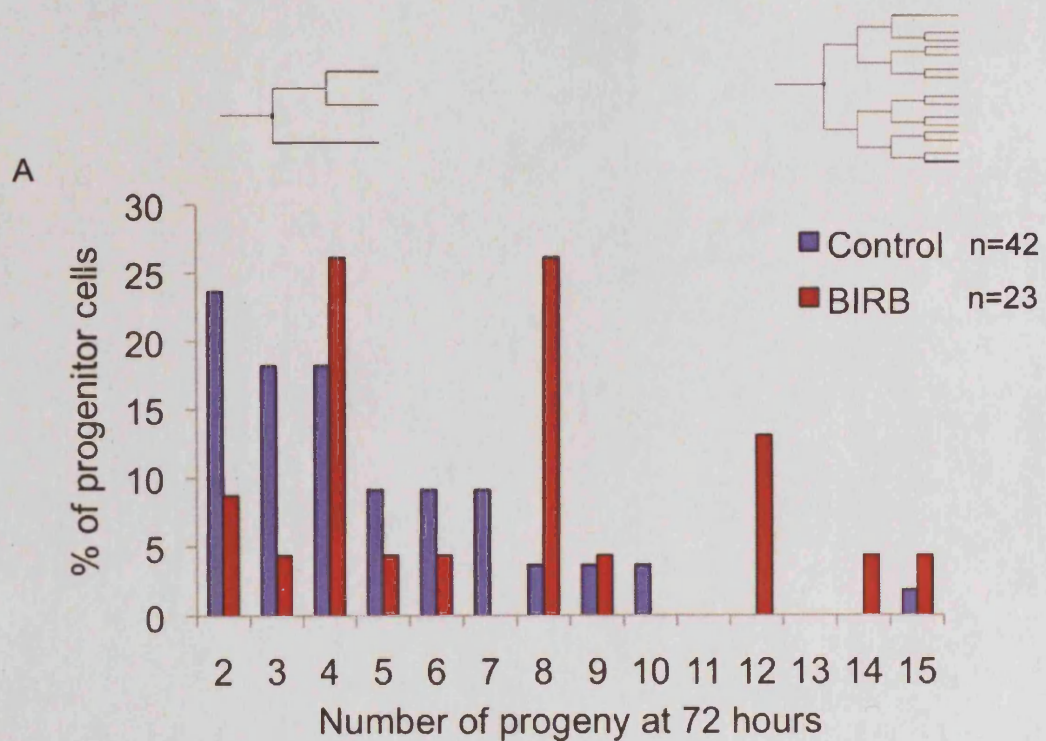
Figure 8.5. Impact of BIRB796 on the clonal potential of (A) AG16409(N)^{hTert} and (B) AG03141(WS)^{hTert} cells.

Bars represent the proportion of progenitor cells that generate a given number of progeny within 72 hours. n = number of lineages analysed. Schematic representations of example lineages that generate 3 or 15 progeny are indicated above panel A.

Chapter 9   General Discussion

This study arises from a background of evidence that suggests that WS cells undergo increased levels of SIPS. This includes the observation that WS cells have a truncated lifespan, senescent-like morphology including prominent stress fibres and elevated levels of activated p38 (Davis et al. 2005; Davis et al. 2006). Here, the proposal was that GI syndrome cells could share similar properties – not least a putative common dependence on p38-mediated pathways. The study reveals a commonality of response to p38 inhibitors amongst normal and GI primary cells and that following alleviation of stress from telomere attrition hTert-immortalised cells remain susceptible to SIPS. The thesis highlights successful approaches to testing the impact of p38 inhibitors by teasing out the nature of cellular heterogeneity arising from different sources, with implications for *in vitro* studies in carcinogenesis, senescence and physiological controls of cell proliferation.

The primary aim of this thesis was to *identify any differences in fibroblast behaviour that may be indicative of SIPS in cells undergoing low levels of GI*, such as those derived from individuals with GI syndromes. The findings (Chapter 3) indicate that a number of the GI syndrome strains, including AG18375(RTS), GM07166(NBS), GM01774(DKC), GM18366(SS), all three HGPS strains and both LIG4 strains, have a truncated lifespan compared to normal cells, which may potentially reflect increased levels of SIPS in these cells. Reduced growth capacity compared to normal controls has been previously reported for BS, CSA and HGPS (Goldstein 1979; Thompson and Holliday 1983), but not for NBS, LIG4, RTS or SS, therefore this study provides novel information regarding the growth potential of these cells. Furthermore, these studies provide a coherent parallel comparison of growth potential in primary cell strains with different genetic backgrounds. Consistent with previous findings in the literature (Absher and Absher 1976; Absher et al. 1974; Cristofalo et al. 1998a; Martin and Sprague 1973; Passos and von Zglinicki 2007; Pious et al. 1964), the current study revealed marked

235

heterogeneity in the growth potential of different normal cell strains as well as between strains from the same GI syndrome. These findings suggest that there are inherent differences in the level of commitment to senescence (SIPS and/or replicative senescence) in primary cells that are not dependent on genetic background. Given that the assumption in this thesis is that the proportion of senescent cells in a population increases over time, the most likely explanation for the observed inter-strain differences are that they are due to differences in passage histories of the individual strains. These issues are discussed further below.

Studies using a range of p38 inhibitors with different modes of action suggest that whether p38 inhibition was achieved by induction of a conformational change in the active site of p38 (e.g. BIRB796) or by blocking p38 activation but not its phosphorylation (e.g. SB203580), the impact of inhibition consistently increased the growth potential. This reveals a commonality of p38 inhibitor responses in primary cell strains. Furthermore, the findings suggest that both normal and GI syndrome cell strains in culture undergo some degree of p38-mediated proliferation restraint that can be relieved by p38 inhibition. Given the previous evidence that p38 inhibition does not prevent telomere-attrition driven replicative senescence and thus has a reduced effect on cells that are close to replicative senescence (Davis et al. 2005), the observation here that some cell strains show a truncated lifespan and yet have a relatively normal response to p38 inhibitors, suggests that these cells may simply be closer to replicative senescence due to strain history. In contrast, other strains, such as GM18366(SS) and to a greater extent GM07166(NBS), show a striking response to p38 inhibition, suggesting that the reduced replicative potential of these cells is derived from a greater commitment to SIPS.

An extensive screen of the cellular morphology of these cells was also undertaken *to identify any morphological features that were indicative of cells undergoing SIPS, such as stress fibre presentation, and to assess the feasibility of such features as biomarkers of differences in the underlying commitment to*

senescence in these cells. The findings show that a complex relationship exists between growth arrest and the presentation of stress fibres, suggesting that stress fibre presentation accompanied enlargement as might be expected given the functional co-relationship. However, there were no clear trends relating stress fibre presentation with genetic background. These findings raise the need for a more quantitative assessment of cellular morphology, perhaps using cell size, rather than stress fibre presentation, as a marker of growth arrest. All cell strains tested showed a reduction in the proportion of enlarged cells following p38 inhibition. In general, these effects were minor, with the majority of cell stains showing a similar response as normal cells. However, some exceptions were observed, for example, both GM07166(NBS) and GM18366(SS) cell strains showed a higher proportion of enlarged cells, with cells estimated to be much larger than those observed in normal strains, and showed greater responses to p38 inhibitors. It is likely that the degree of enlargement relates simply to the time spent in arrest. Therefore the frequency of event detection and the degree of enlargement will be dependent upon the rate of proliferation of non-arrested cells and the effective dilution of arrested cells at subsequent passages. It is reasonable to suggest that GI syndrome cells have an added layer of complexity due to the impact of the molecular defect on each of these features.

Overall, these studies provide valuable information regarding the heterogeneity in growth potential and cellular morphology of primary fibroblasts. Importantly, heterogeneity could not be ascribed primarily to differences in genetic background. Given the complications associated with the uncertain replicative histories of some of the cell strains used, this study underlines the difficulty of comparing GI syndrome cell strains that may have different degrees of commitment to senescence due to telomere attrition. Thus the findings highlight the need to disassemble the complexity and history of these primary cell systems in order to study the impact of SIPS.

Given the restricted replicative potential of some GI strains, and the lack of availability of early passage culture the project sought *to establish an hTert*

immortalised panel of cell strains for more extensive studies in which lifespan is not limited (Chapter 5). The findings showed that ectopic expression of hTert is sufficient to extend the lifespan of all of the above cell strains beyond their normal senescence point. Importantly, the current study shows that RTS cells can be immortalised by ectopic expression of hTert, something that was not previously known. This provides a valuable measure for the study of *RECQL4* helicase gene mutation. Thus, the work successfully established a bank of hTert-immortalised AG16409(N), AG18371(RTS), GM02548(BS), GM07166(NBS), GM01856(CSA), AG11498(HGPS) and GM17523(LIG4) cell strains, providing a comparative resource. Pragmatically, the panel addresses the problems associated with working with primary fibroblasts that have a limited replicative lifespan, and provides a way of generating enough cells for further analysis. Importantly for this thesis, the implicit removal of stress signals associated with telomere attrition, that may obscure the impact of any endogenously generated stress signals, provides a unique opportunity to examine inherent differences in the cellular response to damage or p38 inhibitors in a panel with known molecular defects (addressed below).

The next aim of the thesis was *to assess the activation status of p38 in primary cells undergoing low levels of GI*. Here, studies revealed that the level of p38 activation in GI syndrome cells is similar to that observed for normal cells, although some inter-strain (and intra-GI syndrome) variation is observed. Given these findings, there are two possible explanations for the impact of p38 inhibitors on the growth potential and morphology of these cells. First, it is possible that relatively small changes in p38 activation are translatable into significant changes in the parameter of *in vitro* growth potential due to the exponential nature of growth changes over time and therefore the expansion of differences with time. Studies focusing on changes in p38 activation at a single cell level may provide a means of assessing the p38 activation status in informative cells when these are relatively infrequent in the population (see below). Secondly, it is possible that the small changes in replicative potential observed for most cultures are due to a combination of p38 inhibition and other off-target effects. The observation was

made that VX745, which is deemed to be highly specific for p38 (Lee and Dominguez 2005), consistently shows the smallest effects on cell growth. Thus action on off-targets may contribute to the observed impact of the p38 inhibitors. However, it was proposed that the use of multiple inhibitors, reducing the impact of specific off-target effects, confirm p38 involvement.

The finding that hTert-immortalisation reduced the level of detectable p38 activation in normal cells, but not in GI syndrome cells, suggests that the major stress signals giving rise to growth restraint in normal cells is due to telomere attrition, whereas GI syndrome cells may have the added burden of SIPS. These findings suggest that the hTert panel provides an accessible model in which to study the differences in commitment to SIPS in GI syndrome cells compared with normal cells.

The hTert panel was deployed in a range of studies aimed at *investigating whether hTert-immortalised GI cells remain susceptible to SIPS following exposure to DNA-damaging genotoxic agents* (Chapter 6). The findings indicate that all cell strains show hypersensitivity to DNA damage induced by at least one of the agents tested (see table). Specifically, all strains, with the exception of LIG4 cells, showed hypersensitivity to CPT. This may relate to the distinct S-phase (in cycle) selectivity of CPT. There is little consistent evidence in the literature for the sensitivity of GI syndromes with known molecular defects to damage induced by genotoxic agents. Thus, the present study provides a unique opportunity for coherent comparison of the sensitivity of GI syndrome cell strains to general genotoxic damage using a standard technique. Although there is some evidence in the literature for the sensitivity of GI syndrome cells, such as WS and BS, to genotoxic agents (Mao et

Table 9.1. Summary of drug sensitivities in hTert-immortalised GI syndrome fibroblasts

Syndrome	Molecular defect	Previous evidence of sensitivity to DNA damage	Evidence of sensitivity to DNA damage from current study
RTS	RECQL4	YES (CPT, DOX, H_2O_2)	YES (CPT, CisPt)
CSA	CSA	YES (CPT, 4NQO)	YES (CPT, 4NQO)
BS	BLM	YES (CPT, CisPt)	YES (CPT, DOX)
NBS	NBS1	YES (CPT)	YES (4NQO)
LIG4	LIG4	YES (CisPt)	YES (DOX)
HGPS	Lamin A (LMNA)	YES (CPT)	YES (CPT, DOX, CisPt)
WS	WRN	YES (CPT, 4NQO)	YES (CPT)

al. 2010) (Table 6.1), other syndromes, such as LIG4 and HGPS, have yet to be studied. Recently, two systematic studies of the sensitivity of RTS cells to a panel of genotoxic agents have been reported, both of which show conflicting results (Cabral et al. 2008; Jin et al. 2008). As a critique of such studies, here it is noted that Cabral et al evaluated cytotoxicity based on cell proliferation and MMT survival test after only 4 days, whereas Jin et al used a colony forming assay performed after 10-14 days. The MTT assay is a gross measure of residual metabolic activity in which arrested cells would provide a persistent signal. Jin et al did not consider the kinetic limitations of a colony forming assay. In addition, there were differences in the concentrations and exposure times to each of the drugs between the two studies. This raises the issues associated with comparing results from studies that have used different cell types (e.g. lymphocytes or fibroblasts that have different restraints on proliferation, such as contact inhibition) and the use of virally transformed cells in which checkpoint dysfunction may obscure the results.

Overall, the findings indicate that despite hTert-immortalisation cells remain susceptible to SIPS. The study also shows that recovery from CPT treatment in normal, CSA and BS cells was not affected by BIRB796, suggesting that p38 inhibition alone is insufficient to relieve the restraint on cell cycle progression following CPT-induced DNA damage. Here it is suggested that arrest mediated by checkpoint activation in response to DNA damage supersedes p38 restraint. Whether or not p38 is functionally a minor component of a damage checkpoint response in human fibroblasts remains unclear.

A further investigation was undertaken *to address whether the hTert panel members show any differences in cell cycle dynamics, in particular in cell cycle arrest, that may be indicative of differences in the level of commitment to SIPS.* Here the working hypothesis was that differences in replicative potential reflect the degrees of commitment to long-term exit (senescence) from the cell cycle, reflecting the probability of transition between "out of cycle" and subsequent "re-entry". These studies clearly showed the capacity of BIRB796 to act acutely and consistently increase the proportion of cells that were designated as in cycle

(G_2+S) within 24 hours. The findings suggest that BIRB796 can trigger cells to re-enter the cell cycle within one cell cycle transit and thus provide information regarding the likely target population for BIRB796 action. This view supports the earlier finding that there is a common mechanism that limits retention in or re-entry into cycle in all cells that it is dependent, at least in part, on p38. Furthermore, these findings support and expand previous evidence in the literature that p38 is involved in growth arrest (Bulavin and Fornace 2004; Maruyama et al. 2009; Yee et al. 2004). It is reasonable to suggest that the p38 restraint acts primarily at the G_1/S transition in limiting re-entry into cycle in quiescent cells, since this is the primary physiological site for proliferation restraint.

Clonogenic analysis of the GI syndrome panel revealed differences in the clonogenic potential between strains suggesting that some strains show a greater level of growth restraint. WS have been shown previously to have a reduced clonogenic potential but little information is available for the other syndromes. Therefore, this study provides novel information regarding the growth potential of these cells. The observation that BIRB796 increased the clonogenic potential of all cells supports the previous suggestion of a commonality of p38 restraint in these cells. Here it is noted that clonogenic potential, as determined by colony formation is a composite of absolute ability to form viable daughters upon cell division and the capacity for colony expansion. Further analysis of the impact of BIRB796 on the clonogenic potential of WS cells revealed that BIRB796 increases the proportion of cells that remain in cycle and therefore contribute to colony expansion, resulting in an increase in clonogenic potential. Together, these findings suggest that a subpopulation of cells that are BIRB796-responsive, are essentially "out of cycle". Thus, different cell strains may simply differ from each other on the basis of the proportion of cells available for BIRB796 action. Overall, these studies indicate that stimulation of a non-clonogenic fraction of varying size underpins the increase in the clonogenic potential of these cells and explains the increase in population following BIRB796 treatment.

The findings from the previous chapters revealed the presence of subpopulations of cells that are undergoing SIPS and suggest that the relative proportions of these subpopulations may impact upon the overall replicative potential of the strain. However, the findings also revealed that analysis at a whole population level did not have the resolution to fully examine the variation in the degree of commitment to cell cycle exit and the impact of p38 inhibition on this. This challenge was addressed in the last chapter by attempting to disassemble the complexity of cellular response to inhibition given the expectation of heterogeneity within the cellular systems. Here, the exemplars of RTS and WS cells were studied to determine the extent of the differences in commitment to cell cycle exit at a single cell level in these cells.

There were three fundamental aims of the final study. The first was *to assess whether RTS and WS cells show a difference in the probability of entering mitosis compared to normal cells.* The findings that both primary and hTert-immortalised RTS and WS cells show a significant increase in the proportion of non-dividing cells compared to their normal counterparts, suggest that the reduced replicative potential seen at both a whole population level and in the clonogenic analyses can be ascribed to an increase in SIPS in these cells. The findings support the original hypothesis that a small increase in the number of cells that exit the cell cycle due to SIPS can result in a dramatically reduced replicative potential (Figure 1.6). These findings support previous observations in the literature that WS cells show features of cells undergoing SIPS (Davis et al. 2005; Davis et al. 2006) and provide more definitive evidence of the differences in the proportions of cells that may be undergoing SIPS in WS. These studies also provide previously unreported evidence for an increased level of SIPS occurring in RTS cells. The observation that BIRB796 increases the proportion of cells that can enter cell division further supports the idea that all cells are undergoing some degree of SIPS and that the transition between in and out of cycle is mediated, at least in part, by p38 function.

The second aim was *to assess whether RTS and WS cells traverse the cell cycle at the same rate as normal cells.* The findings show that WS cells have an elongated cell cycle transit time as indicated by a longer average IMT compared to normal cells, whereas RTS cells have an IMT comparable to that of the normal reference. This is consistent with previous studies showing that WS cells have a prolonged S-phase (Poot et al. 1992) and suggests that the increased IMT in WS cells is due to slower progression through S-phase, most likely due to an increase in replication fork stalling (Rodriguez-Lopez et al. 2007). The observation here that BIRB796 reduces the cell cycle transit time of WS cells but not RTS or normal cells, suggests that WS cells have an added restraint on their progression through the cell cycle that is limited, at least in part, by p38.

The third aim of the final study was *to determine the lineage characteristics of WS cells compared to normal cells.* Initial studies suggest that once a cell has been identified as being capable of division, the number of progeny produced from a single progenitor cell is weighted towards the generation of fewer progeny in WS, with a reduction in the maximum number of progeny produced from a single progenitor cell in WS compared to normal cells. These findings suggest that the reduced replicative potential of WS cells may be due to the dual effects of a greater proportion of non-dividing cells and a reduced clonal potential of those that divide. However, it is important to note that the latter feature findings may be affected by the elongated IMT for WS and therefore further studies over a longer period of time may be required to fully assess the differences in lineage characteristics of WS and normal cells.

9.1 Conclusion and cell cycle model

In conclusion, the findings from this study suggest that p38 is involved in growth restraint in primary and hTert-immortalised cells. It is reasonable to suggest that this occurs primarily at G_1/S transition. The observation that all cell strains tested responded to p38 inhibitors suggests that all are undergoing some degree of p38-mediated growth restraint - most likely to be due to sub-optimal culture conditions. The current study provided a view of the heterogeneity in primary cell

strains and raised the issue of differences in replicative histories as a means for generating heterogeneity observable at a given culture age. The generation of the hTert panel provided a unique opportunity to study the impact of endogenously (as a result of GI) and exogenously (induced by DNA-damaging agents) generated stress signals in a system not limited by replicative lifespan. Differences in the clonogenic potential between members of the hTert panel are ascribed to inherent differences in growth restraint. Here it is proposed that growth restraint is a compound of differences in the commitment to (or probability of) cell cycle exit and subsequent likelihood of re-entry – representing the observable differences in the commitment to SIPS in these cells.

The current study provides an in-depth analysis of the extent to which there are differences in the proportion of cells that show division capacity in cell strains with known molecular defects. Here, both RTS and WS cells are shown to contain a greater proportion of non-dividing cells compared to the normal reference strain (Figure 9.1). p38 inhibition reduces the proportion of non-dividing cells, suggesting that p38 stimulates cells to re-enter the cell cycle. Based on the findings in this thesis, it is reasonable to suggest that the cellular response to GI includes an increase in the level of commitment to cell cycle exit.
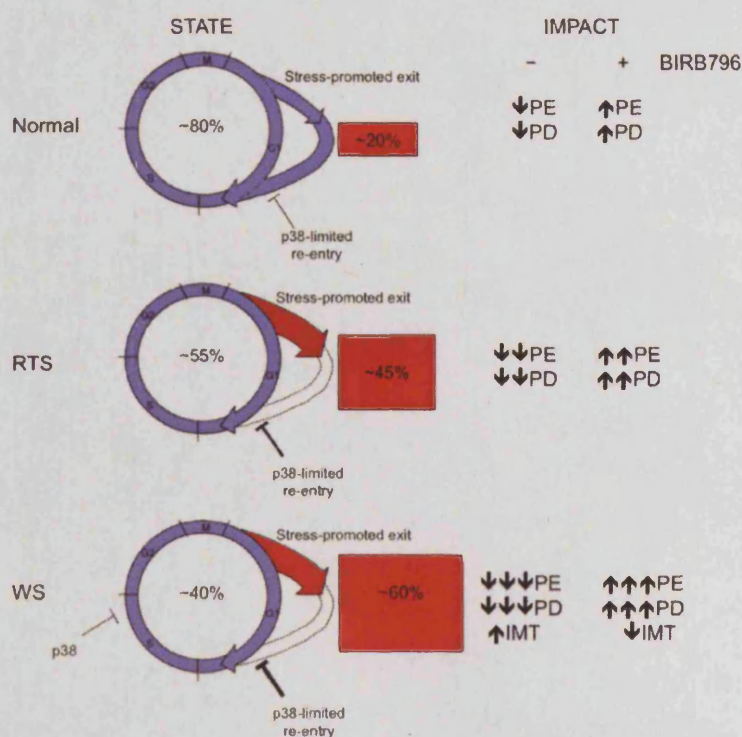

Figure 9.1. Population status of young unperturbed (no overt checkpoint activation) fibroblast cultures governed by p38 restraint

According to the method of analysis there is a hierarchy of observable SIPS effects and the impact of p38 inhibition. When cultures are analysed over long periods (e.g. population doublings over multiple passages), the main effect is the exit rate with p38 inhibition permitting a larger cohort of cells to contribute to culture growth. When tracking over the medium term (e.g. population expansion capacity as in a clonogenic assay set at a given colony size to qualify for 'clonogenicity') the degree of lineage asymmetry plays a critical role in generation of progeny from a progenitor. Finally analysis over the short term (as in single cell tracking) reveals fundamental differences in IMT that may arise from genetically determined defects in cell cycle traverse overlaid by a stochastic probability of cell cycle re-entry following cell division. Given this complexity the degree of response to p38 inhibition needs to be interpreted within the limits of a given assay.

In an attempt to explain the role of p38 in progression to SIPS based on the findings from this study, a mechanistic model is proposed (see figure). This model suggests that there are a number of restrains on growth potential, one of which can be ascribed to p38 function. The model suggests that p38 may be activated in response to low levels of stress, such as endogenously generated stress in GI syndromes or compromised normal cells. Additional over-riding restraints (e.g. an activated DNA damage checkpoint), imposed as part of a response to higher levels of stress, predominate in the response to DNA damaging agents. In keeping with this model, in a system in which the level of stress is negligible, p38 inhibition would have no detectable effect on progression through the cell cycle given the difficulty of identifying informative cells. Similarly, in a system that was exposed to high levels of damage (e.g. exposure to CPT) an over-riding checkpoint would be activated and therefore p38 inhibition would have no effect. In contrast, in systems that were experiencing low levels of endogenous stress, such as GI syndrome cells, the checkpoint would not be activated or sustained and therefore p38 plays a limiting (and therefore inhibitor responsive) role in growth restraint. In this model no distinction is made between p38 being a minor part of checkpoint response or a weak response pathway distal to checkpoint exit. Thus, p38 inhibition would have an effect on growth potential and it is reasonable to suggest that the impact of p38

inhibition would differ depending on the level of stress. On the other hand, in a physiological system low levels of p38-mediated proliferative restraint may act to guide longer term tissue kinetics and dynamics and therefore become a critical factor in the generation of the multisystem disorder presented by GI panel diseases (e.g. sub-optimal growth and altered tissues in WS).

9.2 Future direction

The suggestions for future study include:

1. Application of single-cell tracking. Successful application of single-cell analysis methods to identify inherent differences in the growth potential of RTS and WS cells compared to normal cells in Chapter 9 support the feasibility of this approach for studying heterogeneous fibroblast populations. These studies show that this approach provides a means of identifying differences in the commitment to division and allows lineage analysis to identify differences in the clonal expansion potential of these cells. This approach has the added advantage that relatively few cells are required for analysis compared to whole population analyses such as flow cytometry and is therefore ideal when working with limited resources such as primary GI syndrome cells. This method could be improved by using an automated cell lineage tracker that encodes the microscopy images and deposits data in relational databases mining by bioinformatics tools. Software tools such as ProgeniTRAK along with the associated database – ProgeniDB, have been shown to ease the burden of analysing large data sets associated with this type of study (Khan et al. 2007). This approach could be applied to other GI syndrome cells to identify the quantitative differences in commitment to division in these strains. It my also be interesting to monitor the changes in cell size following BIRB796 treatment to investigate whether a change in morphology is indicative of an increased probability of division.

2. Improvement of techniques to assess p38 activation. Measurement of p38 activation status by Western blot in chapter 5 indicates that identifying phosphorylation patterns in informative cells may be problematic given that a relatively small change in phosphorylation levels may be sufficient to alter growth

potential. Evidence in the literature suggests that p38 shuttles between the cytoplasm and the nucleus depending on the phosphorylation status (Crabtree and Olson 2002; Gomez del Arco et al. 2000; Porter et al. 2000; Wu et al. 2003), for example, p38 is localised in the cytoplasm in untreated HeLa cells but translocates to the nucleus following UV treatment. Similarly, a significant proportion of p38 is shown to translocate from the cytoplasm into the nucleus following treatment with the receptor activator of NF-κB ligand (RANKL), a known upstream activator of the p38 pathway (Matsumoto et al. 2004). It was therefore postulated that subcellular localisation rather than phosphorylation status *per se* could be used to determine the activation status of p38 on a cell-by-cell basis using immunofluorescence (IF). Preliminary studies show that it is possible to identify cells in which p38 has translocated to the nucleus (Figure 9.2); however, the effect is more subtle than that previously seen for cells that have been exposed to genotoxic
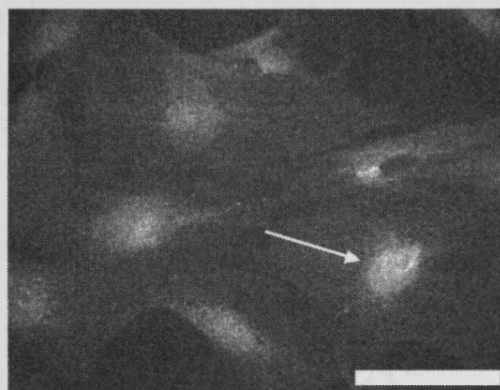
Figure 9.2. Subcellular localisation of p38 as measured by IF. Arrow indicates a cell with nuclear localisation of p38.

agents. Future studies should therefore include attempts to identify a threshold value for the biologically relevant ratio of nuclear versus cytoplasmic signals. Subcellular localisation of p38 could be used in future studies to determine the proportion of cells that have activated p38 in relation to critical cell cycle events (using additional protein/phosphorylation/location markers) such as stress signalling, checkpoint activation, mitotic entry and cell enlargement in arrest. Here methods for the abrogation of checkpoint responses (e.g. as realised in virally transformed or cancer cells) would be highly informative.

3. Identification of other syndromes that show an increased propensity for SIPS. The findings from the current study provide some evidence that defects in NBS1, ATR and WRN result in a reduced replicative potential and altered cellular morphology that may indicate increased SIPS in these cells. Thus, it is

possible that the probability of entering SIPS is dependent on the nature of the pathway that is defective.

ATR responds to a broad spectrum of DNA damage substrates and is crucial for maintaining genomic stability during S-phase (Cimprich and Cortez 2008). The Mre11, Rad50 and Nbs1 proteins form the MRN complex, which is involved in the cellular DNA damage response (Lavin 2007). Although MRN complex function is widely accepted to play a role in ATM activation in response
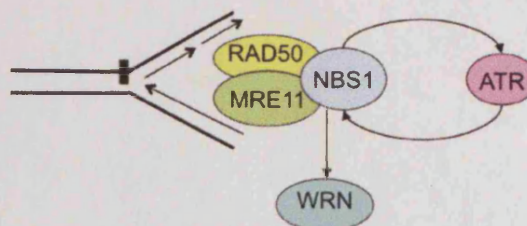
Figure 9.3. Schematic representation of the role of WRN, ATR and MRN complex in resolution of stalled replication forks.

to DSBs (Lee and Paull 2007), its role in ATR activation and downstream signaling in response to different types of damage is less clear. Some evidence in the literature suggests that when replication forks are stalled (such as following UV exposure), MRN is required upstream of ATR to facilitate ATR activation, but is also a downstream substrate of ATR (NBS1 is phosphorylated by ATR) (Olson et al. 2007). WRN has been shown to associate with the MRN complex via binding to NBS1 *in vitro* and *in vivo* (Cheng et al. 2004). This provides support for a model in which NBS1 recruits WRN at stalled replication forks (Figure 9.3). Taken together, these findings suggest a functional link between the three syndromes, WS, NBS and SS, with partially overlapping phenotypes in a pathway that responds to DNA damage.

Further studies of SIPS using a more vigorous panel of markers in a larger panel of SS, WS and NBS cells would be warranted. Furthermore, examination of cells from other syndromes, such as AT like-disorder (ATLD), which have defects in MRE11 may also be of interest. However, any future studies should not be undertaken without full recognition of the heterogeneity between fibroblast strains and care should be taken to study cell strains with known replicative histories and fully characterised mutations.

4. Improvements in the recognition of cell cycle exit in heterogeneous populations. The findings in chapter 4 raised the need for a more quantitative approach to analysis of cellular morphology and suggest that cell size may be a better indicator of differences in proliferation potential than stress-fibre presentation. Further support for this was provided by time-lapse microscopy studies in chapter 8, using image analysis software to identify the size of individual cells, which showed that enlarged cells correlated with a reduced probability of division. These studies appear to have sufficient resolution to identify the relationship between cell

Figure 9.4. (A) CyTRAK Orange staining of nucleus and cytoplasm. (B) Increase in CyTRAK Orange signal in response to CPT treatment.

cycle exit and cell size but are labour-intensive. One approach is to use a reporter for arrest. It was postulated that an agent that stains both the nucleus and the cytoplasm could be used to distinguish between cell cycle exit and cell cycle position on the basis of increased cell size. Preliminary studies using the investigational agent CyTRAK Orange™ showed that this agent stains both the nucleus and the cytoplasm (Figure 9.4A) and that the CyTRAK Orange™ signal increases in cells in which cell cycle arrest is artificially induced using CPT (20 nM for 48 hours; figure 9.4B). Spectral differences allow CyTRAK Orange™ to be combined with other agents, for example, 5-dodecanoylaminofluorescein di-β-D-galactopyranoside (C12FDG), a fluorogenic substrate for βgal activity that can be used to detect senescence cells *in vitro* (Debacq-Chainiaux et al. 2009; Noppe et al. 2009); therefore, CyTRAK Orange™ could potentially be used in future studies to distinguish between a cell that is long-term arrested and one that is senescent.

Appendix A   Prevention of accelerated ageing in Werner

syndrome fibroblasts

A.1 Introduction

One of the hallmarks of WS is that primary dermal fibroblasts derived from WS individuals manifest a much-reduced replicative lifespan than normal fibroblasts (Faragher et al. 1993; Salk et al. 1981; Tollefsbol and Cohen 1984). This premature senescence of WS fibroblasts has been postulated as a major contributor to the accelerated ageing of mitotic tissues *in vivo* in this syndrome (Kipling et al. 2004). WS fibroblasts also divide more slowly than normal cells in part due to an increased S-phase of the cell cycle (Poot et al. 1992; Takeuchi et al. 1982), and have an elevated level of replication fork stalling (Rodriguez-Lopez et al. 2002). Primary WS cells display genome instability, manifested by an elevated rate of chromosomal translocation and genomic deletions (Fukuchi et al. 1989), and are hypersensitive to a subset of DNA damaging agents (Comai and Li 2004), suggesting that the WRN protein plays a key role in the cellular response to specific types of DNA damage. In addition, WS is associated with an increased level of pro-oxidant stress (Pagano et al. 2005), and pro-oxidant stress is associated with increased genomic instability and premature cellular senescence, and has been linked to ageing, diabetes, cancer, atherosclerosis and osteoporosis, all features of WS (Pagano et al. 2005).

As with normal cells, senescent WS fibroblasts have an elevated production of pro-inflammatory cytokines and inflammatory markers such as ICAM-1 (Choi et al. 2001; Kumar et al. 1993). WS individuals have markedly elevated plasma levels of ICAM-1 (Murano et al. 1997) and TNFα (Yokote et al. 2004), both of which are associated with inflammatory diseases (Holtmann and Neurath 2004; Witkowska 2005). Moreover, WS fibroblasts, even at low population doublings, have an

enlarged cellular morphology with extensive F-actin stress fibres and resemble senescent normal fibroblasts (Davis et al. 2005; Davis et al. 2006).

Overall, WS fibroblasts resemble normal cells that have undergone stress-induced premature senescence (SIPS). SIPS is known to result from activation of the p38 signalling pathway (Huot et al. 1997; Wang et al. 2002) and the genome instability seen in WS, increased pro-oxidant state, and the frequent replication fork stalling seen in WS cells, all provide a plausible trigger for intracellular stress in WS cells and a possible involvement for p38 signalling in inducing the shortened replicative life span. To test this WS fibroblasts were cultured in the presence of p38 inhibitors SB203580 and BIRB 796.

Please note that all data in this appendix have been provided courtesy of my supervisor Dr T. Davis and are shown here only as supporting data.

A.2   p38 inhibitors prevent the shortened lifespan of WS fibroblasts

WS fibroblast strain AG03141 was seeded into T25 culture vessels in EMEM supplemented with SB203580 at 2.5 µM and grown with daily re-feeding (with fresh inhibitor) until the cells reached replicative senescence. Control cells were grown in EMEM supplemented with the drug carrier DMSO (0.1 %). Cells were passaged either every five days or when they reached approximately 75 % confluency.

Control cells achieved 22.04 PDs at a maximal growth rate of 0.14 PD/day (Figure A1, graph a). In contrast AG03141(WS) cells grown in the presence of SB203580 achieved 40.84 PDs, well within the range seen for normal adult dermal fibroblasts, at a maximal growth rate of 0.32 PD/day (Davis et al. 2005). As these cultures were initiated when the cells had already achieved 9 PD this is equivalent to an increase in experimental lifespan of 144% (40.84-9)/(22.04-9) x 100%.

In a separate experiment a different batch of AG03141(WS) cells (initiated when they had reached 14 PDs) were cultured in the presence or absence of BIRB 796 at 2.5 µM. In this case the control cells did 20.72 ± 0.09 PDs with a maximal

growth rate of 0.21 PD/day (Figure A1, graph b). In both experiments the AG03141(WS) control cells reached a total of approximately 21 to 22 PDs, showing the shortened lifespan typical of WS cells. When cultured in the presence of BIRB796 the maximal growth rate increased to 0.37 PD/day and the lifespan to 32.77 ± 0.34 PD (Figure A1, graph b). Whilst this lifespan is not as great in PD terms as seen with SB202580 it must be noted that the two experiments were initiated with cells of different replicative age. As measured as a percentage of experimental lifespan, however, the lifespan with BIRB796 is (32.77-14)/(20.72-14) x 100% = 279% of the control cells, an increase of 179%. As it has been shown that the lifespan extension of WS cells treated with p38 inhibitors is inversely proportional to the replicative age of the culture when drug treatment began (Davis et al. 2005), then if cultures with BIRB 796 were initiated at 9 PD and achieved an experimental lifespan increase of 279%, the BIRB 96 treated cells would have reached 41.7 PD. This inverse correlation has been seen many times (Davis et al. 2007).

Thus, treatment using the p38 inhibitors SB203580 and BIRB796 essentially prevents the shortened lifespan and slow growth rates seen in AG03141(WS) dermal fibroblasts.

A.3   p38 inhibitors rescue the abnormal morphology of WS cells

A major characteristic of WS fibroblasts is that, even when young, they have an altered morphology with extensive F-actin stress fibres resembling that of senescent cells (Davis et al. 2005) [Figure A2, panels a and c show the AG03141 cells used for the growth experiment in Figure A1 graph a at 10 PD]. Treatment with the p38 inhibitor SB203580 reverts this morphology to that more reminiscent of young normal dermal fibroblasts (Figure A2, panels b and d show the SB203580 treated AG03141(WS) cells used for the growth experiment in Figure A1 graph a at 12 PD). A similar effect is seen when the p38 inhibitor BIRB796 is used (Figure A2, panels e and f show the cells used for the growth experiment in Figure A1 graph b).

Thus, treatment using the p38 inhibitors SB203580 and BIRB796 essentially reverts the abnormal senescent-like morphology seen in AG03141 WS dermal fibroblasts to that resembling normal dermal fibroblasts (Davis et al. 2005).
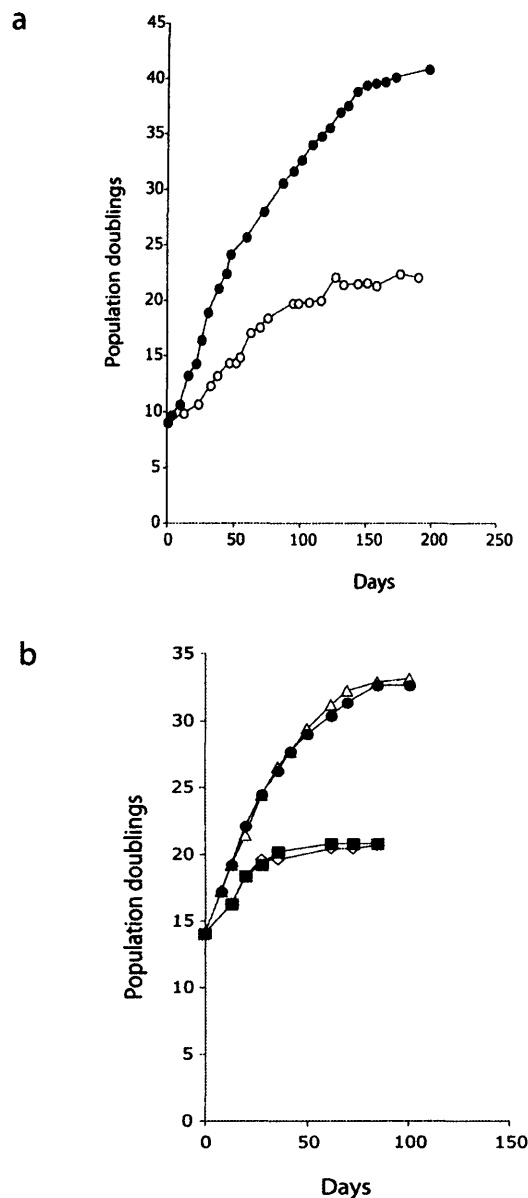
Figure A1. Growth of AG03141(WS) fibroblasts in the presence or absence of p38 inhibitors.

Panel a) SB203580: Open circles are control cells, closed circles are cells treated with SB203580; (b) BIRB796: closed squares and open diamonds are control cells, closed circles and open triangles are BIRB796 treated cells. Growth is measured as cumulative population doublings versus days.

a

b

Brightfield

c

d

phalloidin-
FITC

young control
AG03141 cells

young SB203580 treated
AG03141 cells

e

f

Brightfield

young control
AG03141 cells

young BIRB 796 treated
AG03141 cells
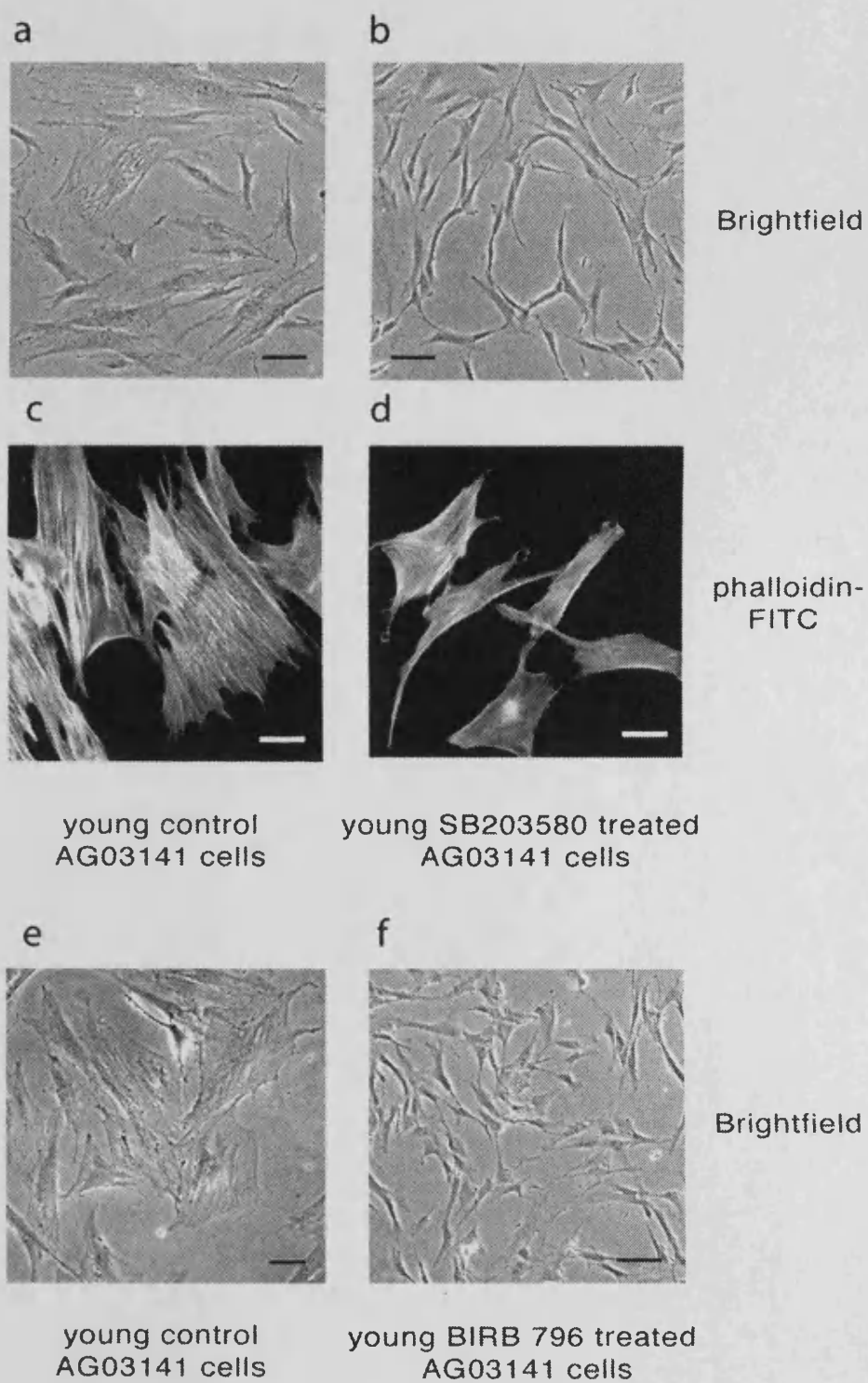
Figure A2. Morphology of AG03141(WS) cells.

Panels a, b, e and f bright field views of AG03141(WS) cells; c and d AG03141(WS) cells stained with phalloidin-FITC. Black bars are 100 μm, white bars are 50 μm.

Appendix B Determination of suitable p38 inhibitor

regimes for cellular growth experiments

B.1 Introduction

All p38 inhibitors show various degrees of cross-kinase specificity, including the inhibition of cell cycle kinases such as cdk2, growth related kinases such as c-Raf1, and other stress-related kinases such as c-Jun (Bain et al. 2007; Godl and Daub 2004). Thus, as these inhibitors are being used to prevent putative stress-induced cellular growth arrest, the ideal inhibitor concentration is the minimum that fully inhibits p38 and that leads to the maximal growth rate of the cells. Thus, a series of titrations were undertaken to determine these parameters for each drug of choice.

Please note that all data in this appendix have been provided courtesy of my supervisor Dr T. Davis and are shown here only as supporting data.

B.2   p38 inhibitor titrations

The cells used for the drug titrations were human HCA2 neonatal dermal foreskin fibroblasts immortalised by ectopic expression of the human telomerase reverse transcriptase protein subunit hTert (Wyllie et al. 2000). These cells were used simply as a model test bed for the efficacy of p38 inhibitors to inhibit anisomycin-induced p38 activity due to ease of use (Bagley et al. 2010). Cells were seeded onto 100 mm dishes in EMEM (composition described in Methods section) and allowed to settle for 24 hours at 37°C. The medium was replaced with EMEM containing a p38 inhibitor at various concentrations for 2 hours at 37°C after which the cells were exposed to anisomycin at 30 μM for 45 minutes. Controls were either DMSO alone or DMSO with anisomycin treatment. The cells were then collected and protein extracted as described (Bagley et al. 2006). The levels of HSP27 and p-HSP27 were determined by ELISA assay as described (Bagley et al. 2007).

Figure B1 shows that the IC_{50} for SB203580 inhibition of p38 (as measured by inhibition of HSP27 phosphorylation) is approximately 20 nM, and the maximal inhibition is at 1.0 µM. BIRB796 (Regan et al. 2002) was synthesised for the current studies in the Cardiff University School of Chemistry (Bagley et al. 2006) and has an IC_{50} less than 10 nM with maximal p38 inhibition achieved at 10 nM (Figure B2). VX745 (Natarajan and Doherty 2005) was synthesised for the current studies in the Cardiff University School of Chemistry (Bagley et al. 2007), and has an IC_{50} between 10 nM and 100 nM with maximal inhibition at 500 nM (Figure B3). All these values are in agreement with the published literature for *in vivo* cellular assays (Goldstein and Gabriel 2005; Regan et al. 2002).

B.3   Effects of p38 inhibitors on the growth rate of WS AG03141[hTert] cells

To determine the effects of these inhibitors on cellular growth hTert-immortalised AG03141(WS) cells were used (Wyllie et al. 2000). These cells retain several of the characteristics of primary WS cells in that they grow slowly and have an altered enlarged cellular morphology with extensive F-actin stress fibres, features which are corrected by growth in SB203580 (Davis et al. 2005; Davis et al. 2006). Cells were grown in EMEM containing inhibitors at various concentrations for a total of 42 days at 37°C to determine growth rate. The medium was changed daily with the addition of fresh inhibitor as it has been shown that this is required to attain maximal growth rate (Davis et al. 2005; Davis et al. 2006). Cells were passaged every three to five days (or when the cells reached approximately 75% confluency, whichever was the soonest) and the cells counted. Cumulative population doublings were measured as PD = $\log(N_t-N_o)/\log2$, where N_t is number counted and N_o is number seeded.

Figure B4 shows the effects of increasing inhibitor concentration on the growth rate of the cells. For SB203580 the maximal growth rate (PDs/day) is achieved at 2.5 µM, for BIRB796 it is 2.5 µM, and for VX745 it is 500 nM. Thus these drug concentrations were chosen for the growth regimes of the progeroid cells. Note that for both SB203580 and BIRB796 the maximal growth rate is achieved at a concentration well above that required to maximally inhibit p38.

## B.4   Time courses for each p38 inhibitor in AG03141(WS)^{hTert} cells

Finally, it was established that these drug concentrations remain fully active as p38 inhibitors over the 24-hour period between medium replacements (Figure B5). AG03141(WS)^{hTert} cells were plated onto 100 mm dishes in EMEM and left for 24 hours to settle. Then the medium was replaced with EMEM containing SB203580, BIRB796 or VX745 at the chosen concentration and the cells incubated at 37°C for between 2 and 24 hours, after which the cells were stimulated with anisomycin at 30 µM for 45 minutes. Controls were either DMSO alone or DMSO with anisomycin treatment. The cells were then collected and protein extracted as described (Bagley et al. 2006). The levels of HSP27 and p-HSP27 were determined by ELISA assay as described (Bagley et al. 2007). The data in Figure B5 shows that the p38 inhibitors remain fully capable of inhibiting the anisomycin induced p38 activity after 24 hours. Thus a re-feeding time of 24 hours was chosen for the growth experiments.

B.5   SB203580 and BIRB 796 inhibit JNK activity.

Many p38 inhibitors also inhibit the related stress-induced c-Jun kinases JNK1 and JNK2, at least *in vitro* (Godl and Daub 2004). Thus the ability of SB203580, BIRB796 and VX745 to inhibit total JNK activity in human cells was assessed in anisomycin treated HCA2^{hTert} cells as described for p38 activity (Section B2). Cells were seeded onto 100 mm dishes in EMEM and allowed to settle for 24 hours at 37°C. The medium was replaced with EMEM containing a p38 inhibitor at various concentrations for 2 hours at 37°C after which the cells were exposed to anisomycin at 30 µM for 45 minutes. Controls were either DMSO alone or DMSO with anisomycin treatment. The cells were then collected and protein extracted as described. The levels of c-Jun and phospho(S63)c-Jun were determined by ELISA assay as described (Bagley et al. 2010). Figure B6 shows the ratio of p-c-Jun/c-Jun for each of the three p38 inhibitors. As can be seen, VX745 has no inhibitory activity for JNK1/2 as the ratio of p-c-Jun/c-Jun in anisomycin treated cells does not increase with increasing VX745 concentration. In contrast, BIRB796 significantly inhibits the JNKs above 10 µM but not significantly

at 2.5 µM, whilst SB203580 may inhibit cellular JNK1/2 at concentrations >25 µM (Bagley et al. 2010). As these ELISAs are measuring the JNK1/2 substrate c-Jun these data do not rule out the possibility that these inhibitors inhibit one of the JNKs but not the other.

p38 inhibitor SB203580
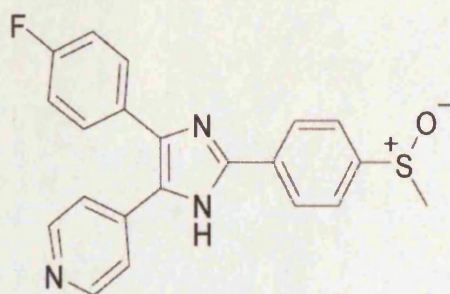
4-(4-Fluorophenyl)-2-(4-methylsulfonylphenyl)-5-(4-pyridyl)-1*H*-imidazole
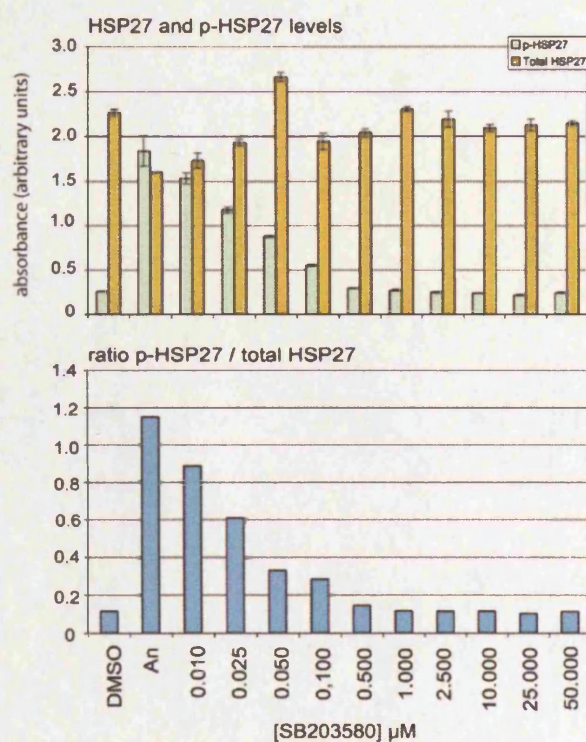
Figure B1. Titration of p38 inhibitor SB203580 in HCA2[hTert] cells.

The top panels are HSP27 and p-HSP27 protein levels, the bottom panels are the ratio of the phosphorylated protein to total protein. Controls were DMSO treated cells (DMSO), and anisomycin stimulated DMSO treated cells (An). 0.0010 to 50.000 are cells treated with SB203580 from 10 nM to 50 μM.

p38 inhibitor BIRB 796
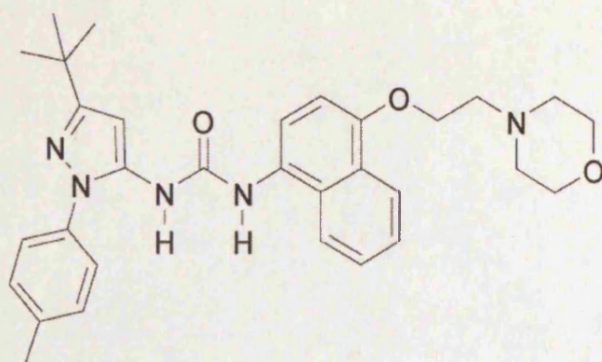
1-[3-*tert*-Butyl-1-*p*-tolyl-1*H*-pyrazol-5-yl]-3-[4-(2-morpholin-4-yl-ethoxy)naphthalen-1-yl]urea

Regan *et al.*, (2002) *J. Med. Chem.* **45**: 2994-3008
Data on current synthesis from Bagley *et al.*, (2006) *Org. Biomol. Chem.* **4**: 4158-4164
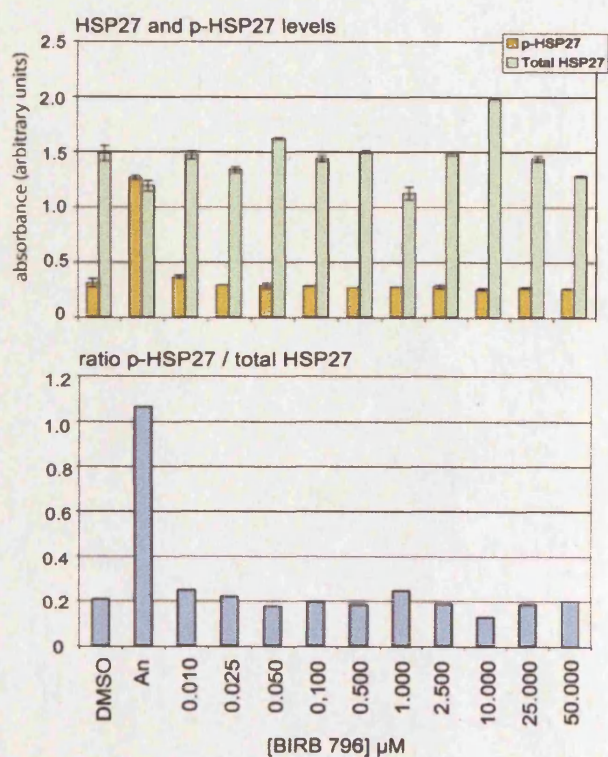
Figure B2. Titration of p38 inhibitor BIRB796 in HCA2[hTERT] cells.

Panels are as in Figure B1.

260

p38 inhibitor VX-745
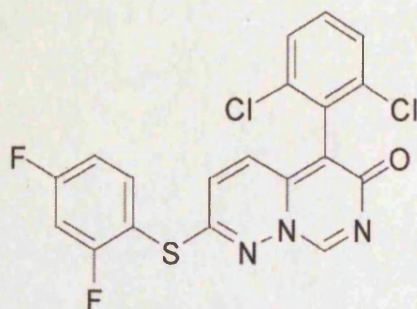
5-(2,6-Dichlorophenyl)-2-(2,4-difluorophenylthio)-6H-pyrimido[1,6-b]pyridazin-6-one

Natarajan *et al.*, (2005) *Curr. Top. Med. Chem.* **5**: 987-1003
Data on current synthesis from Bagley *et al.*, (2007) *Bioorg. Med. Chem. Lett.* **17**: 5107-5110
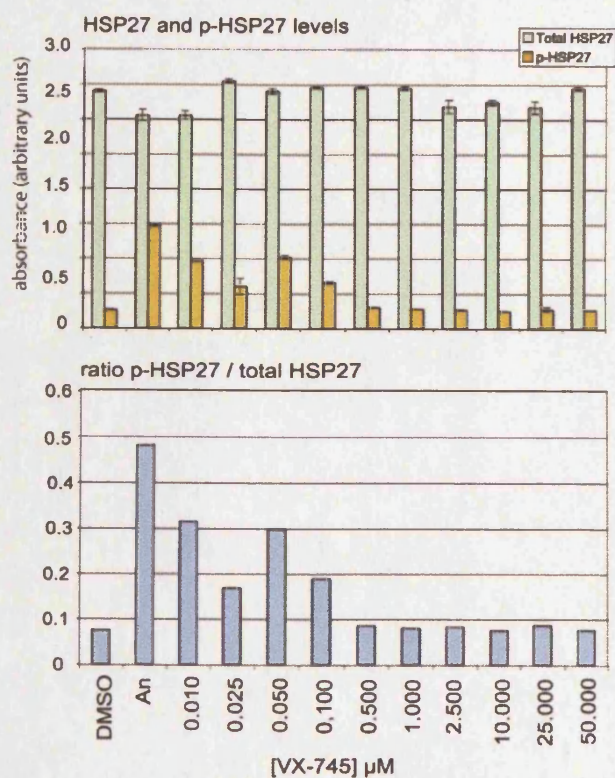
Figure B3. Titration of p38 inhibitor VX745 in HCA2[hTERT] cells.

Panels are as in Figure B1.
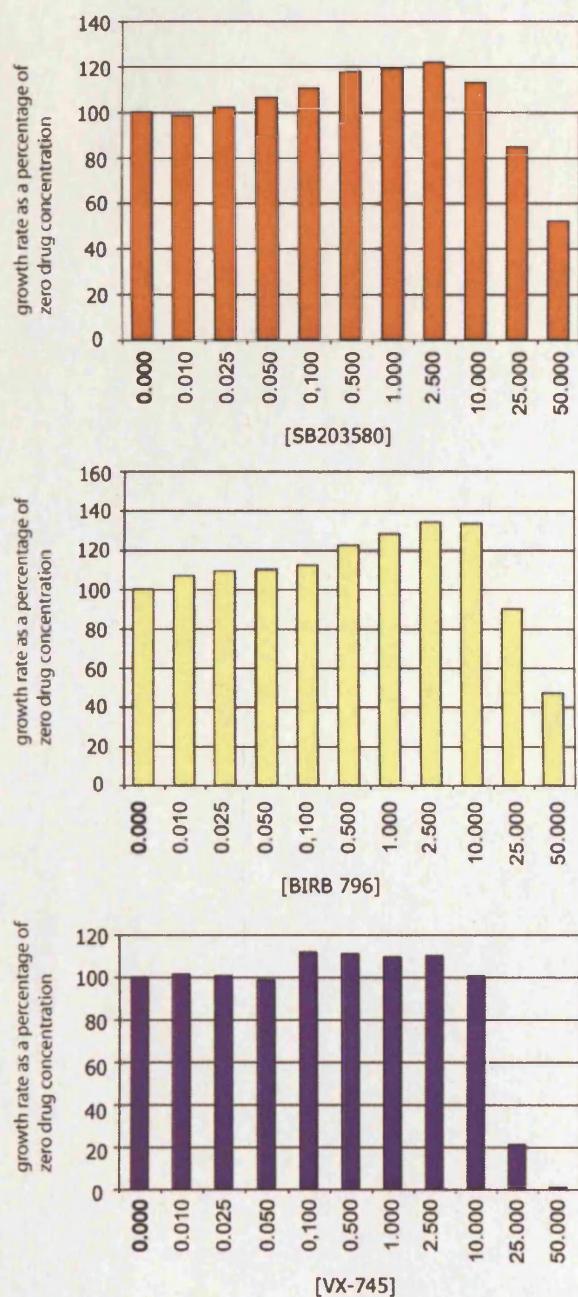
Figure B4. Growth rates of AG3141^{hTERT}(WS) cells treated with p38 inhibitors.

Growth rates are plotted as a percentage of the growth rate in the absence of p38 inhibitor. 0.000 are cells treated only with DMSO (0.1%), 0.010 to 50.000 are cells treated with p38 inhibitors from 10 nM to 50 µM.
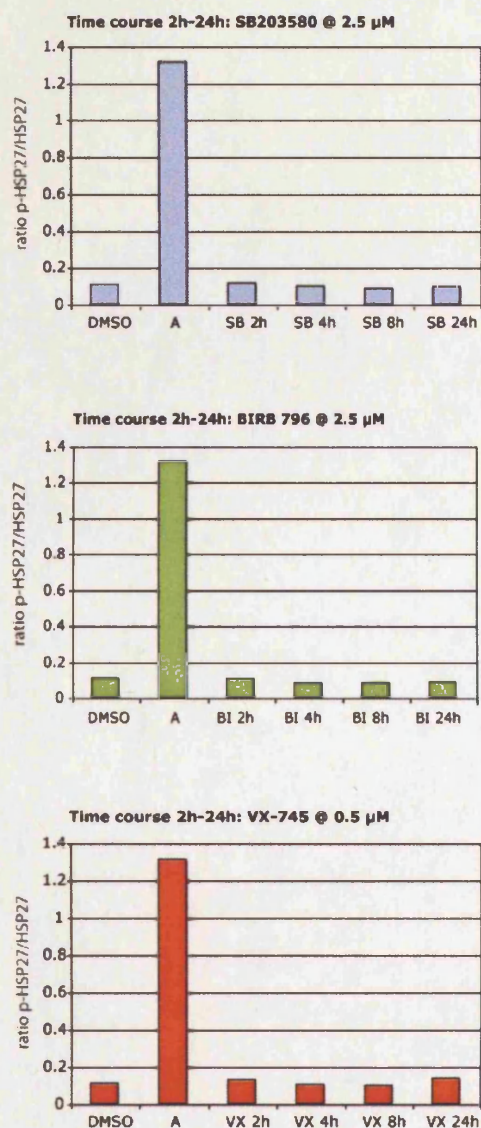
Figure B5. Time courses for activity of p38 inhibitors in AG03141^{hTERT}(WS) cells.

The ratio of p-HSP27/HSP27 is plotted against time of incubation prior to anisomycin stimulation. Control is DMSO only and An = Anisomycin stimulation only. The drug concentration used is given above each panel and the times of incubation are given below the panels.

263
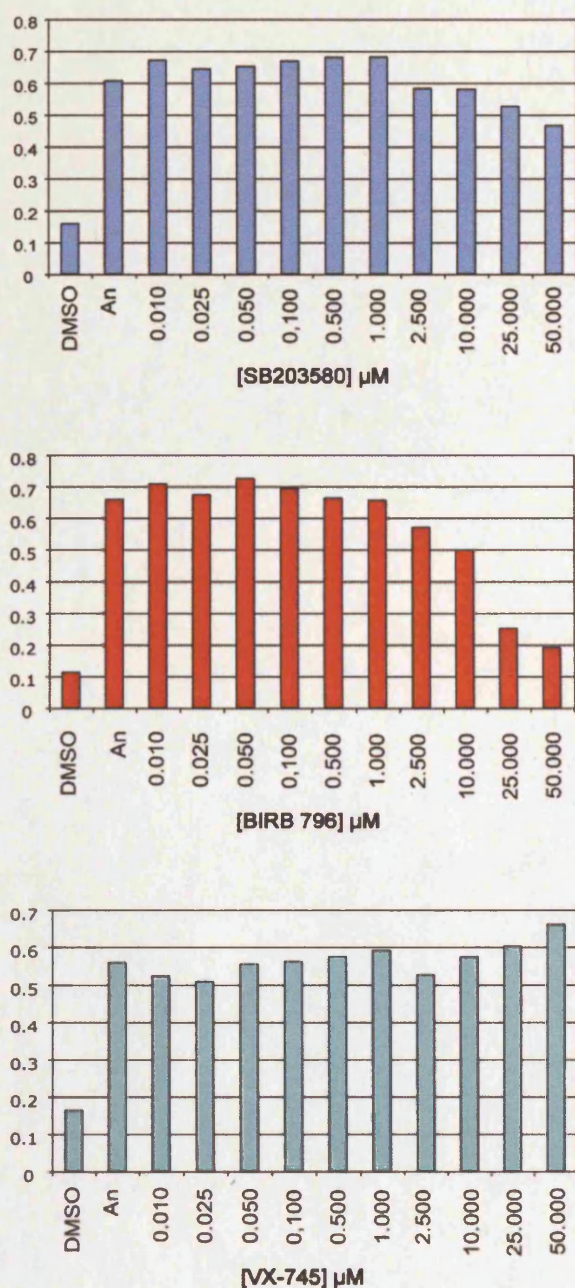
Figure B6. Effects of p38 inhibitors on total JNK activity in HCA2^{hTERT} cells.

Panels are the ratio of p-c-Jun/c-Jun. Controls were DMSO treated cells (DMSO), and anisomycin stimulated DMSO treated cells (An). 0.010 to 50.000 are cells treated with p38 inhibitors from 10 nM to 50 μM.

264

References

Abou-Zahr, F. et al. 1999. Normal expression of the Fanconi anemia proteins FAA and FAC and sensitivity to mitomycin C in two patients with Seckel syndrome. *Am J Med Genet* 83(5), pp. 388-391.

Abraham, R. T. 2001. Cell cycle checkpoint signaling through the ATM and ATR kinases. *Genes Dev* 15(17), pp. 2177-2196.

Absher, P. M. and Absher, R. G. 1976. Clonal variation and aging of diploid fibroblasts. Cinematographic studies of cell pedigrees. *Exp Cell Res* 103(2), pp. 247-255.

Absher, P. M. et al. 1974. Genealogies of clones of diploid fibroblasts. Cinemicrophotographic observations of cell division patterns in relation to population age. *Exp Cell Res* 88(1), pp. 95-104.

Aebi, U. et al. 1986. The nuclear lamina is a meshwork of intermediate-type filaments. *Nature* 323(6088), pp. 560-564.

Agami, R. and Bernards, R. 2000. Distinct initiation and maintenance mechanisms cooperate to induce G1 cell cycle arrest in response to DNA damage. *Cell* 102(1), pp. 55-66.

Agarwal, M. L. et al. 1998. The p53 network. *J Biol Chem* 273(1), pp. 1-4.

Aguilera, A. and Gomez-Gonzalez, B. 2008. Genome instability: a mechanistic view of its causes and consequences. *Nat Rev Genet* 9(3), pp. 204-217.

Alberts, B. et al. 2002. *Molecular biology of the cell*. 4th ed. New York: Garland Science.

Alcorta, D. A. et al. 1996. Involvement of the cyclin-dependent kinase inhibitor p16 (INK4a) in replicative senescence of normal human fibroblasts. *Proc Natl Acad Sci U S A* 93(24), pp. 13742-13747.

Alderton, G. K. et al. 2004. Seckel syndrome exhibits cellular features demonstrating defects in the ATR-signalling pathway. *Hum Mol Genet* 13(24), pp. 3127-3138.

Allen, R. D. 1985. New observations on cell architecture and dynamics by video-enhanced contrast optical microscopy. *Annu Rev Biophys Biophys Chem* 14, pp. 265-290.

Allshire, R. C. et al. 1989. Human telomeres contain at least three types of G-rich repeat distributed non-randomly. *Nucleic Acids Res* 17(12), pp. 4611-4627.

Allsopp, R. C. et al. 1992. Telomere length predicts replicative capacity of human fibroblasts. *Proc Natl Acad Sci U S A* 89(21), pp. 10114-10118.

Alonso, G. et al. 2000. Differential activation of p38 mitogen-activated protein kinase isoforms depending on signal strength. *J Biol Chem* 275(51), pp. 40641-40648.

Ambrosino, C. and Nebreda, A. R. 2001. Cell cycle regulation by p38 MAP kinases. *Biol Cell* 93(1-2), pp. 47-51.

Anderson, G. R. 2001. Genomic instability in cancer. *current science* 81(5).

Anindya, R. et al. 2010. A ubiquitin-binding domain in Cockayne syndrome B required for transcription-coupled nucleotide excision repair. *Mol Cell* 38(5), pp. 637-648.

Antoccia, A. et al. 2006. Nijmegen breakage syndrome and functions of the responsible protein, NBS1. *Genome Dyn* 1, pp. 191-205.

Arellano, M. and Moreno, S. 1997. Regulation of CDK/cyclin complexes during the cell cycle. *Int J Biochem Cell Biol* 29(4), pp. 559-573.

Armanios, M. et al. 2005. Haploinsufficiency of telomerase reverse transcriptase leads to anticipation in autosomal dominant dyskeratosis congenita. *Proc Natl Acad Sci U S A* 102(44), pp. 15960-15964.

Armanios, M. Y. et al. 2007. Telomerase mutations in families with idiopathic pulmonary fibrosis. *N Engl J Med* 356(13), pp. 1317-1326.

Artandi, S. E. 2006. Telomeres, telomerase, and human disease. *N Engl J Med* 355(12), pp. 1195-1197.

Assoian, R. K. and Zhu, X. 1997. Cell anchorage and the cytoskeleton as partners in growth factor dependent cell cycle progression. *Curr Opin Cell Biol* 9(1), pp. 93-98.

Azzarone, B. and Macieira-Coelho, A. 1982. Heterogeneity of the kinetics of proliferation within human skin fibroblastic cell populations. *J Cell Sci* 57, pp. 177-187.

Bachrati, C. Z. and Hickson, I. D. 2003. RecQ helicases: suppressors of tumorigenesis and premature aging. *Biochem J* 374(Pt 3), pp. 577-606.

Bagley, M. C. et al. 2007. Rapid synthesis of VX-745: p38 MAP kinase inhibition in Werner syndrome cells. *Bioorg Med Chem Lett* 17(18), pp. 5107-5110.

266

Bagley, M. C. et al. 2006. Microwave-assisted synthesis of N-pyrazole ureas and the p38alpha inhibitor BIRB 796 for study into accelerated cell ageing. *Org Biomol Chem* 4(22), pp. 4158-4164.

Bagley, M. C. et al. 2010. Synthesis of the highly selective p38 MAPK inhibitor UR13756 for possible therapeutic use in Werner syndrome. *Future Med Chem* 2(2), pp. 193-201.

Bain, J. et al. 2007. The selectivity of protein kinase inhibitors: a further update. *Biochem J* 408(3), pp. 297-315.

Baird, D. M. et al. 2004. Normal telomere erosion rates at the single cell level in Werner syndrome fibroblast cells. *Hum Mol Genet* 13(14), pp. 1515-1524.

Baker, P. B. et al. 1981. Cardiovascular abnormalities in progeria. Case report and review of the literature. *Arch Pathol Lab Med* 105(7), pp. 384-386.

Balin, A. K. et al. 1977. The effect of oxygen and vitamin E on the lifespan of human diploid cells in vitro. *J Cell Biol* 74(1), pp. 58-67.

Bamezai, R. and Shiraishi, Y. 1986. Cell cycle progression and SCE rate of Bloom syndrome cells with/without co-cultivation in the presence/absence of normal cells. *Exp Cell Res* 164(1), pp. 163-173.

Barnes, D. E. et al. 1998. Targeted disruption of the gene encoding DNA ligase IV leads to lethality in embryonic mice. *Curr Biol* 8(25), pp. 1395-1398.

Barnouin, K. et al. 2002. H2O2 induces a transient multi-phase cell cycle arrest in mouse fibroblasts through modulating cyclin D and p21Cip1 expression. *J Biol Chem* 277(16), pp. 13761-13770.

Beausejour, C. M. et al. 2003. Reversal of human cellular senescence: roles of the p53 and p16 pathways. *EMBO J* 22(16), pp. 4212-4222.

Ben-Omran, T. I. et al. 2005. A patient with mutations in DNA Ligase IV: clinical features and overlap with Nijmegen breakage syndrome. *Am J Med Genet A* 137A(3), pp. 283-287.

Ben-Porath, I. and Weinberg, R. A. 2005. The signals and pathways activating cellular senescence. *Int J Biochem Cell Biol* 37(5), pp. 961-976.

Benndorf, R. et al. 1994. Phosphorylation and supramolecular organization of murine small heat shock protein HSP25 abolish its actin polymerization-inhibiting activity. *J Biol Chem* 269(32), pp. 20780-20784.

Bessler, M. et al. 2007. Dysfunctional telomeres and dyskeratosis congenita. *Haematologica* 92(8), pp. 1009-1012.

Bladier, C. et al. 1997. Response of a primary human fibroblast cell line to H2O2: senescence-like growth arrest or apoptosis? *Cell Growth Differ* 8(5), pp. 589-598.

Blander, G. et al. 2003. Superoxide dismutase 1 knock-down induces senescence in human fibroblasts. *J Biol Chem* 278(40), pp. 38966-38969.

Blander, G. et al. 1999. Physical and functional interaction between p53 and the Werner's syndrome protein. *J Biol Chem* 274(41), pp. 29463-29469.

Blasco, M. A. 2003. Mammalian telomeres and telomerase: why they matter for cancer and aging. *Eur J Cell Biol* 82(9), pp. 441-446.

Bobabilla-Morales, L. et al. 2003. Chromosome instability induced in vitro with mitomycin C in five Seckel syndrome patients. *Am J Med Genet A* 123A(2), pp. 148-152.

Bode, A. M. and Dong, Z. 2007. The functional contrariety of JNK. *Mol Carcinog* 46(8), pp. 591-598.

Boder, E. and Sedgwick, R. P. 1958. Ataxia-telangiectasia; a familial syndrome of progressive cerebellar ataxia, oculocutaneous telangiectasia and frequent pulmonary infection. *Pediatrics* 21(4), pp. 526-554.

Bodnar, A. G. et al. 1998. Extension of life-span by introduction of telomerase into normal human cells. *Science* 279(5349), pp. 349-352.

Boldt, S. et al. 2002. The role of MAPK pathways in the action of chemotherapeutic drugs. *Carcinogenesis* 23(11), pp. 1831-1838.

Bond, J. A. et al. 1994. Escape from senescence in human diploid fibroblasts induced directly by mutant p53. *Oncogene* 9(7), pp. 1885-1889.

Borgne, A. and Meijer, L. 1996. Sequential dephosphorylation of p34(cdc2) on Thr-14 and Tyr-15 at the prophase/metaphase transition. *J Biol Chem* 271(44), pp. 27847-27854.

Brack, C. et al. 2000. EMBO WORKSHOP REPORT: Molecular and cellular gerontology Serpiano, Switzerland, September 18-22, 1999. *EMBO J* 19(9), pp. 1929-1934.

Bragado, P. et al. 2007. Apoptosis by cisplatin requires p53 mediated p38alpha MAPK activation through ROS generation. *Apoptosis* 12(9), pp. 1733-1742.

Braig, M. et al. 2005. Oncogene-induced senescence as an initial barrier in lymphoma development. *Nature* 436(7051), pp. 660-665.

Brancho, D. et al. 2003. Mechanism of p38 MAP kinase activation in vivo. *Genes Dev* 17(16), pp. 1969-1978.

Brandes, D. et al. 1972. Ultrastructural and cytochemical changes in cultured human lung cells. *J Ultrastruct Res* 39(5), pp. 465-483.

Bridger, J. M. and Kill, I. R. 2004. Aging of Hutchinson-Gilford progeria syndrome fibroblasts is characterised by hyperproliferation and increased apoptosis. *Exp Gerontol* 39(5), pp. 717-724.

Brosh, R. M., Jr. et al. 2002. Biochemical characterization of the DNA substrate specificity of Werner syndrome helicase. *J Biol Chem* 277(26), pp. 23236-23245.

Brown, J. P. et al. 1997. Bypass of senescence after disruption of p21CIP1/WAF1 gene in normal diploid human fibroblasts. *Science* 277(5327), pp. 831-834.

Brown, W. T. 1992. Progeria: a human-disease model of accelerated aging. *Am J Clin Nutr* 55(6 Suppl), pp. 1222S-1224S.

Brugarolas, J. et al. 1999. Inhibition of cyclin-dependent kinase 2 by p21 is necessary for retinoblastoma protein-mediated G1 arrest after gamma-irradiation. *Proc Natl Acad Sci U S A* 96(3), pp. 1002-1007.

Buda, F. et al. 2003. O2 evolution in the Fenton reaction. *Chemistry* 9(14), pp. 3436-3444.

Bulavin, D. V. et al. 2002. p38 and Chk1 kinases: different conductors for the G(2)/M checkpoint symphony. *Curr Opin Genet Dev* 12(1), pp. 92-97.

Bulavin, D. V. and Fornace, A. J., Jr. 2004. p38 MAP kinase's emerging role as a tumor suppressor. *Adv Cancer Res* 92, pp. 95-118.

Bulavin, D. V. et al. 2001. Initiation of a G2/M checkpoint after ultraviolet radiation requires p38 kinase. *Nature* 411(6833), pp. 102-107.

Bulavin, D. V. et al. 2003. Loss of oncogenic H-ras-induced cell cycle arrest and p38 mitogen-activated protein kinase activation by disruption of Gadd45a. *Mol Cell Biol* 23(11), pp. 3859-3871.

Bulavin, D. V. et al. 2004. Inactivation of the Wip1 phosphatase inhibits mammary tumorigenesis through p38 MAPK-mediated activation of the p16(Ink4a)-p19(Arf) pathway. *Nat Genet* 36(4), pp. 343-350.

Bulavin, D. V. et al. 1999. Phosphorylation of human p53 by p38 kinase coordinates N-terminal phosphorylation and apoptosis in response to UV radiation. *EMBO J* 18(23), pp. 6845-6854.

Burdon, R. H. et al. 1989. Cell proliferation and oxidative stress. *Free Radic Res Commun* 7(3-6), pp. 149-159.

Burks, L. M. et al. 2007. Nuclear import and retention domains in the amino terminus of RECQL4. *Gene* 391(1-2), pp. 26-38.

Burton, D. G. 2009. Cellular senescence, ageing and disease. *Age (Dordr)* 31(1), pp. 1-9.

Burton, D. G. et al. 2005. Bridging the gap: ageing, pharmacokinetics and pharmacodynamics. *J Pharm Pharmacol* 57(6), pp. 671-679.

Burton, D. G. et al. 2007. Cyclin D1 overexpression permits the reproducible detection of senescent human vascular smooth muscle cells. *Ann N Y Acad Sci* 1119, pp. 20-31.

Buscemi, G. et al. 2001. Chk2 activation dependence on Nbs1 after DNA damage. *Mol Cell Biol* 21(15), pp. 5214-5222.

Cabral, R. E. et al. 2008. Identification of new RECQL4 mutations in Caucasian Rothmund-Thomson patients and analysis of sensitivity to a wide range of genotoxic agents. *Mutat Res* 643(1-2), pp. 41-47.

Campisi, J. 1997a. Aging and cancer: the double-edged sword of replicative senescence. *J Am Geriatr Soc* 45(4), pp. 482-488.

Campisi, J. 1997b. The biology of replicative senescence. *Eur J Cancer* 33(5), pp. 703-709.

Campisi, J. 1998. The role of cellular senescence in skin aging. *J Investig Dermatol Symp Proc* 3(1), pp. 1-5.

Campisi, J. 1999. Replicative senescence and immortalization. In: Stein, G.S. et al. eds. *The molecular basis of cell cycle and growth.* New York: Wiley-Liss, pp. 348-373.

Campisi, J. 2001. Cellular senescence as a tumor-suppressor mechanism. *Trends Cell Biol* 11(11), pp. S27-31.

Campisi, J. 2005. Senescent cells, tumor suppression, and organismal aging: good citizens, bad neighbors. *Cell* 120(4), pp. 513-522.

Campisi, J. and d'Adda di Fagagna, F. 2007. Cellular senescence: when bad things happen to good cells. *Nat Rev Mol Cell Biol* 8(9), pp. 729-740.

Cano, E. et al. 1994. Anisomycin-activated protein kinases p45 and p55 but not mitogen-activated protein kinases ERK-1 and -2 are implicated in the induction of c-fos and c-jun. *Mol Cell Biol* 14(11), pp. 7352-7362.

Cao, H. et al. 2004. CKN1 (MIM 216400): mutations in Cockayne syndrome type A and a new common polymorphism. *J Hum Genet* 49(1), pp. 61-63.

Capell, B. C. et al. 2009. From the rarest to the most common: insights from progeroid syndromes into skin cancer and aging. *J Invest Dermatol* 129(10), pp. 2340-2350.

Capp, C. et al. 2009. Drosophila RecQ4 has a 3'-5' DNA helicase activity that is essential for viability. *J Biol Chem* 284(45), pp. 30845-30852.

Capper, R. et al. 2007. The nature of telomere fusion and a definition of the critical telomere length in human cells. *Genes Dev* 21(19), pp. 2495-2508.

Carnero, A. and Hannon, G. J. 1998. The INK4 family of CDK inhibitors. *Curr Top Microbiol Immunol* 227, pp. 43-55.

Carney, J. P. et al. 1998. The hMre11/hRad50 protein complex and Nijmegen breakage syndrome: linkage of double-strand break repair to the cellular DNA damage response. *Cell* 93(3), pp. 477-486.

Carter, S. K. 1975. Adriamycin-a review. *J Natl Cancer Inst* 55(6), pp. 1265-1274.

Casanovas, O. et al. 2000. Osmotic stress regulates the stability of cyclin D1 in a p38SAPK2-dependent manner. *J Biol Chem* 275(45), pp. 35091-35097.

Casper, A. M. et al. 2004. Chromosomal instability at common fragile sites in Seckel syndrome. *Am J Hum Genet* 75(4), pp. 654-660.

Casper, A. M. et al. 2002. ATR regulates fragile site stability. *Cell* 111(6), pp. 779-789.

Castro, P. et al. 2003. Cellular senescence in the pathogenesis of benign prostatic hyperplasia. *Prostate* 55(1), pp. 30-38.

Cervenka, J. et al. 1979. Seckel's dwarfism: analysis of chromosome breakage and sister chromatid exchanges. *Am J Dis Child* 133(5), pp. 555-556.

Chaganti, R. S. et al. 1974. A manyfold increase in sister chromatid exchanges in Bloom's syndrome lymphocytes. *Proc Natl Acad Sci U S A* 71(11), pp. 4508-4512.

Chang, B. D. et al. 1999. Role of p53 and p21waf1/cip1 in senescence-like terminal proliferation arrest induced in human tumor cells by chemotherapeutic drugs. *Oncogene* 18(34), pp. 4808-4818.

Chang, E. and Harley, C. B. 1995. Telomere length and replicative aging in human vascular tissues. *Proc Natl Acad Sci U S A* 92(24), pp. 11190-11194.

Chang, S. et al. 2004. Essential role of limiting telomeres in the pathogenesis of Werner syndrome. *Nat Genet* 36(8), pp. 877-882.

Chatgilialoglu, C. and O'Neill, P. 2001. Free radicals associated with DNA damage. *Exp Gerontol* 36(9), pp. 1459-1471.

Chen, J. et al. 1996. Cyclin-binding motifs are essential for the function of p21CIP1. *Mol Cell Biol* 16(9), pp. 4673-4682.

Chen, J. H. et al. 2007. DNA damage, cellular senescence and organismal ageing: causal or correlative? *Nucleic Acids Res* 35(22), pp. 7417-7428.

Chen, J. L. and Greider, C. W. 2004. Telomerase RNA structure and function: implications for dyskeratosis congenita. *Trends Biochem Sci* 29(4), pp. 183-192.

Chen, Q. and Ames, B. N. 1994. Senescence-like growth arrest induced by hydrogen peroxide in human diploid fibroblast F65 cells. *Proc Natl Acad Sci U S A* 91(10), pp. 4130-4134.

Chen, Q. M. et al. 1998. Molecular analysis of H2O2-induced senescent-like growth arrest in normal human fibroblasts: p53 and Rb control G1 arrest but not cell replication. *Biochem J* 332 (Pt 1), pp. 43-50.

Chen, Z. et al. 2001. MAP kinases. *Chem Rev* 101(8), pp. 2449-2476.

Cheng, W. H. et al. 2004. Linkage between Werner syndrome protein and the Mre11 complex via Nbs1. *J Biol Chem* 279(20), pp. 21169-21176.

Choi, D. et al. 2001. Telomerase expression prevents replicative senescence but does not fully reset mRNA expression patterns in Werner syndrome cell strains. *FASEB J* 15(6), pp. 1014-1020.

Cimprich, K. A. and Cortez, D. 2008. ATR: an essential regulator of genome integrity. *Nat Rev Mol Cell Biol* 9(8), pp. 616-627.

Clarke, A. R. et al. 1994. p53 dependence of early apoptotic and proliferative responses within the mouse intestinal epithelium following gamma-irradiation. *Oncogene* 9(6), pp. 1767-1773.

Coffer, P. J. et al. 1995. UV activation of receptor tyrosine kinase activity. *Oncogene* 11(3), pp. 561-569.

Collado, M. et al. 2005. Tumour biology: senescence in premalignant tumours. *Nature* 436(7051), p. 642.

Comai, L. and Li, B. 2004. The Werner syndrome protein at the crossroads of DNA repair and apoptosis. *Mech Ageing Dev* 125(8), pp. 521-528.

Constantinou, A. et al. 2000. Werner's syndrome protein (WRN) migrates Holliday junctions and co-localizes with RPA upon replication arrest. *EMBO Rep* 1(1), pp. 80-84.

Coppe, J. P. et al. 2006. Secretion of vascular endothelial growth factor by primary human fibroblasts at senescence. *J Biol Chem* 281(40), pp. 29568-29574.

Coppede, F. and Migliore, L. 2010. DNA repair in premature aging disorders and neurodegeneration. *Curr Aging Sci* 3(1), pp. 3-19.

Coulthard, L. R. et al. 2009. p38(MAPK): stress responses from molecular mechanisms to therapeutics. *Trends Mol Med* 15(8), pp. 369-379.

Crabtree, G. R. and Olson, E. N. 2002. NFAT signaling: choreographing the social lives of cells. *Cell* 109 Suppl, pp. S67-79.

Crews, C. M. et al. 1992. The primary structure of MEK, a protein kinase that phosphorylates the ERK gene product. *Science* 258(5081), pp. 478-480.

Cristofalo, V. J. 2005. SA beta Gal staining: biomarker or delusion. *Exp Gerontol* 40(10), pp. 836-838.

Cristofalo, V. J. et al. 1998a. Relationship between donor age and the replicative lifespan of human cells in culture: a reevaluation. *Proc Natl Acad Sci U S A* 95(18), pp. 10614-10619.

Cristofalo, V. J. and Kabakjian, J. 1975. Lysosomal enzymes and aging in vitro: subcellular enzyme distribution and effect of hydrocortisone on cell life-span. *Mech Ageing Dev* 4(1), pp. 19-28.

Cristofalo, V. J. and Kritchevsky, D. 1969. Cell size and nucleic acid content in the diploid human cell line WI-38 during aging. *Med Exp Int J Exp Med* 19(6), pp. 313-320.

Cristofalo, V. J. et al. 1989. Alterations in the responsiveness of senescent cells to growth factors. *J Gerontol* 44(6), pp. 55-62.

Cristofalo, V. J. et al. 1998b. Age-dependent modifications of gene expression in human fibroblasts. *Crit Rev Eukaryot Gene Expr* 8(1), pp. 43-80.

Cuenda, A. and Rousseau, S. 2007. p38 MAP-kinases pathway regulation, function and role in human diseases. *Biochim Biophys Acta* 1773(8), pp. 1358-1375.

D'Amours, D. and Jackson, S. P. 2002. The Mre11 complex: at the crossroads of dna repair and checkpoint signalling. *Nat Rev Mol Cell Biol* 3(5), pp. 317-327.

Dahl, K. N. et al. 2006. Distinct structural and mechanical properties of the nuclear lamina in Hutchinson-Gilford progeria syndrome. *Proc Natl Acad Sci U S A* 103(27), pp. 10271-10276.

Davidson, H. R. and Connor, J. M. 1988. Dyskeratosis congenita. *J Med Genet* 25(12), pp. 843-846.

Davis, R. J. 2000. Signal transduction by the JNK group of MAP kinases. *Cell* 103(2), pp. 239-252.

Davis, T. et al. 2010. Evaluating the role of p38 MAP kinase in growth of Werner syndrome fibroblasts. *Ann N Y Acad Sci* 1197, pp. 45-48.

Davis, T. et al. 2005. Prevention of accelerated cell aging in Werner syndrome using a p38 mitogen-activated protein kinase inhibitor. *J Gerontol A Biol Sci Med Sci* 60(11), pp. 1386-1393.

Davis, T. et al. 2006. Prevention of accelerated cell aging in the Werner syndrome. *Ann N Y Acad Sci* 1067, pp. 243-247.

Davis, T. and Kipling, D. 2009. Assessing the role of stress signalling via p38 MAP kinase in the premature senescence of ataxia telangiectasia and Werner syndrome fibroblasts. *Biogerontology* 10(3), pp. 253-266.

Davis, T. et al. 2007. The role of cellular senescence in Werner syndrome: toward therapeutic intervention in human premature aging. *Ann N Y Acad Sci* 1100, pp. 455-469.

Davoli, T. et al. 2010. Persistent telomere damage induces bypass of mitosis and tetraploidy. *Cell* 141(1), pp. 81-93.

De Bont, R. and van Larebeke, N. 2004. Endogenous DNA damage in humans: a review of quantitative data. *Mutagenesis* 19(3), pp. 169-185.

de Lange, T. 2005. Shelterin: the protein complex that shapes and safeguards human telomeres. *Genes Dev* 19(18), pp. 2100-2110.

de Lange, T. et al. 1990. Structure and variability of human chromosome ends. *Mol Cell Biol* 10(2), pp. 518-527.

De Sandre-Giovannoli, A. et al. 2003. Lamin a truncation in Hutchinson-Gilford progeria. *Science* 300(5628), p. 2055.

de Waard, H. et al. 2004. Different effects of CSA and CSB deficiency on sensitivity to oxidative DNA damage. *Mol Cell Biol* 24(18), pp. 7941-7948.

Debacq-Chainiaux, F. et al. 2009. Protocols to detect senescence-associated beta-galactosidase (SA-betagal) activity, a biomarker of senescent cells in culture and in vivo. *Nat Protoc* 4(12), pp. 1798-1806.

Deng, Q. et al. 2004. High intensity ras signaling induces premature senescence by activating p38 pathway in primary human fibroblasts. *J Biol Chem* 279(2), pp. 1050-1059.

Der Kaloustian, V. M. et al. 1996. Possible new variant of Nijmegen breakage syndrome. *Am J Med Genet* 65(1), pp. 21-26.

Der Kaloustian, V. M. et al. 1990. Clonal lines of aneuploid cells in Rothmund-Thomson syndrome. *Am J Med Genet* 37(3), pp. 336-339.

Derijard, B. et al. 1994. JNK1: a protein kinase stimulated by UV light and Ha-Ras that binds and phosphorylates the c-Jun activation domain. *Cell* 76(6), pp. 1025-1037.

Desai-Mehta, A. et al. 2001. Distinct functional domains of nibrin mediate Mre11 binding, focus formation, and nuclear localization. *Mol Cell Biol* 21(6), pp. 2184-2191.

Devault, A. et al. 1991. Concerted roles of cyclin A, cdc25+ mitotic inducer, and type 2A phosphatase in activating the cyclin B/cdc2 protein kinase at the G2/M phase transition. *Cold Spring Harb Symp Quant Biol* 56, pp. 503-513.

Devriendt, K. et al. 1997. Skewed X-chromosome inactivation in female carriers of dyskeratosis congenita. *Am J Hum Genet* 60(3), pp. 581-587.

Di Leonardo, A. et al. 1994. DNA damage triggers a prolonged p53-dependent G1 arrest and long-term induction of Cip1 in normal human fibroblasts. *Genes Dev* 8(21), pp. 2540-2551.

Digweed, M. et al. 1999. Nijmegen breakage syndrome: consequences of defective DNA double strand break repair. *Bioessays* 21(8), pp. 649-656.

Dimri, G. P. et al. 1995. A biomarker that identifies senescent human cells in culture and in aging skin in vivo. *Proc Natl Acad Sci U S A* 92(20), pp. 9363-9367.

Dokal, I. 1996. Dyskeratosis congenita: an inherited bone marrow failure syndrome. *Br J Haematol* 92(4), pp. 775-779.

Dokal, I. 2000. Dyskeratosis congenita in all its forms. *Br J Haematol* 110(4), pp. 768-779.

Dokal, I. et al. 1992. Dyskeratosis congenita fibroblasts are abnormal and have unbalanced chromosomal rearrangements. *Blood* 80(12), pp. 3090-3096.

Drachtman, R. A. and Alter, B. P. 1992. Dyskeratosis congenita: clinical and genetic heterogeneity. Report of a new case and review of the literature. *Am J Pediatr Hematol Oncol* 14(4), pp. 297-304.

Drachtman, R. A. and Alter, B. P. 1995. Dyskeratosis congenita. *Dermatol Clin* 13(1), pp. 33-39.

Drapkin, R. et al. 1996. Human cyclin-dependent kinase-activating kinase exists in three distinct complexes. *Proc Natl Acad Sci U S A* 93(13), pp. 6488-6493.

Draviam, V. M. et al. 2004. Chromosome segregation and genomic stability. *Curr Opin Genet Dev* 14(2), pp. 120-125.

Drayton, S. and Peters, G. 2002. Immortalisation and transformation revisited. *Curr Opin Genet Dev* 12(1), pp. 98-104.

Duan, J. et al. 2005. Irreversible cellular senescence induced by prolonged exposure to H2O2 involves DNA-damage-and-repair genes and telomere shortening. *Int J Biochem Cell Biol* 37(7), pp. 1407-1420.

Duker, N. J. 2002. Chromosome breakage syndromes and cancer. *Am J Med Genet* 115(3), pp. 125-129.

el-Deiry, W. S. et al. 1993. WAF1, a potential mediator of p53 tumor suppression. *Cell* 75(4), pp. 817-825.

el-Khateeb, M. et al. 1999. Reactions of cisplatin hydrolytes with methionine, cysteine, and plasma ultrafiltrate studied by a combination of HPLC and NMR techniques. *J Inorg Biochem* 77(1-2), pp. 13-21.

Elmore, L. W. et al. 2005. Evasion of a single-step, chemotherapy-induced senescence in breast cancer cells: implications for treatment response. *Clin Cancer Res* 11(7), pp. 2637-2643.

Elmore, L. W. et al. 2002. Adriamycin-induced senescence in breast tumor cells involves functional p53 and telomere dysfunction. *J Biol Chem* 277(38), pp. 35509-35515.

Enslen, H. et al. 1998. Selective activation of p38 mitogen-activated protein (MAP) kinase isoforms by the MAP kinase kinases MKK3 and MKK6. *J Biol Chem* 273(3), pp. 1741-1748.

Epstein, C. J. et al. 1966. Werner's syndrome a review of its symptomatology, natural history, pathologic features, genetics and relationship to the natural aging process. *Medicine (Baltimore)* 45(3), pp. 177-221.

Eriksson, M. et al. 2003. Recurrent de novo point mutations in lamin A cause Hutchinson-Gilford progeria syndrome. *Nature* 423(6937), pp. 293-298.

Errington, R. J. et al. 2005a. Advanced microscopy solutions for monitoring the kinetics and dynamics of drug-DNA targeting in living cells. *Adv Drug Deliv Rev* 57(1), pp. 153-167.

Errington, R. J. et al. 2010. Single cell nanoparticle tracking to model cell cycle dynamics and compartmental inheritance. *Cell Cycle* 9(1), pp. 121-130.

Errington, R. J. et al. 2005b. Time-lapse microscopy approaches to track cell cycle progression at the single-cell level. *Curr Protoc Cytom* Chapter 12, p. Unit 12 14.

Evans, T. et al. 1983. Cyclin: a protein specified by maternal mRNA in sea urchin eggs that is destroyed at each cleavage division. *Cell* 33(2), pp. 389-396.

Eyers, P. A. et al. 1998. Conversion of SB 203580-insensitive MAP kinase family members to drug-sensitive forms by a single amino-acid substitution. *Chem Biol* 5(6), pp. 321-328.

Faivre, L. and Cormier-Daire, V. 2001. Seckel Syndrome. [Online]. Available at.

Faivre, L. et al. 2002. Clinical and genetic heterogeneity of Seckel syndrome. *Am J Med Genet* 112(4), pp. 379-383.

Fan, W. and Luo, J. 2008. RecQ4 facilitates UV light-induced DNA damage repair through interaction with nucleotide excision repair factor xeroderma pigmentosum group A (XPA). *J Biol Chem* 283(43), pp. 29037-29044.

Faragher, R. G. et al. 1993. The gene responsible for Werner syndrome may be a cell division "counting" gene. *Proc Natl Acad Sci U S A* 90(24), pp. 12030-12034.

Faragher, R. G. and Kipling, D. 1998. How might replicative senescence contribute to human ageing? *Bioessays* 20(12), pp. 985-991.

Featherstone, C. and Jackson, S. P. 1998. DNA repair: the Nijmegen breakage syndrome protein. *Curr Biol* 8(17), pp. R622-625.

Feldser, D. M. and Greider, C. W. 2007. Short telomeres limit tumor progression in vivo by inducing senescence. *Cancer Cell* 11(5), pp. 461-469.

Feng, J. et al. 1995. The RNA component of human telomerase. *Science* 269(5228), pp. 1236-1241.

Fernandez-Palazzi, F. et al. 1992. Report on a case of Hutchinson-Gilford progeria, with special reference to orthopedic problems. *Eur J Pediatr Surg* 2(6), pp. 378-382.

Forrester, H. B. et al. 2000. Computerized video time-lapse analysis of apoptosis of REC:Myc cells X-irradiated in different phases of the cell cycle. *Radiat Res* 154(6), pp. 625-639.

Franchitto, A. et al. 2008. Replication fork stalling in WRN-deficient cells is overcome by prompt activation of a MUS81-dependent pathway. *J Cell Biol* 183(2), pp. 241-252.

Frank, K. M. et al. 2000. DNA ligase IV deficiency in mice leads to defective neurogenesis and embryonic lethality via the p53 pathway. *Mol Cell* 5(6), pp. 993-1002.

Franken, N. A. et al. 2006. Clonogenic assay of cells in vitro. *Nat Protoc* 1(5), pp. 2315-2319.

Franklin, T. B. et al. 2005. The role of heat shock proteins Hsp70 and Hsp27 in cellular protection of the central nervous system. *Int J Hyperthermia* 21(5), pp. 379-392.

Freshney, N. W. et al. 1994. Interleukin-1 activates a novel protein kinase cascade that results in the phosphorylation of Hsp27. *Cell* 78(6), pp. 1039-1049.

Friedberg, E. C. 2001. How nucleotide excision repair protects against cancer. *Nat Rev Cancer* 1(1), pp. 22-33.

Friedberg, E. C. et al. 1979. Human diseases associated with DNA repair. *Adv Rad Biol* 8, pp. 85-174.

Friedberg, E. C. et al. 2006. *DNA repair and mutagenesis*. Washington: ASM Press.

Frippiat, C. et al. 2001. Subcytotoxic H2O2 stress triggers a release of transforming growth factor-beta 1, which induces biomarkers of cellular senescence of human diploid fibroblasts. *J Biol Chem* 276(4), pp. 2531-2537.

Frippiat, C. et al. 2002. Signal transduction in H2O2-induced senescence-like phenotype in human diploid fibroblasts. *Free Radic Biol Med* 33(10), pp. 1334-1346.

Frisa, P. S. and Jacobberger, J. W. 2010. Cytometry of chromatin bound Mcm6 and PCNA identifies two states in G1 that are separated functionally by the G1 restriction point. *BMC Cell Biol* 11, p. 26.

Fry, M. and Loeb, L. A. 1999. Human werner syndrome DNA helicase unwinds tetrahelical structures of the fragile X syndrome repeat sequence d(CGG)n. *J Biol Chem* 274(18), pp. 12797-12802.

Fryer, L. G. et al. 2002. Protein kinase inhibitors block the stimulation of the AMP-activated protein kinase by 5-amino-4-imidazolecarboxamide riboside. *FEBS Lett* 531(2), pp. 189-192.

Fujiwara, Y. et al. 1977. A retarded rate of DNA replication and normal level of DNA repair in Werner's syndrome fibroblasts in culture. *J Cell Physiol* 92(3), pp. 365-374.

Fukuchi, K. et al. 1989. Mutator phenotype of Werner syndrome is characterized by extensive deletions. *Proc Natl Acad Sci U S A* 86(15), pp. 5893-5897.

Furth, J. J. 1991. The steady-state levels of type I collagen mRNA are reduced in senescent fibroblasts. *J Gerontol* 46(3), pp. B122-124.

Garcia, C. K. et al. 2007. Human diseases of telomerase dysfunction: insights into tissue aging. *Nucleic Acids Res* 35(22), pp. 7406-7416.

German, J. 1969. Bloom's syndrome. I. Genetical and clinical observations in the first twenty-seven patients. *Am J Hum Genet* 21(2), pp. 196-227.

German, J. and Ellis, N. A. 1998. Bloom syndrome. In: Vogelstein, B. and Kinzler, K.W. eds. *The genetic basis of human cancer.* New York: McGraw-Hill, pp. 301-315.

German, J. et al. 2007. Syndrome-causing mutations of the BLM gene in persons in the Bloom's Syndrome Registry. *Hum Mutat* 28(8), pp. 743-753.

German, J. et al. 1977. Bloom's syndrome. IV. Sister-chromatid exchanges in lymphocytes. *Am J Hum Genet* 29(3), pp. 248-255.

Gilford, H. 1904. Ateleiosis and progeria: continuous youth and premature old age. *British Medical Journal* 2, pp. 914-918.

Girard, F. et al. 1991. Cyclin A is required for the onset of DNA replication in mammalian fibroblasts. *Cell* 67(6), pp. 1169-1179.

Gisselsson, D. et al. 2001. Telomere dysfunction triggers extensive DNA fragmentation and evolution of complex chromosome abnormalities in human malignant tumors. *Proc Natl Acad Sci U S A* 98(22), pp. 12683-12688.

Glotzer, M. et al. 1991. Cyclin is degraded by the ubiquitin pathway. *Nature* 349(6305), pp. 132-138.

Godl, K. and Daub, H. 2004. Proteomic analysis of kinase inhibitor selectivity and function. *Cell Cycle* 3(4), pp. 393-395.

Godl, K. et al. 2003. An efficient proteomics method to identify the cellular targets of protein kinase inhibitors. *Proc Natl Acad Sci U S A* 100(26), pp. 15434-15439.

Goldman, R. D. et al. 2002. Nuclear lamins: building blocks of nuclear architecture. *Genes Dev* 16(5), pp. 533-547.

Goldman, R. D. et al. 2004. Accumulation of mutant lamin A causes progressive changes in nuclear architecture in Hutchinson-Gilford progeria syndrome. *Proc Natl Acad Sci U S A* 101(24), pp. 8963-8968.

Goldstein, D. M. and Gabriel, T. 2005. Pathway to the clinic: inhibition of P38 MAP kinase. A review of ten chemotypes selected for development. *Curr Top Med Chem* 5(10), pp. 1017-1029.

Goldstein, D. M. et al. 2010. Selective p38alpha inhibitors clinically evaluated for the treatment of chronic inflammatory disorders. *J Med Chem* 53(6), pp. 2345-2353.

Goldstein, S. 1979. Studies on age-related diseases in cultured skin fibroblasts. *J Invest Dermatol* 73(1), pp. 19-23.

Goldstein, S. et al. 1978. Chronologic and physiologic age affect replicative life-span of fibroblasts from diabetic, prediabetic, and normal donors. *Science* 199(4330), pp. 781-782.

Goloudina, A. et al. 2003. Regulation of human Cdc25A stability by Serine 75 phosphorylation is not sufficient to activate a S phase checkpoint. *Cell Cycle* 2(5), pp. 473-478.

Gomez del Arco, P. et al. 2000. A role for the p38 MAP kinase pathway in the nuclear shuttling of NFATp. *J Biol Chem* 275(18), pp. 13872-13878.

Gorbunova, V. et al. 2002. Expression of human telomerase (hTERT) does not prevent stress-induced senescence in normal human fibroblasts but protects the cells from stress-induced apoptosis and necrosis. *J Biol Chem* 277(41), pp. 38540-38549.

Goto, M. et al. 1996. Excess of rare cancers in Werner syndrome (adult progeria). *Cancer Epidemiol Biomarkers Prev* 5(4), pp. 239-246.

Graham, F. L. et al. 1977. Characteristics of a human cell line transformed by DNA from human adenovirus type 5. *J Gen Virol* 36(1), pp. 59-74.

Grawunder, U. et al. 1997. Activity of DNA ligase IV stimulated by complex formation with XRCC4 protein in mammalian cells. *Nature* 388(6641), pp. 492-495.

Greenberg, S. B. et al. 1977. Cell size in aging monolayer cultures. *In Vitro* 13(5), pp. 297-300.

Greider, C. W. 1999. Telomeres do D-loop-T-loop. *Cell* 97(4), pp. 419-422.

Greider, C. W. and Blackburn, E. H. 1985. Identification of a specific telomere terminal transferase activity in Tetrahymena extracts. *Cell* 43(2 Pt 1), pp. 405-413.

Griffith, E. et al. 2008. Mutations in pericentrin cause Seckel syndrome with defective ATR-dependent DNA damage signaling. *Nat Genet* 40(2), pp. 232-236.

Groisman, R. et al. 2003. The ubiquitin ligase activity in the DDB2 and CSA complexes is differentially regulated by the COP9 signalosome in response to DNA damage. *Cell* 113(3), pp. 357-367.

Gruenbaum, Y. et al. 2005. The nuclear lamina comes of age. *Nat Rev Mol Cell Biol* 6(1), pp. 21-31.

Guan, K. L. et al. 1994. Growth suppression by p18, a p16INK4/MTS1- and p14INK4B/MTS2-related CDK6 inhibitor, correlates with wild-type pRb function. *Genes Dev* 8(24), pp. 2939-2952.

Guay, J. et al. 1997. Regulation of actin filament dynamics by p38 map kinase-mediated phosphorylation of heat shock protein 27. *J Cell Sci* 110 (Pt 3), pp. 357-368.

Gum, R. J. et al. 1998. Acquisition of sensitivity of stress-activated protein kinases to the p38 inhibitor, SB 203580, by alteration of one or more amino acids within the ATP binding pocket. *J Biol Chem* 273(25), pp. 15605-15610.

Gupta, V. and Kumar, A. 2010. Dyskeratosis congenita. *Adv Exp Med Biol* 685, pp. 215-219.

Halbert, C. L. et al. 1991. The E7 gene of human papillomavirus type 16 is sufficient for immortalization of human epithelial cells. *J Virol* 65(1), pp. 473-478.

Hale, K. K. et al. 1999. Differential expression and activation of p38 mitogen-activated protein kinase alpha, beta, gamma, and delta in inflammatory cell lineages. *J Immunol* 162(7), pp. 4246-4252.

Hall, M. et al. 1995. Evidence for different modes of action of cyclin-dependent kinase inhibitors: p15 and p16 bind to kinases, p21 and p27 bind to cyclins. *Oncogene* 11(8), pp. 1581-1588.

Hall-Jackson, C. A. et al. 1999. Effect of SB 203580 on the activity of c-Raf in vitro and in vivo. *Oncogene* 18(12), pp. 2047-2054.

Han, J. et al. 1994. A MAP kinase targeted by endotoxin and hyperosmolarity in mammalian cells. *Science* 265(5173), pp. 808-811.

Han, J. and Sun, P. 2007. The pathways to tumor suppression via route p38. *Trends Biochem Sci* 32(8), pp. 364-371.

Han, Z. et al. 2002. Role of p21 in apoptosis and senescence of human colon cancer cells treated with camptothecin. *J Biol Chem* 277(19), pp. 17154-17160.

Haq, R. et al. 2002. Constitutive p38HOG mitogen-activated protein kinase activation induces permanent cell cycle arrest and senescence. *Cancer Res* 62(17), pp. 5076-5082.

Harfst, E. et al. 2000. Normal V(D)J recombination in cells from patients with Nijmegen breakage syndrome. *Mol Immunol* 37(15), pp. 915-929.

Harley, C. B. et al. 1990. Telomeres shorten during ageing of human fibroblasts. *Nature* 345(6274), pp. 458-460.

Harper, J. W. et al. 1995. Inhibition of cyclin-dependent kinases by p21. *Mol Biol Cell* 6(4), pp. 387-400.

Hartlerode, A. J. and Scully, R. 2009. Mechanisms of double-strand break repair in somatic mammalian cells. *Biochem J* 423(2), pp. 157-168.

Hartwell, L. H. et al. 2001. *Nobelprize.org* [Online]. Available at: [Accessed:

Hartwell, L. H. and Weinert, T. A. 1989. Checkpoints: controls that ensure the order of cell cycle events. *Science* 246(4930), pp. 629-634.

Havelka, A. M. et al. 2007. Mechanisms of action of DNA-damaging anticancer drugs in treatment of carcinomas: is acute apoptosis an "off-target" effect? *Mini Rev Med Chem* 7(10), pp. 1035-1039.

Hayflick, L. 1965. The Limited in Vitro Lifetime of Human Diploid Cell Strains. *Exp Cell Res* 37, pp. 614-636.

Hayflick, L. and Moorhead, P. S. 1961. The serial cultivation of human diploid cell strains. *Exp Cell Res* 25, pp. 585-621.

Hazzalin, C. A. et al. 1997. Effects of the inhibition of p38/RK MAP kinase on induction of five fos and jun genes by diverse stimuli. *Oncogene* 15(19), pp. 2321-2331.

Heald, R. et al. 1993. Human wee1 maintains mitotic timing by protecting the nucleus from cytoplasmically activated Cdc2 kinase. *Cell* 74(3), pp. 463-474.

Heiss, N. S. et al. 1999. Dyskerin localizes to the nucleolus and its mislocalization is unlikely to play a role in the pathogenesis of dyskeratosis congenita. *Hum Mol Genet* 8(13), pp. 2515-2524.

Heiss, N. S. et al. 1998. X-linked dyskeratosis congenita is caused by mutations in a highly conserved gene with putative nucleolar functions. *Nat Genet* 19(1), pp. 32-38.

Henning, K. A. et al. 1995. The Cockayne syndrome group A gene encodes a WD repeat protein that interacts with CSB protein and a subunit of RNA polymerase II TFIIH. *Cell* 82(4), pp. 555-564.

Herbig, U. et al. 2006. Cellular senescence in aging primates. *Science* 311(5765), p. 1257.

Hermeking, H. et al. 1997. 14-3-3 sigma is a p53-regulated inhibitor of G2/M progression. *Mol Cell* 1(1), pp. 3-11.

Hickson, I. D. 2003. RecQ helicases: caretakers of the genome. *Nat Rev Cancer* 3(3), pp. 169-178.

Hickson, I. D. et al. 2001. Role of the Bloom's syndrome helicase in maintenance of genome stability. *Biochem Soc Trans* 29(Pt 2), pp. 201-204.

Hiel, J. A. et al. 2000. Nijmegen breakage syndrome. The International Nijmegen Breakage Syndrome Study Group. *Arch Dis Child* 82(5), pp. 400-406.

Hirai, H. et al. 1995. Novel INK4 proteins, p19 and p18, are specific inhibitors of the cyclin D-dependent kinases CDK4 and CDK6. *Mol Cell Biol* 15(5), pp. 2672-2681.

Hiyama, H. et al. 1997. Regulated ectopic expression of cyclin D1 induces transcriptional activation of the cdk inhibitor p21 gene without altering cell cycle progression. *Oncogene* 14(21), pp. 2533-2542.

Hoeijmakers, J. H. 2009. DNA damage, aging, and cancer. *N Engl J Med* 361(15), pp. 1475-1485.

Hofer, A. C. et al. 2005. Shared phenotypes among segmental progeroid syndromes suggest underlying pathways of aging. *J Gerontol A Biol Sci Med Sci* 60(1), pp. 10-20.

Holtmann, M. H. and Neurath, M. F. 2004. Differential TNF-signaling in chronic inflammatory disorders. *Curr Mol Med* 4(4), pp. 439-444.

Honda, R. et al. 1993. Dephosphorylation of human p34cdc2 kinase on both Thr-14 and Tyr-15 by human cdc25B phosphatase. *FEBS Lett* 318(3), pp. 331-334.

Honda, S. and Matsuo, M. 1983. Shortening of the in vitro lifespan of human diploid fibroblasts exposed to hyperbaric oxygen. *Exp Gerontol* 18(5), pp. 339-345.

Howard, A. and Pelc, S. 1953. Synthesis of deoxyribonucleic acid in normal and irradiated cells and its relation to chromosome breakage. *Heredity* 6((Suppl)), pp. 261-273.

Hsiang, Y. H. et al. 1985. Camptothecin induces protein-linked DNA breaks via mammalian DNA topoisomerase I. *J Biol Chem* 260(27), pp. 14873-14878.

Hsiang, Y. H. and Liu, L. F. 1988. Identification of mammalian DNA topoisomerase I as an intracellular target of the anticancer drug camptothecin. *Cancer Res* 48(7), pp. 1722-1726.

Huang, S. et al. 2005. Correction of cellular phenotypes of Hutchinson-Gilford Progeria cells by RNA interference. *Hum Genet* 118(3-4), pp. 444-450.

Huang, S. et al. 2008. Accelerated telomere shortening and replicative senescence in human fibroblasts overexpressing mutant and wild-type lamin A. *Exp Cell Res* 314(1), pp. 82-91.

Huot, J. et al. 1997. Oxidative stress-induced actin reorganization mediated by the p38 mitogen-activated protein kinase/heat shock protein 27 pathway in vascular endothelial cells. *Circ Res* 80(3), pp. 383-392.

Huot, J. et al. 1996. HSP27 phosphorylation-mediated resistance against actin fragmentation and cell death induced by oxidative stress. *Cancer Res* 56(2), pp. 273-279.

Huot, J. et al. 1995. Characterization of 45-kDa/54-kDa HSP27 kinase, a stress-sensitive kinase which may activate the phosphorylation-dependent protective function of mammalian 27-kDa heat-shock protein HSP27. *Eur J Biochem* 227(1-2), pp. 416-427.

Hustinx, T. W. et al. 1979. Karyotype instability with multiple 7/14 and 7/7 rearrangements. *Hum Genet* 49(2), pp. 199-208.

Hutchinson, J. 1886. Case of congenital absence of hair, with atrophic condition of skin and its appendages, in a boy whose mother had been almost wholly bald from alopecia areata from teh age of six. *Lancet I* 923.

Imlay, J. A. et al. 1988. Toxic DNA damage by hydrogen peroxide through the Fenton reaction in vivo and in vitro. *Science* 240(4852), pp. 640-642.

Iordanov, M. S. et al. 1997. Ribotoxic stress response: activation of the stress-activated protein kinase JNK1 by inhibitors of the peptidyl transferase reaction and by sequence-specific RNA damage to the alpha-sarcin/ricin loop in the 28S rRNA. *Mol Cell Biol* 17(6), pp. 3373-3381.

Ishikawa, F. 2006. Cellular senescence as a stress response. *Cornea* 25(10 Suppl 1), pp. S3-6.

Itahana, K. et al. 2003. Control of the replicative life span of human fibroblasts by p16 and the polycomb protein Bmi-1. *Mol Cell Biol* 23(1), pp. 389-401.

Iwasa, H. et al. 2003. Mitogen-activated protein kinase p38 defines the common senescence-signalling pathway. *Genes Cells* 8(2), pp. 131-144.

Jaattela, M. and Wissing, D. 1992. Emerging role of heat shock proteins in biology and medicine. *Ann Med* 24(4), pp. 249-258.

Jacobs, J. J. and de Lange, T. 2004. Significant role for p16INK4a in p53-independent telomere-directed senescence. *Curr Biol* 14(24), pp. 2302-2308.

Jaeschke, A. et al. 2006. JNK2 is a positive regulator of the cJun transcription factor. *Mol Cell* 23(6), pp. 899-911.

Jeffrey, P. D. et al. 1995. Mechanism of CDK activation revealed by the structure of a cyclinA-CDK2 complex. *Nature* 376(6538), pp. 313-320.

Jeggo, P. A. 1998. DNA breakage and repair. *Adv Genet* 38, pp. 185-218.

Jeyapalan, J. C. et al. 2007. Accumulation of senescent cells in mitotic tissue of aging primates. *Mech Ageing Dev* 128(1), pp. 36-44.

Jiang, X. R. et al. 1999. Telomerase expression in human somatic cells does not induce changes associated with a transformed phenotype. *Nat Genet* 21(1), pp. 111-114.

Jiang, Y. et al. 1996. Characterization of the structure and function of a new mitogen-activated protein kinase (p38beta). *J Biol Chem* 271(30), pp. 17920-17926.

Jiang, Y. et al. 1997. Characterization of the structure and function of the fourth member of p38 group mitogen-activated protein kinases, p38delta. *J Biol Chem* 272(48), pp. 30122-30128.

Jin, W. et al. 2008. Sensitivity of RECQL4-deficient fibroblasts from Rothmund-Thomson syndrome patients to genotoxic agents. *Hum Genet* 123(6), pp. 643-653.

Johnson, F. B. et al. 2001. The Saccharomyces cerevisiae WRN homolog Sgs1p participates in telomere maintenance in cells lacking telomerase. *Embo J* 20(4), pp. 905-913.

Jones, C. J. et al. 2000. Evidence for a telomere-independent "clock" limiting RAS oncogene-driven proliferation of human thyroid epithelial cells. *Mol Cell Biol* 20(15), pp. 5690-5699.

Jowsey, P. A. et al. 2004. Human PTIP facilitates ATM-mediated activation of p53 and promotes cellular resistance to ionizing radiation. *J Biol Chem* 279(53), pp. 55562-55569.

Kamath-Loeb, A. S. et al. 2000. Functional interaction between the Werner Syndrome protein and DNA polymerase delta. *Proc Natl Acad Sci U S A* 97(9), pp. 4603-4608.

Kamath-Loeb, A. S. et al. 2001. Interactions between the Werner syndrome helicase and DNA polymerase delta specifically facilitate copying of tetraplex and hairpin structures of the d(CGG)n trinucleotide repeat sequence. *J Biol Chem* 276(19), pp. 16439-16446.

Kastan, M. B. and Bartek, J. 2004. Cell-cycle checkpoints and cancer. *Nature* 432(7015), pp. 316-323.

Kelland, L. R. 1993. New platinum antitumor complexes. *Crit Rev Oncol Hematol* 15(3), pp. 191-219.

Kelland, L. R. 2000. A new resistance mechanism to cisplatin? *Drug Resist Updat* 3(3), pp. 139-141.

Kerzendorfer, C. and O'Driscoll, M. 2009. Human DNA damage response and repair deficiency syndromes: linking genomic instability and cell cycle checkpoint proficiency. *DNA Repair (Amst)* 8(9), pp. 1139-1152.

Khan, I. A. et al. 2007. ProgeniDB: a novel cell lineage database for generation associated phenotypic behavior in cell-based assays. *Cell Cycle* 6(7), pp. 868-874.

Kill, I. R. et al. 1994. The expression of proliferation-dependent antigens during the lifespan of normal and progeroid human fibroblasts in culture. *J Cell Sci* 107 (Pt 2), pp. 571-579.

Kim, G. Y. et al. 2002. The stress-activated protein kinases p38 alpha and JNK1 stabilize p21(Cip1) by phosphorylation. *J Biol Chem* 277(33), pp. 29792-29802.

Kim, N. W. et al. 1994. Specific association of human telomerase activity with immortal cells and cancer. *Science* 266(5193), pp. 2011-2015.

King, R. W. et al. 1994. Mitosis in transition. *Cell* 79(4), pp. 563-571.

Kipling, D. et al. 2004. What can progeroid syndromes tell us about human aging? *Science* 305(5689), pp. 1426-1431.

Kishi, H. et al. 2001. Osmotic shock induces G1 arrest through p53 phosphorylation at Ser33 by activated p38MAPK without phosphorylation at Ser15 and Ser20. *J Biol Chem* 276(42), pp. 39115-39122.

Kitao, S. et al. 1998. Cloning of two new human helicase genes of the RecQ family: biological significance of multiple species in higher eukaryotes. *Genomics* 54(3), pp. 443-452.

Knight, S. et al. 1998. Dyskeratosis Congenita (DC) Registry: identification of new features of DC. *Br J Haematol* 103(4), pp. 990-996.

Ko, L. J. and Prives, C. 1996. p53: puzzle and paradigm. *Genes Dev* 10(9), pp. 1054-1072.

Kobayashi, J. et al. 2002. NBS1 localizes to gamma-H2AX foci through interaction with the FHA/BRCT domain. *Curr Biol* 12(21), pp. 1846-1851.

Kolch, W. 2000. Meaningful relationships: the regulation of the Ras/Raf/MEK/ERK pathway by protein interactions. *Biochem J* 351 Pt 2, pp. 289-305.

Kool, J. et al. 2003. Induction of ATF3 by ionizing radiation is mediated via a signaling pathway that includes ATM, Nibrin1, stress-induced MAPkinases and ATF-2. *Oncogene* 22(27), pp. 4235-4242.

Kosako, H. et al. 1992. Xenopus MAP kinase activator is a serine/threonine/tyrosine kinase activated by threonine phosphorylation. *EMBO J* 11(8), pp. 2903-2908.

Kraakman-van der Zwet, M. et al. 1999. Immortalization and characterization of Nijmegen Breakage syndrome fibroblasts. *Mutat Res* 434(1), pp. 17-27.

Kraemer, K. H. et al. 2007. Xeroderma pigmentosum, trichothiodystrophy and Cockayne syndrome: a complex genotype-phenotype relationship. *Neuroscience* 145(4), pp. 1388-1396.

Krishnamurthy, J. et al. 2004. Ink4a/Arf expression is a biomarker of aging. *J Clin Invest* 114(9), pp. 1299-1307.

Krtolica, A. and Campisi, J. 2002. Cancer and aging: a model for the cancer promoting effects of the aging stroma. *Int J Biochem Cell Biol* 34(11), pp. 1401-1414.

Kruk, P. A. et al. 1995. DNA damage and repair in telomeres: relation to aging. *Proc Natl Acad Sci U S A* 92(1), pp. 258-262.

Kumar, S. et al. 1999. Pyridinylimidazole compound SB 203580 inhibits the activity but not the activation of p38 mitogen-activated protein kinase. *Biochem Biophys Res Commun* 263(3), pp. 825-831.

Kumar, S. et al. 1997. Novel homologues of CSBP/p38 MAP kinase: activation, substrate specificity and sensitivity to inhibition by pyridinyl imidazoles. *Biochem Biophys Res Commun* 235(3), pp. 533-538.

Kumar, S. et al. 1993. Expression of interleukin-1 alpha and beta in early passage fibroblasts from aging individuals. *Exp Gerontol* 28(6), pp. 505-513.

Kumata, Y. et al. 2007. Possible involvement of RecQL4 in the repair of double-strand DNA breaks in Xenopus egg extracts. *Biochim Biophys Acta* 1773(4), pp. 556-564.

Kyriakis, J. M. and Avruch, J. 2001. Mammalian mitogen-activated protein kinase signal transduction pathways activated by stress and inflammation. *Physiol Rev* 81(2), pp. 807-869.

Landry, J. et al. 1989. Heat shock resistance conferred by expression of the human HSP27 gene in rodent cells. *J Cell Biol* 109(1), pp. 7-15.

Lans, H. and Hoeijmakers, J. H. 2006. Cell biology: ageing nucleus gets out of shape. *Nature* 440(7080), pp. 32-34.

Larizza, L. et al. 2006. Rothmund-Thomson syndrome and RECQL4 defect: splitting and lumping. *Cancer Lett* 232(1), pp. 107-120.

Lavin, M. F. 2007. ATM and the Mre11 complex combine to recognize and signal DNA double-strand breaks. *Oncogene* 26(56), pp. 7749-7758.

Lavoie, J. N. et al. 1995. Modulation of cellular thermoresistance and actin filament stability accompanies phosphorylation-induced changes in the oligomeric structure of heat shock protein 27. *Mol Cell Biol* 15(1), pp. 505-516.

Lee, J. C. et al. 1999. p38 mitogen-activated protein kinase inhibitors--mechanisms and therapeutic potentials. *Pharmacol Ther* 82(2-3), pp. 389-397.

Lee, J. C. et al. 1994. A protein kinase involved in the regulation of inflammatory cytokine biosynthesis. *Nature* 372(6508), pp. 739-746.

Lee, J. H. and Paull, T. T. 2007. Activation and regulation of ATM kinase activity in response to DNA double-strand breaks. *Oncogene* 26(56), pp. 7741-7748.

Lee, M. R. and Dominguez, C. 2005. MAP kinase p38 inhibitors: clinical results and an intimate look at their interactions with p38alpha protein. *Curr Med Chem* 12(25), pp. 2979-2994.

Lee, S. et al. 2002. MAPK signaling is involved in camptothecin-induced cell death. *Mol Cells* 14(3), pp. 348-354.

Lemaire, M. et al. 2006. CDC25B phosphorylation by p38 and MK-2. *Cell Cycle* 5(15), pp. 1649-1653.

Lengauer, C. et al. 1997. Genetic instability in colorectal cancers. *Nature* 386(6625), pp. 623-627.

Lew, D. J. and Kornbluth, S. 1996. Regulatory roles of cyclin dependent kinase phosphorylation in cell cycle control. *Curr Opin Cell Biol* 8(6), pp. 795-804.

Li, B. and Comai, L. 2000. Functional interaction between Ku and the werner syndrome protein in DNA end processing. *J Biol Chem* 275(50), p. 39800.

Li, Z. et al. 1996. The primary structure of p38 gamma: a new member of p38 group of MAP kinases. *Biochem Biophys Res Commun* 228(2), pp. 334-340.

Licht, C. L. et al. 2003. Cockayne syndrome group B cellular and biochemical functions. *Am J Hum Genet* 73(6), pp. 1217-1239.

Lin, A. W. et al. 1998. Premature senescence involving p53 and p16 is activated in response to constitutive MEK/MAPK mitogenic signaling. *Genes Dev* 12(19), pp. 3008-3019.

Lin, A. W. and Lowe, S. W. 2001. Oncogenic ras activates the ARF-p53 pathway to suppress epithelial cell transformation. *Proc Natl Acad Sci U S A* 98(9), pp. 5025-5030.

Lindahl, T. 1993. Instability and decay of the primary structure of DNA. *Nature* 362(6422), pp. 709-715.

Lindahl, T. and Wood, R. D. 1999. Quality control by DNA repair. *Science* 286(5446), pp. 1897-1905.

Lindor, N. M. et al. 1996. Rothmund-Thomson syndrome in siblings: evidence for acquired in vivo mosaicism. *Clin Genet* 49(3), pp. 124-129.

Lindor, N. M. et al. 2000. Rothmund-Thomson syndrome due to RECQ4 helicase mutations: report and clinical and molecular comparisons with Bloom syndrome and Werner syndrome. *Am J Med Genet* 90(3), pp. 223-228.

Linskens, M. H. et al. 1995. Cataloging altered gene expression in young and senescent cells using enhanced differential display. *Nucleic Acids Res* 23(16), pp. 3244-3251.

Lipetz, J. and Cristofalo, V. J. 1972. Ultrastructural changes accompanying the aging of human diploid cells in culture. *J Ultrastruct Res* 39(1), pp. 43-56.

Lisnock, J. et al. 1998. Molecular basis for p38 protein kinase inhibitor specificity. *Biochemistry* 37(47), pp. 16573-16581.

Little, J. B. et al. 1995. Absence of radiation-induced G1 arrest in two closely related human lymphoblast cell lines that differ in p53 status. *J Biol Chem* 270(19), pp. 11033-11036.

Liu, J. et al. 2004. c-Jun N-terminal protein kinase 1 (JNK1), but not JNK2, is essential for tumor necrosis factor alpha-induced c-Jun kinase activation and apoptosis. *Mol Cell Biol* 24(24), pp. 10844-10856.

Logar, D. B. et al. 2007. Expression of bone resorption genes in osteoarthritis and in osteoporosis. *J Bone Miner Metab* 25(4), pp. 219-225.

Lopez-Girona, A. et al. 1999. Nuclear localization of Cdc25 is regulated by DNA damage and a 14-3-3 protein. *Nature* 397(6715), pp. 172-175.

Lowe, S. W. et al. 1994. p53 status and the efficacy of cancer therapy in vivo. *Science* 266(5186), pp. 807-810.

Lowe, S. W. and Sherr, C. J. 2003. Tumor suppression by Ink4a-Arf: progress and puzzles. *Curr Opin Genet Dev* 13(1), pp. 77-83.

Luzzatto, L. and Karadimitris, A. 1998. Dyskeratosis and ribosomal rebellion. *Nat Genet* 19(1), pp. 6-7.

Ly, D. H. et al. 2000. Mitotic misregulation and human aging. *Science* 287(5462), pp. 2486-2492.

Maciera-Coelho, A. et al. 1971. Changes in lysosomal associated structures in human fibroblasts kept in resting phase. *Proc Soc Exp Biol Med* 138(2), pp. 712-718.

Macris, M. A. et al. 2006. Biochemical characterization of the RECQ4 protein, mutated in Rothmund-Thomson syndrome. *DNA Repair (Amst)* 5(2), pp. 172-180.

Malanga, M. and Althaus, F. R. 2005. The role of poly(ADP-ribose) in the DNA damage signaling network. *Biochem Cell Biol* 83(3), pp. 354-364.

Malumbres, M. and Barbacid, M. 2005. Mammalian cyclin-dependent kinases. *Trends Biochem Sci* 30(11), pp. 630-641.

Manke, I. A. et al. 2005. MAPKAP kinase-2 is a cell cycle checkpoint kinase that regulates the G2/M transition and S phase progression in response to UV irradiation. *Mol Cell* 17(1), pp. 37-48.

Mann, M. B. et al. 2005. Defective sister-chromatid cohesion, aneuploidy and cancer predisposition in a mouse model of type II Rothmund-Thomson syndrome. *Hum Mol Genet* 14(6), pp. 813-825.

Mao, F. J. et al. 2010. The Human WRN and BLM RecQ Helicases Differentially Regulate Cell Proliferation and Survival after Chemotherapeutic DNA Damage. *Cancer Res.*

Maraschio, P. et al. 2001. A novel mutation and novel features in Nijmegen breakage syndrome. *J Med Genet* 38(2), pp. 113-117.

Marciniak, R. A. et al. 2000. Dyskeratosis congenita, telomeres and human ageing. *Trends Genet* 16(5), pp. 193-195.

Marciniak, R. A. et al. 1998. Nucleolar localization of the Werner syndrome protein in human cells. *Proc Natl Acad Sci U S A* 95(12), pp. 6887-6892.

Marinissen, M. J. et al. 2001. Regulation of gene expression by the small GTPase Rho through the ERK6 (p38 gamma) MAP kinase pathway. *Genes Dev* 15(5), pp. 535-553.

Marquez, N. et al. 2003. Single cell tracking reveals that Msh2 is a key component of an early-acting DNA damage-activated G2 checkpoint. *Oncogene* 22(48), pp. 7642-7648.

Marrone, A. and Dokal, I. 2004. Dyskeratosis congenita: molecular insights into telomerase function, ageing and cancer. *Expert Rev Mol Med* 6(26), pp. 1-23.

Marsh, J. C. et al. 1992. "Stem cell" origin of the hematopoietic defect in dyskeratosis congenita. *Blood* 79(12), pp. 3138-3144.

Martin, G. M. 1978. Genetic syndromes in man with potential relevance to the pathobiology of aging. *Birth Defects Orig Artic Ser* 14(1), pp. 5-39.

Martin, G. M. et al. 1999. What geriatricians should know about the Werner syndrome. *J Am Geriatr Soc* 47(9), pp. 1136-1144.

Martin, G. M. and Sprague, C. A. 1973. Symposium on in vitro studies related to atherogenesis. Life histories of hyperplastoid cell lines from aorta and skin. *Exp Mol Pathol* 18(2), pp. 125-141.

Martin, G. M. et al. 1970. Replicative life-span of cultivated human cells. Effects of donor's age, tissue, and genotype. *Lab Invest* 23(1), pp. 86-92.

Maruyama, J. et al. 2009. Stress-activated MAP kinase cascades in cellular senescence. *Curr Med Chem* 16(10), pp. 1229-1235.

Maser, R. S. et al. 1997. hMre11 and hRad50 nuclear foci are induced during the normal cellular response to DNA double-strand breaks. *Mol Cell Biol* 17(10), pp. 6087-6096.

Maser, R. S. et al. 2001. An alternative mode of translation permits production of a variant NBS1 protein from the common Nijmegen breakage syndrome allele. *Nat Genet* 27(4), pp. 417-421.

Massague, J. 2004. G1 cell-cycle control and cancer. *Nature* 432(7015), pp. 298-306.

Matsukawa, J. et al. 2004. The ASK1-MAP kinase cascades in mammalian stress response. *J Biochem* 136(3), pp. 261-265.

Matsumoto, M. et al. 2004. Essential role of p38 mitogen-activated protein kinase in cathepsin K gene expression during osteoclastogenesis through association of NFATc1 and PU.1. *J Biol Chem* 279(44), pp. 45969-45979.

Matsumura, T. 1980. Multinucleation and polyploidization of aging human cells in culture. *Adv Exp Med Biol* 129, pp. 31-38.

Matsuno, K. et al. 2006. The N-terminal noncatalytic region of Xenopus RecQ4 is required for chromatin binding of DNA polymerase alpha in the initiation of DNA replication. *Mol Cell Biol* 26(13), pp. 4843-4852.

Matsuura, S. et al. 2004. Nijmegen breakage syndrome and DNA double strand break repair by NBS1 complex. *Adv Biophys* 38, pp. 65-80.

Mayer, R. J. and Callahan, J. F. 2006. p38 MAP kinase inhibitors: A future therapy for inflammatory diseases. *Today Therapeutic Strategies* 3(1), pp. 49-54.

Mayne, L. V. and Lehmann, A. R. 1982. Failure of RNA synthesis to recover after UV irradiation: an early defect in cells from individuals with Cockayne's syndrome and xeroderma pigmentosum. *Cancer Res* 42(4), pp. 1473-1478.

McEachern, M. J. et al. 2000. Telomeres and their control. *Annu Rev Genet* 34, pp. 331-358.

McGowan, C. H. and Russell, P. 1993. Human Wee1 kinase inhibits cell division by phosphorylating p34cdc2 exclusively on Tyr15. *EMBO J* 12(1), pp. 75-85.

McGowan, C. H. and Russell, P. 1995. Cell cycle regulation of human WEE1. *EMBO J* 14(10), pp. 2166-2175.

Mehlen, P. et al. 1996. Human hsp27, Drosophila hsp27 and human alphaB-crystallin expression-mediated increase in glutathione is essential for the protective activity of these proteins against TNFalpha-induced cell death. *EMBO J* 15(11), pp. 2695-2706.

Meier, R. et al. 1996. Cellular stresses and cytokines activate multiple mitogen-activated-protein kinase kinase homologues in PC12 and KB cells. *Eur J Biochem* 236(3), pp. 796-805.

Miao, Z. H. et al. 2006. 4-nitroquinoline-1-oxide induces the formation of cellular topoisomerase I-DNA cleavage complexes. *Cancer Res* 66(13), pp. 6540-6545.

Michishita, E. et al. 1998. DNA topoisomerase inhibitors induce reversible senescence in normal human fibroblasts. *Biochem Biophys Res Commun* 253(3), pp. 667-671.

Mikhailov, A. et al. 2004. Topoisomerase II and histone deacetylase inhibitors delay the G2/M transition by triggering the p38 MAPK checkpoint pathway. *J Cell Biol* 166(4), pp. 517-526.

Millis, A. J. et al. 1992a. Differential expression of metalloproteinase and tissue inhibitor of metalloproteinase genes in aged human fibroblasts. *Exp Cell Res* 201(2), pp. 373-379.

Millis, A. J. et al. 1992b. Metalloproteinase and TIMP-1 gene expression during replicative senescence. *Exp Gerontol* 27(4), pp. 425-428.

Minamino, T. et al. 2002. Endothelial cell senescence in human atherosclerosis: role of telomere in endothelial dysfunction. *Circulation* 105(13), pp. 1541-1544.

Minamino, T. et al. 2003. Ras induces vascular smooth muscle cell senescence and inflammation in human atherosclerosis. *Circulation* 108(18), pp. 2264-2269.

Miozzo, M. et al. 1998. Chromosomal instability in fibroblasts and mesenchymal tumors from 2 sibs with Rothmund-Thomson syndrome. *Int J Cancer* 77(4), pp. 504-510.

Mitchell, J. R. et al. 1999a. A box H/ACA small nucleolar RNA-like domain at the human telomerase RNA 3' end. *Mol Cell Biol* 19(1), pp. 567-576.

Mitchell, J. R. et al. 1999b. A telomerase component is defective in the human disease dyskeratosis congenita. *Nature* 402(6761), pp. 551-555.

Mitsui, Y. and Schneider, E. L. 1976. Relationship between cell replication and volume in senescent human diploid fibroblasts. *Mech Ageing Dev* 5(1), pp. 45-56.

Mohaghegh, P. et al. 2001. The Bloom's and Werner's syndrome proteins are DNA structure-specific helicases. *Nucleic Acids Res* 29(13), pp. 2843-2849.

Momparler, R. L. et al. 1976. Effect of adriamycin on DNA, RNA, and protein synthesis in cell-free systems and intact cells. *Cancer Res* 36(8), pp. 2891-2895.

Morales, C. P. et al. 1999. Absence of cancer-associated changes in human fibroblasts immortalized with telomerase. *Nat Genet* 21(1), pp. 115-118.

Morgan, D. O. 1995. Principles of CDK regulation. *Nature* 374(6518), pp. 131-134.

Morgan, D. O. 1997. Cyclin-dependent kinases: engines, clocks, and microprocessors. *Annu Rev Cell Dev Biol* 13, pp. 261-291.

Morgan, D. O. 2007. *The Cell Cycle: Principles of Control.* London: New Science Press in association with Oxford University Press.

Morgenstern, J. P. and Land, H. 1990. Advanced mammalian gene transfer: high titre retroviral vectors with multiple drug selection markers and a complementary helper-free packaging cell line. *Nucleic Acids Res* 18(12), pp. 3587-3596.

Morris, M. C. et al. 2000. An essential phosphorylation-site domain of human cdc25C interacts with both 14-3-3 and cyclins. *J Biol Chem* 275(37), pp. 28849-28857.

Moser, M. J. et al. 1997. The proofreading domain of Escherichia coli DNA polymerase I and other DNA and/or RNA exonuclease domains. *Nucleic Acids Res* 25(24), pp. 5110-5118.

Moser, M. J. et al. 1999. WRN mutations in Werner syndrome. *Hum Mutat* 13(4), pp. 271-279.

Moyzis, R. K. et al. 1988. A highly conserved repetitive DNA sequence, (TTAGGG)n, present at the telomeres of human chromosomes. *Proc Natl Acad Sci U S A* 85(18), pp. 6622-6626.

Mueller, P. R. et al. 1995. Myt1: a membrane-associated inhibitory kinase that phosphorylates Cdc2 on both threonine-14 and tyrosine-15. *Science* 270(5233), pp. 86-90.

Mueller, S. N. et al. 1980. Cellular senescence in a cloned strain of bovine fetal aortic endothelial cells. *Science* 207(4433), pp. 889-891.

Murano, S. et al. 1997. Increased blood plasminogen activator inhibitor-1 and intercellular adhesion molecule-1 as possible risk factors of atherosclerosis in Werner syndrome. *Gerontology* 43 Suppl 1, pp. 43-52.

Murray, A. W. 2004. Recycling the cell cycle: cyclins revisited. *Cell* 116(2), pp. 221-234.

Musich, P. R. and Zou, Y. 2009. Genomic instability and DNA damage responses in progeria arising from defective maturation of prelamin A. *Aging (Albany NY)* 1(1), pp. 28-37.

Naka, K. et al. 2004. Stress-induced premature senescence in hTERT-expressing ataxia telangiectasia fibroblasts. *J Biol Chem* 279(3), pp. 2030-2037.

Nakamura, T. M. et al. 1997. Telomerase catalytic subunit homologs from fission yeast and human. *Science* 277(5328), pp. 955-959.

Nance, M. A. and Berry, S. A. 1992. Cockayne syndrome: review of 140 cases. *Am J Med Genet* 42(1), pp. 68-84.

Nanni, S. et al. 2007. Matrix metalloproteinases in premature coronary atherosclerosis: influence of inhibitors, inflammation, and genetic polymorphisms. *Transl Res* 149(3), pp. 137-144.

Narita, M. et al. 2003. Rb-mediated heterochromatin formation and silencing of E2F target genes during cellular senescence. *Cell* 113(6), pp. 703-716.

Natarajan, S. R. and Doherty, J. B. 2005. P38 MAP kinase inhibitors: evolution of imidazole-based and pyrido-pyrimidin-2-one lead classes. *Curr Top Med Chem* 5(10), pp. 987-1003.

Naumanen, P. et al. 2008. Mechanisms of actin stress fibre assembly. *J Microsc* 231(3), pp. 446-454.

Navarro, C. L. et al. 2006. Molecular bases of progeroid syndromes. *Hum Mol Genet* 15 Spec No 2, pp. R151-161.

Negrini, S. et al. 2010. Genomic instability--an evolving hallmark of cancer. *Nat Rev Mol Cell Biol* 11(3), pp. 220-228.

Nelms, B. E. et al. 1998. In situ visualization of DNA double-strand break repair in human fibroblasts. *Science* 280(5363), pp. 590-592.

Niggli, H. J. et al. 1989. Mitomycin C-induced postmitotic fibroblasts retain the capacity to repair pyrimidine photodimers formed after UV-irradiation. *Mutat Res* 219(4), pp. 231-240.

Noda, A. et al. 1994. Cloning of senescent cell-derived inhibitors of DNA synthesis using an expression screen. *Exp Cell Res* 211(1), pp. 90-98.

Noppe, G. et al. 2009. Rapid flow cytometric method for measuring senescence associated beta-galactosidase activity in human fibroblasts. *Cytometry A* 75(11), pp. 910-916.

Nunoshiba, T. and Demple, B. 1993. Potent intracellular oxidative stress exerted by the carcinogen 4-nitroquinoline-N-oxide. *Cancer Res* 53(14), pp. 3250-3252.

O'Driscoll, M. et al. 2001. DNA ligase IV mutations identified in patients exhibiting developmental delay and immunodeficiency. *Mol Cell* 8(6), pp. 1175-1185.

O'Driscoll, M. et al. 2004. An overview of three new disorders associated with genetic instability: LIG4 syndrome, RS-SCID and ATR-Seckel syndrome. *DNA Repair (Amst)* 3(8-9), pp. 1227-1235.

O'Driscoll, M. et al. 2003. A splicing mutation affecting expression of ataxia-telangiectasia and Rad3-related protein (ATR) results in Seckel syndrome. *Nat Genet* 33(4), pp. 497-501.

Ochs, H. D. et al. 1997. *Primary immunodeficieny diseases, a molecular and genetics approach.* Oxford: Oxford University Press.

Ohtsubo, M. et al. 1995. Human cyclin E, a nuclear protein essential for the G1-to-S phase transition. *Mol Cell Biol* 15(5), pp. 2612-2624.

Olovnikov, A. M. 1973. A theory of marginotomy. The incomplete copying of template margin in enzymic synthesis of polynucleotides and biological significance of the phenomenon. *J Theor Biol* 41(1), pp. 181-190.

Olsen, C. L. et al. 2002. Raf-1-induced growth arrest in human mammary epithelial cells is p16-independent and is overcome in immortal cells during conversion. *Oncogene* 21(41), pp. 6328-6339.

Olson, E. et al. 2007. The Mre11-Rad50-Nbs1 complex acts both upstream and downstream of ataxia telangiectasia mutated and Rad3-related protein (ATR) to regulate the S-phase checkpoint following UV treatment. *J Biol Chem* 282(31), pp. 22939-22952.

Opresko, P. L. et al. 2004. The Werner syndrome helicase and exonuclease cooperate to resolve telomeric D loops in a manner regulated by TRF1 and TRF2. *Mol Cell* 14(6), pp. 763-774.

Opresko, P. L. et al. 2002. Telomere-binding protein TRF2 binds to and stimulates the Werner and Bloom syndrome helicases. *J Biol Chem* 277(43), pp. 41110-41119.

Oren, M. 1999. Regulation of the p53 tumor suppressor protein. *J Biol Chem* 274(51), pp. 36031-36034.

Orren, D. K. et al. 2002. The Werner syndrome helicase/exonuclease (WRN) disrupts and degrades D-loops in vitro. *Biochemistry* 41(46), pp. 13483-13488.

Ostler, E. L. et al. 2000. Telomerase and the cellular lifespan: implications of the aging process. *J Pediatr Endocrinol Metab* 13 Suppl 6, pp. 1467-1476.

Ouellette, M. M. et al. 2000. The establishment of telomerase-immortalized cell lines representing human chromosome instability syndromes. *Hum Mol Genet* 9(3), pp. 403-411.

Ouyang, K. J. et al. 2008. Homologous recombination and maintenance of genome integrity: cancer and aging through the prism of human RecQ helicases. *Mech Ageing Dev* 129(7-8), pp. 425-440.

Packer, L. and Fuehr, K. 1977. Low oxygen concentration extends the lifespan of cultured human diploid cells. *Nature* 267(5610), pp. 423-425.

Pagano, G. et al. 2005. Multiple involvement of oxidative stress in werner syndrome phenotype. *Biogerontology* 6(4), pp. 233-243.

Pagano, M. et al. 1992. Cyclin A is required at two points in the human cell cycle. *EMBO J* 11(3), pp. 961-971.

Palmero, I. et al. 1997. Accumulation of p16INK4a in mouse fibroblasts as a function of replicative senescence and not of retinoblastoma gene status. *Oncogene* 15(5), pp. 495-503.

Pan, J. et al. 2010. Reactive oxygen species-activated Akt/ASK1/p38 signaling pathway in nickel compound-induced apoptosis in BEAS 2B cells. *Chem Res Toxicol* 23(3), pp. 568-577.

Pardee, A. B. 1974. A restriction point for control of normal animal cell proliferation. *Proc Natl Acad Sci U S A* 71(4), pp. 1286-1290.

Pargellis, C. et al. 2002. Inhibition of p38 MAP kinase by utilizing a novel allosteric binding site. *Nat Struct Biol* 9(4), pp. 268-272.

Park, W. Y. et al. 2001. Gene profile of replicative senescence is different from progeria or elderly donor. *Biochem Biophys Res Commun* 282(4), pp. 934-939.

Parrinello, S. et al. 2003. Oxygen sensitivity severely limits the replicative lifespan of murine fibroblasts. *Nat Cell Biol* 5(8), pp. 741-747.

Passos, J. F. et al. 2010. Feedback between p21 and reactive oxygen production is necessary for cell senescence. *Mol Syst Biol* 6, p. 347.

Passos, J. F. and von Zglinicki, T. 2007. Methods for cell sorting of young and senescent cells. *Methods Mol Biol* 371, pp. 33-44.

Pearson, G. et al. 2001. Mitogen-activated protein (MAP) kinase pathways: regulation and physiological functions. *Endocr Rev* 22(2), pp. 153-183.

Pellegrin, S. and Mellor, H. 2007. Actin stress fibres. *J Cell Sci* 120(Pt 20), pp. 3491-3499.

Peltomaki, P. 2001. DNA mismatch repair and cancer. *Mutat Res* 488(1), pp. 77-85.

Perry, M. E. et al. 1993. The mdm-2 gene is induced in response to UV light in a p53-dependent manner. *Proc Natl Acad Sci U S A* 90(24), pp. 11623-11627.

Petkovic, M. et al. 2005. The human Rothmund-Thomson syndrome gene product, RECQL4, localizes to distinct nuclear foci that coincide with proteins involved in the maintenance of genome stability. *J Cell Sci* 118(Pt 18), pp. 4261-4269.

Petrini, J. H. 1999. The mammalian Mre11-Rad50-nbs1 protein complex: integration of functions in the cellular DNA-damage response. *Am J Hum Genet* 64(5), pp. 1264-1269.

Petrini, J. H. 2000. The Mre11 complex and ATM: collaborating to navigate S phase. *Curr Opin Cell Biol* 12(3), pp. 293-296.

Phong, M. et al. 2010. The p38 MAPK promotes cell survival in response to DNA damage but is not required for G2 DNA damage checkpoint in human cancer cells. *Molecular Cell Biology*.

Pichierri, P. and Franchitto, A. 2004. Werner syndrome protein, the MRE11 complex and ATR: menage-a-trois in guarding genome stability during DNA replication? *Bioessays* 26(3), pp. 306-313.

Pichierri, P. et al. 2000. Werner's syndrome cell lines are hypersensitive to camptothecin-induced chromosomal damage. *Mutat Res* 456(1-2), pp. 45-57.

Pignolo, R. J. et al. 1992. Skin fibroblasts from aged Fischer 344 rats undergo similar changes in replicative life span but not immortalization with caloric restriction of donors. *Exp Cell Res* 201(1), pp. 16-22.

Pines, J. 1991. Cyclins: wheels within wheels. *Cell Growth Differ* 2(6), pp. 305-310.

Pines, J. 1995. Cyclins and cyclin-dependent kinases: theme and variations. *Adv Cancer Res* 66, pp. 181-212.

Pious, D. A. et al. 1964. Clonal Growth of Primary Human Cell Cultures. *Exp Cell Res* 33, pp. 495-507.

Pollex, R. L. and Hegele, R. A. 2004. Hutchinson-Gilford progeria syndrome. *Clin Genet* 66(5), pp. 375-381.

Pommier, Y. et al. 1994. Cellular determinants of sensitivity and resistance to DNA topoisomerase inhibitors. *Cancer Invest* 12(5), pp. 530-542.

Pommier, Y. et al. 2003. Repair of and checkpoint response to topoisomerase I-mediated DNA damage. *Mutat Res* 532(1-2), pp. 173-203.

Poon, R. Y. et al. 1996. Cyclin-dependent kinases are inactivated by a combination of p21 and Thr-14/Tyr-15 phosphorylation after UV-induced DNA damage. *J Biol Chem* 271(22), pp. 13283-13291.

Poot, M. et al. 2002. Werner syndrome diploid fibroblasts are sensitive to 4-nitroquinoline-N-oxide and 8-methoxypsoralen: implications for the disease phenotype. *FASEB J* 16(7), pp. 757-758.

Poot, M. et al. 1999. Werner syndrome lymphoblastoid cells are sensitive to camptothecin-induced apoptosis in S-phase. *Hum Genet* 104(1), pp. 10-14.

Poot, M. et al. 1992. Impaired S-phase transit of Werner syndrome cells expressed in lymphoblastoid cell lines. *Exp Cell Res* 202(2), pp. 267-273.

Poot, M. et al. 2001. Werner syndrome cells are sensitive to DNA cross-linking drugs. *FASEB J* 15(7), pp. 1224-1226.

Poplawski, T. et al. 2009. [Non-homologous DNA end joining--new proteins, new functions, new mechanisms]. *Postepy Biochem* 55(1), pp. 36-45.

Poppe, B. et al. 2001. Chromosomal aberrations in Bloom syndrome patients with myeloid malignancies. *Cancer Genet Cytogenet* 128(1), pp. 39-42.

Porter, C. M. et al. 2000. Identification of amino acid residues and protein kinases involved in the regulation of NFATc subcellular localization. *J Biol Chem* 275(5), pp. 3543-3551.

Postiglione, A. et al. 1996. Premature aging in Werner's syndrome spares the central nervous system. *Neurobiol Aging* 17(3), pp. 325-330.

Potter, A. J. et al. 2002. Flow cytometric analysis of the cell cycle phase specificity of DNA damage induced by radiation, hydrogen peroxide and doxorubicin. *Carcinogenesis* 23(3), pp. 389-401.

Price, J. S. et al. 2002. The role of chondrocyte senescence in osteoarthritis. *Aging Cell* 1(1), pp. 57-65.

Prince, P. R. et al. 1999. Cell fusion corrects the 4-nitroquinoline 1-oxide sensitivity of Werner syndrome fibroblast cell lines. *Hum Genet* 105(1-2), pp. 132-138.

Rai, P. 2010. Oxidation in the nucleotide pool, the DNA damage response and cellular senescence: Defective bricks build a defective house. *Mutat Res.*

Raingeaud, J. et al. 1995. Pro-inflammatory cytokines and environmental stress cause p38 mitogen-activated protein kinase activation by dual phosphorylation on tyrosine and threonine. *J Biol Chem* 270(13), pp. 7420-7426.

Raman, M. et al. 2007. TAO kinases mediate activation of p38 in response to DNA damage. *EMBO J* 26(8), pp. 2005-2014.

Ramirez, R. D. et al. 2001. Putative telomere-independent mechanisms of replicative aging reflect inadequate growth conditions. *Genes Dev* 15(4), pp. 398-403.

Ranganathan, V. et al. 2001. Rescue of a telomere length defect of Nijmegen breakage syndrome cells requires NBS and telomerase catalytic subunit. *Curr Biol* 11(12), pp. 962-966.

Rapin, I. et al. 2000. Cockayne syndrome and xeroderma pigmentosum. *Neurology* 55(10), pp. 1442-1449.

Rebbaa, A. et al. 2003. Caspase inhibition switches doxorubicin-induced apoptosis to senescence. *Oncogene* 22(18), pp. 2805-2811.

Rechsteiner, M. and Rogers, S. W. 1996. PEST sequences and regulation by proteolysis. *Trends Biochem Sci* 21(7), pp. 267-271.

Regan, J. et al. 2002. Pyrazole urea-based inhibitors of p38 MAP kinase: from lead compound to clinical candidate. *J Med Chem* 45(14), pp. 2994-3008.

Regan, J. et al. 2003. The kinetics of binding to p38MAP kinase by analogues of BIRB 796. *Bioorg Med Chem Lett* 13(18), pp. 3101-3104.

Reinhardt, H. C. et al. 2007. p53-deficient cells rely on ATM- and ATR-mediated checkpoint signaling through the p38MAPK/MK2 pathway for survival after DNA damage. *Cancer Cell* 11(2), pp. 175-189.

Ren, Y. et al. 2003. Three novel mutations responsible for Cockayne syndrome group A. *Genes Genet Syst* 78(1), pp. 93-102.

Resnick, I. B. et al. 2002. Nijmegen breakage syndrome: clinical characteristics and mutation analysis in eight unrelated Russian families. *J Pediatr* 140(3), pp. 355-361.

Resnitzky, D. et al. 1995. Cyclin A-associated kinase activity is rate limiting for entrance into S phase and is negatively regulated in G1 by p27Kip1. *Mol Cell Biol* 15(8), pp. 4347-4352.

Rheinwald, J. G. and Green, H. 1975. Serial cultivation of strains of human epidermal keratinocytes: the formation of keratinizing colonies from single cells. *Cell* 6(3), pp. 331-343.

Ridley, A. J. et al. 2005. Characterisation of novel mutations in Cockayne syndrome type A and xeroderma pigmentosum group C subjects. *J Hum Genet* 50(3), pp. 151-154.

Roberson, R. S. et al. 2005. Escape from therapy-induced accelerated cellular senescence in p53-null lung cancer cells and in human lung cancers. *Cancer Res* 65(7), pp. 2795-2803.

Rodemann, H. P. et al. 1989. Selective enrichment and biochemical characterization of seven human skin fibroblasts cell types in vitro. *Exp Cell Res* 180(1), pp. 84-93.

Rodriguez-Lopez, A. M. et al. 2002. Asymmetry of DNA replication fork progression in Werner's syndrome. *Aging Cell* 1(1), pp. 30-39.

Rodriguez-Lopez, A. M. et al. 2003. Characterisation of the interaction between WRN, the helicase/exonuclease defective in progeroid Werner's syndrome, and an essential replication factor, PCNA. *Mech Ageing Dev* 124(2), pp. 167-174.

Rodriguez-Lopez, A. M. et al. 2007. Correction of proliferation and drug sensitivity defects in the progeroid Werner's Syndrome by Holliday junction resolution. *Rejuvenation Res* 10(1), pp. 27-40.

Roninson, I. B. 2003. Tumor cell senescence in cancer treatment. *Cancer Res* 63(11), pp. 2705-2715.

Rothmund, A. 1868. Uber cataracte in Verbindung mit einer eigenthuemlichen hautdegeneration. *Albrecht von Graefes Arch Klin Opthal* 14, pp. 159-182.

Rouse, J. et al. 1994. A novel kinase cascade triggered by stress and heat shock that stimulates MAPKAP kinase-2 and phosphorylation of the small heat shock proteins. *Cell* 78(6), pp. 1027-1037.

Roussel, M. F. 1999. The INK4 family of cell cycle inhibitors in cancer. *Oncogene* 18(38), pp. 5311-5317.

Roux, P. P. and Blenis, J. 2004. ERK and p38 MAPK-activated protein kinases: a family of protein kinases with diverse biological functions. *Microbiol Mol Biol Rev* 68(2), pp. 320-344.

Rubin, H. 1997. Cell aging in vivo and in vitro. *Mech Ageing Dev* 98(1), pp. 1-35.

Rudner, A. D. and Murray, A. W. 1996. The spindle assembly checkpoint. *Curr Opin Cell Biol* 8(6), pp. 773-780.

Russo, C. A. et al. 1995. An anoxia inducible endonuclease and enhanced DNA breakage as contributors to genomic instability in cancer. *Cancer Res* 55(5), pp. 1122-1128.

Sagan, D. et al. 2009. The DNA repair protein NBS1 influences the base excision repair pathway. *Carcinogenesis* 30(3), pp. 408-415.

Salk, D. et al. 1981. Systematic growth studies, cocultivation, and cell hybridization studies of Werner syndrome cultured skin fibroblasts. *Hum Genet* 58(3), pp. 310-316.

Sancar, A. et al. 2004. Molecular mechanisms of mammalian DNA repair and the DNA damage checkpoints. *Annu Rev Biochem* 73, pp. 39-85.

Sanchez, I. and Dynlacht, B. D. 2005. New insights into cyclins, CDKs, and cell cycle control. *Semin Cell Dev Biol* 16(3), pp. 311-321.

Sanchez-Prieto, R. et al. 2000. A role for the p38 mitogen-acitvated protein kinase pathway in the transcriptional activation of p53 on genotoxic stress by chemotherapeutic agents. *Cancer Res* 60(9), pp. 2464-2472.

Sangrithi, M. N. et al. 2005. Initiation of DNA replication requires the RECQL4 protein mutated in Rothmund-Thomson syndrome. *Cell* 121(6), pp. 887-898.

Satyanarayana, A. et al. 2008. p21 Inhibits Cdk1 in the absence of Cdk2 to maintain the G1/S phase DNA damage checkpoint. *Mol Biol Cell* 19(1), pp. 65-77.

Satyanarayana, A. and Kaldis, P. 2009. Mammalian cell-cycle regulation: several Cdks, numerous cyclins and diverse compensatory mechanisms. *Oncogene* 28(33), pp. 2925-2939.

Savage, S. A. et al. 2008. TINF2, a component of the shelterin telomere protection complex, is mutated in dyskeratosis congenita. *Am J Hum Genet* 82(2), pp. 501-509.

Scaffidi, P. and Misteli, T. 2005. Reversal of the cellular phenotype in the premature aging disease Hutchinson-Gilford progeria syndrome. *Nat Med* 11(4), pp. 440-445.

Schafer, K. A. 1998. The cell cycle: a review. *Vet Pathol* 35(6), pp. 461-478.

Schieven, G. L. 2005. The biology of p38 kinase: a central role in inflammation. *Curr Top Med Chem* 5(10), pp. 921-928.

Schieven, G. L. 2009. The p38alpha kinase plays a central role in inflammation. *Curr Top Med Chem* 9(11), pp. 1038-1048.

Schmitt, C. A. et al. 2002. A senescence program controlled by p53 and p16INK4a contributes to the outcome of cancer therapy. *Cell* 109(3), pp. 335-346.

Schneider, E. L. and Mitsui, Y. 1976. The relationship between in vitro cellular aging and in vivo human age. *Proc Natl Acad Sci U S A* 73(10), pp. 3584-3588.

Schulz, V. P. et al. 1996. Accelerated loss of telomeric repeats may not explain accelerated replicative decline of Werner syndrome cells. *Hum Genet* 97(6), pp. 750-754.

Sclafani, R. A. and Holzen, T. M. 2007. Cell cycle regulation of DNA replication. *Annu Rev Genet* 41, pp. 237-280.

Seckel, H. P. G. 1960. Bird-headed dwarfs: Studies in developmental anthropology including human proportions.Springfield, Illinois: Thomas, CT.

Seemanova, E. et al. 1985. Familial microcephaly with normal intelligence, immunodeficiency, and risk for lymphoreticular malignancies: a new autosomal recessive disorder. *Am J Med Genet* 20(4), pp. 639-648.

Segurado, M. and Tercero, J. A. 2009. The S-phase checkpoint: targeting the replication fork. *Biol Cell* 101(11), pp. 617-627.

Seluanov, A. et al. 2001. Change of the death pathway in senescent human fibroblasts in response to DNA damage is caused by an inability to stabilize p53. *Mol Cell Biol* 21(5), pp. 1552-1564.

Sengupta, S. et al. 2005. Tumor suppressor p53 represses transcription of RECQ4 helicase. *Oncogene* 24(10), pp. 1738-1748.

Serrano, M. et al. 1997. Oncogenic ras provokes premature cell senescence associated with accumulation of p53 and p16INK4a. *Cell* 88(5), pp. 593-602.

Seshadri, T. and Campisi, J. 1990. Repression of c-fos transcription and an altered genetic program in senescent human fibroblasts. *Science* 247(4939), pp. 205-209.

Shapiro, G. I. and Harper, J. W. 1999. Anticancer drug targets: cell cycle and checkpoint control. *J Clin Invest* 104(12), pp. 1645-1653.

Shay, J. W. and Wright, W. E. 2005. Senescence and immortalization: role of telomeres and telomerase. *Carcinogenesis* 26(5), pp. 867-874.

She, Q. B. et al. 2000. ERKs and p38 kinase phosphorylate p53 protein at serine 15 in response to UV radiation. *J Biol Chem* 275(27), pp. 20444-20449.

Shelton, D. N. et al. 1999. Microarray analysis of replicative senescence. *Curr Biol* 9(17), pp. 939-945.

Shen, J. and Loeb, L. A. 2001. Unwinding the molecular basis of the Werner syndrome. *Mech Ageing Dev* 122(9), pp. 921-944.

Sherr, C. J. 1994. G1 phase progression: cycling on cue. *Cell* 79(4), pp. 551-555.

Sherr, C. J. et al. 1994. D-type cyclins and their cyclin-dependent kinases: G1 phase integrators of the mitogenic response. *Cold Spring Harb Symp Quant Biol* 59, pp. 11-19.

Sherr, C. J. and McCormick, F. 2002. The RB and p53 pathways in cancer. *Cancer Cell* 2(2), pp. 103-112.

Shi, Y. et al. 2003. Elimination of protein kinase MK5/PRAK activity by targeted homologous recombination. *Mol Cell Biol* 23(21), pp. 7732-7741.

Shifrin, V. I. and Anderson, P. 1999. Trichothecene mycotoxins trigger a ribotoxic stress response that activates c-Jun N-terminal kinase and p38 mitogen-activated protein kinase and induces apoptosis. *J Biol Chem* 274(20), pp. 13985-13992.

Shiloh, Y. 1997. Ataxia-telangiectasia and the Nijmegen breakage syndrome: related disorders but genes apart. *Annu Rev Genet* 31, pp. 635-662.

Shiloh, Y. 2003. ATM and related protein kinases: safeguarding genome integrity. *Nat Rev Cancer* 3(3), pp. 155-168.

Siddik, Z. H. 2002. Biochemical and molecular mechanisms of cisplatin resistance. *Cancer Treat Res* 112, pp. 263-284.

Siddik, Z. H. 2003. Cisplatin: mode of cytotoxic action and molecular basis of resistance. *Oncogene* 22(47), pp. 7265-7279.

Sidorova, J. M. et al. 2008. The RecQ helicase WRN is required for normal replication fork progression after DNA damage or replication fork arrest. *Cell Cycle* 7(6), pp. 796-807.

Singh, D. K. et al. 2010. The involvement of human RECQL4 in DNA double-strand break repair. *Aging Cell*.

Smith, P. J. et al. 2006. Cell cycle dynamics and challenges for CDK targeting. In: Smith, P.J. and Yue, E.W. eds. *Inhibitors of cyclin-dependent kinases as anti-tumour agents*. Boca Ranton (FL): CRC Press, pp. 3-19.

Smith, P. J. and Jones, C., J. 2000. *DNA Recombination and Repair*. Oxford University Press.

Smith, P. J. et al. 2007. Mitotic bypass via an occult cell cycle phase following DNA topoisomerase II inhibition in p53 functional human tumor cells. *Cell Cycle* 6(16), pp. 2071-2081.

Sonoda, E. et al. 1999. Sister chromatid exchanges are mediated by homologous recombination in vertebrate cells. *Mol Cell Biol* 19(7), pp. 5166-5169.

Squires, S. et al. 1993. Hypersensitivity of Cockayne's syndrome cells to camptothecin is associated with the generation of abnormally high levels of double strand breaks in nascent DNA. *Cancer Res* 53(9), pp. 2012-2019.

Stansel, R. M. et al. 2001. T-loop assembly in vitro involves binding of TRF2 near the 3' telomeric overhang. *EMBO J* 20(19), pp. 5532-5540.

Stavropoulos, D. J. et al. 2002. The Bloom syndrome helicase BLM interacts with TRF2 in ALT cells and promotes telomeric DNA synthesis. *Hum Mol Genet* 11(25), pp. 3135-3144.

Stein, B. et al. 1997. p38-2, a novel mitogen-activated protein kinase with distinct properties. *J Biol Chem* 272(31), pp. 19509-19517.

Stein, G. H. et al. 1999. Differential roles for cyclin-dependent kinase inhibitors p21 and p16 in the mechanisms of senescence and differentiation in human fibroblasts. *Mol Cell Biol* 19(3), pp. 2109-2117.

Stetler, R. A. et al. 2009. HSP27: mechanisms of cellular protection against neuronal injury. *Curr Mol Med* 9(7), pp. 863-872.

Stewart, S. A. and Weinberg, R. A. 2006. Telomeres: cancer to human aging. *Annu Rev Cell Dev Biol* 22, pp. 531-557.

Stokoe, D. et al. 1992a. MAPKAP kinase-2; a novel protein kinase activated by mitogen-activated protein kinase. *EMBO J* 11(11), pp. 3985-3994.

Stokoe, D. et al. 1992b. Identification of MAPKAP kinase 2 as a major enzyme responsible for the phosphorylation of the small mammalian heat shock proteins. *FEBS Lett* 313(3), pp. 307-313.

Suwaki, N. et al. 2010. Dose-dependent changes in cyclin D1 in response to 4-nitroquinoline 1-oxide-induced DNA damage. *Arch Biochem Biophys* 497(1-2), pp. 55-61.

Suzuki, T. et al. 2009. DNA helicase activity in purified human RECQL4 protein. *J Biochem* 146(3), pp. 327-335.

Syrrou, M. et al. 1995. Seckel syndrome in a family with three affected children and hematological manifestations associated with chromosome instability. *Genet Couns* 6(1), pp. 37-41.

Takekawa, M. et al. 2000. p53-inducible wip1 phosphatase mediates a negative feedback regulation of p38 MAPK-p53 signaling in response to UV radiation. *EMBO J* 19(23), pp. 6517-6526.

Takeuchi, F. et al. 1982. Prolongation of S phase and whole cell cycle in Werner's syndrome fibroblasts. *Exp Gerontol* 17(6), pp. 473-480.

Tan, Y. et al. 1996. FGF and stress regulate CREB and ATF-1 via a pathway involving p38 MAP kinase and MAPKAP kinase-2. *EMBO J* 15(17), pp. 4629-4642.

Tao, W. and Levine, A. J. 1999. P19(ARF) stabilizes p53 by blocking nucleo-cytoplasmic shuttling of Mdm2. *Proc Natl Acad Sci U S A* 96(12), pp. 6937-6941.

Tauchi, H. et al. 2002. Nbs1 is essential for DNA repair by homologous recombination in higher vertebrate cells. *Nature* 420(6911), pp. 93-98.

Taylor, W. R. and Stark, G. R. 2001. Regulation of the G2/M transition by p53. *Oncogene* 20(15), pp. 1803-1815.

te Poele, R. H. et al. 2002. DNA damage is able to induce senescence in tumor cells in vitro and in vivo. *Cancer Res* 62(6), pp. 1876-1883.

Thannhauser, S. J. 1945. Werner's syndrome (progeria of the adult) and Rothmund's syndrome: two types of closely related heredofamilial atrophic dermatosis with juvenile cataracts and endocrine features. A critcal study of five new cases *Ann Int Med* 23, pp. 559-625.

Thompson, K. V. and Holliday, R. 1983. Genetic effects on the longevity of cultured human fibroblasts. II. DNA repair deficient syndromes. *Gerontology* 29(2), pp. 83-88.

Thompson, S. L. et al. 2010. Mechanisms of chromosomal instability. *Curr Biol* 20(6), pp. R285-295.

Thomson, M. S. 1936. Poikiloderma congenitale. *Arch Dermatol* 75, pp. 236-244.

Thornton, T. M. and Rincon, M. 2009. Non-classical p38 map kinase functions: cell cycle checkpoints and survival. *Int J Biol Sci* 5(1), pp. 44-51.

Tice, R. R. et al. 1979. Cytokinetic analysis of the impaired proliferative response of peripheral lymphocytes from aged humans to phytohemagglutinin. *J Exp Med* 149(5), pp. 1029-1041.

Tollefsbol, T. O. and Cohen, H. J. 1984. Werner's syndrome: An underdiagnosed disorder resembling premature aging. *Age* 7, pp. 75-88.

Tollervey, D. and Kiss, T. 1997. Function and synthesis of small nucleolar RNAs. *Curr Opin Cell Biol* 9(3), pp. 337-342.

Torocsik, B. and Szeberenyi, J. 2000. Anisomycin affects both pro- and antiapoptotic mechanisms in PC12 cells. *Biochem Biophys Res Commun* 278(3), pp. 550-556.

Toussaint, O. et al. 2002. Stress-induced premature senescence and tissue ageing. *Biochem Pharmacol* 64(5-6), pp. 1007-1009.

Toyoshima, H. and Hunter, T. 1994. p27, a novel inhibitor of G1 cyclin-Cdk protein kinase activity, is related to p21. *Cell* 78(1), pp. 67-74.

van der Burgt, I. et al. 1996. Nijmegen breakage syndrome. *J Med Genet* 33(2), pp. 153-156.

van Hoffen, A. et al. 1993. Deficient repair of the transcribed strand of active genes in Cockayne's syndrome cells. *Nucleic Acids Res* 21(25), pp. 5890-5895.

van Steensel, B. et al. 1998. TRF2 protects human telomeres from end-to-end fusions. *Cell* 92(3), pp. 401-413.

Varon, R. et al. 1998. Nibrin, a novel DNA double-strand break repair protein, is mutated in Nijmegen breakage syndrome. *Cell* 93(3), pp. 467-476.

Vasile, E. et al. 2001. Differential expression of thymosin beta-10 by early passage and senescent vascular endothelium is modulated by VPF/VEGF: evidence for

senescent endothelial cells in vivo at sites of atherosclerosis. *FASEB J* 15(2), pp. 458-466.

Vaziri, H. 1997. Critical telomere shortening regulated by the ataxia-telangiectasia gene acts as a DNA damage signal leading to activation of p53 protein and limited life-span of human diploid fibroblasts. A review. *Biochemistry (Mosc)* 62(11), pp. 1306-1310.

Vaziri, H. and Benchimol, S. 1998. Reconstitution of telomerase activity in normal human cells leads to elongation of telomeres and extended replicative life span. *Curr Biol* 8(5), pp. 279-282.

Venema, J. et al. 1990. The genetic defect in Cockayne syndrome is associated with a defect in repair of UV-induced DNA damage in transcriptionally active DNA. *Proc Natl Acad Sci U S A* 87(12), pp. 4707-4711.

Vennos, E. M. et al. 1992. Rothmund-Thomson syndrome: review of the world literature. *J Am Acad Dermatol* 27(5 Pt 1), pp. 750-762.

Verdun, R. E. and Karlseder, J. 2006. The DNA damage machinery and homologous recombination pathway act consecutively to protect human telomeres. *Cell* 127(4), pp. 709-720.

Vermeulen, K. et al. 2003. The cell cycle: a review of regulation, deregulation and therapeutic targets in cancer. *Cell Prolif* 36(3), pp. 131-149.

Vulliamy, T. et al. 2001a. The RNA component of telomerase is mutated in autosomal dominant dyskeratosis congenita. *Nature* 413(6854), pp. 432-435.

Vulliamy, T. et al. 2004. Disease anticipation is associated with progressive telomere shortening in families with dyskeratosis congenita due to mutations in TERC. *Nat Genet* 36(5), pp. 447-449.

Vulliamy, T. J. et al. 1997. Skewed X-inactivation in carriers of X-linked dyskeratosis congenita. *Blood* 90(6), pp. 2213-2216.

Vulliamy, T. J. et al. 2001b. Very short telomeres in the peripheral blood of patients with X-linked and autosomal dyskeratosis congenita. *Blood Cells Mol Dis* 27(2), pp. 353-357.

Vulliamy, T. J. et al. 2005. Mutations in the reverse transcriptase component of telomerase (TERT) in patients with bone marrow failure. *Blood Cells Mol Dis* 34(3), pp. 257-263.

Wahl, G. M. and Carr, A. M. 2001. The evolution of diverse biological responses to DNA damage: insights from yeast and p53. *Nat Cell Biol* 3(12), pp. E277-286.

Walker, D. H. and Maller, J. L. 1991. Role for cyclin A in the dependence of mitosis on completion of DNA replication. *Nature* 354(6351), pp. 314-317.

Wallis, C. V. et al. 2004. Fibroblast clones from patients with Hutchinson-Gilford progeria can senesce despite the presence of telomerase. *Exp Gerontol* 39(4), pp. 461-467.

Walne, A. J. et al. 2007. Genetic heterogeneity in autosomal recessive dyskeratosis congenita with one subtype due to mutations in the telomerase-associated protein NOP10. *Hum Mol Genet* 16(13), pp. 1619-1629.

Wang, L. L. et al. 2003. Association between osteosarcoma and deleterious mutations in the RECQL4 gene in Rothmund-Thomson syndrome. *J Natl Cancer Inst* 95(9), pp. 669-674.

Wang, M. et al. 2006. PARP-1 and Ku compete for repair of DNA double strand breaks by distinct NHEJ pathways. *Nucleic Acids Res* 34(21), pp. 6170-6182.

Wang, W. et al. 2002. Sequential activation of the MEK-extracellular signal-regulated kinase and MKK3/6-p38 mitogen-activated protein kinase pathways mediates oncogenic ras-induced premature senescence. *Mol Cell Biol* 22(10), pp. 3389-3403.

Wang, W. et al. 2000a. Possible association of BLM in decreasing DNA double strand breaks during DNA replication. *Embo J* 19(13), pp. 3428-3435.

Wang, X. et al. 2000b. Involvement of the MKK6-p38gamma cascade in gamma-radiation-induced cell cycle arrest. *Mol Cell Biol* 20(13), pp. 4543-4552.

Wang, X. et al. 1998. Evidence of cisplatin-induced senescent-like growth arrest in nasopharyngeal carcinoma cells. *Cancer Res* 58(22), pp. 5019-5022.

Wang, X. Z. and Ron, D. 1996. Stress-induced phosphorylation and activation of the transcription factor CHOP (GADD153) by p38 MAP Kinase. *Science* 272(5266), pp. 1347-1349.

Warmerdam, D. O. and Kanaar, R. 2010. Dealing with DNA damage: relationships between checkpoint and repair pathways. *Mutat Res* 704(1-3), pp. 2-11.

Werner, O. 1904. *On cataract associated in conjunction with scleroderma.* Doctoral, Doctoral Dissertation, Schmidt and Klaunig, Kiel.

West, M. D. et al. 1989. Replicative senescence of human skin fibroblasts correlates with a loss of regulation and overexpression of collagenase activity. *Exp Cell Res* 184(1), pp. 138-147.

West, M. D. et al. 1996. Altered expression of plasminogen activator and plasminogen activator inhibitor during cellular senescence. *Exp Gerontol* 31(1-2), pp. 175-193.

Westin, E. R. et al. 2007. Telomere restoration and extension of proliferative lifespan in dyskeratosis congenita fibroblasts. *Aging Cell* 6(3), pp. 383-394.

Wick, M. et al. 1994. A novel member of human tissue inhibitor of metalloproteinases (TIMP) gene family is regulated during G1 progression, mitogenic stimulation, differentiation, and senescence. *J Biol Chem* 269(29), pp. 18953-18960.

Widmann, C. et al. 1999. Mitogen-activated protein kinase: conservation of a three-kinase module from yeast to human. *Physiol Rev* 79(1), pp. 143-180.

Wilhelm, D. et al. 1997. The level of intracellular glutathione is a key regulator for the induction of stress-activated signal transduction pathways including Jun N-terminal protein kinases and p38 kinase by alkylating agents. *Mol Cell Biol* 17(8), pp. 4792-4800.

Wilkinson, M. G. and Millar, J. B. 2000. Control of the eukaryotic cell cycle by MAP kinase signaling pathways. *FASEB J* 14(14), pp. 2147-2157.

Wilson, K. P. et al. 1996. Crystal structure of p38 mitogen-activated protein kinase. *J Biol Chem* 271(44), pp. 27696-27700.

Wilson, T. E. et al. 1997. Yeast DNA ligase IV mediates non-homologous DNA end joining. *Nature* 388(6641), pp. 495-498.

Witkowska, A. M. 2005. Soluble ICAM-1: a marker of vascular inflammation and lifestyle. *Cytokine* 31(2), pp. 127-134.

Wong, J. M. and Collins, K. 2006. Telomerase RNA level limits telomere maintenance in X-linked dyskeratosis congenita. *Genes Dev* 20(20), pp. 2848-2858.

Woo, L. L. et al. 2006. The Rothmund-Thomson gene product RECQL4 localizes to the nucleolus in response to oxidative stress. *Exp Cell Res* 312(17), pp. 3443-3457.

Wood, M. L. et al. 1990. Mechanistic studies of ionizing radiation and oxidative mutagenesis: genetic effects of a single 8-hydroxyguanine (7-hydro-8-oxoguanine) residue inserted at a unique site in a viral genome. *Biochemistry* 29(30), pp. 7024-7032.

Wood, M. L. et al. 1992. Genetic effects of oxidative DNA damage: comparative mutagenesis of 7,8-dihydro-8-oxoguanine and 7,8-dihydro-8-oxoadenine in Escherichia coli. *Nucleic Acids Res* 20(22), pp. 6023-6032.

Wood, R. D. et al. 2001. Human DNA repair genes. *Science* 291(5507), pp. 1284-1289.

Woods, C. G. et al. 1995. Severe intrauterine growth retardation with increased mitomycin C sensitivity: a further chromosome breakage syndrome. *J Med Genet* 32(4), pp. 301-305.

Wright, W. E. and Shay, J. W. 2000. Telomere dynamics in cancer progression and prevention: fundamental differences in human and mouse telomere biology. *Nat Med* 6(8), pp. 849-851.

Wu, C. C. et al. 2003. Nuclear factor of activated T cells c is a target of p38 mitogen-activated protein kinase in T cells. *Mol Cell Biol* 23(18), pp. 6442-6454.

Wu, J. et al. 1993. Activation of MAP kinase by a dual specificity Tyr/Thr kinase. *Adv Second Messenger Phosphoprotein Res* 28, pp. 219-225.

Wu, L. et al. 2001. Potential role for the BLM helicase in recombinational repair via a conserved interaction with RAD51. *J Biol Chem* 276(22), pp. 19375-19381.

Wyllie, F. S. et al. 2000. Telomerase prevents the accelerated cell ageing of Werner syndrome fibroblasts. *Nat Genet* 24(1), pp. 16-17.

Xiong, W. et al. 2006. Anisomycin activates p38 MAP kinase to induce LTD in mouse primary visual cortex. *Brain Res* 1085(1), pp. 68-76.

Xiong, Y. 1996. Why are there so many CDK inhibitors? *Biochim Biophys Acta* 1288(1), pp. 01-05.

Xu, X. and Liu, Y. 2009. Dual DNA unwinding activities of the Rothmund-Thomson syndrome protein, RECQ4. *EMBO J* 28(5), pp. 568-577.

Yamazaki, V. et al. 1998. Characterization of cell cycle checkpoint responses after ionizing radiation in Nijmegen breakage syndrome cells. *Cancer Res* 58(11), pp. 2316-2322.

Yanishevsky, R. and Carrano, A. V. 1975. Prematurely condensed chromosomes of dividing and non-dividing cells in aging human cell cultures. *Exp Cell Res* 90(1), pp. 169-174.

Yee, A. S. et al. 2004. The HBP1 transcriptional repressor and the p38 MAP kinase: unlikely partners in G1 regulation and tumor suppression. *Gene* 336(1), pp. 1-13.

Yegorov, Y. E. et al. 1998. Endogenous beta-galactosidase activity in continuously nonproliferating cells. *Exp Cell Res* 243(1), pp. 207-211.

Yin, J. et al. 2004. RECQL4, mutated in the Rothmund-Thomson and RAPADILINO syndromes, interacts with ubiquitin ligases UBR1 and UBR2 of the N-end rule pathway. *Hum Mol Genet* 13(20), pp. 2421-2430.

Ying, K. L. et al. 1990. Rothmund-Thomson syndrome associated with trisomy 8 mosaicism. *J Med Genet* 27(4), pp. 258-260.

Yokote, K. et al. 2004. Dysadipocytokinemia in werner syndrome and its recovery by treatment with pioglitazone. *Diabetes Care* 27(10), pp. 2562-2563.

Yu, C. E. et al. 1996. Positional cloning of the Werner's syndrome gene. *Science* 272(5259), pp. 258-262.

Zelle, B. and Bootsma, D. 1980. Repair of DNA damage after exposure to 4-nitroquinoline-1-oxide in heterokaryons derived from xeroderma pigmentosum cells. *Mutat Res* 70(3), pp. 373-381.

Zetterberg, A. et al. 1995. What is the restriction point? *Curr Opin Cell Biol* 7(6), pp. 835-842.

Zha, S. et al. 2007. Defective DNA repair and increased genomic instability in Cernunnos-XLF-deficient murine ES cells. *Proc Natl Acad Sci U S A* 104(11), pp. 4518-4523.

Zhan, Q. et al. 1999. Association with Cdc2 and inhibition of Cdc2/Cyclin B1 kinase activity by the p53-regulated protein Gadd45. *Oncogene* 18(18), pp. 2892-2900.

Zhang, S. et al. 1995. Rho family GTPases regulate p38 mitogen-activated protein kinase through the downstream mediator Pak1. *J Biol Chem* 270(41), pp. 23934-23936.

Zhang, Y. et al. 2006. The role of NBS1 in DNA double strand break repair, telomere stability, and cell cycle checkpoint control. *Cell Res* 16(1), pp. 45-54.